Technische Universität München

Lehrstuhl für Betriebswissenschaften und Montagetechnik
am Institut für Werkzeugmaschinen und Betriebswissenschaften (*iwb*)

Disaggregation of the Electric Energy Demand of Manufacturing Machines

Christian Johannes Gebbe

Vollständiger Abdruck der von der Fakultät für Maschinenwesen der Technischen Universität München zur Erlangung des akademischen Grades eines

Doktor-Ingenieurs (Dr.-Ing.)

genehmigten Dissertation.

Vorsitzender:	Prof. Dr. Tim C. Lüth
Prüfer der Dissertation:	1. Prof. Dr.-Ing. Gunther Reinhart 2. Prof. Dr. Thomas Hamacher

Die Dissertation wurde am 04.02.2019 bei der Technischen Universität München eingereicht und durch die Fakultät für Maschinenwesen am 22.08.2019 angenommen.

Contents

List of symbols and mathematical notation

In this thesis, the following mathematical notation is used consistently:

j – imaginary unit

x – a variable representing a real number / a continuous or discrete function returning a real number

$x(t)$ – value of the continuous function $x : \mathbb{R} \mapsto \mathbb{R}$ for input t

$\underline{x}$ – a vector

x_k – if $\underline{x}$ is a vector: value of its k^{th} element / if x is a discrete function $x : \mathbb{Z} \mapsto \mathbb{R}$: value of x for input k / else: any of the possibilities described under x

X – a constant such as the period T or the number of items N / a set / a matrix $X \in \mathbb{R}^{m \times n}$ or $X \in \mathbb{C}^{m \times n}$ / a variable representing a complex number / a function returning a complex number

X_{ij} – the element in the i^{th} row and j^{th} column of matrix X

$X(t)$ – value of the continuous function $X : \mathbb{R} \mapsto \mathbb{C}$ for input t

X_k – if X is a discrete function $X : \mathbb{Z} \mapsto \mathbb{C}$: value of X for input k / else: any of the possibilities described under X

Whether x, x_k, X or X_k represents a variable or a function is described explicitly when the specific symbol is introduced. Signals are considered to be functions in this thesis, since they relate a signal value (output) to a certain point in time (input).

The notation above is unusual in parts: in other publications, functions are often expressed including the argument, e.g., $x(t)$. However, this notation is not accurate and can lead to contradictions, as explained in Lee & Varaiya (2011, p. xiv). Moreover, according to norms such as IEC 60050-131:2002 (2002), the voltage, current and active power are written with uppercase letters, whereas they are written with lowercase letters here for consistency reasons. In this way, the current i is also clearly distinguishable from the complex current

harmonic I_n. Frequently used symbols and their meanings are listed in the following Table 0.1.

Table 0.1: List of frequently used symbols

Symbol	Meaning
f	Arbitrary signal
t	Time
k	Time, discretely measured
u	Voltage
i	Electric current
I	Electric current harmonic
p	Active power
q	Reactive power
s	Apparent power
d	Distortion power
z	Z-value, also referred to as standard score
T	Duration of one period in a periodic signal
N	Number of elements
ϕ	Phase angle
ω	Angular frequency
θ	Signal referring to the operating behavior of a two-state load, whose value is either 0 (off) or 1 (on)
ξ	Signal representing the probability of a step change
ϵ	Error
σ	Standard deviation
μ	Mean
$\mathcal{N}$	Gaussian distribution

List of abbreviations

Abbreviations are used sparsely in the thesis. The few abbreviations that are not listed in dictionaries are presented in Table 0.2.

Table 0.2: List of uncommon abbreviations used in this thesis

Abbreviation	Meaning
FSM	Fixed-speed motor
NILM	Nonintrusive load monitoring
PLC	Programming logic controller
UBR	Uncontrolled bridge rectifier
VSD	Variable speed drive

1 Introduction

This chapter describes the initial situation and the problem that this thesis aims to solve. Moreover, the requirements for a potential solution are specified, and the structure of the thesis is explained.

1.1 Initial situation

For many manufacturing companies in Germany increasing the energy efficiency has become a relevant objective (Abele & Reinhart 2011; Putz et al. 2017). For example, the car manufacturing companies BMW AG, Daimler AG, Volkswagen AG and General Motors Company LLC proclaimed that they will reduce the energy consumption per produced vehicle by between 20 % and 45 % (see Tab. 1.1).

Table 1.1: Energy efficiency targets of car manufacturers

Company and source	Reduction target for energy consumption per produced vehicle
BMW AG (BMW AG 2018, p. 55)	45 % between 2006 and 2020
Daimler AG (Daimler AG 2018, p. 119)	25 % between 2015 and 2022 (for Mercedes-Benz car plants)
Volkswagen AG (VW AG 2018, p. 77)	25 % between 2010 and 2018
GM Company LLC (GMC LLC 2018, p. 105)	20 % between 2010 and 2020

Their motivation is manifold. First, by increasing energy efficiency, their energy costs can be reduced. This has become of particular interest since the electricity price for industrial companies in Germany, including taxes, has increased by a factor of 284 % between 2000 and 2018 (see Fig. 1.1). Second, manufacturing companies can reduce their tax burden of the electricity price under certain conditions, according to §10 StromStG (electricity tax act) and §40 EEG (renewable energy sources act). One of these conditions is the implementation of organizational measures according to, e.g., the ISO 500001, EMAS or DIN 16247-1 norm. According to these norms, the companies

must demonstrate a continuous effort and corresponding results regarding the improvement in energy efficiency. Third, some end customers prefer sustainably manufactured products and are willing to pay more for such products (see Fig. 1.2).

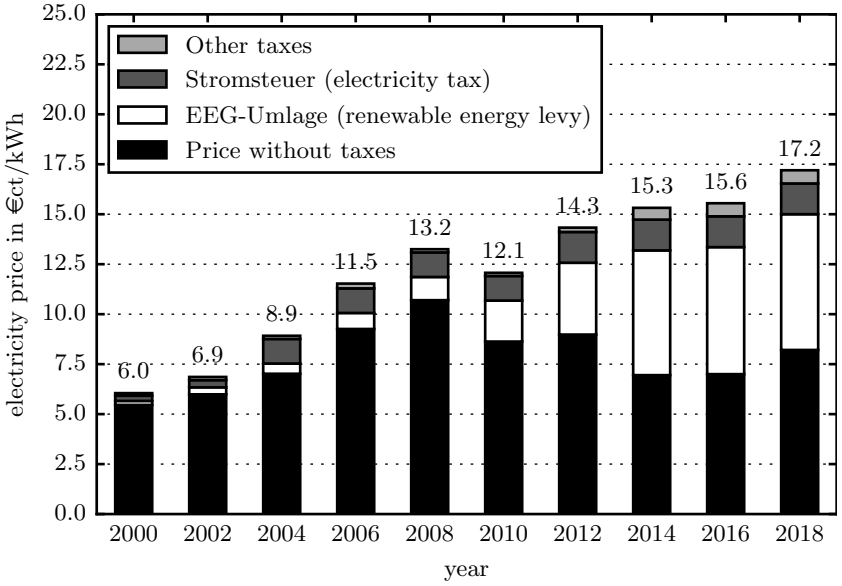

Figure 1.1: Electricity price for industrial customers (BDEW 2018)

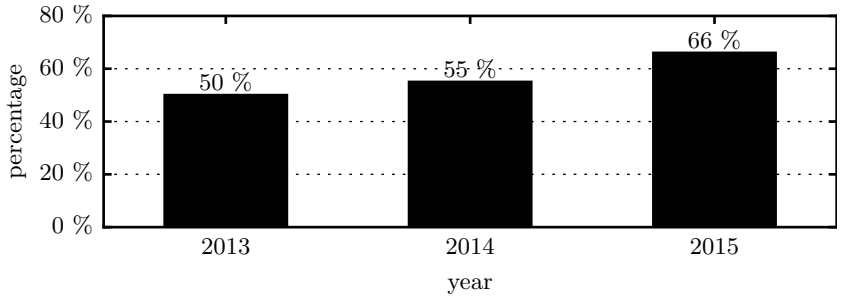

Figure 1.2: Percentage of customers (N=30,000 based on an online survey) that are willing to pay extra for products and services that come from companies committed to positive social and environmental impact (The Nielsen Company LLC 2015, p. 8)

One of the ways in which a manufacturing company can increase energy efficiency is by increasing the electric energy efficiency of its production machines. This area is relevant, since electric energy costs represents approximately 67 % of all energy costs in the mechanical engineering sector (Grassl 2015). About 66 % of the electric energy is converted via machines into mechanical energy, process heating or process cooling in the mechanical engineering sector (Rohde 2017). The residual 34 % of the electric energy is used for illumination, hot water, room heating and cooling as well as information technology. Therefore, in the mechanical engineering sector, the share of the electric energy costs from production machines in the total energy costs of an average company can be estimated to be 50 %.

To increase the electric energy efficiency of an existing production machine, its electric energy demand needs to be reduced while maintaining its value-adding output (Gebbe et al. 2015; Patterson 1996) (see Fig. 1.3).

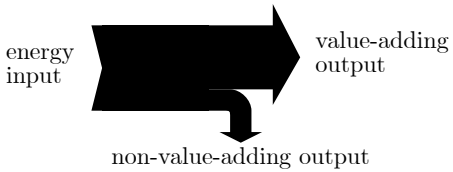

Figure 1.3: Schematic Sankey diagram describing the term energy efficiency. Based on (Patterson 1996)

This can be achieved in the following ways (Reinhart et al. 2010):

- Reduction of the non-value-adding output during idle times;
- Reduction of the non-value-adding output during active times;
- Providing the value-adding output more efficiently by, e.g., substituting components.

Several related examples have been reported in literature and they will be described next:

Reduction of non-value adding output during idle times One possibility is to simply reduce the duration of idle times. This can be achieved through manufacturing scheduling strategies which take into account the energy demand of machines in various states (Ataby et al. 2014; Kohl et al. 2014; Langer et al. 2014; Neugebauer et al. 2012b; Stoldt et al. 2013; Teiwes et al. 2018; Willeke et al. 2016). Another possibility is to turn off parts of the machine, i.e., machine components, which are not necessary at that moment (Li et al. 2011). Turning off machine components can be automated by

modifying the control system of existing machines. This was performed by the Leoni AG, which operated a galvanization process, comprising, among other things, two circulation pumps (Reinhart et al. 2016). These pumps worked under full load the whole time, even during idle times, since no standby mode was available. By retrofitting the pumps for 500 €, a standby mode was introduced, which lead to annual cost savings of approximately 3,000 €. Similarly, in (Steinhilper et al. 2015), a blasting machine was analyzed. It was found that during idle times, an industrial robot as well as a conveyor system for the blasting abrasive, comprising a lifting unit, a screw conveyor and a sieving unit, were unnecessarily active. Through a simple reprogramming, the energy demand during idle times could be reduced by 4.4 kW or 80 %. More examples in which the energy demand of machines during idle times was reduced are presented in (Reinhart et al. 2016): Voith GmbH & Co. KGaA reprogrammed automated weaving looms in several of their plants with the help of the loom manufacturer. Fujitsu Technology Solutions GmbH implemented a new, less energy-consuming standby mode with a longer ramp-up time for an existing soldering unit. BSH Hausgeräte GmbH noticed that one plastic manufacturing machine consumed 50 % as much electric energy in standby mode as in the active mode. While a modification was not economical for the existing machine, improvement measures were derived for the next purchase of a similar machine. In all examples described above the electric energy demand of the machine components was measured at first to quantify their degree of utilization and to estimate the energy saving potential of a new control strategy.

Reduction of non-value adding output during active times Even in active times, machine components can generate non-value-adding output, namely if the output is excessive. In these cases, the energy demand can be reduced by varying the process parameters. For example, the energy efficiency of cleaning systems could often be increased by reducing the duration of the cleaning process or the temperature of the cleaning fluid because these parameters were often defined with a large safety margin (Kübler 2017; Reinhart et al. 2017). The energy demand per cleaned piece could consequently be reduced by approximately 30 % in real-world applications. The fluid temperature of a cleaning basin was also reduced by BSH Hausgeräte GmbH by utilizing an alternative cleaning agent (Reinhart et al. 2016). In a similar manner, Herrmann et al. (2014) suggested reducing the system pressure of the hydraulic fluid in a pressure casting machine, Eberspächer et al. (2014) recommended adjusting the magnetization current of the main drives of a tooling machine during partial load and Denkena et al. (2013) proposed reducing the temperature, duration and raw part volume of a forging process. Apart from the above mentioned process parameters, several authors (Brossog et al. 2014, 2015; Brüggemann & Laumeyer 2013; Senft 2012; Simon

2015) reported that changing the movement paths of industrial robots from linear paths to more circular ones can lead to significant energy savings. Also in these cases, it is advised to measure the electric energy demand of relevant machine components in order to quantify the effect of a parameter change on their electric energy demand. One could argue that it would suffice to measure the electric energy demand of the machine as a whole. However, Popp & Zäh (2014a, b) showed that the electric energy demand of machine as a whole is often not reproducible due to decentralized controls. Therefore, it is at least beneficial to measure the components directly and thus quantify the effect accurately.

Substitution of components Last, machine components have been substituted to increase energy efficiency. A frequent example are electric motors which run at partial load and thus, generally, at a lower than nominal efficiency (Auinger 2001; USDOE 1997). If the motor is substituted with a smaller one, the load factor and accordingly the efficiency increases. Such a substitution is usually only economical if a new motors needs to be purchased in any case, e.g., due to a defect. In these cases, purchasing a smaller motor reduces not only energy costs but also investment costs. The substitution of a motor was recommended in a case study by Böhner et al. (2014), in which one of the main drives in a manufacturing plant had a nominal power of 260 kW but only supplied 179 kW at peak times. Therefore, a downsizing of the current motor into two separate 100 kW motors was advised. This measure was estimated to increase the motor efficiency by nine percentage points on average and thus generate energy cost savings of approximately 14,000 € annually. Similarly, the Leoni AG discovered that two pumps in a closed circuit were significantly overdimensioned. As a result, they removed one of the pumps and installed a variable speed drive on the other pump which resulted in cost savings of 12,000 € per year (Reinhart et al. 2016). In both cases it was necessary to measure the electric energy demand of the motor to determine the load factor and evaluate the saving potential of substituting the motor. Apart from motors, machine components used for energy storage can be substituted. For example, in (Abele et al. 2014), the valves of a hydraulic fluid storage tank, which were free of defects, were substituted with less leaking ones. In doing so, the average power of the hydraulic pump during standby was reduced from 826 W to 5 W. The unexpectedly high leakage rate was discovered by measuring the electric energy demand of the hydraulic pump during standby and noticing the high frequency of turn-on and turn-off events every 27 seconds.

As the examples above demonstrate, measuring the electric energy demand of a production machine **at the component level** is necessary for identifying and subsequently evaluating certain efficiency measures. Therefore, this kind of measurement is recommended by several systematic approaches for improving

the energy efficiency of machines (Abele et al. 2015; Böhner et al. 2014; Dörr et al. 2013; Liebl et al. 2018; Reinhart et al. 2010). It has also been performed in several other case studies analyzing the energy efficiency of tooling machines (Abele et al. 2011; Behrendt et al. 2012; Brecher et al. 2010, 2012; Denkena et al. 2014, 2015; Neugebauer et al. 2010, 2012a) or handling processes (Fleischer et al. 2016). In addition, the energy demand of machine components is a required input for several energy efficiency oriented control systems (Eberspächer et al. 2014; Larek et al. 2011; Verl et al. 2011b).

1.2 Problem statement

Each electric energy demanding machine component represents an (electric) load according to (IEC 60050-151:2001 2001). This definition includes components that convert the input electric energy into another form of electric energy, such as a 24 V power supply. The electric energy demand of any load can be determined by measuring the current flow through the load and the voltage drop across the load. Based on those two signals, the active power demand can be calculated (IEC 60050-113:2011 2011), which represents the time derivative of the electric energy demand (IEC 60050-131:2002 2002).

Therefore, a current clamp needs to be installed at each load of a production machine. In this thesis, it is assumed that only loads that are illustrated in the first level in Fig. 1.4 need to be measured. Loads in deeper levels, such as sensors or actors which are fed by a 24 V power supply, are typically of much lower interest due to their lower energy demand, and are thus not measured. This simplification also allows one to acquire the voltage signal only once, since it is approximately the same for all loads in the first level, as they are connected in a parallel circuit.

While this type of setup can be considered to be the reference measurement method, it is rather expensive and time consuming: First, dozens of current clamps are typically required for a manufacturing machine, since one machine comprises several loads, and most loads draw current on three phases. In combination with a data acquisition device which can record dozens of signals synchronously with a suitable sampling rate in the order of kilohertz, the investment costs for the measurement equipment quickly exceed 10,000 € or 20,000 €. Second, by German law, only a certified electrician can install the current clamps as it requires opening the cabinet box of a machine. Moreover, operating the often complex measurement equipment demands additional competences. Third, the person who installs the current clamps is usually not familiar with the assembly of the electric structure in the cabinet box and needs to consult the wiring diagram provided by the machine manufacturer. Determining which loads need to be measured and finding the appropriate wires to which to attach the current clamps might take hours. Fourth, the wires are

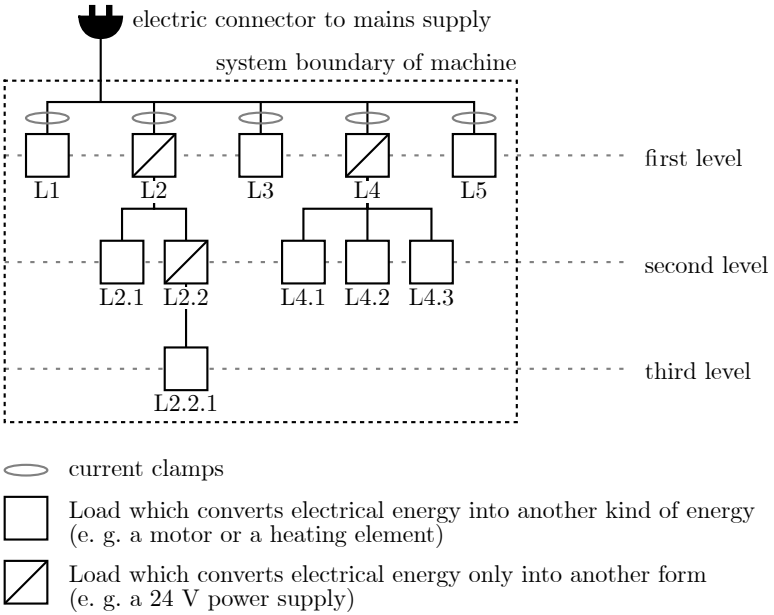

Figure 1.4: Schematic electric structure of a production machine including its components and installed current clamps

usually fastened tightly in the cabinet box with little space around them so that some current clamps cannot be installed due to lack of space. In such cases, only one of the three phases might be measured at once, or an electrician might need to elongate the existing wiring. Fifth, the data acquisition device needs to be configured by labeling the channels, specifying the type of connection (delta, star or any kind of voltage transformer in between) and displaying the signals. Sixth, the recorded data must be validated. Common errors are attaching a current clamp in the wrong direction, accidentally removing a voltage sensor or a current clamp from the data acquisition device, assigning the wrong voltage signal to a current signal or misinterpreting the wiring diagram. Even if everything has been performed correctly, the actual wiring of the machine might deviate from the specifications of the wiring diagram, for example, in terms of permutated phases. In total, the setup for one measurement can easily take several staff hours up to a day, considering all involved persons.

Since the reference measurement method exhibits high purchasing costs for the necessary equipment and a long setup time for each measurement, which translates into high recurring costs, a more economical measurement method is sought after.

1.3 Requirements on solution

An alternative measurement method should be characterized by lower costs and a similar benefit compared to the reference method described above. The cost and benefit depend on the following properties:

- The initial costs depend on the utilized measurement equipment.
- The running costs depend on the effort for each measurement.
- The benefit of a measurement can be characterized by the quality of the measurement result.

Therefore, three related requirement categories are defined in the following.

Requirements on the measurement equipment:

- **The measurement equipment can be used for multiple machines**. Since a medium-sized factory usually contains hundreds of machines, it is essential that the measurement equipment can be used not only for a few selected machines, but for any.
- **The initial costs for the measurement equipment are approximately 10,000 € or less.** The measurement itself does not generate cost savings, and it is not guaranteed that suitable efficiency measures resulting in cost savings can be identified by conducting a measurement. It is thus important that the initial costs are low. Based on the fact that typical energy efficiency measures yield cost savings of the order of magnitude of several thousand euros per year, per machine (see subsection 1.1), initial costs of approximately 10,000 € would be amortized in a few years by finding only one such efficiency measure. Such a reward-to-risk ratio seems appropriate.

Requirements on the effort for each measurement:

- **The measurement method can be executed by non-experts.** While energy managers or members of the energy efficiency team have certain competencies, they are not necessarily certified electricians or knowledgeable in operating production machinery. However, if the execution of a measurement method requires such knowledge, they cannot perform the measurement method themselves, and an expert needs to be called in. This prolongs the measurement process and increases the costs for each measurement.
- **The setup time for a measurement at a new machine requires approximately one hour or less.** Similar to the argument above, any performed measurement should be as time-efficient and hence as

economical as possible, since the benefit is uncertain. Probably more important than the economic aspect is the fact that measurements with a setup time of several hours or days are likely to be postponed, because they are rarely urgent or top-priority matters, neither for an energy manager nor for an electrician. Based on this thought, a setup time of one hour seems sensible, as it can be easily integrated into a typical working day.

Requirements on the measurement result quality:

- **The identified loads make up approximately 80 % or more of the aggregate active power demand.** In theory, it is desirable to know the power demand of every load in a machine. However, in practice, carrying out an energy efficiency measure is only profitable if the cost savings are significant. The reason is that the cost savings must outweigh the costs for planning and executing an efficiency measure. This cannot be achieved with loads exhibiting a low power demand such as a small power supply or a fan venting the cabinet box. Therefore, such loads are not of practical interest. A sensible threshold value is 80 %, based on the Pareto principle (Juran & Gryna 1951) or the ABC analysis (Dickie 1951).
- **The measurement accuracy for each of the identified loads is approximately 85 % or higher.** In this thesis, the term measurement accuracy is defined as

$$acc = 1 - \underbrace{\frac{\int |p_{meas}(t) - p_{ref}(t)| dt}{\int |p_{ref}(t)| dt}}_{\equiv \epsilon}, \tag{1.1}$$

where p_{meas} refers to the active power demand determined by a new measurement method, and p_{ref} represents the "true" active power demand determined by the reference measurement method described above. The subtrahend ϵ is referred to as the measurement error. In principle, an accuracy of 100 % is desirable. However, in practice, it is only necessary to detect those energy deficits that are economically feasible to tackle. This does not hold true for deficits in which the energy demand is only a few percent in excess of what is actually required because, in these cases, the cost savings are less than the costs for carrying out the efficiency measure. Instead, the cost savings and hence the difference between the actual and the required energy demand needs to be significant, e.g., by a factor of 150 % (see subsection 1.1). To detect such a deficit, an accuracy of 85 % is sufficient, since it would measure an excess factor of 150 % as 128-173 %, which is still excessive.

1.4 Scientific approach and structure of thesis

The work in this thesis can be classified as applied research which is defined as "an original investigation undertaken in order to acquire new knowledge [...] directed primarily towards a specific, practical aim or objective" (OECD 2015, p. 29). According to Siegwart (1974, p. 15), it aims at "providing a scientific basis for finding economically viable solutions to relevant problems".

The relevant problem in this thesis was explained in subsection 1.2. It came to the authors attention through discussions with various energy managers involved in the research project Green Factory Bavaria as well as through literature research. In order to find a solution to this problem, first, existing measurement methods were analyzed and assessed (see chapter 3). One promising method works by only measuring the active power demand of the aggregate load (i.e., the entire machine), and then disaggregating it into its parts automatically. While this method has been proven to be successful for determining the active power demand of residential household devices, it has never been applied to machines used in manufacturing. Since its suitability depends on the type of loads present in the aggregate load, an empirical analysis of approximately 150 loads of machines used in manufacturing was carried out (see chapter 4). Based on this analysis, the suitability of the existing disaggregation methods was evaluated in more detail for the most prevalent loads. The evaluation revealed four distinct deficits, which were mathematically proven when possible (see chapter 5). For each of the four deficits a new, improved method was designed (see chapter 6). These new methods were merged into a combined measurement method based on disaggregation and applied to seven machines used in manufacturing (see chapter 7). Based on the application results, the new combined measurement method was assessed according to the criteria defined in section 1.3 (see chapter 8). Finally, the research carried out in this thesis was summarized and future research directions were proposed (see chapter 9).

The structure of this thesis is presented graphically in Fig. 1.5. The dominant part of the scientific work can be characterized as design work according to Balzert et al. (2017, p. 72ff) while chapter 4 and chapter 5 comprise empirical and theoretical work, respectively. All conducted steps were devised to comply to the research principles of replicability, independence, precision and falsification (Recker 2012, p. 16).

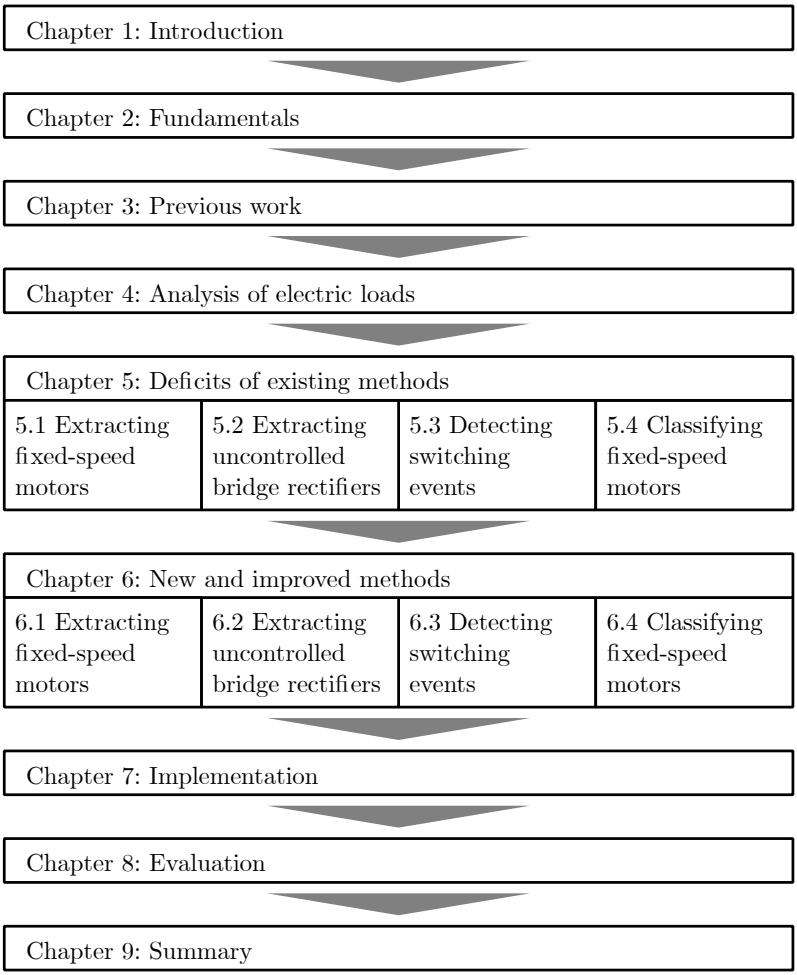

Figure 1.5: Structure of the thesis

2 Fundamentals

In order to prepare the reader for the following chapters, some information taught in (advanced) university courses is briefly summarized in this chapter. Since the main topic of the thesis is the measurement of electrical energy, relevant electrical properties such as the active power, current harmonics and the total harmonic distortion are defined in section 2.2. These definitions make use of the Fourier transform, which is therefore introduced in section 2.1 beforehand. One of the most relevant machine components in this thesis are motors fed by a variable speed drive, which are thus presented in section 2.3. All of the variable speed drives discussed in this thesis comprise rectifiers, whose characteristic current draw is explained in section 2.4. Finally, many signals are classified automatically in this thesis using machine learning methods and the relevant technical terms are hence introduced in section 2.5.

2.1 Fourier transform

The Fourier transform decomposes a signal into its various frequency components (Sung et al. 2002). With the continuous Fourier transform a continuous, integrable signal $f' : \mathbb{R} \mapsto \mathbb{R}$ can be transformed into another continuous signal $F' : \mathbb{R} \mapsto \mathbb{C}$ as

$$F'(v) = \int_{-\infty}^{+\infty} f'(t) e^{-2\pi j v t} dt \ , \tag{2.1}$$

where j represents the imaginary unit, t the time and v the frequency.

Similarly, a discrete signal $f : \mathbb{Z} \mapsto \mathbb{R}$ with $f_k = f'(t_0 + kT)$ with a sampling frequency of T and $k = 0, 1, ..., N-1$ possesses a discrete Fourier transform $F : \mathbb{Z} \mapsto \mathbb{C}$ defined as

$$F_n = \frac{1}{N} \sum_{k=0}^{N-1} f_k e^{-2\pi j (n/N) k} \ , \tag{2.2}$$

where n/N is analogous to the frequency v (Bracewell 1978, p. 260). If f is real valued ($f_k \in \mathbb{R} \forall k$), the symmetry $F_{N-n} = F_n^*$ holds true.

Based on the discrete Fourier transform F, the original signal f can be reconstructed using the inverse discrete Fourier transform:

$$f_k = \sum_{n=0}^{N-1} F_n e^{2\pi jnk/N} \tag{2.3}$$

$$\underbrace{\begin{bmatrix} f_0 \\ f_1 \\ f_2 \\ \vdots \\ f_{N-1} \end{bmatrix}}_{\equiv \underline{f}} = \underbrace{F_0 \begin{bmatrix} 1 \\ 1 \\ 1 \\ \vdots \\ 1 \end{bmatrix}}_{\equiv \underline{f_0}} + \underbrace{F_1 \begin{bmatrix} 1 \\ e^{2\pi j \cdot 1 \cdot 1/N} \\ e^{2\pi j \cdot 1 \cdot 2/N} \\ \vdots \\ e^{2\pi j \cdot 1 \cdot (N-1)/N} \end{bmatrix}}_{\equiv \underline{f_1}} + \ldots + \underbrace{F_{N-1} \begin{bmatrix} 1 \\ e^{2\pi j \cdot (N-1) \cdot 1/N} \\ e^{2\pi j \cdot (N-1) \cdot 2/N} \\ \vdots \\ e^{2\pi j \cdot (N-1) \cdot (N-1)/N} \end{bmatrix}}_{\equiv \underline{f_{N-1}}}$$

The equation above can be understood such that the original signal $\underline{f}$ can be represented as the sum of $\underline{f_0}, \underline{f_1}, ..., \underline{f_{N-1}}$, which are oscillations of a single frequency (see Fig. 2.1). Moreover, it can be demonstrated, that $\underline{f_0}, \underline{f_1}, ..., \underline{f_{N-1}}$ are pairwise orthogonal to each other, since:

$$\begin{aligned} < \underline{f_m}, \underline{f_n} > &= F_m F_n^* \sum_{k=0}^{N-1} e^{2\pi jmk/N} e^{-2\pi jnk/N} \\ &= F_m F_n^* \sum_{k=0}^{N-1} e^{2\pi j(m-n)k/N} \\ &= F_m F_n^* N \delta_{mn} \ , \end{aligned} \tag{2.4}$$

where δ_{mn} represents the Kronecker delta.

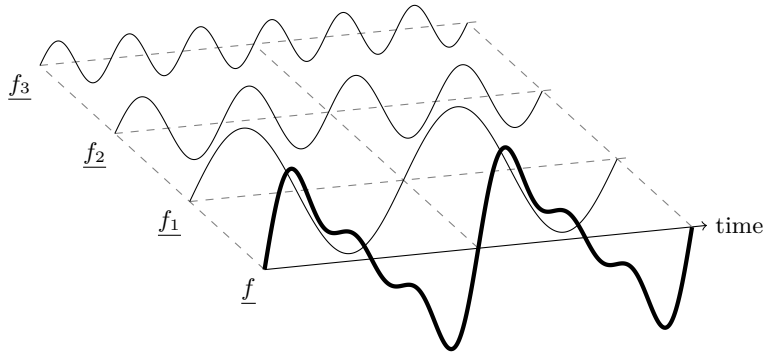

Figure 2.1: The signal $\underline{f}$ can be represented as the sum of $\underline{f_1}$, $\underline{f_2}$ and $\underline{f_3}$

2.2 Electrical properties

The electric power is defined as the derivative with respect to time t of the energy e being transferred or transformed (IEC 60050-113:2011 2011). Based on the measured voltage u and the current i, the instantaneous power p_{inst} can be calculated as

$$p_{inst}(t) \equiv \frac{d}{dt}e(t) = u(t)i(t) \ . \tag{2.5}$$

If the flow of electric charges represented by i is in only one direction, the operating mode is referred to as direct current (DC). If, on the other hand, i changes its direction periodically, one speaks of alternating current (AC). In the latter case, p_{inst} will oscillate with period $T/2$, and instead of the instantaneous power, the more relevant property is the active power p, which is defined as (IEC 60050-131:2002 2002)

$$p(t_0) \equiv \frac{1}{T}\int_{t_0}^{t_0+T} p_{inst}(t)dt \ . \tag{2.6}$$

For a sinusoidal voltage and a linear load, u and i can be represented with $\omega = 2\pi/T$ and $\phi = \alpha - \beta$ as

$$\begin{aligned} u(t) =& \sqrt{2}\hat{u}cos(\omega t + \alpha) = \mathbb{R}\left(\sqrt{2}\underbrace{\hat{u}e^{j\alpha}}_{U}e^{j\omega t}\right) = \mathbb{R}\left(\sqrt{2}Ue^{j\omega t}\right) \text{ and} \\ i(t) =& \sqrt{2}\hat{i}cos(\omega t + \beta) = \mathbb{R}\left(\sqrt{2}\underbrace{\hat{i}e^{j\beta}}_{I}e^{j\omega t}\right) = \mathbb{R}\left(\sqrt{2}Ie^{j\omega t}\right) \ . \end{aligned} \tag{2.7}$$

The instantaneous and active power can then be calculated as

$$\begin{aligned} \Rightarrow p_{inst}(t) =& u(t)i(t) = \mathbb{R}\left(\sqrt{2}Ue^{j\omega t}\right) \cdot \mathbb{R}\left(\sqrt{2}Ie^{j\omega t}\right) \\ =& 2 \cdot \frac{1}{2}\left(Ue^{j\omega t} + U^*e^{-j\omega t}\right)\frac{1}{2}\left(Ie^{j\omega t} + I^*e^{-j\omega t}\right) \\ =& \frac{1}{2}\left(UIe^{2j\omega t} + U^*I^*e^{2j\omega t} + UI^* + U^*I\right) \\ =& \mathbb{R}\left(UIe^{2j\omega t} + UI^*\right) \text{ and} \\ \Rightarrow p(t_0) =& \frac{1}{T}\int_{t_0}^{t_0+T} p(t)dt = \mathbb{R}\left(UI^*\right) = \mathbb{R}\left(|U||I|e^{j(\alpha-\beta)}\right) = |U||I|cos(\phi) \ . \end{aligned} \tag{2.8}$$

In contrast to the above, any periodic, but not necessarily sinusoidal voltage and current can be represented by means of the Fourier transform as (Hanzelka & Milanović 2008)

$$u(t) = \mathbb{R}\left(\sum_{n=0}^{\infty} \sqrt{2} U_n e^{jn\omega t}\right) \text{ and} \tag{2.9}$$
$$i(t) = \mathbb{R}\left(\sum_{n=0}^{\infty} \sqrt{2} I_n e^{jn\omega t}\right) .$$

Each summand represents an oscillation whose angular frequency is an integer multiple n of the base angular frequency ω. Therefore, these summands are also termed harmonics, e.g., the summand with $n = 2$ can be called the second harmonic. Moreover, the vector $[I_0, I_1, \cdots, I_\infty]$ can be referred to as the spectral envelope of the current harmonics. Based on the spectral envelope, the total harmonic distortion (THD) of the current i can be calculated as

$$THD = \frac{\sqrt{|I_2|^2 + |I_3|^2 + |I_4|^2 + \ldots}}{|I_1|} . \tag{2.10}$$

For this general scenario, the active power p and another electric property called the apparent power s can be defined as

$$p(t_0) = \int_{t_0}^{t_0+T} u(t) i(t) dt = \sum_{n=0}^{\infty} |U_n||I_n| cos(\phi_n) \text{ and} \tag{2.11}$$
$$s(t_0) \equiv \sqrt{\frac{1}{T}\int_{t_0}^{t_0+T} u(t)^2 dt} \sqrt{\frac{1}{T}\int_{t_0}^{t_0+T} i(t)^2 dt} = \sqrt{\sum_{n=0}^{\infty} |U_n|^2 \sum_{n=0}^{\infty} |I_n|^2} .$$

Furthermore, Budeanu (1927) proposed defining the reactive power q and the distortion power d as

$$\sqrt{s(t_0)^2 - p(t_0)^2} \equiv \underbrace{\sum_{n=0}^{\infty} |U_n||I_n| sin(\phi_n)}_{q(t_0)} + d(t_0) . \tag{2.12}$$

It is important to note that for an ideal alternating voltage source, $(U_n = 0 | n \neq 1)$, so that $p = |U_1||I_1| cos(\phi_1)$ and $q = |U_1||I_1| sin(\phi_1)$. If the current is also a pure sinus, i.e., $(I_n = 0 | n \neq 1)$, the distortion power is zero, i.e., $d = 0$, and $s^2 = p^2 + q^2$ holds. Even though the power theory of Budeanu (1927) has several disadvantages (Czarnecki 1997), it still remains popular today (Czarnecki 2011; Jeltsema 2015).

2.3 Electric motors

Electric motors are used to convert electrical energy into mechanical energy. In the last century, a wide variety of electrical motor types have been developed. According to Sclater & Traister (2003, p. 346), they can be broadly classified as either AC or DC motors based on their necessary electric energy supply. Alternating current motors can be further partitioned into synchronous and induction motors or single- and poly-phase motors. The classification scheme by Sclater & Traister (2003) is illustrated in Fig. 2.2.

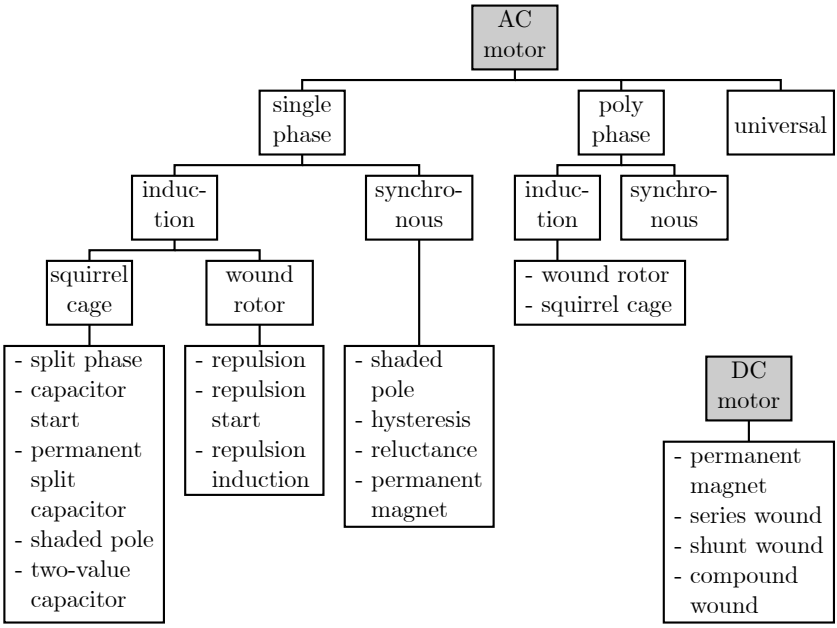

Figure 2.2: Classification of electric motors (Sclater & Traister 2003, p. 346)

One relevant motor, which is not explicitly presented in Fig. 2.2, is the electronically commutated motor, also called brushless DC motor. This motor is similar to the AC synchronous permanent-magnet motor. The difference between them is the wave shape of their induced electromotive force (Krishnan 2001, p. 523; Pillay & Krishnan 1989a, b). It is sinusoidal for AC synchronous permanent-magnet motors and trapezoidal for electronically commutated motors.

In the simplest form, AC and DC motors are directly connected to an AC or DC supply respectively. To vary the motor speed or optimize the performance, motors can be equipped with an additional variable speed drive. A variable speed drive system consists of an electric motor, a power converter and a controller (see Fig. 2.3). There are various ways in which to classify variable speed drive systems, e.g., by application, by power converter type or by motor (Rashid 2007, p. 887 ff). A list of typical applications for variable speed drive systems is presented in Table 2.1, which indicates their importance for manufacturing companies.

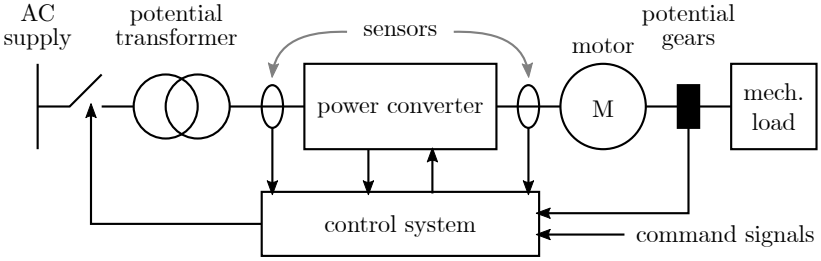

Figure 2.3: Structure of a variable speed drive (Rashid 2007, p. 882)

Table 2.1: Exemplary applications of different variable speed drives (Koschnick & Sattler 2013)

Type of variable speed drive	Exemplary applications
Drive controller for AC motors with a joint DC link	Tooling machines, packaging machines and industrial robots
Drive controller for AC motors (single axis)	Pumps, fans, compressors, extruders, conveyors, cranes and ship propulsion
Drive controller for electronically commutated motors	Pick and place, handling and adjusting
Drive controller for DC motors (single axis)	Rolling mill, cableway and test stands

Due to the importance of AC squirrel cage induction motors for the industry (Rashid 2007, p. 897; Frost & Sullivan 2014; Chaudhary 2015), such drive systems shall be discussed in more detail. In order to change the rotor speed of an induction motor, the number of poles, the slip or the supply frequency can be changed (Krishnan 2001, p. 262). A variable supply frequency from the AC mains can be achieved through a rectifier, a DC-link and a pulse-

width-modulated inverter (see Fig. 2.4). Similarly, the power converter of an AC synchronous permanent-magnet motor drive consists of a rectifier, a DC-link and a pulse-width-modulated inverter (Pillay & Krishnan 1989b; Rasmussen et al. 1997).

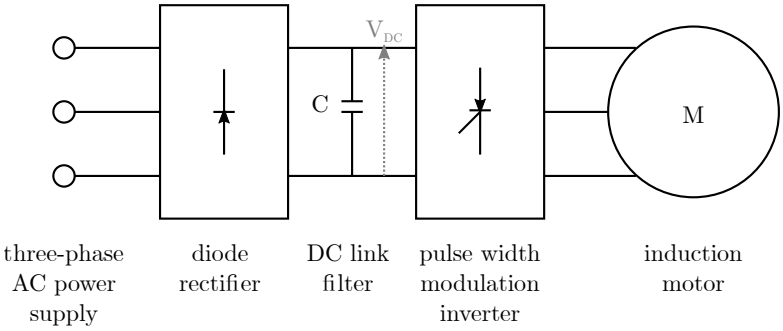

Figure 2.4: Exemplary structure of the power converter of a variable speed drive for an induction motor (Krishnan 2001, p. 314)

2.4 Rectifier circuits

As explained above, several types of variable speed drives comprise rectifiers. Thereby, they exhibit a characteristic current waveform, which can be explained by looking only at the rectifier and modeling the inverter, the connected motor and the mechanical load as a DC source (Wichakool et al. 2009; Xu et al. 1999) or as a simple ohmic resistor (Zhou et al. 2015). The influence of the inverter, motor and mechanical load on the current shape is assumed to be negligible as explained by Xu et al. (1999). The characteristic current waveform depends on the type of rectifier. Here, three types of rectifiers shall be differentiated:

- A single-phase uncontrolled full-wave bridge rectifier;
- A three-phase uncontrolled full-wave bridge rectifier;
- Any type of rectifier (three-phase or single-phase) using power factor correction.

Single-phase uncontrolled bridge rectifier The structure of a single-phase uncontrolled full-wave bridge rectifier is illustrated in Fig. 2.5. In its simplest form, it comprises four diodes, and, as explained above, the load can be modeled as either a DC source or as an ohmic resistor. These options yield the same

result when the current through the resistor is constant, which is approximately true for the scenarios in the following. Therefore, the load was modeled as a resistor R_{load}. The voltage between both ends of the diodes can be calculated as $u_{DC}(t) \approx max(u_L(t), u_N(t)) - min(u_L(t), u_N(t)) \propto |sin(\omega t)|$ (see Fig. 2.5). By introducing a capacitor parallel to the resistor the diodes only become conducting for brief moments when u_{DC} is larger than the voltage across the capacitor. Then, the resulting form of i_L can be described by one narrow peak per half-period (see Fig. 2.5). To limit the magnitude of the DC current, an additional ohmic resistance R_{series} (Xu et al. 1999) or inductance L_{series} (Lee et al. 2005; Zhou et al. 2015) can be introduced in series with the capacitance and R_{load}.

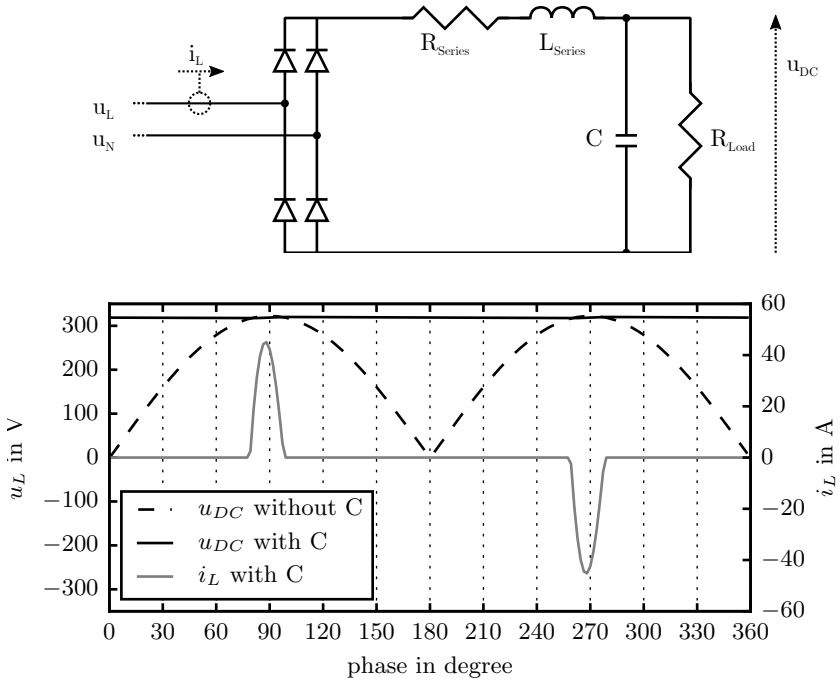

Figure 2.5: Electric circuit used for the simulation of an uncontrolled full-wave single-phase bridge rectifier (top) and simulated voltages and current with $R_{series} = L_{series} = 0$, $R_{load} = 100\ \Omega$ and $C = 10\ mF$ (with C) or $C = 0$ (without C) (bottom)

Three-phase uncontrolled bridge rectifier The structure of a three-phase uncontrolled full-wave bridge rectifier is presented in Fig. 2.6. It strongly resembles the single-phase version. Again, the voltage between both ends of the diodes can be calculated as $u_{DC}(t) \approx max(u_{L1}(t), u_{L2}(t), u_{L3}(t)) - min((u_{L1}(t), u_{L2}(t), u_{L3}(t)))$. Though, in this case, $u_{DC}(t)$ shows a different pattern with a six times shorter period than the AC system. As a consequence, the resulting signals i_{L1}, i_{L2}, i_{L3} typically exhibit two peaks per half-period. The signals are zero for $\phi \in [-30°, 30°] \cup [150°, 210°]$ and around $\phi = 90°$ and $\phi = 270°$. For large values of either the series resistance R_{series} or the inductance L_{series} the current shape may change such that the signal is zero only for $\phi \in [-30°, 30°] \cup [150°, 210°]$ and nonzero otherwise. However, such a current shape was not observed in this thesis.

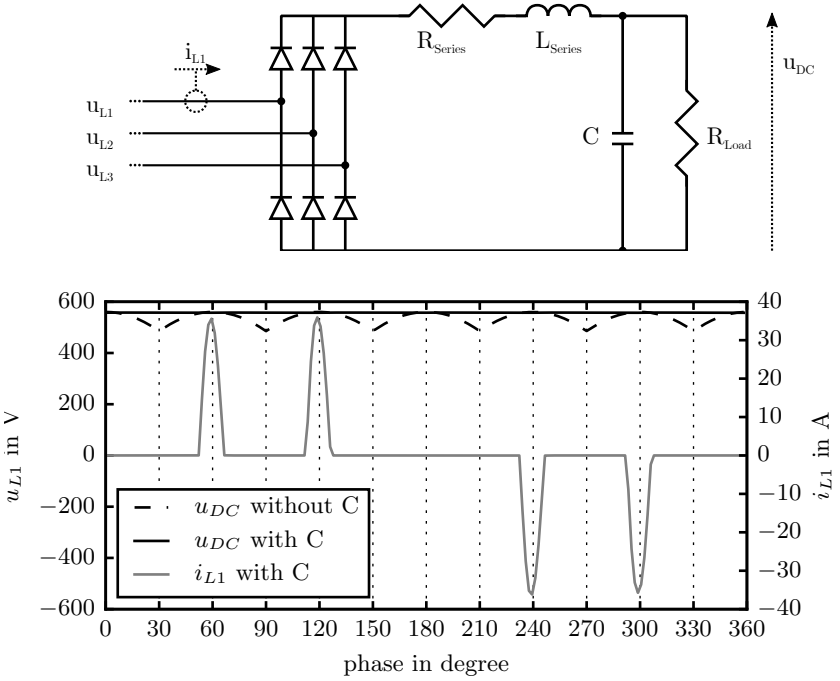

Figure 2.6: Electric circuit used for the simulation of an uncontrolled full-wave three-phase bridge rectifier (top) and simulated voltages and current with $R_{series} = L_{series} = 0$, $R_{load} = 100\ \Omega$ and $C = 10\ mF$ (with C) or $C = 0$ (without C) (bottom)

Rectifier featuring power factor correction Rectifiers featuring power factor correction do not exhibit peaks in the current waveform (see Fig. 2.7). Instead, the current waveform is rather sinusoidal with a typical total harmonic distortion of less than 5 % (Microchip Technology Inc. 2008). This is exactly one of the two purposes of the power factor correction. Apart from reducing the total harmonic distortion, which can cause problems for other electric loads in the same building, it also aims at increasing the power factor $\lambda(t) = |p(t)|/s(t) \approx |p(t)|/\sqrt{p(t)^2 + q(t)^2}$. In other words, it is employed to reduce the demand of the reactive power q. Different topologies using high-frequency switching can be used to achieve this goal (Microchip Technology Inc. 2008).

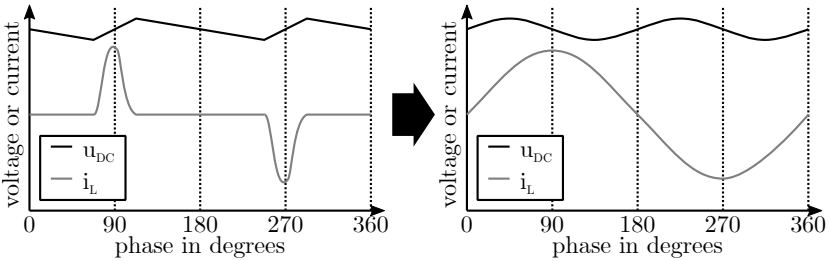

Figure 2.7: Schematic voltage and current of a single-phase uncontrolled full-wave bridge rectifier (left) and a rectifier with power factor correction (right). Based on Microchip Technology Inc. (2008, p. 10).

2.5 Classification in the context of machine learning

According to Mohri et al. (2012), classification is the process of assigning a category to items. In the context of machine learning, items are said to be characterized by features (attributes), and instead of the word category, the word label is rather used. The function that performs the classification can be referred to as the classifier.

A classifier can either be manually specified or it can automatically "learn" a desired behavior based on existing data, i.e., without being explicitly programmed (Koza et al. 1996). In the latter case, it is important to differentiate between supervised and unsupervised learning (Jain et al. 1999). In supervised learning, the classifier learns from training data in which all items are labeled (see Fig. 2.8). After this learning phase or "training", one of these labels is assigned to new, unlabeled data.

In contrast, no labeled (training) data exist in unsupervised learning. Instead, a classifier is constructed such that the given data are grouped into meaningful clusters. All items in one cluster are assigned the same label. In some cases the number of clusters can be specified by the user. Unsupervised classification is often referred to with the term clustering instead of the term classification.

Both supervised and unsupervised learning methods are employed in this thesis to classify electric signals according to their electrical properties with the purpose of identifying the type of an electric load.

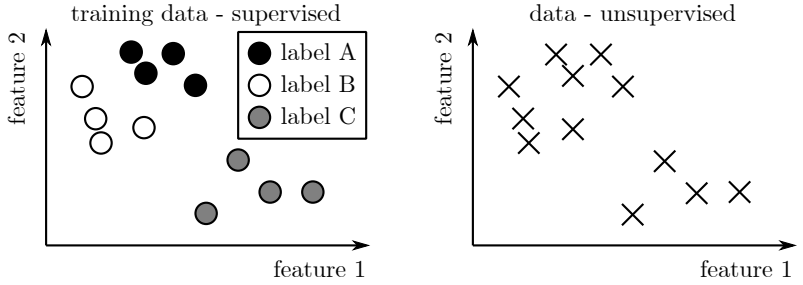

Figure 2.8: Exemplary *labeled* training data in the case of supervised learning and *unlabeled* data in the case of unsupervised learning

3 Previous work

This chapter lists different measurement methods for determining the electric energy demand of machine components, and it assesses their suitability according to the six requirements specified in section 1.3. The term measurement method is defined as the "generic description of a logical organization of operations used in a measurement" by the Joint Committee for Guides in Metrology (JCGM 2012). The term measurement is defined as the "process of experimentally obtaining one or more quantity values that can reasonably be attributed to a quantity" (JCGM 2012).

To assess the measurement methods, it is helpful to differentiate electric loads according to their number of operating states (see Fig. 3.1). Simple loads, which can only be switched on and off and exhibit a constant active power demand when turned on, have just two operating states and can thus be called two-state loads. Other loads may have more than two states, but still a finite number of operating states whose active power demand is constant and pairwise different. These loads are referred to as multi-state loads in this thesis. Last, there are loads in which the active power demand varies continuously. These loads effectively have an infinite amount of operating states, and they are referred to as continuously variable loads.

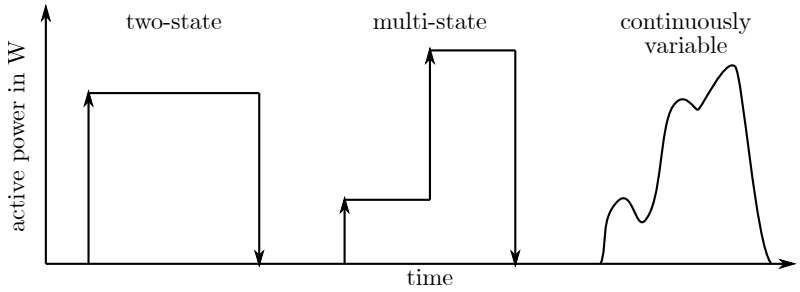

Figure 3.1: The active power demand of a two-state, a multi-state and a continuously variable electric load (from left to right)

The following seven measurement methods will be analyzed:

1. Reference measurement method with mobile equipment (see section 1.2);
2. Reference measurement method with permanently installed equipment;
3. Estimation of the electric energy demand by an expert;
4. Simulation of the electric energy demand;
5. Disaggregation of the measured electric energy demand of the machine by manually controlling the operating status of its components;
6. Disaggregation of the measured electric energy demand of the machine by monitoring the operating status of its components;
7. Disaggregation of the measured electric energy demand of the machine using only the measured voltage and current.

3.1 Reference method with mobile equipment

The most straightforward method to quantify the active power demand of the electric loads in a machine is to measure the voltage and current of each electric load. As described in section 2.2, the active power demand can then be calculated as $p(t_0) \equiv \frac{1}{T} \int_{t_0}^{t_0+T} u(t)i(t)dt$.

In practice, the voltage is measured only once rather than at each electric load. The reason is that the electric loads are normally connected to the mains in a parallel circuit, and in an ideal parallel circuit, the voltage drop across the loads is exactly the same (see Fig. 3.2). In contrast to an ideal parallel circuit, in reality, the wirings have a non-zero electrical impedance, which differs for each electric load due to, e.g., the cable length and the quality of the electric connectors. However, since the impedance of the wiring is typically significantly less than the impedance of the electric load, the assumption of an ideal parallel circuit leads to negligible measurement errors.

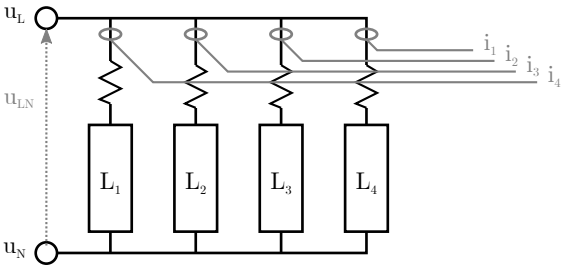

Figure 3.2: In the reference method the current i is measured for each electric load L and the voltage u is only measured once.

As explained in section 1.2, with this measurement method, the true quantity value can be obtained within the accuracy of the measurement equipment. Potential measurement errors can be introduced by all components of the measurement chain, including the voltage and current sensors, the current-to-voltage transducer, the analog-to-digital converters and any transmission unit such as cables in between (Borši et al. 2003; Hofmann 2000). In this application scenario, some of the largest error sources are typically the employed current clamps, which are specified with errors of a few percent relative to the measured value. While current sensors with lower specified errors exist, they tend to be more expensive, bulkier and may not be opened, thereby significantly complicating the installation process. Nevertheless, the requirement of a measurement accuracy of at least 85 % is definitely fulfilled. Moreover, all electric loads can be measured given a sufficient number of current clamps and enough space to attach them.

The costs of the equipment depends significantly on the necessary accuracy and the number of electric loads. The current clamps used in this thesis cost around 150 € per piece (Gossen Metrawatt WZ12b). Assuming that 20 current signals corresponding to approximately seven three-phase electric loads need to be measured, the costs of the current clamps amount to 3,000 €. In addition, a data acquisition system that is capable of synchronously monitoring 20 current channels and three voltage channels amounts to approximately 15,000 € (e.g., Dewesoft DS-Net, National Instruments DAQ) It is possible to build a system out of automation equipment that is not meant for mobile use and thereby decrease the costs to around 5,000 € (e.g., Beckhoff CX5140 in combination with EL3773). However, such systems need to be assembled and programmed after the purchase, resulting in labor costs of approximately 5,000 €. Finally, the costs of cables, voltage clamps and hardware such as a monitor and input devices can be approximated to 1,000 €. In total, the initial costs will most likely exceed 10,000 €.

The disadvantages of this measurement method have already been detailed in section 1.2. Apart from the high initial costs, the time to set up the measurement is long due to the necessary expert competencies, the need to study the machine wiring specifications, the lack of space, the necessary configuration of the measurement equipment and the validation of the recorded signal data.

3.2 Reference method with permanently installed equipment

Similarly to the measurement method described above, the same equipment could be permanently installed, for example, by the machine manufacturer. In

that case, some of the drawbacks mentioned in section 1.2, such as the lack of space and the time to study the wiring diagram, would not apply.

However, since such permanently installed equipment can only be used for the measurement of one machine, the costs for multiple machines would increase many times over.

3.3 Estimation by an expert

Even without any measurement of the voltage or the current, the power demand of the machine components can be estimated by an expert based on the measurement results of similar machinery and specification sheets provided by the machine manufacturer (Eisele 2014). First, all relevant electric loads and the times at which they are switched on or off could be identified with the help of the machine operator. Further, the rated power can be found on the type plate of motors (IEC 60034-16-1:2011 2011) or machines (Directive 2006/42/EC 2006). However, the rated power only refers to a specific operating condition - often full load in continuous duty (USDOE 1997). In contrast, the actual power demand can differ significantly from that value, as the examples in section 1.1 demonstrated. Due to these uncertainties in the estimation, a measurement accuracy of approximately 85 % for all loads is highly unlikely.

Moreover, such an estimation can only be performed by experts, and the necessary time to discuss the electric loads of the machine, analyze its data sheets and find relevant measurement data for comparison can total several hours if performed diligently.

3.4 Simulation of the electric energy demand

Several authors have used simulation models to estimate the power demand of electric loads in machines. For example, in (Eisele 2014), a method was developed to simulate the energy demand of all components of metal cutting machines. This simulation model was then used to minimize the energy demand for a specific product. With the same purpose, a state-based consumption simulation model was developed for a milling machine (Dietmair & Verl 2009; Eberspächer & Verl 2013), with which the energy consumption in idle times could be minimized. Similar work has been reported in (Schmitt et al. 2011; Verl et al. 2011a). Apart from tooling machines components, the energy demand of each of the six axes of an industrial robot was simulated by Brossog et al. (2014, 2015).

By using such models, all relevant electric loads can be simulated, and an accuracy of above 85 % can be reached (Dietmair & Verl 2009; Eisele 2014).

However, an expert is required to perform the simulation, and the necessary setup time to develop an accurate machine model is in the order of days or weeks, not hours. The development costs for this "measurement equipment" is thus significantly larger than 10,000 €.

The greatest disadvantage of this method is that simulation models are machine specific. While the framework and certain parts of the simulation model may be transferable, the majority of the work needs to be performed again for a new machine. Moreover, many machine models are trained with measurement data acquired through the reference method mentioned above (Dietmair & Verl 2009; Eberspächer & Verl 2013). In these cases, the simulation method is not a substitute for the reference measurement method but rather an extension for other problem settings.

3.5 Disaggregation by means of manual control

Another method is to measure only the voltage and current of the aggregate load (i.e., the machine as a whole), and then turn electric loads on and off manually, one by one. In this case, the active power demand p of the manually controlled electric load can be calculated as the difference between the measured aggregate power and the baseline aggregate power before switching on the load as follows:

$$p(t) = p_{agg}(t) - p_{agg}(t_{before}) \ . \tag{3.1}$$

This method can be referred to as disaggregation, since the power demand of the individual loads is estimated based on the power consumption of the aggregate load. Measuring the aggregate load only requires a suitable mobile data acquisition system including three current clamps. Such a system is available for around 2,000 € (e.g., FLUKE 1730).

The accuracy of this method depends on the types of loads and extent to which they can be controlled manually. For example, power supplies often can not be controlled manually, neither can a ventilator cooling a spindle in a machine tool (without modification of the programmable logic controller). Therefore, it is not certain whether the majority of the loads can be measured. Even if each electric load can be controlled manually, it is not guaranteed that a typical process of a machine can be realistically imitated through manual control. Moreover, the power demand of all electric loads contributing to $p_{agg}(t_{before})$ has to be constant, which cannot always be assured.

Performing this measurement method requires the competence to manually control the individual electric loads of the machine, to imitate a typical process and to identify relevant electric loads. While no formal certification is necessary,

such competence can only be acquired through extensive experience in operating machines.

3.6 Disaggregation by means of operating status monitoring

Panten et al. (2016) and Gebbe et al. (2014) proposed using the operating status of electric loads to disaggregate the active power demand of an aggregate load. While Gebbe et al. (2014) focused on disaggregating the power demand of a process chain into the power demand of individual machines, Panten et al. (2016) concentrated on disaggregating the power demand of a machine into the power demand of its individual components, which is the same goal as the one pursued in this thesis. In both cases, the power demand of the components is calculated via a linear regression:

$$\hat{p}_1, \hat{p}_2, \cdots, \hat{p}_N = \underset{p_1, p_2, \cdots p_N}{\operatorname{argmin}} \int \left| p_{agg}(t) - \sum_{n=0}^{N} p_n \theta_n(t) \right|^2 dt \ , \tag{3.2}$$

where $\hat{p}_1, \hat{p}_2, \cdots, \hat{p}_N \in \mathbb{R}$ refer to the estimated power of each load and $\theta_n : \mathbb{Z} \mapsto \{0, 1\}$ to the operating status of a two-state load (either on or off). Each electric load is hence assumed to be a two-state load, and if this condition does not hold true, the accuracy will deteriorate accordingly. Another detrimental situation explained in (Gebbe et al. 2014) occurs if two electric loads are switched on and off at similar times, leading to a linear correlation and numerical instabilities. In conclusion, an accuracy of 85 % can only be achieved in a few cases.

A more important question relates to how the operating status of the electric loads can be obtained. It can be observed manually, which is rarely appropriate, or it can be automatically inferred from analog or digital signals. These signals can be monitored either at different cables in the cabinet box, which would mean a similar effort and similar measurement equipment to those in the reference method, or centrally from the control variables in the programming logic controller (PLC). However, while it is rather straightforward to establish a physical connection with the PLC, the control variables are rarely made easily accessible through, e.g., a OPC-UA server. Instead, a symbol file exported from the program code is necessary, which only the machine manufacturer possesses and is usually hesitant to distribute. Moreover, some electric loads might not be controlled by a central PLC, but by small decentralized control loops. An example would be a simple cooling device, which turns on once a threshold temperature is exceeded.

Adding to this disadvantage, the equipment cost for this measurement method can become high due to the large variety of PLC suppliers and their different

physical and network interfaces. Dealing with different systems will also require expert knowledge. Therefore, this measurement method is only relevant for the following types of companies:

- Those who have a limited variety of PLCs;
- Those who have access to the program code of the PLCs;
- Those whose electric loads can be reasonably approximated as ideal two-state loads;
- Those whose electric loads are centrally controlled by a PLC for each machine.

3.7 Disaggregation using only the voltage and the current

Last, there is the possibility to perform a disaggregation automatically through only a detailed analysis of the current and voltage of the aggregate load. Neither a manual control of the electric loads nor information about their operating statuses is necessary.

This method is often termed nonintrusive load monitoring (NILM) or nonintrusive appliance load monitoring and the number of published papers per year in this area has grown significantly in the past decade (see Fig. 3.3). In this thesis, The term NILM shall refer to measurement methods that estimate the power consumption and operational schedule of electric loads based on *only* a detailed analysis of the measured current and the measured voltage of the aggregate load (Anderson 2014; Berges et al. 2010a; Hart 1992). This is a rather narrow understanding of the term NILM. In a broader sense, additional information such as the operating state of electric loads (Panten et al. 2016), environmental information from light sensors (Berges et al. 2010b), acoustic sensors (Guvensan et al. 2013; Schoofs et al. 2010; Uddin & Nadeem 2012) or contextual information such as the time of the day (Kim et al. 2011; Powers et al. 1991) or location of a person (Harris & Cahill 2005; Yoo et al. 2011) can be used for the disaggregation. Nonintrusive load monitoring can be contrasted with intrusive load monitoring, where a sensor is installed at each electric load (Hart 1992; Ridi et al. 2015). Alternatively, NILM can be referred to as single-point sensing, and intrusive load monitoring can be referred to as distributed sensing (Zoha et al. 2012).

Despite its popularity, **no publication exists today in which NILM has been applied to production machines**. Instead, the primary application area of NILM has been the disaggregation of the electric energy demand of residential households. A few authors have already addressed the industry sector. However, they either focused on the heating, ventilation, and air conditioning (Laughman et al. 2003) or a refrigerated warehouse (Holmegaard & Baun Kjaergaard 2016) or they discussed the challenges and potential solutions theoretically (Adabi et al. 2015). None of them targeted production

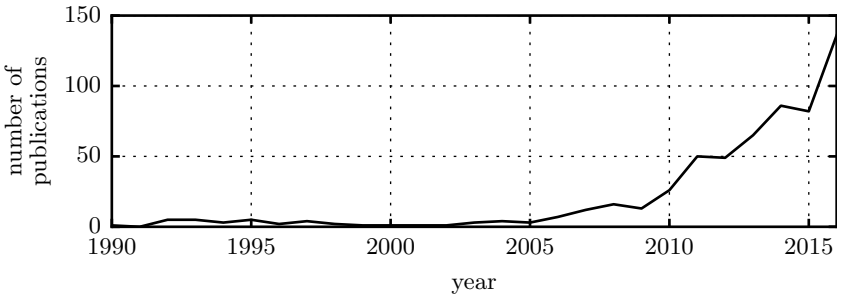

Figure 3.3: Number of publications per year with the topic nonintrusive load monitoring (in different spellings) according to (Elsevier 2018)

machines. Since production machines comprise different electric loads in terms of number, type and operating behavior than residential households, the extent to which existing disaggregation algorithms developed for households are also suitable for production machines is unclear.

The disaggregation method using only the aggregate voltage and the aggregate current is more complex than in cases, where, additionally the operating status of the loads are either controlled or monitored. In fact, to date, the following four different disaggregation routes have been proposed (Zeifman & Roth 2011; Zoha et al. 2012) (see Fig. 3.4) and they will be explained in detail in the next subsections:

- Disaggregation based on switching events,
- Disaggregation as an optimization problem,
- Disaggregation based on correlations,
- Disaggregation using neural networks.

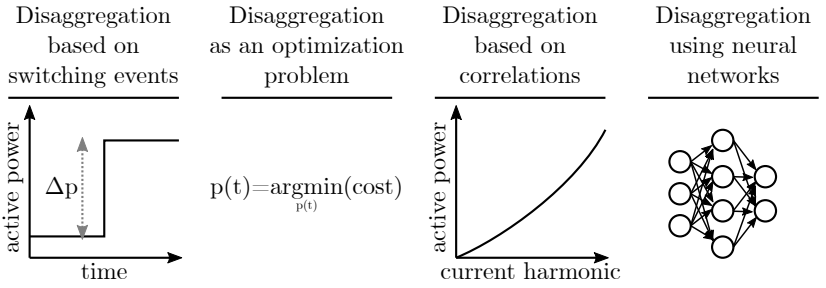

Figure 3.4: Different disaggregation methods using only the measured current and voltage of the aggregate load

Not all four of those methods are suitable for two-state, multi-state and continuously variable loads (see Table 3.1). Moreover, they may need to be trained in some cases, which means that they initially need to be provided with the ground truth and can only perform after the training period (see section 2.5). In this application scenario, it would mean that first the electric energy demand of all components would need to be measured with the reference measurement method. Based on these training data, the disaggregation algorithm can learn the desired result, and only then is it sufficient to measure the aggregate load alone and run the disaggregation algorithm. The necessity of obtaining such training data first stands in contrast to the requirements of a short setup time (see subsection 1.3). Therefore, disaggregation methods requiring training do not represent a valid alternative, and they are only briefly described next.

Table 3.1: Summary of the suitability and training requirement of the four different disaggregation methods using no additional information. The symbols indicate whether a statement is correct ●, correct only in some cases ◑ or incorrect ○.

	Suitable for two-state loads	Suitable for multi-state loads	Suitable for continuously variable loads	Does not require training
Disaggregation based on switching events	●	◑	○	◑
Disaggregation as an optimization problem	●	●	○	◑
Disaggregation based on correlations	○	○	◑	◑
Disaggregation using neural networks	●	●	●	○

In all four methods, it is sufficient to only acquire the voltage and current of the aggregate load (assuming no training is required). The initial investment costs for the hardware are thus only around 2,000 €. In addition, the disaggregation algorithms would need to be implemented either on the device or on an external computer. In either case, the costs can be expected to be less than 10,000 €. Moreover, since the disaggregation is performed automatically, and since the aggregate current and voltage could be measured by connecting a measurement device in series with the electric connector of the machine, this measurement method could be performed by a non-expert within minutes.

3.7.1 Disaggregation based on switching events

The term nonintrusive load monitoring was first introduced by George W. Hart in 1985 (Hart 1985). His idea was based on the observation that each switching event of an appliance, e.g., from on to off or vice versa, leads to a step change in the active power demand and other electric properties such as the reactive power demand (see Fig. 3.5 top). Such a step change can be mathematically represented as a vector $[\Delta p, \Delta q]$, where Δp refers to the magnitude of the step change in the active power and Δq represents the magnitude of the step change in the reactive power. For a two-state load, this vector is approximately the same for each turn-on or turn-off event. On the other hand, different two-state loads are characterized by different vector values. Thereby, it is possible to identify which step changes belong to the same electric load. The complete algorithm can be summarized in five steps:

1. Data acquisition,
2. Event detection,
3. Clustering of events,
4. Estimation of power demand for each load,
5. Labeling of loads.

First, the current and voltage of the aggregate load are measured and relevant electric properties are calculated (see section 2.2). Second, step changes are detected in both the active and reactive power by calculating the difference between any two consecutive steady states (see Fig. 3.5 top). If an event is detected, its feature vector $[\Delta p, \Delta q]$ is extracted. Third, once all events in a timeframe are detected, they are clustered according to their absolute features values. Since Hart (1985) used two features, the clustering can be easily represented in a two-dimensional plane (see Fig. 3.5 bottom). Each cluster is assumed to be a different appliance. Fourth, for each cluster, its active power demand is estimated as $p(t) = \theta(t)p_{on}$, where $\theta(t) = \{0, 1\}$ represents the operating state of the load (either on or off) and can be inferred from the detected events in a cluster, and $p_{on} \in \mathbb{R}$ represents the constant active power demand in the on-state, which can be calculated as the average of all detected step-change magnitudes in a cluster. Fifth, a cluster can be labeled as a specific appliance type, e.g., a dishwasher or an oven, based on its feature values and its calculated duration in the on and off states. For this purpose, either a-priori information or training data is necessary.

The actual implementation of the algorithm is more complex as described above, since in reality, more complex situations can arise:

First, the voltage in the grid fluctuates so that even for a simple ohmic resistor the step change Δp calculated as $\Delta p = u \cdot i = u^2/R$ is not constant. Therefore,

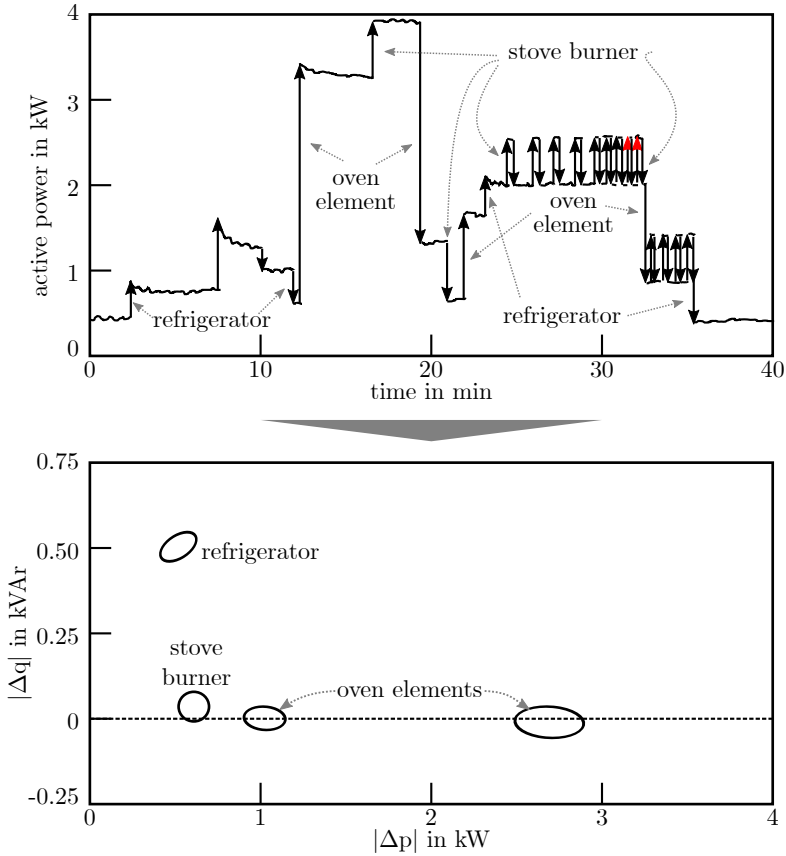

Figure 3.5: Characteristic step changes in the active power demand (top), which can be clustered (bottom). Based on (Hart 1992).

instead of the active power p, a normalized active power p_{norm} is used instead which is defined as

$$p_{norm} = (U_{norm}/u)^2 \, p = (U_{norm}/u)^2 \, (u^2/R) = U_{norm}^2/R = const \ , \quad (3.3)$$

where U_{norm} is a constant, for example, $U_{norm} = 230 \ V$ in Europe.

Second, the algorithm above is only suitable for two-state loads. However, Hart (1985) observed that some appliances have multiple operating states, for example, a washing machine. In these cases, there are not just two, but more transitions between the states, whose magnitude differs. Therefore, these transitions will not be grouped in the same cluster, which makes the situation much more complex. For such appliances, Hart laid out ideas in (Hart 1985) and sketched out a "tentative" algorithm in (Hart 1992). In this algorithm the appliances are modeled as finite-state machines and learned by hypothesizing several possibilities and choosing the one that best fits the data according to a number of heuristics. After one finite-state machine is learned, its events are removed from the data so that they are learned one by one.

Third, it may be that two appliances coincidentally turn on or off at the same time. This would lead to two missed events of known appliances, plus a new event, which, in general, will not be grouped in a cluster and thus represents an outlier. To resolve these situations, an anomaly resolution system is built into the disaggregation approach. It works by searching for appliances with missed events, which, because of the missed events, are estimated to be switched on or off twice in a row, against common sense.

Fourth, the above-mentioned approach described the scenario in which all the measured data are processed at once after the measurement has been performed. In contrast, in most applications, it is desired that the measurement data are processed close to real time. This complicates the clustering process, and dynamic algorithms become necessary. While the algorithms become more sophisticated, the general idea remains the same.

The structure of recent disaggregation methods based on switching events is still the same as in Hart's original algorithm. However, several additions and improvements have since been made:

- More features than only the active and reactive power have been used to classify switching events.
- Different classification and labeling procedures have been tested.
- Different methods for estimating the power demand of each cluster have been proposed.

3.7.1.1 More features

As additional features, current harmonics, voltage noise, transients and V-I-trajectories have been suggested.

Harmonics Several authors have pointed out that two different appliances may lead to the same step change $[\Delta p, \Delta q]$ when switched on. This would lead to an inability to distinguish them in the best case, and to an appliance being estimated to be switched on or off twice in a row in the worst case. For this reason, Akbar & Khan (2007); Bernard & Marx (2016); Bernard et al. (2015); Laughman et al. (2003) used the step changes in the harmonics of the measured aggregate current as additional features. In this way, Laughman et al. (2003) were able to differentiate between a computer and a light bulb, even though they had similar $[\Delta p, \Delta q]$ values.

The vector of all harmonics is often referred to as the spectral envelope (see section 2.2 and Fig. 3.6), and efficient ways in which to calculate it are discussed in (Shaw & Laughman 2007). In (Bernard & Marx 2016; Bernard et al. 2015), the current harmonics were calculated until the 11th order, which correlates to a frequency of 550 Hz in the European grid. Therefore, according to the Nyquist–Shannon sampling theorem (Shannon 1949), the sample rate has to be at least 1,100 Hz. In practice though, sampling rates of several kilohertz are used to calculate the harmonics.

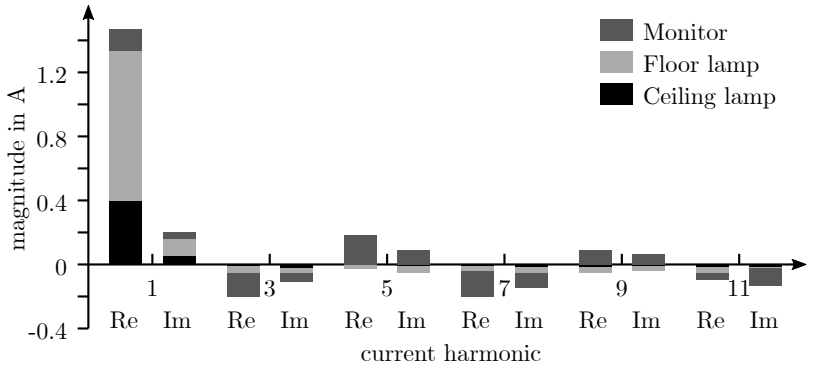

Figure 3.6: Part of the spectral envelope of the current from a monitor, floor lamp and ceiling lamp. "Re" stands for the real part and "Im" for the imaginary part of the current harmonic (Bernard et al. 2015).

Srinivasan et al. (2006) also used the spectral envelope of the measured aggregate current as the only feature to classify electric loads after a supervised training period. However, in this paper, the absolute values of the harmonics were used as features instead of the step changes in the harmonics. In this way, all possible combinations of the operating states of 8-10 loads were measured or simulated and used for training the classifier. However, this approach does not seem practical (Zeifman & Roth 2011) because in a house with 40 two-state loads, $2^{40} = 1.10 \cdot 10^{12}$ combinations would need to be learned. Moreover, integration of new appliances would require excessive retraining.

Voltage noise An additional feature for the classification can be extracted when using sampling rates in the high kilohertz to megahertz range for the voltage. Patel et al. (2007) were the first to observe that solid-state switched electric loads, such as switch mode power supplies used for consumer appliances, generate high-frequency electromagnetic interference during steady state operation, which propagates through a home's power wiring (see Fig. 3.7.)

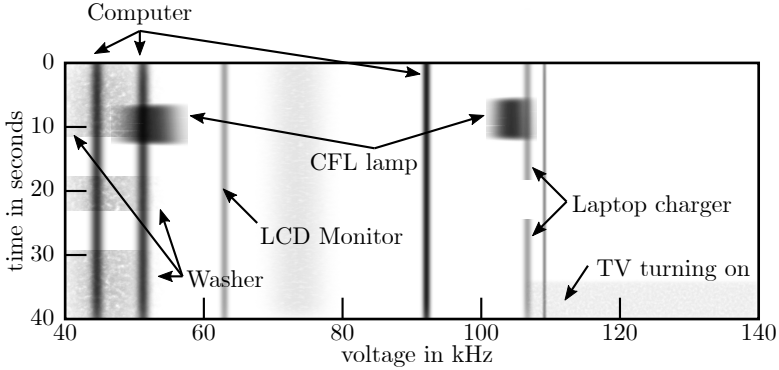

Figure 3.7: Steady state voltage noise from various appliances (Gupta et al. 2010)

Based on the findings of Patel et al. (2007), Gupta et al. (2010) tested a disaggregation based on only this feature in seven different homes with 7 to 20 appliances, and they reported an average classification accuracy of 94 % for the switching events after a supervised training period. One disadvantage was that not all appliances generated voltage noise in their operation. Examples are devices with large resistive loads such as electric stoves or dryers as well as the majority of washing machines.

Gupta et al. (2010) also tested whether devices of the same model yield similar features. While this was true for eight LCD screens, the voltage noise

spectra of four compact fluorescent lights, which were purchased as a package, were shifted slightly such that the peak of the voltage noise varied between 50-55 kHz. Moreover, it was observed that the features of an LCD screen were influenced by the touch of a hand (Gupta 2014, p. 92) and that the features of a TV monitor were affected by the type of screen content (Gupta 2014, p. 88). In fact, it was even possible to predict the type of movie for a TV monitor after a training period.

Transient features All previously mentioned features are extracted from the electric properties in the steady state. In contrast, features can also be obtained from the transient state, which Shenkman (2006, p. 2) describes as follows: "an electrical system is said to be in transient state when the variables are changed non-periodically, i.e., when the system is not in steady-state. The transient-state vanishes with time and a new steady-state regime appears."

Sultanem (1991) noticed that appliances generate different transient responses when turned on (see Fig. 3.8). Therefore, in the disaggregation procedure, the duration of the transient active power is used to distinguish between the loads in addition to the $[\Delta p, \Delta q]$ features.

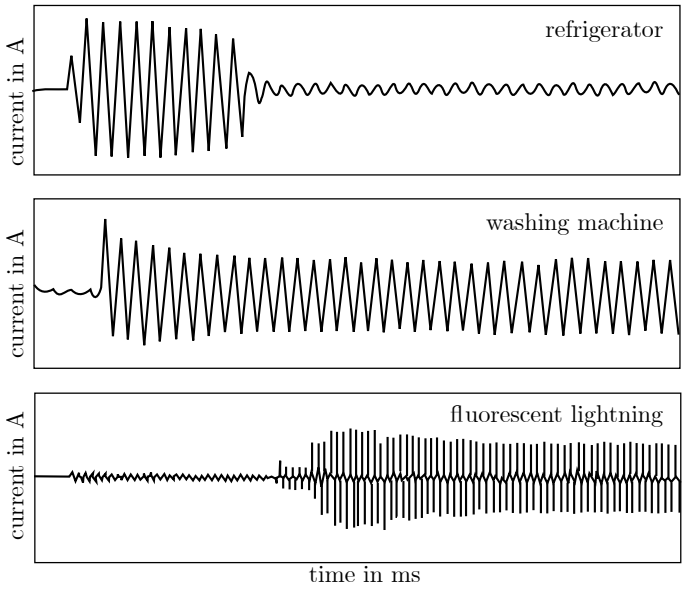

Figure 3.8: Transient currents of various appliances when switched on (Sultanem 1991)

Similarly, Leeb et al. (1993) described that the "transient behavior of a typical load is intimately related to the physical task that the load performs" based on a load survey conducted in Leeb (1993). In this survey, Leeb (1993) analyzed and explained the transient behavior of linear loads, electrothermal loads, electromechanical loads (further partitioned into DC machines, induction machines and synchronous machines) as well as power electronic loads. As a result, Leeb (1993); Leeb et al. (1993) used the pattern of the transient active and reactive power for classification. Since the transients can be several seconds or even minutes long, they are prone to overlap with another turn-on transient. They consequently only used those segments of the transient that varied the most - those segments were dubbed v-sections. The comparison was performed using a transversal filter. The same approach was utilized in (Norford & Leeb 1996).

Two years later, Leeb et al. (1995) proposed using the elements of the spectral envelope of the transient aggregate current as features. In contrast to section 2.2, where the elements of the spectral envelope are constant for at least one period, Leeb used time-varying coefficients by calculating the Fourier series coefficients in a sliding window manner - for more information see (Sanders et al. 1991). These time-varying coefficients were then used for a classification similar to the one described in (Leeb 1993; Leeb et al. 1993).

Instead of the Fourier series coefficients, Camps et al. (1994) used the coefficients from a wavelet transform of the transient power for classification. While Camps et al. (1994) used it to classify power system disturbances, Cole & Albicki (1998) laid out the idea to classify electric loads with it – apparently not aware of Leebs similar work in the earlier years because Leeb et al. (1995) was neither cited nor mentioned in the paper. Due to the computational effort to compute wavelets, Cole & Albicki (1998) actually proposed approximating the transient active power of electric loads with a linear slope (see Fig. 3.9). Only the idea was presented; no classification was performed with a case study.

From 2007 to 2012 Hsueh-Hsien Chang analyzed several ways in which to use the transient state for classification. In (Chang et al. 2007, 2008, 2010, 2012; Yang et al. 2007), the energy in the transient state $e = \int_{t_{start}}^{t_{end}} p(t)dt$ was used as a feature, and it was classified using different types of neural networks. In addition, in (Chang et al. 2012), the duration of the transient was used as well.

Patel et al. (2007), who focused on voltage noise caused by electromagnetic interference (see above), observed not only steady state voltage noise, but also transient voltage noise and they described the frequency range between 0.5 kHz and 5 kHz as an effective range for analysis. They performed a fast Fourier transform on the measured voltage and classified its coefficients

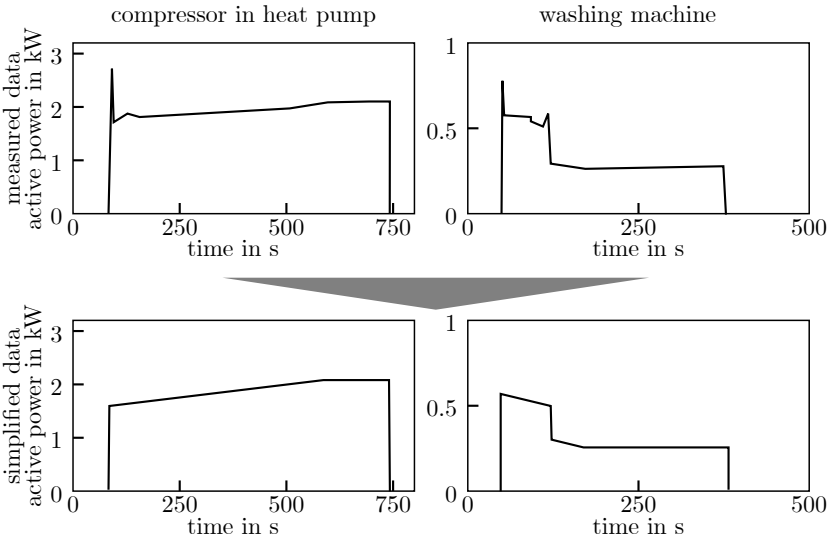

Figure 3.9: Approximation of the transient active power with a linear slope (Cole & Albicki 1998)

using a support vector machine. This classification method was tested for five different houses over a six-week period. After extensively training the classifier, classification accuracies between 84 and 92 % were achieved for each house. The same features were also classified using a simple majority classifier, leading to accuracies below 8 %, which demonstrates that the accuracy is significantly influenced by the choice of the classifier. Classifying electric loads using the transient voltage noise was also analyzed by Cox et al. (2006), albeit without reporting quantitative results.

v-i trajectories Lam et al. (2007) proposed extracting features from the v-i trajectories (see Fig. 3.10) of loads to classify appliances. Examples of the features extracted from a shape are its asymmetry, its looping direction, its area and its curvature of the mean line. The voltage and current were normalized before creating the v-i trajectory so that their magnitude becomes irrelevant. While Lam et al. (2007) were able to cluster dozens of typical household appliances into meaningful groups, it seems that all appliances were measured individually. This scenario is much easier than working with aggregate currents, and it is questionable whether the classification would work as well with aggregate currents. Since (Lam et al. 2007), no other work on v-i trajectories in the context of disaggregation is known to the author.

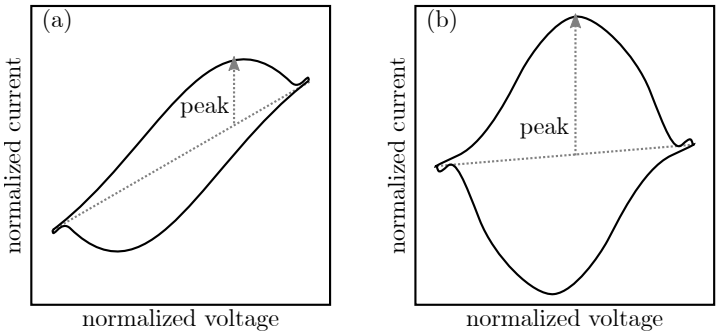

Figure 3.10: v-i trajectories of a radio (left) and a CD-player (right) operating in standby mode (Lam et al. 2007)

3.7.1.2 Classification and labeling procedure

It is important to differentiate between classification methods for switching events which require training data (supervised learning) and those who do not (unsupervised learning) (see section 2.5).

Unsupervised classification is more commonly referred to as clustering, and it was employed in the original method by Hart (1985). Different clustering methods have been tested, for example k-means clustering (Hart 1985), genetic k-means (Gonçalves et al. 2011), mean-shift clustering (Barsim et al. 2014) and hierarchical clustering (Jazizadeh et al. 2014) . The clustering results can be further evaluated, e.g., by estimating finite-state machines that can also represent multi-state loads. For this purpose, Baranski & Voss (2004b) employed a genetic algorithm. In the unsupervised case, labeling of the loads can only be performed based on manual a-priori knowledge. For example, the power factor of each load defined as $\lambda = |p|/s$ (IEC 60050-131:2002 2002) indicates whether a load is resistive or rather inductive or capacitive. Resistive loads with a high active power demand are often electric heating elements in households. In addition to the power factor, the transient current could be used for labeling through manually defined rules, as Sultanem (1991) describes that some appliances exhibit characteristic transient currents.

In contrast, the supervised classification comprises a training stage, in which the features of all electric loads are learned. This greatly simplifies the classification, since the classes are already defined, and the algorithm only has to assign a new event to the most likely class. Several different classification methods have been used for this purpose, such as a nearest neighbor classifier, a Gaussian Naive Bayes classifier, decision trees, support vector machines and artificial neural networks (Berges et al. 2009, 2011; Patel et al. 2007; Srinivasan et al.

2006; Zoha et al. 2012). Further, Liang et al. (2010a) proposed combining several classifiers via a committee decision mechanism. This means that each classifier is run in parallel, and the final result is chosen based on either the most common occurrence, the least unified residue or the maximum-likelihood. In supervised classification not only the classification, but also the labeling process is much simpler. Since all events in the training phase are labeled with a name, any new events simply inherit the name of the assigned class.

As Hart (1992) has stated, the unsupervised classification is "clearly superior from the user's point of view", because it requires less work. On the other hand, it generally yields a lower accuracy compared to the supervised classification. In this thesis, only the unsupervised classification is relevant because a minimal setup time is required (see section 1.3).

3.7.1.3 Estimation of power demand of each load

While the estimation of the power demand based on the clustering results is straightforward in principle, already Hart (1992) employed additional sanity checks and proposed a tentative algorithm to handle multi-state loads by representing them as finite-state machines.

A slightly different method for this purpose was proposed by Baranski & Voss (2004a, b). According to this method, first all possible finite-state machines based on the clustering results are generated. Then, for each potential finite-state machine, all possible time sequences are evaluated individually using a quality criterion. To this end, the problem was reformulated as a shortest path problem (Ahuja et al. 1990) and solved using a dynamic programming algorithm similar to the Viterbi algorithm. Finally, the sum of the active power demand of all appliances is evaluated to find overlapping events.

Another method is described by Shao et al. (2012). After a steady state extraction, they employed a combination of probabilistic sequential mining and motif mining to find repetitive episodes in a time series. Based on these results, the individual appliances and their active power demand is estimated.

3.7.2 Disaggregation as an optimization problem

In the original paper by Hart (1985), the active power demand of each load is estimated one by one without taking into account the measured aggregate active power demand. In contrast, several approaches try to match p_{agg} as close as possible by formulating the disaggregation problem as an optimization problem. Therefore, the operating behavior of each load has been modeled in one of two ways:

- As a simple two-state load, resulting in a combinatorial optimization;
- As a hidden Markov model or variants thereof.

While the disaggregation method formulated as an optimization problem can be performed alone, some authors have used the results of the disaggregation method based on switching events as fixed parameters for the optimization, such as the times at which switching events were detected (Egarter et al. 2013) or the magnitude of the step changes (Hart 1992).

Combinatorial optimization Already in (Hart 1992) but also later in (Batra et al. 2014; Liang et al. 2010a, b) it has been described that the disaggregation problem can be formulated as a combinatorial optimization problem:

$$\hat{\underline{\theta}}(t) = \underset{\underline{\theta}(t)}{\operatorname{argmin}} \int \left(p_{agg}(t) - \sum_{n=1}^{N} \theta_n(t) \hat{p_n} \right)^2 dt \ , \tag{3.4}$$

where $\underline{\theta} = [\theta_1, \theta_2, \cdots, \theta_N]$ represents the operating states of the N identified loads in the classification, and $\hat{p_1}, \hat{p_2}, \ldots, \hat{p_N}$ refers to the estimated active power demand of each load. Since only integer values are permitted for $\theta_1, \theta_2, \ldots, \theta_N$ (either zero or one), equation 3.4 represents an integer optimization problem. This idea was implemented by Egarter et al. (2013) and tested for simulated data. Egarter et al. (2013) added the constraint that appliances could only turn on at times when an edge was detected. Despite assuming a perfect edge detection and a-priori knowledge about $\hat{p_1}, \hat{p_2}, \ldots, \hat{p_N}$, a detection percentage of only 80 % was reported in the presence of five different loads. The detection percentage drops further once unknown loads are added to the aggregate signal $p_{agg}(t)$.

Combinatorial optimization was also tested by Suzuki et al. (2008). Instead of fitting the aggregate active power demand, they targeted the measured aggregate current, which resulted in the following equation:

$$\hat{\underline{\theta}}(t) = \underset{\underline{\theta}(t)}{\operatorname{argmin}} \int \left(i_{agg}(t) - \sum_{n=1}^{N} \theta_n(t) \hat{i}_n \right)^2 dt \ , \tag{3.5}$$

where $\hat{i_1}, \hat{i_2}, \ldots, \hat{i_N}$ represents the mean current of one period of the N loads. After a training period, they achieved accuracies between 73 and 97 % for the power demand of a residential household for five different days.

However, as (Hart 1992) and Parson (Parson 2013) already cautioned, a challenge with optimization is overfitting. Imagine, for example, three estimated loads with $\hat{p_1} = 100\ W$, $\hat{p_2} = 200\ W$ and $\hat{p_3} = 301\ W$. If $p_{agg}(t) = 300\ W$, hen the best fit would be a summation of the first two power demands. However, if the measured aggregate power changes slightly to $p_{agg}(t) = 301\ W$, the best fit would be that only the load represented by the third cluster is active.

Moreover, the event detection and classification steps are likely to yield at least some errors. In these cases, an optimization does not make sense, because p_{agg} cannot be explained by the detected events and clusters. In contrast, an optimization will try to minimize the difference between the estimated and measured aggregate power as much as possible. Last, some loads have a continuously variable power demand. Such loads cannot be represented with the appliance models $p(t) = \theta(t)p_{on}$ above. If the model would be extended accordingly, the problem would be significantly underdetermined.

Hidden Markov Models In the optimization approaches presented above the active power demand of the appliances was modeled as $p(t) = \theta(t)p_{on}$ with $\theta(t) = 0, 1$ and the model parameters $\underline{\theta}(t) = \theta_1, \theta_2, \ldots, \theta_N$ and $\underline{p} = p_1, p_2, \ldots, p_N$ are determined using any suitable optimization algorithm. In contrast to this simple model, more sophisticated mathematical models can be used to describe the operating behavior of appliances.

To this end, Kim et al. (2011) proposed modeling all appliances with a factorial hidden Markov model, which is a special variant of a Markov model. A Markov model is a finite-state machine in which the future state depends only on the current state and not on any past states. While in simple Markov models the states are directly observable, in hidden Markov models only an output is observable, which depends on the current state (see Fig. 3.11). A hidden Markov model can be used to describe the behavior of any multi-state appliance, since the active power demand can be represented by the output, and the operating states of the appliance correspond to the hidden states.

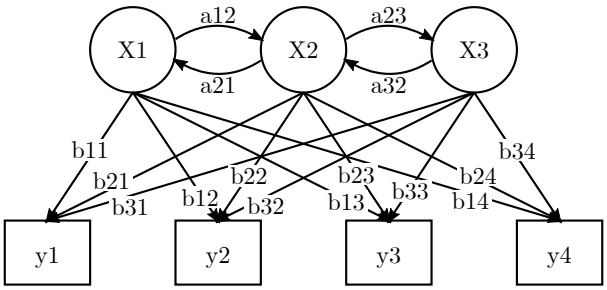

Figure 3.11: Structure of an exemplary hidden Markov model
x — states
y — possible observations
a — state transition probabilities
b — output probabilities

However, a residential household comprises not one but usually $n \gg 1$ number of appliances, hence a combination of hidden Markov models is necessary. This can be achieved through a *factorial* hidden Markov model, in which the hidden state is represented by a vector $\underline{s_t} = [s_t^1, s_t^2, \cdots, s_t^n]$, where each s_t^i with $i = 1, 2, \ldots, n$ refers to the state of the appliance i at time t, e.g., $x1$ or $x2$ (Ghahramani & Jordan 1996). To reduce the computational complexity, it is often assumed that the transitions of each appliance occur independently from each other. Such a factorial hidden Markov model is represented in Fig. 3.12. Moreover, in (Kolter & Jaakkola 2012), the output y of the factorial hidden Markov model is modeled as a Gaussian distribution as $y_t = \mathcal{N}\left(\sum_{i=1}^{n} \underline{\mu}(s_t^i), \Sigma\right)$, where $\mathcal{N}(\mu, \sigma^2)$ represents the Gaussian distribution, $\underline{\mu}(s_t^i) \in \mathbb{R}^m$ refers to the mean observed output of state i at time t, $\Sigma \in \mathbb{R}^{mxm}$ is the variance matrix and the parameter m represents the number of observed features. That the assumption of a Gaussian distribution for the active power demand of one appliance state is justified has been previously demonstrated by Kim et al. (2011).

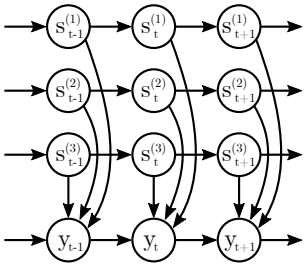

Figure 3.12: Structure of a constrained factorial hidden Markov model (Ghahramani & Jordan 1996)

Different kinds of factorial hidden Markov models were employed in (Johnson & Willsky 2013; Kim et al. 2011; Kolter & Jaakkola 2012; Parson 2014; Parson et al. 2014). Kolter & Jaakkola (2012) reported disaggregation accuracies between 90-100 % for synthesized data, Johnson & Willsky (2013) a mean accuracy of 80 % for a manually selected subset of the data published in (Kolter & Johnson 2011) and Parson (2014); Parson et al. (2014) a normalized mean error between approximately -40 % and +25 % in a real case study with cold appliances.

3.7.3 Disaggregation based on correlations

The disaggregation methods presented so far are only applicable to two-state and multi-state loads. In contrast, the disaggregation method based on cor-

relation is primarily applied to continuously variable loads. It relies on the correlation between the active power demand and the current harmonics. More precisely, a mapping function $f : \mathbb{R} \mapsto \mathbb{R}$ is required, which relates a particular *aggregate* current harmonic I^n_{agg} to the active power of an *individual* electric load $p_{ind} = f(I^n_{agg})$.

The existing publications concerning disaggregation methods based on correlation differ in terms of how this mapping function is determined. They can be grouped in three clusters:

- Laughman et al. (2003); Lee (2003) and Lee et al. (2005)
- Wichakool et al. (2009),
- Wichakool et al. (2015).

All individual methods were primarily developed for uncontrolled bridge rectifiers. As described in section 2.4, these rectifiers exhibit a characteristic waveform that differs significantly from a pure sinus and thus contains significant fractions of current harmonics. Moreover, uncontrolled bridge rectifiers are often found in variable speed drives (see section 2.3), whose continuously variable active power demand could thus be extracted with these methods. The suitability of the individual methods for the three types of rectifiers defined in section 2.4 is summarized in Table 3.2

Table 3.2: Suitability of the existing disaggregation methods based on correlation (subsec. 3.7.3) for different types of rectifiers: suitable ●, suitable if transferred ◑ and not suitable ○.

	three-phase uncontrolled bridge rectifier	single-phase uncontrolled bridge rectifier	rectifiers with power factor control
Laughman et al. (2003); Lee (2003); Lee et al. (2005)	●	◑	○
Wichakool et al. (2009)	●	○	○
Wichakool et al. (2015)	●	●	○

Laughman et al. (2003); Lee (2003); Lee et al. (2005): Laughman et al. (2005) noticed that the temporal behavior of the magnitude of the fifth and seventh current harmonic is closely related to the temporal behavior of the active power (see Fig. 3.13).

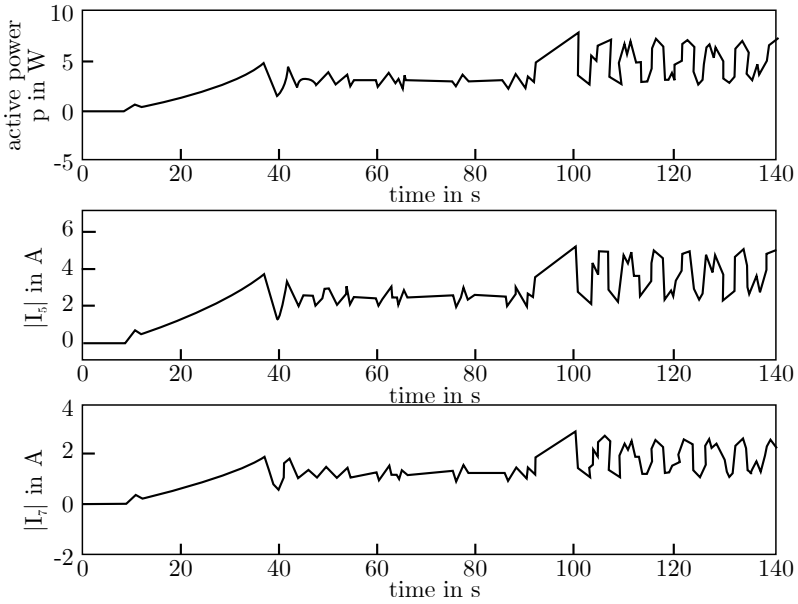

Figure 3.13: Temporal behavior of the magnitude of the fifth and seventh current harmonic as well as of the active power demand (Laughman et al. 2003)

Therefore, they proposed that the active power demand of a variable speed drive featuring an uncontrolled bridge rectifier can be estimated based on the measured aggregate current if the following two conditions hold true:

1. The magnitude of the fifth or seventh harmonic of the aggregate current is dominated by the uncontrolled bridge rectifier. This can be mathematically expressed for the case of the fifth harmonic as

$$|I_5^{agg}| = |I_5^{UBR}| + |I_5^A| + |I_5^B| + |I_5^C| + \ldots \approx |I_5^{UBR}| \tag{3.6}$$
$$\Leftrightarrow |I_5^{UBR}| \gg |I_5^A| + |I_5^B| + |I_5^C| + \ldots \ ,$$

   where $|I_5|$ represents the magnitude of the fifth current harmonic, the superscript UBR stands for uncontrolled bridge rectifier, and the superscripts A, B and C represent any other loads part of the aggregate load.

2. The functional relation between the active power demand and the magnitude of the fifth or seventh harmonic is known. This means that a function $f_5 : \mathbb{R} \mapsto \mathbb{R}$ of $f_7 : \mathbb{R} \mapsto \mathbb{R}$ is known, which fulfills

$$p^{UBR} = f_5(|I_5^{UBR}|) = f_7(|I_7^{UBR}|). \tag{3.7}$$

If both conditions hold true, the active power demand of the uncontrolled bridge rectifier can be estimated in one of the following two ways:

$$p^{UBR} = f_5(|I_5^{UBR}|) \approx f_5(|I_5^{agg}|) \ , \qquad (3.8)$$
$$p^{UBR} = f_7(|I_7^{UBR}|) \approx f_7(|I_7^{agg}|) \ .$$

While Laughman et al. (2003) only laid out the idea of the algorithm, it was implemented in (Lee 2003; Lee et al. 2005). Instead of looking at the correlation between the active power demand and the aggregate current harmonics, they examined the correlation between the active power demand and an aggregate electric property s_n, which they defined as

$$s_n \equiv \sqrt{p_k^2 + q_k^2} \ , \text{ where} \qquad (3.9)$$
$$p_n \equiv \frac{1}{T} \int_{t-T}^{t} i(s) \ U_{peak} \ cos(2\pi k/T) ds \ , \text{ and}$$
$$q_n \equiv \frac{1}{T} \int_{t-T}^{t} i(s) \ U_{peak} \ sin(2\pi k/T) ds \ ,$$

where i refers to the measured aggregate current, and $U_{peak} = const$ represents the peak voltage magnitude. This formula is similar to the formula for calculating the magnitude of the complex current harmonic $|I_k|$ via a continuous Fourier transform (see section 2.1).

According to Lee et al. (2005), the functions f_5 and f_7, which relate the active power demand of a variable speed drive with s_5 and s_7 respectively, may be derived analytically given the precise circuit schematic, control scheme, and mechanical loading conditions of the variable speed drive. However, this information are rarely available. Thus, in (Lee 2003; Lee et al. 2005) the function was determined statistically by collecting data over a period of one day (see Fig. 3.14). The relation was mapped with the model

$$s_n^{agg} = a \cdot \left(p^{UBR}\right)^b \Leftrightarrow p^{UBR} = \sqrt[b]{s_n^{agg}/a} = f_k(s_n^{agg}) \ , \qquad (3.10)$$

where the parameters a and b were fitted using a least squares regression.

Lee (2003); Lee et al. (2005) applied the disaggregation algorithm on the measurement data of a test building which comprised two variable speed drives featuring a three-phase uncontrolled bridge rectifier for a supply and an exhaust fan. To this end, only f_5 was used, not f_7. Since the disaggregation result was not compared to direct measurements of the variable speed drive, no accuracy evaluation could be reported.

After the disaggregation, Lee et al. (2005) also removed any colored noise from the aggregate active power demand based on the assumption that all the colored noise is a result of the uncontrolled bridge rectifier. The purpose is to only leave white noise, for which the event based disaggregation methods are modeled.

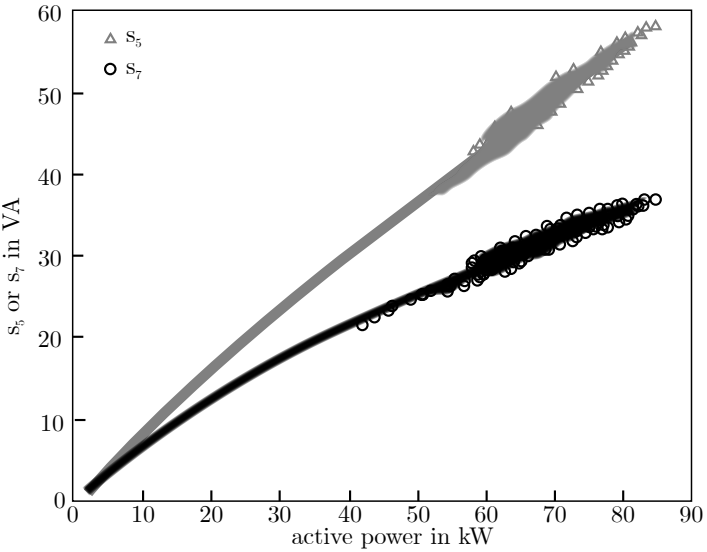

Figure 3.14: Correlation between the active power demand and s_5 and s_7 (Lee et al. 2005)

Wichakool et al. (2009) Wichakool et al. (2009) proposed another way in which to determine a mapping function based on the current harmonics. Instead of mapping *one* current harmonic to the active power demand, they proposed mapping *several* higher current harmonics to the first (complex) current harmonic I_1. As described in section 2.2, for ideal voltage sources, the active power demand can be calculated as $p = \mathbb{R}(U_1 {I_1}^*)$. Since U_1 of the uncontrolled bridge rectifier is the same as the measured one of the aggregate load, by estimating I_1 the active power demand of the uncontrolled bridge rectifier can be calculated. Analogous to the correlation method described above, it is assumed that the higher harmonics are only generated by the uncontrolled bridge rectifier.

To determine this mapping function, Wichakool et al. (2009) require neither a statistical analysis nor knowledge about the specific electronic structure of the bridge rectifier. Instead, they used a rather sophisticated mathematical derivation based on the discrete Fourier transform in combination with heuristic approximations. A detailed summary is presented in section A.3.

They applied it to a test case comprising one variable speed drive featuring an uncontrolled bridge rectifier and one resistive load, and they reported disaggregation accuracies close to 100 % for the variable speed drive.

Wichakool et al. (2015) Later, Wichakool et al. (2015) considered not only uncontrolled bridge rectifiers, but also other continuously variable appliances such as computers or light dimmers (see current waveform in Fig. 3.15). More exactly, the new method is applicable to any appliance, whose current is real-valued, periodic, point symmetric, approximately band-limited and exhibits regions in which the current is zero. Again, they determined a mapping function between multiple higher current harmonics and the first current harmonic through a different mathematical derivation in combination with heuristic approximations (see details in subsection A.3).

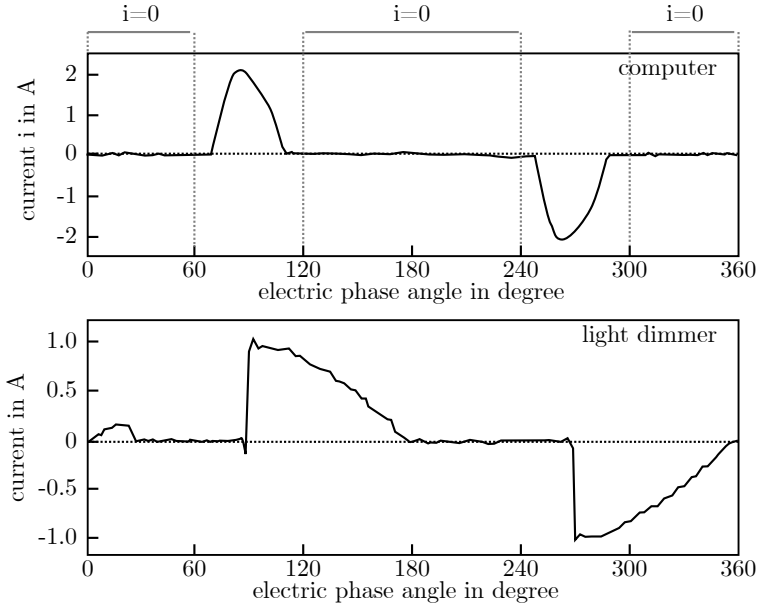

Figure 3.15: Current waveform of a computer (top) and a light dimmer (bottom) (Wichakool et al. 2015)

Wichakool et al. (2015) applied this disaggregation method on three test cases. In all test cases the aggregate load was composed of one continuously variable load and one two-state load. For the continuously variable load, a variable speed drive featuring an uncontrolled bridge rectifier, a computer and a dimmable light were chosen. The graphical representations of the disaggregation results in Wichakool et al. (2015) indicate a high accuracy of close to 100 %, even though it was not quantified.

3.7.4 Disaggregation using neural networks

A rather recent idea is to use deep neural networks for the disaggregation of a power demand. However, as mentioned earlier (see section 3.7) these methods require training data, which stands in contrast to the requirements of a short setup time. Thus, these methods are only presented briefly.

One of the earliest publications in this field comes from Mauch & Yang (2015). They advocate a special class of neural networks named recurrent neural networks. These networks are characterized by the fact that information in the network can be passed from one time step to another. This makes them suited to classify data *sequences*. However, if the relevant information components are far apart from each other in the sequence, the basic form of recurrent neural networks cannot correlate such information in practice. Therefore, Mauch & Yang (2015) used a special kind of recurrent neural network called long short term memory network, which does not exhibit this drawback (for more information, see (Hochreiter & Schmidhuber 1997)).

Its input layer corresponds to a sequence of the aggregate power demand, while its output layer represents the sequence of the power demand of a single appliance at the same time. This means that one such network can only extract one appliance out of an aggregate power demand. In order to extract all appliances, it is necessary to run multiple networks in parallel and merge their results. Moreover, the network requires supervised learning (see section 2.5). Mauch & Yang (2015) applied this disaggregation method on a house with 18 appliances. They ran three networks in parallel for a fridge, a dishwasher and a microwave, respectively. Their normalized root mean square error ranged from 33 to 74 %.

A subsequent paper from Mauch & Yang (2016) analyzed a combination of a hidden Markov model and deep neural networks. Also here, multiple estimators have to be run in parallel to disaggregate the power of the aggregate load. The application to a case study demonstrated improvement compared to the method explained in their previous paper.

Kelly & Knottenbelt (2015) compared three different types of deep neural network architectures:

- A long short term memory network similar to the one used in (Mauch & Yang 2015) (see disaggregation result in Fig. 3.16);
- A denoising autoencoder neural network;
- A deep neural network, in which the appliance is modeled as a two-state load. To achieve this, the network outputs only three parameters, namely the start and stop time of the appliance as well as its average power demand.

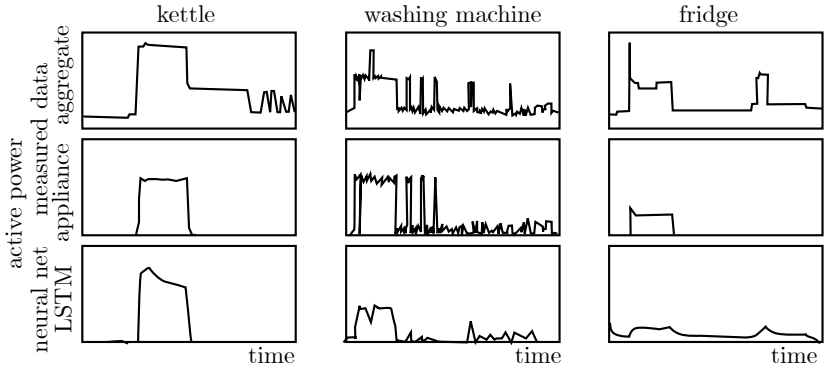

Figure 3.16: The measured aggregate power demand (top row), the measured appliance power demand (middle row) and the estimated appliance power demand when using the long short term memory (LSTM) neural network (bottom row) (Kelly & Knottenbelt 2015)

These disaggregation methods were applied to real data. It turned out that the second and third network outperformed the long short term memory network in terms of mean absolute error. They also yielded superior results compared to the approaches based on a combinatorial optimization and factorial hidden Markov models (see sections above). The denoising autoencoder network was further analyzed and extended in (Bonfigli et al. 2018) (see structure in Fig. 3.17).

The advantage of deep neural networks is that any type power sequence can be trained and subsequently estimated, including the one from variable speed drives. Moreover, deep neural networks are currently investigated in many other fields (Schmidhuber 2015) so that an advancement of these methods can be expected. On the other hand, deep neural networks require a significant amount of training due to their high degree of freedom. For example, the networks used by Kelly & Knottenbelt (2015) comprise 1-150 mio. parameters. Another more important disadvantage is that the estimation is not anchored to the physical understanding of the operation behavior of the loads. This leads to unusual estimation results compared to other disaggregation methods. For example, Mauch & Yang (2015) have reported that the estimation results have a low-pass characteristic, meaning that the power profiles do not exhibit the expected rectangular shape but rather a smoothed version (see Fig. 3.16). Similarly, Bansal (2017) has stated that the disaggregation result changes when adding a constant baseline. Such a change would not affect the event-based disaggregation at all.

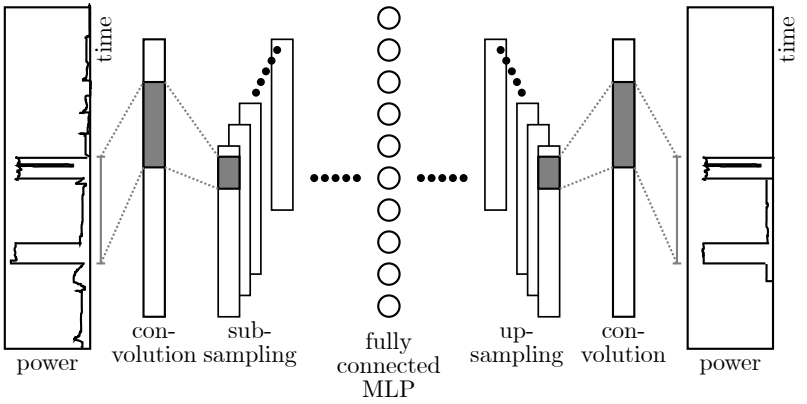

Figure 3.17: Structure of the denoising autoencoder deep neural network used in (Bonfigli et al. 2018)

3.8 Comparison of measurement methods

Based on the explanations above, the degree to which the requirements are fulfilled by the seven measurement methods are summarized in Table 3.3. While the reference method provides high accuracy, the equipment costs and the effort for the measurement are higher than allowed. The measurement method through estimation by experts does not comply with the requirement of being executable by nonexperts. Moreover, its accuracy is most likely less than 85 %. A prediction of the active power demand using simulation models can achieve a high accuracy given a sufficiently complex energy model of a machine. However, as described earlier, such models are usually trained with measurement data and thus represent an extension of the reference measurement method rather than a substitute.

Another option is to only measure the current and voltage of the aggregate load and to infer the active power demands of the individual loads by controlling them manually. This method completes all requirements at least partially. However, some loads cannot be controlled manually (without a significant alteration of the machine) and others are difficult to control manually in such a way, that the actual operation is imitated. Such conditions impair the accuracy. Moreover, it is necessary to be familiar with the machine to be measured, which may require expert knowledge. For those reasons, the measurement method does not fulfill the requirements completely.

Using the operating status of the individual loads to disaggregate the active power demand of the machine can lead to suitable accuracies for two-state

Table 3.3: Comparison of the seven measurement methods with respect to the requirements described in section 1.3. Requirements are either fulfilled completely ●, partially ◑ or not at all ○.

	Usable for multiple machines	Investment costs less than 10.000 €	Executable by non-experts	Setup time less than one hour	Identification of most loads	Accuracy of 85 % or more
1. Reference method mobile equipment	●	○	○	○	●	●
2. Reference method stationary equipment	○	○	○	○	●	●
3. Estimation by an expert	●	●	○	◑	●	○
4. Simulation methods	◑	○	○	○	●	◑
5. Disaggregation by means of controlling	●	●	◑	◑	◑	◑
6. Disaggregation by means of monitoring	◑	◑	◑	○	●	◑
7. Disaggregation using only voltage and current	●	●	●	●	●	**?**

and multi-state loads. However, it will not work, if the electric load has a continuously variable power demand. More importantly, it is difficult to monitor the operating status of all electric loads in the majority of cases, since a connection to the programmable logic controller and sensitive information from the machine manufacturer are necessary.

This stands in contrast to the last measurement method, in which the disaggregation of the aggregate load is performed based on only a detailed analysis of the current and the voltage. Since in this case only the aggregate current and voltage have to be measured, the equipment costs are low, and the measurement can be executed by a non-expert. In applications in the residential sector, most loads could be identified, and the disaggregation yielded an accuracy of 85 % or more.

However, so far, this kind of disaggregation has never been applied to the active power demand of machines used in manufacturing. Hence, the level of accuracy that can be achieved for this problem setting is not clear, since the relevant

conditions such as the number of electric loads, their type and their operating behavior are likely to be different than in the residential problem setting. If a suitable accuracy can be attained, this method would meet all requirements. Due to this prospect, this disaggregation method shall be examined further, and the following questions shall be answered:

- What type of electric loads do machines used in manufacturing comprise and how do they operate?
- To what extent can the active power demand of the most prevalent load types in such machines be extracted with the existing methods? What are current challenges and how can they be overcome?
- What measurement accuracy can be achieved with this method?

These questions are addressed in the next chapters: First, 151 electric loads of 18 machines used in manufacturing are classified in chapter 4. For the most common load types the extent to which the existing disaggregation methods are applicable is assessed. Based on this analysis, the current challenges are summarized in chapter 5. For each challenge, a solution in the form of a new or an improved method is developed and presented in chapter 6. Finally, the disaggregation is performed on the active power demand of seven manufacturing machines in chapter 7, and the resulting accuracy values are critically discussed.

4 Analysis of electric loads

As stated in chapter 3, the accuracy of the measurement method in which the electric energy demand of an aggregate load is disaggregated using only the measured voltage and current depends on the type of the constituent loads and their operating behavior. To find out which types of loads exist in machines used in manufacturing, 151 loads in 18 machines are classified in section 4.2. Therefore, a suitable classification scheme is first determined in section 4.1. The most common load types are more closely examined in terms of their operating behavior in section 4.3. Based on this information, the suitability of existing disaggregation methods for the most common loads is evaluated in section 4.4.

4.1 Classification system for electric loads

According to Jacob (2004) a classification system can be defined as "a system of classes, ordered according to a predetermined set of principles and used to organize a set of entities [into groups]". Hence, in order to classify electric loads, it is important to decide on the principle according to which they shall be grouped. To this end, the following seven possibilities are evaluated:

- Classification according to the type of appliance,
- Classification according to the operating behavior of a load,
- Classification according to existing norms relevant for manufacturing,
- Classification according to the position in the control hierarchy,
- Classification according to the electric properties of a load„
- Classification according to the type of energy output,
- Classification according to the type of energy conversion.

According to appliance type When disaggregating the total power demand of households, electric loads are often classified according to their home appliance type and –group. For example, Zimmermann et al. (2012, p. 245) classified electric loads as a fridge-freezer, a refrigerator, an upright freezer, a chest freezer or a wine cooler. All these home appliance types belong to the larger appliance group of cold appliances. Other possible groups are cooking appliances, washing and drying appliances, heating and cooling appliances, water heating appliances, lighting, computer sites, audiovisual sites and other appliances. Similarly, Wang & Zheng (2012) proposed the following classes: major appliances

(including refrigerators, washing machines, plasma TVs, air conditioners), household appliances, kitchen appliances, sound and image as well as health and beauty equipment. Many authors (Berges et al. 2010a; Ducange et al. 2014; Egarter et al. 2015; Gulati et al. 2014; Wang & Zheng 2011) only used the classification by home appliance type (and not by appliance group) with classes such as food cutters, hair dryers, ovens, refrigerators, waffle irons, clothes dryers, toasters and irons. While this classification is easy to follow for residential households, the electric loads of manufacturing machines do not fit into these classes.

According to operating behavior Another prominent classification scheme in nonintrusive load monitoring literature is the distinction of electric loads according to their operating mode (see introduction in chapter 3). Using this principle, four different classes are proposed in (Hart 1992; Zeifman & Roth 2011; Zoha et al. 2012):

- Class 1 - appliances with only two states of operation (On/Off), e.g., a toaster or a table lamp;
- Class 2 - appliances with a finite number of operating states such as on, off and standby, e.g., a washing machine or a stove burner;
- Class 3 - appliances with a continuously variable active power demand (and thus infinite operating states), e.g., a power drill or a light dimmer;
- Class 4 - appliances of class 1 that remain active throughout weeks or months, e.g., a smoke detector or a telephone.

Similarly, Wang & Zheng (2011) distinguished between three classes based on the operating mode of the appliance:

- Appliances with a variable active power demand and a high switching frequency, e.g., a washing machine;
- Appliances with a variable active power demand and a low switching frequency, e.g., a television, an air-conditioning or a stereo;
- Appliances with only two states of operation, e.g., a heater, a refrigerator or a cooker.

Further, the duty types S1-S10 defined in the (IEC 60034-1:2017 2017), which describe different operating modes, could be used as classes. The analysis of the operating mode is also helpful for electric loads in machines used in manufacturing. However, this classification system has two imprecisions. First, appliances of class 3 are always an aggregate of the electric loads of class 1. An example is the washing machine, which usually consists of a heating element, a motor for rotation and a motor driving the lye pump. Another example is a stove, whose different discrete power levels are achieved by switching on ohmic heating elements in various combinations. Hence, it is questionable, whether

class 3 is actually necessary. Second, appliances of class 4 and of class 1 can have the same electric characteristics despite being assigned to different classes. This would mean that only two classes may be relevant in the end, which is a low number for differentiating electric loads.

According to existing norms relevant for manufacturing One of the most frequently used classification systems in manufacturing is described in the (DIN 8580:2003-09 2003) and can be employed to organize manufacturing processes. However, there is no clear link between a class of manufacturing processes and electric loads. To perform a manufacturing process either several electric loads (for example, in a complex milling machine) or no electric loads at all (manual process) may be used. Other relevant norms apply to machine elements, such as bearings (e.g., DIN 611), screws (e.g., DIN 267-27) or gear wheels (e.g., DIN ISO 3952-2). While these elements may be part of an electric load such as a motor, they do not offer suitable principles according to which electric loads could be classified.

According to position in control hierarchy Schmitt et al. (2011) discussed various classification schemes for energy consumers in cutting machine tools, and they proposed the following classes: control systems, machine components (further divided into main components and auxiliary components) as well as common supply systems. This type of classification system reflects the control hierarchy in machine tools, but it does not consider the electric properties of the electric loads at all. Therefore, it is not recommended for the purpose of disaggregation.

According to electric properties Another option is to characterize the loads according to their electric properties or elemental load type. To this end, Barker et al. (2013) proposed using the classes resistive loads, inductive loads, capacitive loads and non-linear loads. However, the boundaries between these classes are soft. Moreover, the class non-linear loads comprises significantly different types of electric loads and the total number of classes is low.

According to type of energy output Another option is to classify electric loads according to the type of output energy into which the electric input energy is converted. One possibility is to define the following four types of energy, including subtypes: inner energy (comprising thermal, chemical and nuclear energy), mechanical energy (kinetic and potential energy), electrical energy and radiation energy (Feynman et al. 2011, section 4-4). Such energy forms are not precisely defined though, since, for example, macroscopic thermal energy can also be considered as microscopic kinetic energy. Moreover, these

classes seem too broad for the classification of electric loads. For example, both an electric furnace and an industrial refrigeration unit convert electrical energy into thermal energy and would thus be assigned to the same class despite their significantly different structures. Furthermore, a heat pump comprising three motors driving a pump, a compressor and a ventilator could be classified as an aggregate electric load producing thermal energy, or instead, each motor could be assigned to the class kinetic energy. Due to these imprecisions, this classification system is not recommended.

According to type of energy conversion A new proposal is to classify electric loads according to the dominant "type" of energy conversion. While no such types have been defined in literature, each energy conversion process follows a physical law or a combination of physical laws. For example, the conversion from electrical energy to thermal energy in an electric furnace can be described using Joule's first law. In contrast, in an industrial refrigeration unit based on vapor-compression, the electrical energy is first converted into mechanical energy in a motor, which can be described using the Lorentz force law. The motor drives a compressor, which increases the pressure of a fluid used to transfer thermal energy from one point to another. The relevant aspect is that the conversion of the electrical energy can be described with the Lorentz force law. While classifying according to the type of energy conversion is related to classifying according to the type of energy output, the former classification system is more precise and offers an even finer distinction. For example, the conversion of electrical energy into mechanical energy could be described with either the Lorentz force law or the inverse piezoelectric effect (which is a combination of Hooke's law and the electric permittivity of a material). Moreover, it seems likely that the type of energy conversion strongly affects the electric properties of loads, which are used for the disaggregation process.

Summary In summary, all classification principles, except for the physical law governing the energy conversion, were found to be unsuitable in one way or another (see Table 4.1). In contrast, classifying loads according to the physical law governing the energy conversion promises a clear distinction and many relevant classes. Most importantly, the electric properties in each class are likely to be similar so that all loads in one class can be treated similarly during disaggregation. For these reasons, electric loads are classified according to the physical law governing the energy conversion in the following section.

Table 4.1: Summary of potential classification systems and their suitability

Classification according to ...	Classes	Suitability
... type of appliance	Toaster, refrigerator, washing machine, television, ...	Not suitable because existing classes for household appliances are not applicable to electric loads in manufacturing machines.
... operating behavior	Two states (On/Off), multiple states (On/Off/Standby), infinite states (variable), always on	Not suitable because only two classes may be relevant, which would allow for little separation.
... existing manufacturing norms	Casting, forming, separating, joining, coating, changing of material properties	Not suitable because there is no direct link between the manufacturing process and the necessary electric loads.
... electrical properties	Resistive, capacitive, inductive, non-linear	Not suitable because the boundaries in between the classes are soft. Moreover, the number of classes is low
... position in control hierarchy	Control system, main components, auxiliary components, supply system	Not suitable because electric loads with similar properties could be grouped into different categories.
... type of energy output	Thermal energy, chemical energy, mechanical energy, radiation energy, electric energy, ...	Not suitable because a toaster and refrigerator would both be grouped into the class thermal energy despite their different structures.
... type of energy conversion	Joule's first law, Lorentz force law, Faraday's law of electrolysis, Lorentz force law, inverse piezoelectric effect, radiative recombination, specific electronic circuits such as magnetrons or inverters, ...	Suitable

4.2 Occurrence of classes in case study

Using the classification system based on the type of energy conversion, the electric loads of 18 machines used in manufacturing were analyzed (see Table 4.2).

These machines were selected for the analysis based on two criteria. First, the machines should vary in terms of their purpose and their structure, so that the analysis is generally valid. Thus, several different manufacturing processes according to (DIN 8580:2003-09 2003) are represented by the selected machines including primary shaping, forming, separation and joining. Moreover, auxiliary machines such as industrial robots, external cooling devices and quality control machines were included in the analysis because they can be found in most factories. Second, all selected machines comprise three to 40 electric loads, otherwise the challenge of the disaggregation was either deemed as too low or as too high. The number 40 was chosen based on the fact that a typical residential household consists of $30-50$ appliances (Zeifman & Roth 2011).

Table 4.2: List of analyzed machines

Description of analyzed machine	Number of machines
Vacuum-based handling equipment for carbon composites	1
Six-axis industrial robot	1
Machine for folding cardboard boxes	1
Selective laser sintering machine	2
External cooling device	2
Optical quality control system for battery separator foils	1
Thermoform machine	1
Water jet cutting machine	1
Milling machine	1
Plasma cleaning system	1
Ultrasonic cleaning system	2
Heated washing basin	1
Food shredding machine	1
Food mixing machine	2
Total	**18**

As was illustrated in Fig. 1.4, some of the loads in a machine, such as DC power supplies or variable speed drives, convert the electric energy into another form, which is then transferred to another electric load in the machine. In these cases, both loads, e.g., the variable speed drive and the motor, are presented in the analysis.

The result of the classification according to the type of energy conversion is that approximately 92 % of the 151 analyzed electric loads belong to one of the following classes (see Fig. 4.1 and details in A.1):

- Lorentz force (motor),
- Variable speed drive + Lorentz force (motor),
- Joule heating,
- Rectifier + electronic load (e.g., programmable logic controller).

The residual 8 % represented different electric loads, which all required varying types of power converters. Among those loads are compact fluorescent lamps, semiconductor laser diodes, ultrasonic actuators and capacitive plasma generators.

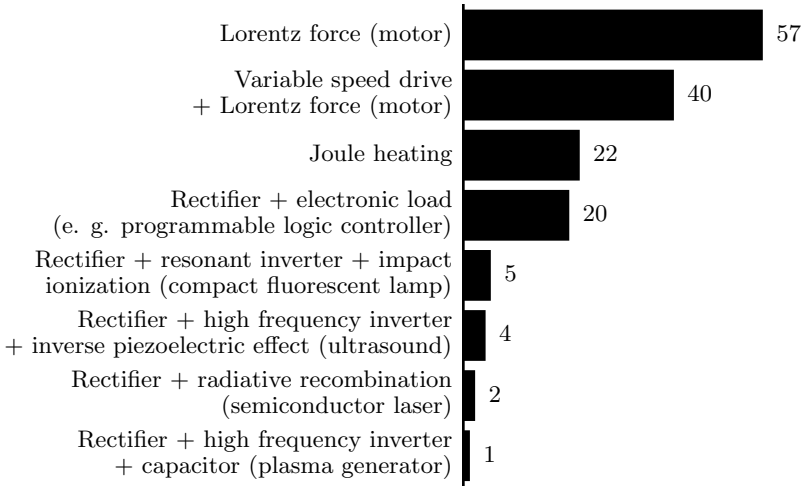

Figure 4.1: Distribution of the analyzed electric loads (N=151)

The motors could be further partitioned by looking at their mechanical load (see Table 4.3). Around 85 % of the analyzed fixed-speed motors drove either a pump, a fan or a compressor. The difference between these three mechanical loads is that a pump transfers a liquid from a region of low pressure to a region of high pressure, whereas a fan moves a gas with adding negligible amounts of pressure to it, and a compressor raises the pressure of a gas significantly (Marchildon & Mody 2006). The residual 15 % of the fixed-speed motors moved other types of mechanical loads such as a conveyor belt. Among the motors controlled by a variable speed drive, only one instance moved a pump, while four instances moved a fan, and all other 35 instances moved other types of mechanical loads.

Table 4.3: Distribution of the mechanical loads of the motors

	Fan	Pump	Compressor	Other mechanical load	**Total**
Motor	26	16	7	8	**57**
Variable speed drive + motor	4	1	0	35	**40**

4.3 Operating behavior of the most frequent classes

As section 4.2 demonstrated, the four most prevalent loads in machines used for manufacturing are fixed-speed motors, motors fed by a variable speed drive, Joule heating elements and rectifiers supplying different types of other electronic loads. For those four load classes, the operating behavior is examined next because it determines which disaggregation algorithms can be applied to them (see Table 3.1). A summary of the results is presented in Table 4.4.

Table 4.4: Operating behavior of the four most common load classes. The symbols indicate whether all loads ●, some loads ◑ or no loads ○ of the same type exhibit that particular operating behavior.

	Two-state	Multi-state	Continuously variable	Comment
Fixed-speed motor	◑	○	◑	Depends on mechanical load.
Variable speed drive + motor	○	○	●	
Joule heating element	●	○	○	
Rectifier + electronics	◑	○	◑	Depends on electronic load. May be approximated as a two-state load.

Fixed-speed motor Motors without a variable speed drive run at fixed speed. In most cases observed in this thesis their active power demand was approximately constant (see Fig. 4.2 top). However, when the mechanical load changes, the active power demand of the motor does so too. For example, the active

power demand of a motor driving a vacuum pump depicted in the bottom of Fig. 4.2 changes approximately ±20 % around the mean value of $P = 750\ W$.

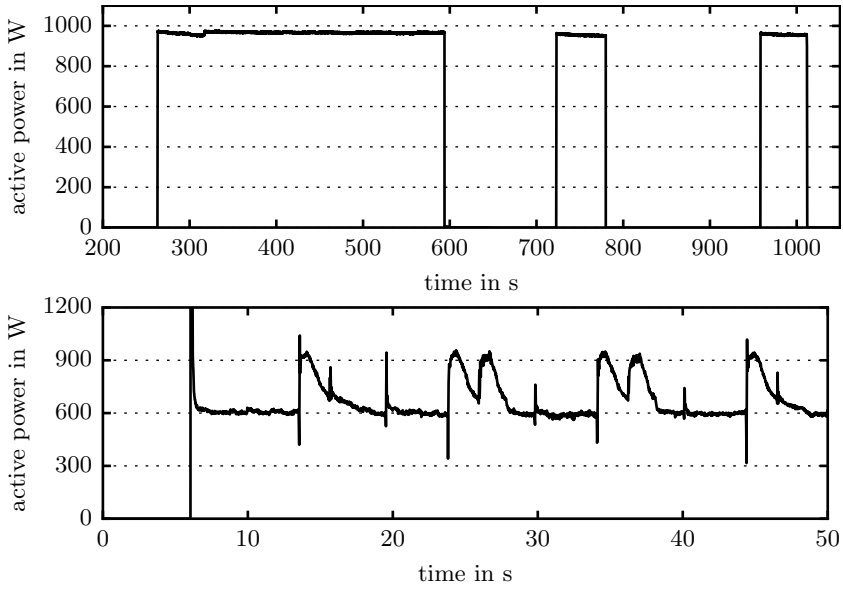

Figure 4.2: Active power demand of two different fixed-speed motors, of which one has an approximately constant mechanical load (top) and the other a varying mechanical load (bottom)

Variable speed drive + motor Variable speed drives are installed for the purpose of deliberately varying the motor output power. Therefore, they are a prime example of a continuously variable load (see Fig. 4.3). Moreover, they are important electric loads in terms of their relative electric energy demand in several machine types such as tooling machines or six-axis robots.

Joule heating The operating behavior of simple ohmic heating elements in production machines closely resembles that of an ideal two-state load. While it could be expected that the resistance of such loads changes when the loads become warmer or cooler, such an effect was not observed, or at least, it was found to be negligible in this thesis. However, what was observed was a frequent switching behavior of these loads within up to 100 ms (see Fig. 4.4). If the active power demand is calculated by averaging the instantaneous power over 10 periods according to the (IEC 61000-4-30:2015 2015), corresponding to

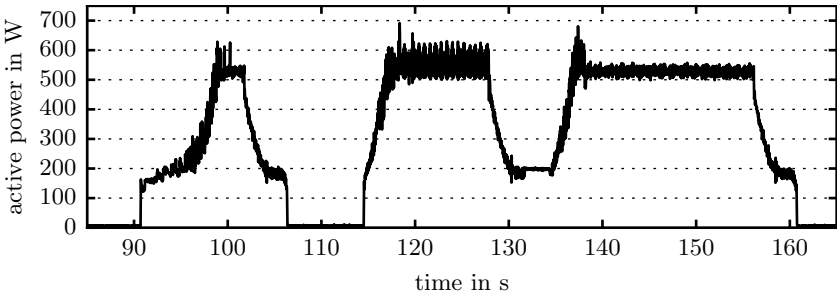

Figure 4.3: Active power demand of a motor fed by a variable speed drive

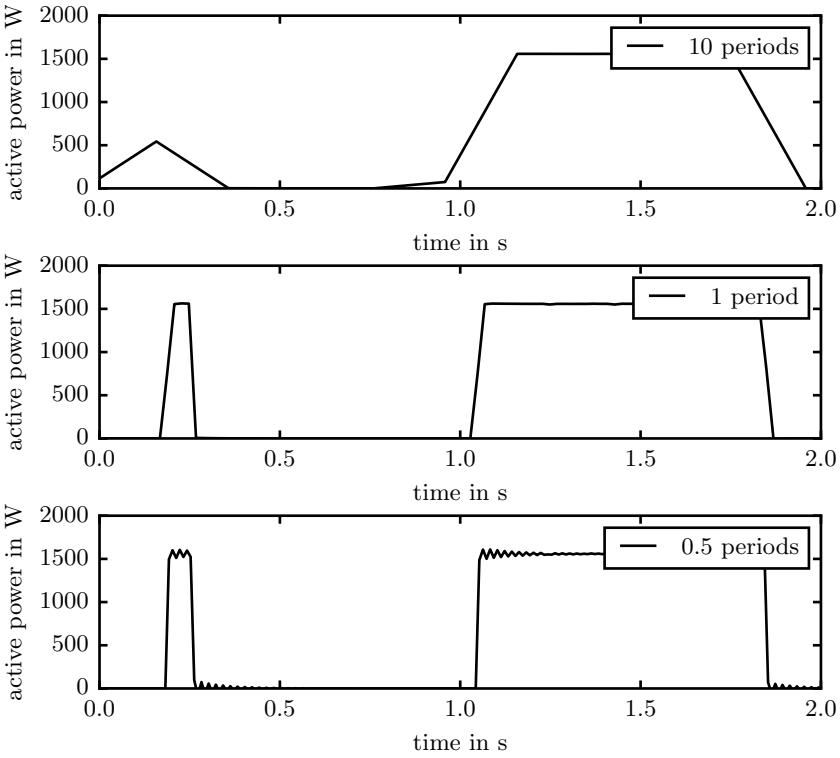

Figure 4.4: Active power demand of a heating element calculated from the instantaneous power with different averaging time periods

approximately 200 ms, the actual steady states become blurred out, which impedes the disaggregation. Therefore, the instantaneous power is averaged over only one period in the whole thesis. Decreasing the average period even further to a half-period resulted in oscillations of the active power demand, which again would impede the disaggregation.

Rectifier + electronic load The active power demand of rectifiers supplying electronic loads such as programmable logic controllers may change over time depending on its electronic load. Thus, they may represent a continuously variable load. An example is illustrated in Fig. 4.5, where the active power demand fluctuates by ±20 % around the mean value of $P = 150\ W$. However, the magnitude of the active power demand generally tends to be small, compared to the aggregate power. In other words, the rectifier and its attached electronic loads are rarely the main power consumer. Moreover, it is questionable whether any profitable efficiency measures could be implemented for rectifiers supplying electronic loads. Hence, this load class may be approximated with two states in most practical cases, even if it leads to accuracies below 85 %, since such loads are rarely of any real interest to the energy manager.

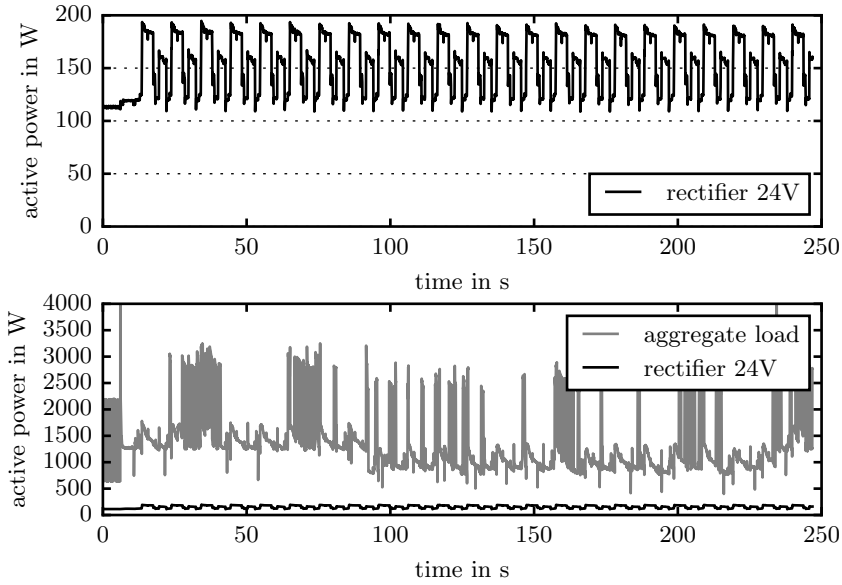

Figure 4.5: Active power demand of a rectifier (top and bottom), in comparison with the active power demand of the aggregate load (bottom)

4.4 Suitability of existing disaggregation algorithms

As described in section 3.7, four different disaggregation methods exist:

- Disaggregation based on switching events,
- Disaggregation as an optimization problem,
- Disaggregation based on correlations,
- Disaggregation using neural networks.

In the following section, only the disaggregation method based on switching events and the one based on correlations will be considered further. The disaggregation method using neural networks was already discarded in subsection 3.7 because it requires training, which stands in contrast to the requirements specified in subsection 1.3. Furthermore, the disaggregation method formulated as an optimization problem does not offer any advantage over the disaggregation method based on switching events because no multi-state loads were observed in the case study (see Table 4.4). Instead, it has the disadvantage of being less rooted to the physical interpretation of a signal, thereby being more likely to overfit signals and mask detection errors. The suitability of the remaining two disaggregation methods for the four most prevalent load types identified in section 4.2 is evaluated in Table 4.5.

The disaggregation method based on switching events is only suitable for loads that have two operating states. Since the active power demand of rectifiers can often be reasonably approximated with two states (see section 4.3), the method can also be applied to them. In contrast, the disaggregation method based on correlation is primarily suited to continuously variable loads. However, not all continuously variable loads can be extracted through disaggregation, but only those with a high total harmonic distortion (see equation 2.10), such as uncontrolled bridge rectifiers (see subsection 3.7.3). While all variable speed drives observed in this thesis comprised uncontrolled bridge rectifiers, not all rectifiers feeding diverse electronics were of this rectifier type. Instead, some of them seemed to feature a power factor control, so that the disaggregation method based on correlation cannot be applied. Similarly, the disaggregation method based on correlation cannot be employed for fixed-speed motors.

In conclusion, the existing disaggregation method based on switching events and the existing disaggregation method based on correlation could be combined, so that the active power demand of all uncontrolled bridge rectifiers and all two-state loads could be extracted (see diagram of such a combined method in Fig. 4.6). Furthermore, the two-state loads could be labeled according to a-priori knowledge, for example, by their power factor $\lambda = |p|/s$ or by their step-change magnitude (see subsubsection 3.7.1.2).

Table 4.5: Suitability of the existing disaggregation methods for the four most prevalent loads. The symbols indicate whether a disaggregation method is suitable ●, suitable only to a certain degree ◑ or not suitable ○.

Type of load	Operating behavior	Features uncontrolled bridge rectifier	Disaggregation based on switching events	Disaggregation based on correlations
Fixed-speed motor	Two-State	irrelevant	●	○
Fixed-speed motor	Variable	no	○	○
Variable speed drive + motor	Variable	yes	○	●
Joule heating element	Two-State	irrelevant	●	○
Rectifier + electronics	Two-State	irrelevant	●	○
Rectifier + electronics	Variable	yes	◑	●
Rectifier + electronics	Variable	no	◑	○

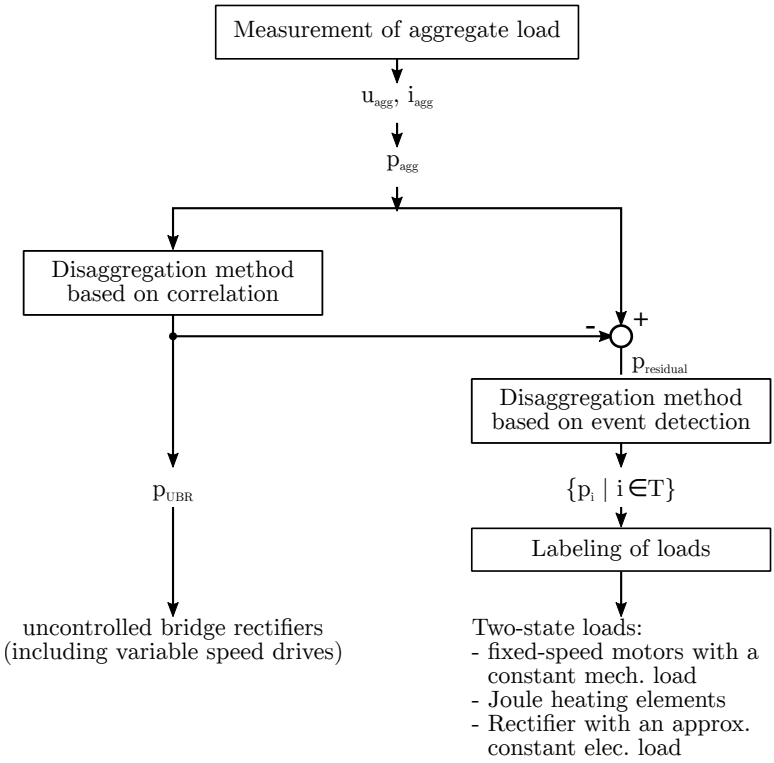

Figure 4.6: Flow chart of a preliminary combined disaggregation method

5 Deficits of existing methods

In chapter 4 it was identified that the four most common loads in production machines are fixed-speed motors, motors fed by a variable speed drive featuring an uncontrolled bridge rectifier, Joule heating elements and rectifiers supplying different types of electronics. Based on their operating behavior, the suitability of existing disaggregation algorithms for these load types was assessed, and a preliminary combined disaggregation method was proposed (see Fig. 4.6).

However, this preliminary method exhibits several deficits, which are summarized below and explained in detail in the following sections:

1. As Table 4.5 indicates, there are currently no disaggregation methods with which fixed-speed motors exhibiting a continuously variable active power demand due to a varying mechanical load can be extracted.
2. Motors fed by a variable speed drive featuring an uncontrolled bridge rectifier can be extracted using the disaggregation method based on correlation. However, this method has several disadvantages:
   - It requires training, otherwise an accuracy of at least 85 % cannot be guaranteed.
   - It is susceptible to other loads generating current harmonics.
   - It does not work in the case where both a three-phase and a single-phase uncontrolled bridge rectifier are present in the load.
   - It only estimates the active power demand or the fundamental current harmonic, but not directly the current of the uncontrolled bridge rectifier. This is adverse if other methods work directly on the current such as classifying the transient current (see below).
3. Two-state loads can be extracted from an aggregate load using the disaggregation method based on switching events. However, the current methods for detecting such events and determining their step-change magnitude may lead to inappropriate results, particularly in the case of inrush currents or in the presence of continuously variable loads.
4. Fixed-speed motors represented the most frequent load class in the case study (see Fig. 4.1). Hence, it would be advantageous if these loads could be further differentiated automatically. To this end, a differentiation according to their mechanical load, e.g., a fan or a pump (see Table 4.3), based on the transient turn-on current has been indicated in literature. However, whether such a differentiation is actually feasible has never been tested.

5.1 Deficits in extracting fixed-speed motors

Fixed-speed motors can exhibit a continuously variable active power demand if their mechanical load changes over time. An example thereof was illustrated in the bottom of Fig. 4.2, in which the active power demand of a motor driving a vacuum pump is depicted. This power demand changes periodically between approximately 600 W and 950 W within a few seconds. In contrast to variable speed drives featuring uncontrolled bridge rectifiers, the current waveform of fixed-speed motors is approximately sinusoidal (see Fig. 5.1) and does not exhibit any characteristic shapes or current harmonics. In fact, for that particular signal, the total harmonic distortion according to equation 2.10 is only 4 % in contrast to a value of 116 % for a variable speed drive featuring an uncontrolled bridge rectifier installed in the same machine. Therefore, the disaggregation algorithm based on correlations with characteristic current harmonics is not suitable for fixed-speed motors.

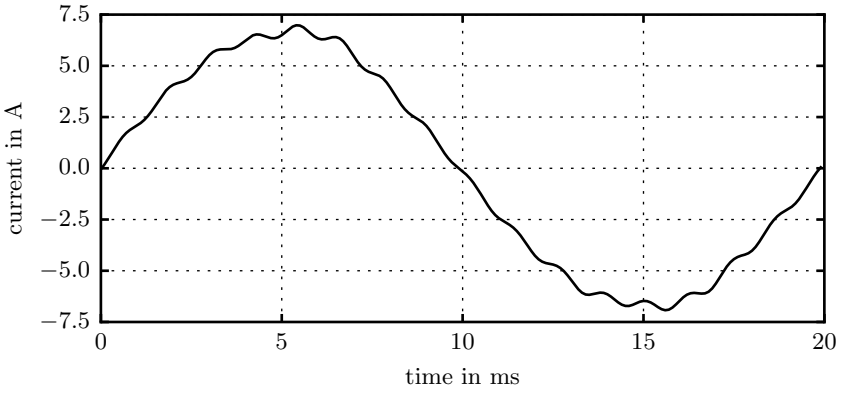

Figure 5.1: Current of a fixed-speed motor with a continuously variable power demand (same load as in Fig. 4.2 bottom)

5.2 Deficits in extracting uncontrolled bridge rectifiers

As described in subsection 3.7.3, three different types of disaggregation methods for uncontrolled bridge rectifiers (and hence also for variable speed drives featuring uncontrolled bridge rectifiers) can be differentiated:

- Method described in (Laughman et al. 2003; Lee 2003; Lee et al. 2005),
- Method described in (Wichakool et al. 2009),
- Method described in (Wichakool et al. 2015).

All of the methods extract a load based on an existing correlation between the aggregate current harmonics and the active power demand of the specific load (or the first current harmonic of the load with which the active power demand can be calculated). They differ in terms of how this correlation in the form of a mapping function is determined.

Laughman et al. (2003); Lee (2003); Lee et al. (2005) suggested determining a mapping function f_5 or f_7 such that $p^{UBR} = f_5(|I_5^{agg}|)$ or $p^{UBR} = f_7(|I_7^{agg}|)$, either through exact knowledge of the electronic structure of the uncontrolled bridge rectifier or through training data. However, the exact electronic structure is rarely known and the need for training data violates the requirement of a short setup time (see section 1.3). Therefore, it is not possible to infer an *exact* mapping function within the constraints of the problem setting. Instead, it is analyzed next whether an *approximate*, generally valid mapping function exists, that is applicable to all uncontrolled bridge rectifiers and does not require training data for each measurement. It will be revealed that such a function has several disadvantages:

- A low accuracy,
- A high susceptibility to other loads exhibiting current harmonics,
- An inapplicability if the aggregate load comprises both a three-phase and a single-phase uncontrolled bridge rectifier,
- An inability to extract the current directly.

These disadvantages also hold true in a similar way for the mapping functions proposed by Wichakool et al. (2009, 2015). In these two publications, the mapping function relates not one but multiple aggregate current harmonics to the first current harmonic of, e.g., an uncontrolled bridge rectifier so that the mapping function takes the form $I_1^{UBR} = F(I_5^{agg}, I_7^{agg}, \dots)$. However, since the mathematical derivation of this mapping function depends on many parameters, it is more difficult to explicitly prove these disadvantages. One would need to run the sophisticated derivation for all parameter combinations and multiple test cases, which seems hardly adequate. Instead, both methods are explained in detail in the attachment A.3, and either the inaccuracies are

explicitly pointed out or an example is provided, where an accuracy of 85 % cannot be achieved.

5.2.1 Low accuracy

In order to evaluate the accuracy of an approximate, generally valid mapping function for uncontrolled bridge rectifiers, the current draw of several such rectifiers, which differ in terms of their electric components, is first simulated. Then, an analysis is conducted to determine whether a mapping function inferred from *one* rectifier is also valid for a *different* rectifier. Only three-phase uncontrolled bridge rectifiers are henceforth analyzed since they are more commonly mentioned in literature (see subsection 3.7.3). However, the analysis could be carried out analogously for single-phase bridge rectifiers.

The electronic structure of a three-phase uncontrolled bridge rectifier was already described in section 2.4 and it is presented again in the top of Fig. 5.2. Six different three-phase uncontrolled bridge rectifiers A,B,C,D,E,F are simulated next. They differ in terms of their values for C, R_{series} and L_{series} (see Table 5.1). For each rectifier the current draw is simulated for the values of $R_{load} \in [10, 15, 20, 30, 40, 80, 160, 320, 640, 1000]\ \Omega$ (see Fig. 5.2 middle). Based on the simulated current draw, the active power demand as well as the fifth and seventh current harmonic are calculated and plotted in a diagram (see Fig. 5.2 bottom). This is performed for all six rectifiers, resulting in the two diagrams presented in Fig. 5.3. Details concerning the simulation and more intermediate results can be found in A.2. As Fig. 5.3 illustrates, the relation between p and $|I_5|$ or p and $|I_7|$ differs significantly for the six different rectifiers, especially for larger values of p. The difference is the largest for the rectifiers D and E.

Table 5.1: Parameters used in the simulation of the six different rectifiers A-F

Rectifier	C *in* F	R_{series} *in* Ω	L_{series} *in* mH
A	0.001	0.1	none
B	0.001	0.5	none
C	0.001	0.1	0.5
D	1	0.1	none
E	1	0.8	none
F	1	0.1	0.2

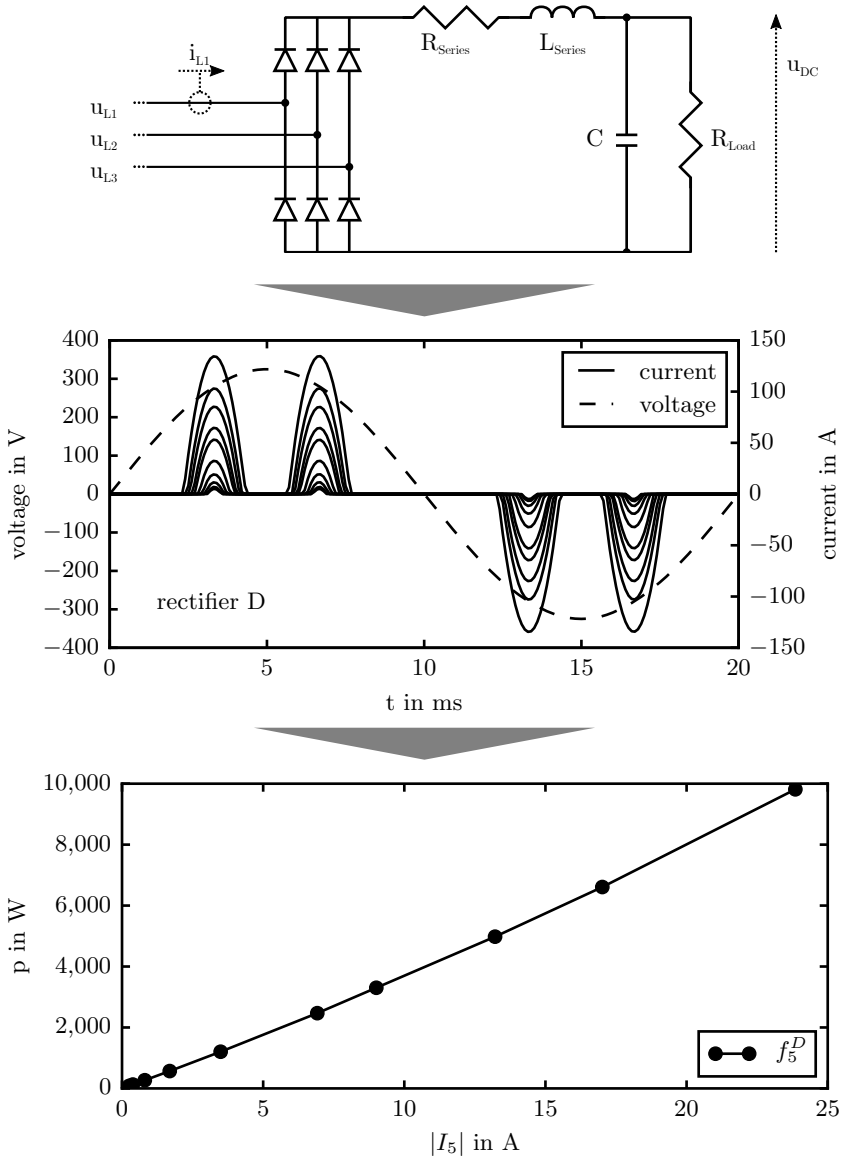

Figure 5.2: A three-phase uncontrolled bridge rectifiers (structure at top) defined by the parameters C, R_{series} and L_{series} was simulated for different values of R_{load}. Based on the simulated current and voltage (middle), the active power demand and the current harmonics were calculated and plotted (bottom).

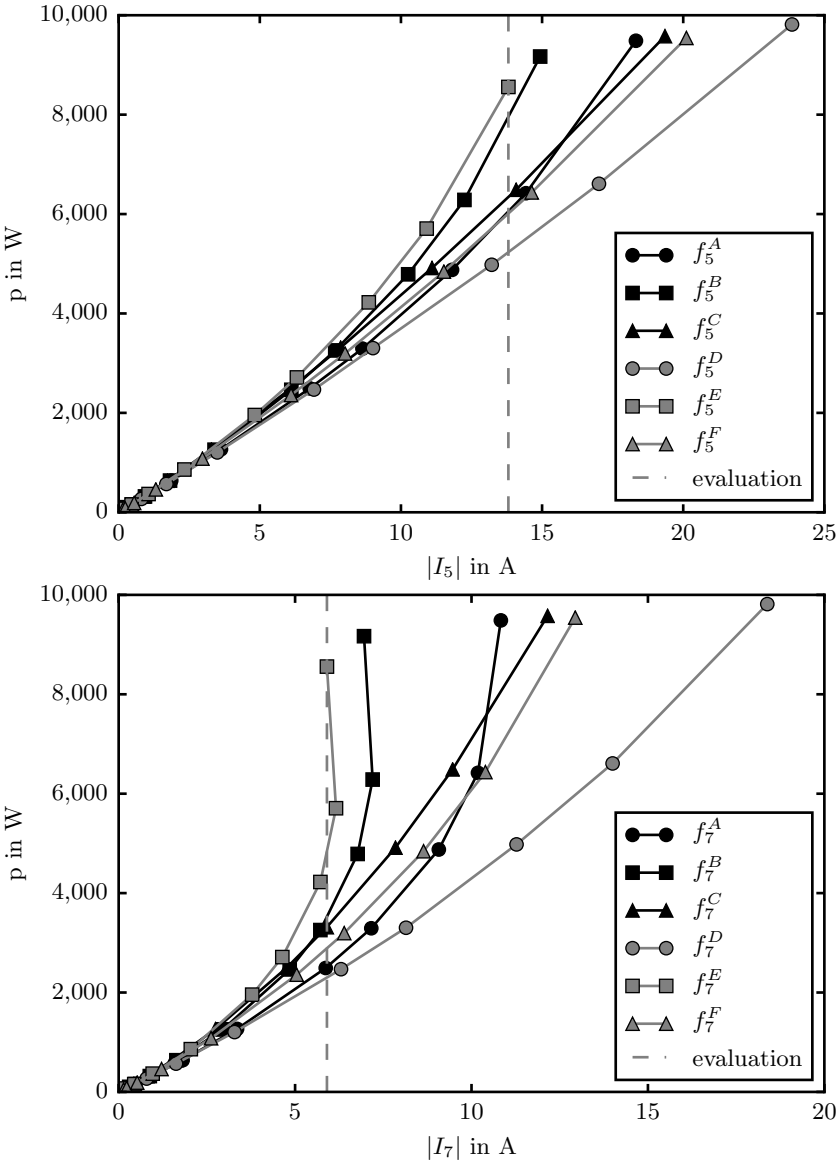

Figure 5.3: Plot of p with respect to $|I_5|$ (top) and $|I_7|$ (bottom) for the six different rectifiers A-F defined in Table 5.1 and the same varying load

Assuming that the approximate mapping function f_n^{estim}, mapping either $|I_5|$ or $|I_7|$ on p, is inferred from the mean value of the curves from rectifiers D and E, i.e., $f_n^{estim}(|I_n|) = 0.5 \cdot \left(f_n^D(|I_n|) + f_n^E(|I_n|)\right)$, the accuracy of such a function for rectifiers D and E can be compared with the exact mapping functions $f_n^D(|I_n|)$ and $f_n^E(|I_n|)$, respectively. In this case, the error ϵ for the rectifier D can be calculated as

$$\epsilon_D(|I_n|) = \frac{|p_{estim} - p_{real}|}{|p_{real}|} = \frac{\left|f_n^{estim}(|I_n|) - f_n^D(|I_n|)\right|}{|f_n^D(|I_n|)|} \,, \tag{5.1}$$

where p_{estim} represents the active power demand defined by the approximate mapping function, and p_{real} refers to the one defined by the exact mapping functions for rectifier D. The error $\epsilon_E(|I_n|)$ for rectifier E can be calculated in the same way.

For the values of $|I_5|$ and $|I_7|$ marked with a dashed vertical line in Fig. 5.3, the estimation error ϵ ranges from 19 % to 136 % depending on the rectifier and whether $|I_5|$ or $|I_7|$ was used for the estimation (see Table 5.2). In conclusion, the required accuracy of 85 % cannot be achieved using an approximate mapping function, at least not for all cases.

Table 5.2: Calculation of the estimation error ϵ according to equation 5.1. The values are drawn from the data presented in Fig. 5.3

	$n = 5$	$n = 7$
$\|I_n\|$ in A	13.8	5.9
$f_n^D(\|I_n\|)$ in W	5,233	2,302
$f_n^E(\|I_n\|)$ in W	8,557	8,557
$f_n^{estim}(\|I_n\|)$ in W	6,895	5,430
$\epsilon_D(\|I_n\|)$	32 %	136 %
$\epsilon_E(\|I_n\|)$	19 %	37 %

5.2.2 Susceptibility to current harmonics from other loads

Apart from the accuracy, another vulnerability of any mapping function approach is that the fifth and seventh current harmonic of the aggregate load may be generated not only by the uncontrolled bridge rectifier but also by other electric loads. Assuming that another electric load generates a fifth or seventh current harmonic with the same magnitude and phase as the uncontrolled

bridge rectifier, the estimation error with the mapping function approach is approximately 100 %, and the measurement accuracy is thus 0 %:

$$\begin{aligned} p_{real} &= f(|I_5^{VSD}|) \\ p_{estim} &= f(|I_5^{agg}|) \\ &= f|(I_5^{VSD}| + |I_5^{other}|) \\ &= f(2 \cdot |I_5^{VSD}|) \\ &\approx 2 \cdot f(|I_5^{VSD}|) \\ \Rightarrow acc &= 1 - \frac{|p_{estim} - p_{real}|}{|p_{real}|} \approx 1 - \frac{2-1}{1} = 0 \ . \end{aligned} \tag{5.2}$$

5.2.3 Inapplicability if two different types of uncontrolled bridge rectifier are present

Another disadvantage of the disaggregation method based on correlation is that it is not suitable if both a three-phase and a single-phase uncontrolled bridge rectifier are present in the aggregate load (see example in Fig. 5.4). The reason is that both loads exhibit similar current harmonics, which cannot be differentiated by looking at the current harmonics alone.

5.2.4 Inability to extract the current

Finally, the method only estimates the active power demand or the fundamental current harmonic of, e.g., an uncontrolled bridge rectifier. Those values are calculated once per period, and it is thus not possible to infer the current waveform from them. However, this may be desirable if either the current of the uncontrolled bridge rectifier or the current from the residual loads is further processed.

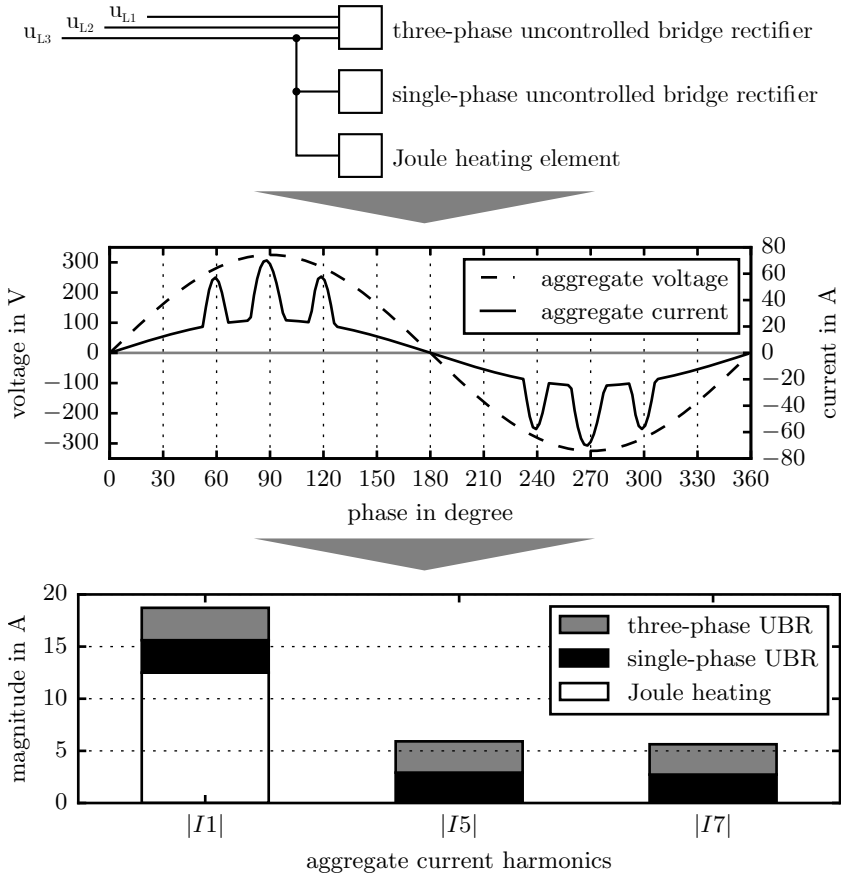

Figure 5.4: Example of an aggregate load on u_{L3} comprising both a three-phase and a single-phase uncontrolled bridge rectifier as well as a Joule heating element (top). Despite the fact that the peaks in the aggregate current (middle) can be clearly associated with either the three-phase or the single-phase uncontrolled bridge rectifier, it is not possible to extract their currents because they exhibit similar current harmonics (bottom).

5.3 Deficits in detecting switching events

According to Anderson et al. (2012), three types of methods for detecting events in the form of step changes have been proposed in literature: expert heuristics, matching filters and probabilistic methods (see Table 5.3). The following section only considers the probabilistic method by Luo et al. (2002) which was also adapted with minor changes by Berges et al. (2011); Jin et al. (2011). Methods using matching filters are omitted because they require a mask generated from training, which stands in contrast to the required short setup time (see section 1.3). Similarly, methods based on expert heuristics are discarded because they are not robust against fluctuations of the aggregate signal due to noise or the presence of continuously variable loads (Luo et al. 2002).

Table 5.3: Comparison of methods for detecting events in the form of step changes. The symbols indicate whether a method fulfills a requirement ● or not ○.

Type of method	Does not require training	Is robust against fluctuations
Expert heuristics, e.g., (Hart 1985)	●	○
Matching filters, e.g., (Leeb et al. 1995)	○	●
Probabilistic methods, e.g., (Luo et al. 2002)	●	●

The probabilistic method by Luo et al. (2002) for determining step changes can be described using the following three functions:

- $\xi : \mathbb{Z} \mapsto \mathbb{R}$ for calculating the probability of a step change, including the parameter ξ_{thres} to decide whether or not a step change has occurred;
- $\Delta f : \mathbb{Z} \mapsto \mathbb{R}$ for determining the step-change magnitude for each detected event;
- $\hat{f} : \mathbb{Z} \mapsto \mathbb{R}$ for reconstructing the original signal based on the detected step changes.

These functions are explained in more detail next, and they are applied to a simulated signal in Fig. 5.5. Thereafter, the disadvantages of this method are explained, namely a low robustness against narrow peaks and a dissimilarity between the reconstructed and the original signal.

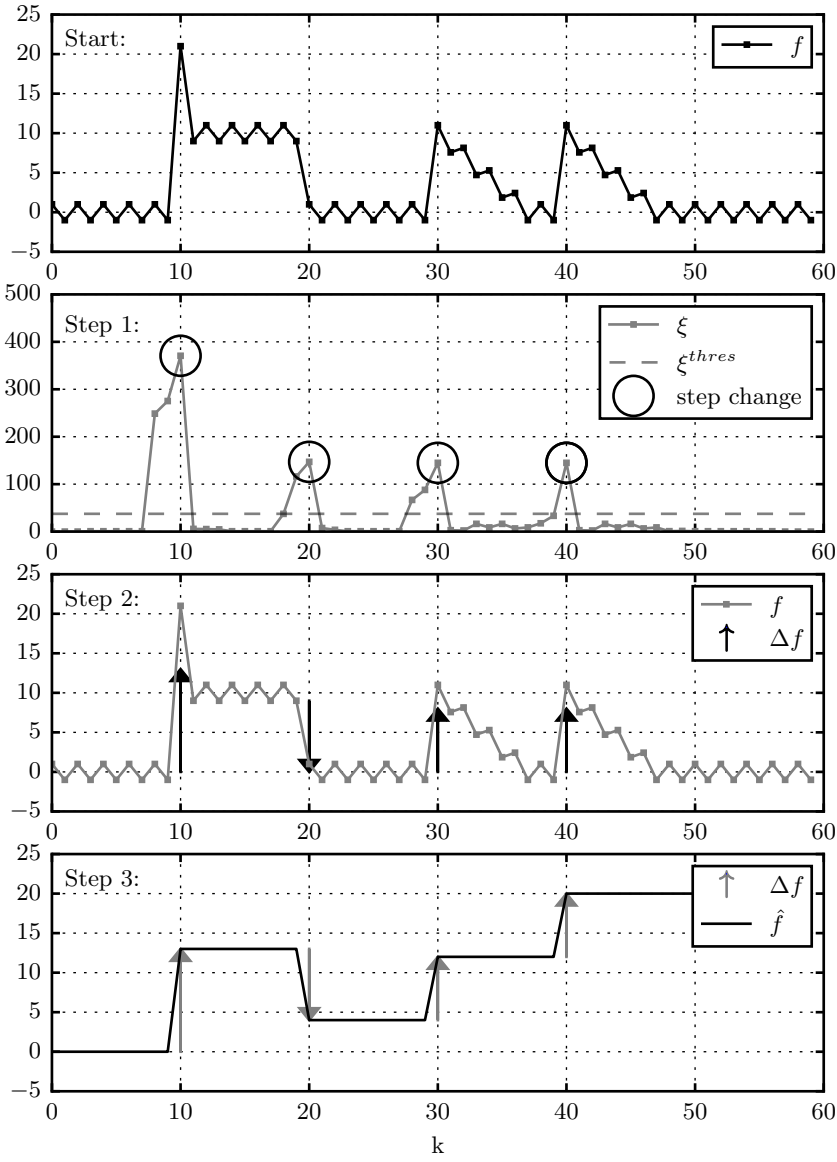

Figure 5.5: Approach for detecting events with probabilistic methods for a simulated signal f (top row): first the probability of a step change ξ is determined (second row), and then the step-change magnitude Δf is calculated (third row). Based on these step changes, the original signal can be reconstructed $\hat{f}$ (bottom row). Here, $N_D = N_P = 3$ was chosen so that $\xi^{thres} = N_D/2{\cdot}5^2 = 37.5$.

Determine probability of step change using ξ: First, for each point k, a pre-event window $P_k = \{k-1, k-2, \ldots, k-N_P\}$ and a detection window $D_k = \{k, k+1, \ldots, k+(N_D-1)\}$ are defined. Based on these windows, the test statistic function ξ is defined as

$$\xi_k = ln\left(\frac{\prod_{i\in D_k}\mathcal{N}(f_i,\mu_D,\sigma_D)}{\prod_{i\in D_k}\mathcal{N}(f_i,\mu_P,\sigma_P)}\right) , \tag{5.3}$$

where $\mathcal{N}(x,\mu,\sigma)$ represents the normal distribution and f_i refers to the signal value at time i. Moreover, μ_D and σ_D represent the mean and standard deviation of $(f_i|i \in D_k)$ and μ_P and σ_P refer to the mean and standard deviation of $(f_i|i \in P_k)$.

The equation can be more easily understood as a summation of three factors:

$$\begin{aligned}
\xi_k =& ln\left(\frac{\prod_{i\in D_k}\mathcal{N}(f_i,\mu_D,\sigma_D)}{\prod_{i\in D_k}\mathcal{N}(f_i,\mu_P,\sigma_P)}\right) = \sum_{i\in D_k} ln\frac{\mathcal{N}(f_i,\mu_D,\sigma_D)}{\mathcal{N}(f_i,\mu_P,\sigma_P)} \\
&= \sum_{i\in D_k} ln\left(\frac{\frac{1}{\sqrt{2\pi\sigma_D^2}}exp\left(-\frac{1}{2}\left(\frac{f_i-\mu_D}{\sigma_D}\right)^2\right)}{\frac{1}{\sqrt{2\pi\sigma_P^2}}exp\left(-\frac{1}{2}\left(\frac{f_i-\mu_P}{\sigma_P}\right)^2\right)}\right) \\
&= \sum_{i\in D_k} ln\left(\frac{\sigma_P}{\sigma_D}exp\left(-\frac{1}{2}\left(\frac{f_i-\mu_D}{\sigma_D}\right)^2+\frac{1}{2}\left(\frac{f_i-\mu_P}{\sigma_P}\right)^2\right)\right) \\
&= \sum_{i\in D_k} ln\left(\frac{\sigma_P}{\sigma_D}\right) + \sum_{i\in D_k} ln\left(exp\left(-\frac{1}{2}\left(\frac{f_i-\mu_D}{\sigma_D}\right)^2+\frac{1}{2}\left(\frac{f_i-\mu_P}{\sigma_P}\right)^2\right)\right) \\
&= N_D ln\left(\frac{\sigma_P}{\sigma_D}\right) - \underbrace{\frac{1}{2}\sum_{i\in D_k}\left(\frac{f_i-\mu_D}{\sigma_D}\right)^2}_{=N_D} + \frac{1}{2}\sum_{i\in D_k}\left(\underbrace{\frac{f_i-\mu_P}{\sigma_P}}_{\equiv z_i}\right)^2 \\
&= N_D ln\left(\frac{\sigma_P}{\sigma_D}\right) - \frac{N_D}{2} + \frac{1}{2}\sum_{i\in D_k} z_i^2 \ .
\end{aligned} \tag{5.4}$$

In conclusion, the indicator represents a sum of three values: the logarithmic ratio of σ_P/σ_D times the number of samples in the detection window N_D, a constant value of -$N_D/2$, and the sum of the squared standard score (sometimes also called the z-value) z_i of the values f_i with respect to the normal distribution defined by μ_P and σ_P. The most relevant part is the standard score z_i. If a step change has occurred, z_i and hence ξ are high.

In order to find a suitable threshold value, the case $\sigma_D = \sigma_P$ will be analyzed, which often holds approximately true:

$$\begin{aligned}\xi_k =& N_D \underbrace{ln\left(\frac{\sigma_P}{\sigma_P}\right)}_{=0} - \frac{N_D}{2} + \frac{1}{2}\sum_{i \in D_k}\left(\frac{f_i - \mu_P}{\sigma_P}\right) \\ =& \cdots = \frac{N_D}{2}\left(\frac{\mu_D - \mu_P}{\sigma_P}\right)^2 .\end{aligned} \tag{5.5}$$

This means that for $\sigma_D = \sigma_P$, the test statistic represents the squared standard score of μ_D with respect to the normal distribution defined by μ_P and σ_P, multiplied by the number of samples in the detection window and 0.5. Based on this information, a threshold value ξ^{thres} can be easily defined by requiring that μ_D is at least, e.g., five standard scores away from μ_P, such that $\xi^{thres} = N_D/2 \cdot 5^2$. A standard score of five occurs only once in about two million values for an ideal Gaussian distribution. Therefore, false positives should be rare. Here, false positives should be even rarer because the mean of the standard scores is used.

Determine magnitude of step change using Δf: After a step change has been detected for a particular point, its magnitude can be straightforwardly calculated with the function Δf, which is defined here as

$$\Delta f_k = \begin{cases} \mu_D - \mu_P & \dots \text{if a step change is detected at } k \\ 0 & \dots \text{otherwise} \end{cases} . \tag{5.6}$$

Reconstruct signal using $\hat{f}$: Based on the detected step changes, the original signal can be reconstructed using the function $\hat{f}$, which can be defined as

$$\hat{f}_k = f_0 + \sum_{k' \leq k} \Delta f_{k'} . \tag{5.7}$$

While reconstruction is not necessary in the actual disaggregation, it is similar to what occurs in the clustering and estimation step (see subsection 3.7.1). Therefore, if the reconstruction of the signal using $\hat{f}$ closely resembles the original signal, it is likely that the accuracy of the disaggregation is high. Inversely, if the reconstructed signal does not resemble the original signal, the disaggregation accuracy is likely to be low.

5.3.1 Low robustness against narrow peaks

The active power demand of fixed-speed motors often closely resembles the signal $(f_k|0 \leq k \leq 30)$ displayed in Fig. 5.5: While there appears to be a constant steady state when the motor is active, there is initially a high peak due to an inrush current (Scheda 1986). This peak leads to an overestimation of the step-change magnitude, as can be seen in Fig. 5.5.

Moreover, the probability of a step change is higher for the turn-on event (at $k = 10$ in Fig. 5.5) than for the turn-off event (at $k = 20$), which seems undesirable, since the real absolute step-change magnitude is the same for those two events. In fact, it can be demonstrated that ξ yields nearly the same probability for a narrow delta peak f^p as for an actual step change f^s with the same magnitude m (see Fig. 5.6). More specifically, the following values shall be assumed:

- For the signal f^s,
  - $(f_k^s|k \geq k^*) = \begin{cases} \mu_P + \sigma & \text{for even } k \\ \mu_P - \sigma & \text{for odd } k \end{cases}$ and
  - $(f_k^s|k < k^*) = \begin{cases} \mu_P + m + \sigma & \text{for even } k \\ \mu_P + m - \sigma & \text{for odd } k \end{cases}$.
- For the signal f^p,
  - $(f_k^p|k \neq k^*) = \begin{cases} \mu_P + \sigma & \text{for even } k \\ \mu_P - \sigma & \text{for odd } k \end{cases}$ and
  - $(f_k^p|k = k^*) = \begin{cases} \mu_P + m + \sigma & \text{for even } k \\ \mu_P + m - \sigma & \text{for odd } k \end{cases}$.

Moreover, $m \gg N_D \cdot \sigma$ and $N_D > 1$ shall hold true. Then, it can be demonstrated that the probabilities only differ by a factor of N_D:

$$\begin{aligned} &\text{for } f^s: && \xi_{k^*} \overset{\text{see eq. 5.5}}{=} \frac{N_D}{2}\left(\frac{\mu_D - \mu_P}{\sigma_P}\right)^2 = \frac{N_D}{2}\left(\frac{m}{\sigma}\right)^2, \\ &\text{for } f^p: && \xi_{k^*} \overset{\text{see sec. A.5}}{\approx} \frac{1}{2}\left(\frac{m}{\sigma}\right)^2. \end{aligned} \tag{5.8}$$

These findings can be demonstrated with a graphical example, in which $\mu_P = 0$, $\sigma = 1$, $m = 10$, $N_D = 4$, $k^* = 10$ and $\xi^{thres} = (N_D/2) \cdot 5^2 = 50$ (see Fig. 5.6). Then, the test statistic becomes $\xi_{k^*} = 200$ for signal f^s and $\xi_{k^*} = 60$ for signal f^p. In comparison, equation 5.8 yields very similar values, namely 200 and 50, respectively. Thus, the narrow delta peak in f^s would be misclassified as a step change.

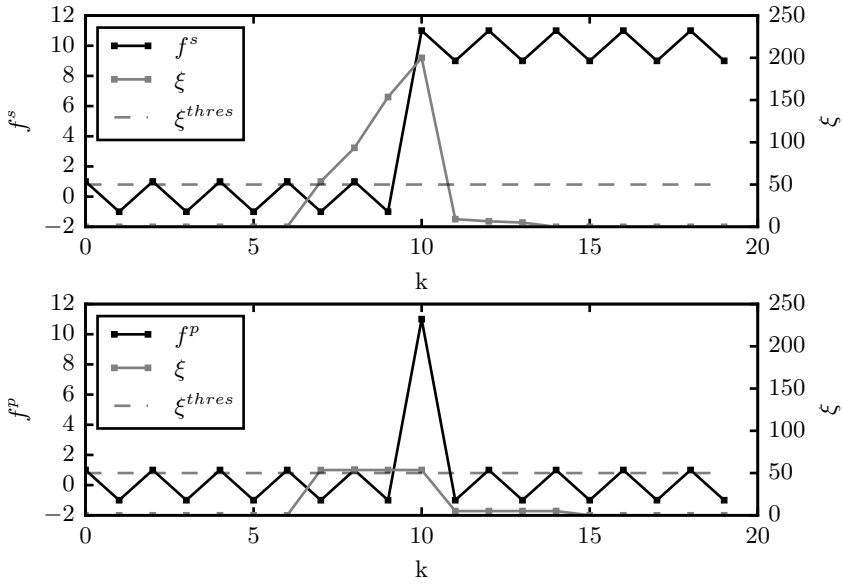

Figure 5.6: Two signals representing an actual step change (top) and a narrow delta peak (bottom)

5.3.2 Dissimilarity between reconstructed and original signal

As Fig. 5.5 also illustrates, the reconstructed signal does not resemble the original signal at all. This is due to two reasons. First, different step-change magnitudes were determined for the turn-on event at $k = 10$ and the turn-off event at $k = 20$, even though they should be the same. Second, gradual changes between $30 \leq k < 40$ and $40 \leq k < 50$ due to, e.g., a fixed-speed motor with a varying mechanical load, are not accounted for at all. Thus, it is likely that the disaggregation accuracy is low too.

5.4 Deficits in classifying fixed-speed motors

As the analysis of electric loads in machines used for manufacturing indicated (see section 4.2), nearly 40 % of them are fixed-speed motors, which can be further classified according to the mechanical load they drive (a fan, a pump, a compressor or any other mechanical load). This raises the following question: does a simple, generally valid classifier exist that can differentiate motors according to their mechanical loads?

A positive answer to this question has been indicated by Sultanem (1991), who describes that pump-operated appliances typically exhibit long transients when turned on, and also by Leeb et al. (1993), who state that the "transient behavior of a typical load is intimately related to the physical task that the load performs". However, no one has examined that question in more detail. Instead, previous papers dealing with features extracted from the transient state examined whether a classifier exists that can differentiate between, e.g., a motor, a linear load and a fluorescent lamp (see paragraph titled "transient state" in subsection 3.7.1 and detailed summary in Table A.3). In addition, previous studies exhibit three other imperfections:

First, in nearly all case studies, only 3-5 electric loads were used to validate the classifier, which is a small sample size. A noteworthy exception is the study by Patel et al. (2007), who classified the appliances of six houses, which probably comprised dozens of electric loads. However, Patel et al. (2007) used the voltage noise as a feature, which is not examined here since it requires data acquisition hardware in the megahertz range.

Second, no one has compared the features extracted from the transient state with each other, for example, in terms of their effect on the classification accuracy. Instead, most papers have only analyzed one particular feature from the transient state. A comparison between the features proposed in different papers is not feasible, since different data sets have been used to assess the quality of the proposed features.

Third, previous works did not clearly differentiate between using the measured *motor* current and using the measured *aggregate* current for classification. This is relevant because even if a classification is possible using the motor current, it is not necessarily possible using the aggregate current. In fact, the degree of accuracy with which the transient motor current can be extracted from the aggregate current has not been analyzed yet.

6 New and improved methods

For each of the four deficits explained in detail in chapter 5, either a new (in a case where no previous method existed) or an improved method (in a case where a method already existed but exhibited deficits) is presented next:

1. New method for extracting fixed-speed motors with a varying mechanical load;
2. Improved method for extracting uncontrolled bridge rectifiers, which were present in all variable speed drives analyzed in this thesis;
3. Improved method for detecting events and determining their step changes;
4. New method for classifying fixed-speed motors according to their mechanical loads.

For each method, the general approach is described first, followed by a more detailed description of the algorithm. Thereafter, each method is validated. All methods can be merged into a combined measurement method based on disaggregation, which is depicted in Fig. 6.1 (compare with the preliminary combined method presented in Fig. 4.6). This measurement method is later applied to seven machines used in manufacturing in chapter 7.

This combined method works in the following way. First, the voltage and current of the aggregate load are measured using appropriate data acquisition hardware. Second, the current of any one phase and/or three phase uncontrolled bridge rectifiers is extracted from the aggregate current according to the disaggregation method described in section 6.2. Whether any type of bridge rectifier is present in the aggregate load or not is identified automatically (see section 6.2). Thereafter, the current from the bridge rectifiers is subtracted from the aggregate load. Based on the residual aggregate current and the aggregate voltage, relevant electric properties such as the active power, the reactive power and the current harmonics are calculated. Third, using these properties, switching events are detected (see section 6.3) and clustered according to the disaggregation method based on switching events. Each distinct cluster is assumed to be a two-state load. Fourth, any potential fixed-speed motors exhibiting a continuously variable power demand due to a varying mechanical load are extracted (see section 6.1). Fifth, all two-state loads that were extracted using the disaggregation method based on switching events are labeled according to, e.g., the power factor $\lambda = p/s$ (see subsubsection 3.7.1.2).

Fixed-speed motors can be further classified according to their mechanical loads by analyzing their transient current (see section 6.4).

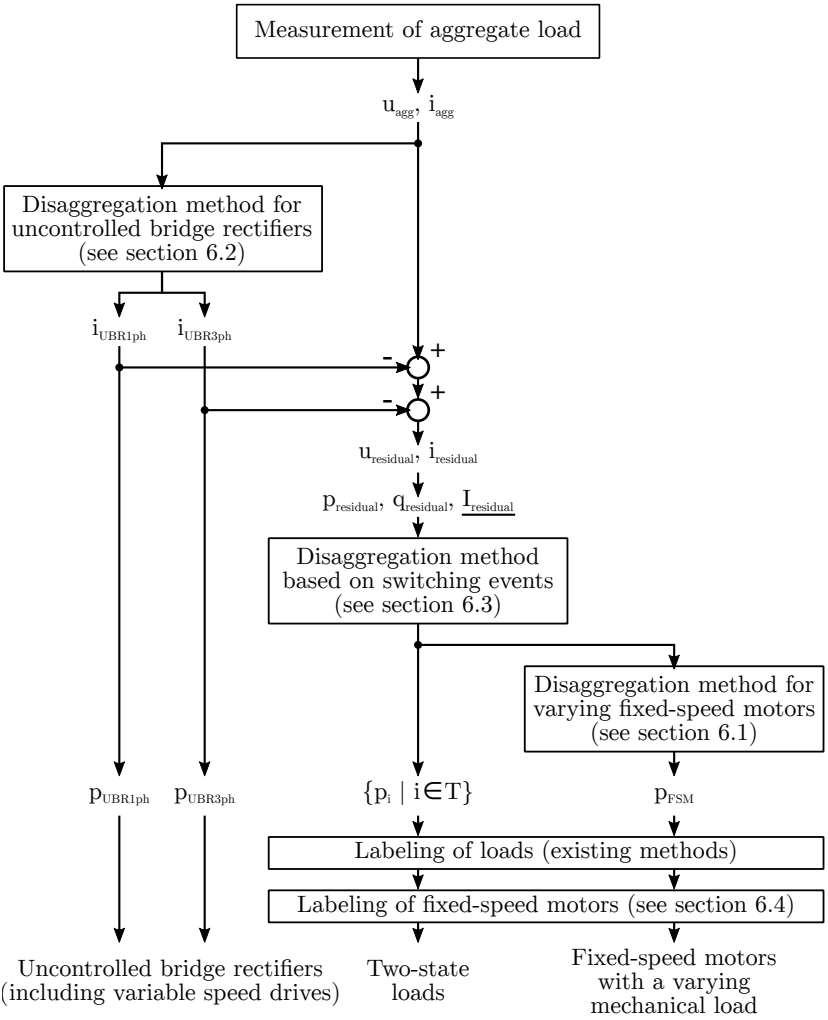

Figure 6.1: Flow chart of the combined measurement method based on disaggregation

6.1 Method for extracting fixed-speed motors

6.1.1 Approach

An algorithm was developed for a situation in which the following conditions hold true:

- The aggregate load consists of only one fixed-speed motor whose active power demand varies continuously, and any number of two-state loads and uncontrolled bridge rectifiers.
- The fixed-speed motors with a continuously variable power demand exhibits a characteristic step change in the active power demand and in the current harmonics when switched on and off.
- There is a significant linear correlation between at least one current harmonic of the *aggregate* load and the continuously variable active power demand of the fixed-speed motor.

In this case, the continuously variable active power demand of the fixed-speed motor can be estimated by performing the following steps (see Fig. 6.2):

1. Perform the existing disaggregation method for uncontrolled bridge rectifiers as well as the disaggregation method based on switching events (see flow chart in Fig. 6.1).
2. Calculate the difference Δp_{agg} between the sum of the estimated active power demand of the loads and the measured aggregate active power.
3. Identify a specific current harmonic I_x, which correlates linearly with Δp_{agg} and identify the to which it belongs to.
4. Perform a linear fit between Δp_{agg} and I_x.
5. Estimate the active power demand of the fixed-speed motor p_{FSM} through the linear fit.

The algorithm is based on the following idea: In order to derive a continuously variable active power demand of a specific load based on only measurements of the aggregate load, it is necessary that one aggregate feature can be uniquely associated with this load. To this end, only two electrical properties have been proposed in literature so far, namely high frequency voltage noise (see subsubsection 3.7.1.1) and current harmonics (see subsection 3.7.3). High frequency harmonics could not be analyzed in this thesis because it requires expensive measurement equipment featuring a sample frequency of 1 MHz. Current harmonics have been used for the disaggregation of uncontrolled bridge rectifiers, which are characterized by a high total harmonic distortion of more than 100 % (see section 5.1). Moreover, the relation between the current harmonics and the active power demand can be analytically determined (see subsection 5.2). In contrast, the current of fixed-speed motors only exhibits

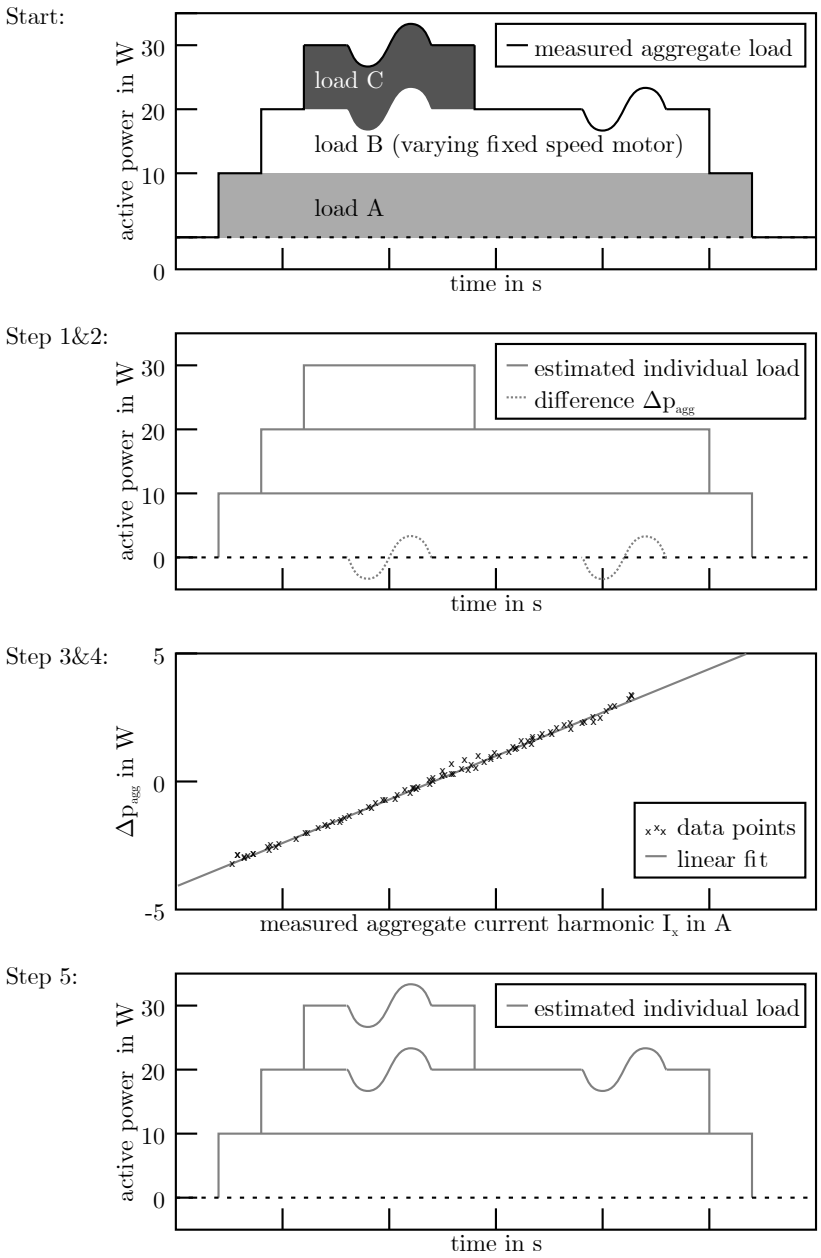

Figure 6.2: Approach for extracting fixed-speed motors with a varying mechanical load.

a total harmonic distortion of a few percent and there is no obvious relation between any current harmonic and the active power demand. Nevertheless, it was found that a significant linear correlation between a current harmonic and the active power demand *can* exist.

An interesting question is when and why such a linear correlation exists. While the relation between current harmonics and the fundamental current harmonic (with which the active power demand can be calculated) can be easily analytically determined for several electric loads such as uncontrolled bridge rectifiers, light dimmers and ideal line commuted converters (Grady 2012), it cannot be derived in a similar way for fixed-speed motors. Grady (2012) notes that single-phase motors typically have a low total harmonic distortion of around 10 % because the current becomes nonlinear when the motor is operated with peak flux densities beyond the saturation knee, but he does not specify a quantitative relation. Moreover, almost all ideal electric loads in AC systems generate only odd harmonics, since loads typically affect the positive and negative cycles symmetrically (Chapman 2005). However, in the validation example (see subsection 6.1.3) the linear relation between an *even* current harmonic and the active power demand is used. Reasons for even harmonics are either loads such as diodes or imperfections of AC loads, such as tolerances in transformer windings, commutation reactances and deviations in the firing times of thyristors (Buddingh 2003). However, in general, even harmonics seem to be scarcely described in literature (Barros et al. 2007), and it is difficult to specify the conditions under which a linear correlation between the active power demand and an even current harmonic exists.

6.1.2 Detailed algorithm

As mentioned above, the algorithm comprises five steps:

1. Perform the existing disaggregation methods.
2. Calculate the difference Δp_{agg}.
3. Identify the correlation between Δp_{agg} and I_x.
4. Perform a linear fit between Δp_{agg} and I_x.
5. Estimate the active power demand of the fixed-speed motor using the linear fit.

Step 1: Perform existing disaggregation methods First, any loads featuring uncontrolled bridge rectifiers (in particular, variable speed drives) are extracted using the new disaggregation algorithm described in 6.2. Thereafter, the power demand of all two-state loads is estimated using the event-based disaggregation algorithm described in section 3.7.1. Since it is assumed that the

fixed-speed motor with the continuously variable power demand also exhibits a characteristic step change, it is first estimated as a two-state load.

Step 2: Calculate difference Δp_{agg} Second, the difference between the measured aggregate power and the sum of the estimated power demands is calculated as

$$\Delta p_{agg}(t) = p_{agg}^{meas}(t) - \underbrace{\left(\sum_{UBR} p_{UBR}^{est}(t) + \sum_{i} \theta_i^{est}(t) p_i^{est} \right)}_{\equiv p_{agg}^{est}} , \tag{6.1}$$

where the first subtrahend represents the estimated active power demand of all loads featuring uncontrolled bridge rectifiers, and the second subtrahend refers to the estimated active power demand of all two-state electric loads of the aggregate load. The second subtrahend includes the fixed-speed motor with a continuously variable power demand, since it also exhibits a characteristic step change (see assumption above). If the active power demand of all loads was estimated correctly, $\Delta p_{agg}(t)$ contains only the fluctuations of the active power demand of the fixed-speed motor. With real data, it is beneficial to slightly smoothen Δp_{agg} using a median filter because otherwise imprecisely detected switching times lead to narrow peaks in Δp_{agg}.

Step 3: Identify correlation Third, two tests are executed for each harmonic I_n and for each two-state load i:

- The correlation between Δp_{agg} and the measured aggregate current harmonic $|I_n^{agg}|$ is tested using the Pearson correlation coefficient for the time windows defined by θ_i^{est}. The Pearson correlation coefficient is calculated as

$$\rho(x, y) = \frac{\sum_{i=1}^{n} (x_i - \overline{x})(y_i - \overline{y})}{\sqrt{\sum_{i=1}^{n} (x_i - \overline{x})^2 \sum_{i=1}^{n} (y_i - \overline{y})^2}} , \tag{6.2}$$

  where x refers to $|I_n^{agg}|$, and y represents Δp_{agg}.
- It is tested, whether a significant step change was detected for the harmonic $|I_n^{agg}|$ when the load i is turned on and off. Therefore, the step-change magnitude of $|I_n^{agg}|$ at switching times is compared to its usual noisiness quantified with the coefficient of variation.

If both tests return positive results for a harmonic $|I_{n*}^{agg}|$ and a specific load indicated by the subscript FSM in the following steps, then this suggests that the continuous variable power demand can be estimated based on the harmonic $n*$.

Step 4: Perform linear fit Fourth, a linear fit is performed, and its parameters are returned using

$$m^*, b^* = \underset{m,b}{\operatorname{argmin}} \int \left| \theta_{FSM}^{est}(t) \cdot \left[\Delta p_{agg}(t) + p_{FSM}^{est} - (m \cdot |I_{n*}^{agg}|(t) + b) \right] \right| dt \ . \tag{6.3}$$

Step 5: Estimate using linear fit Fifth and finally, the estimated active power demand of load i^* is substituted by

$$p_{FSM}^{est,new}(t) = \theta_{FSM}^{est}(t) \cdot (m^* \cdot |I_{n*}^{agg}|(t) + b^*) \ . \tag{6.4}$$

Extension to more complicated cases In contrast to the assumption that the aggregate load comprises only one fixed-speed motor whose power consumption varies continuously, the disaggregation algorithm presented above is also applicable to aggregate loads comprising two fixed-speed motors with a continuously variable power demand, under the condition that the regions in which their power varies, do not overlap. If they do overlap, the aggregate power will not display a significant linear correlation with any of the harmonics, and hence the algorithm will stop at step three.

For this scenario, an estimation of the individual power demands is still conceivable. One approach would be to linearly fit not one but multiple fixed-speed motors in equation 6.3, i.e.,

$$\underline{m^*}, \underline{b^*} = \underset{\underline{m},\underline{b}}{\operatorname{argmin}} \underbrace{\int \left| \Delta p_{agg}(t) + \sum_{i \in FSM} \theta_i^{est}(t) p_i^{est} - (m_i \cdot |I_n^{agg}|(t) + b_i) \right| dt}_{\epsilon} \ , \tag{6.5}$$

where the sum iterates over all fixed-speed motors that might have a continuously variable power demand. Furthermore, $\underline{m} = m_1, m_2, \ldots$ and $\underline{b} = b_1, b_2, \ldots$.

However, assuming two fixed-speed motors with a continuously variable active power demand, the equation already allows for four degrees of freedom. With such a high freedom, many signals can be fitted to the measured aggregate active power demand even though no correlation might exist. This should be prevented. To this end, Gebbe et al. (2017a) proposed first performing a fit in which only the parameter b is variable. Then, the same fit is performed again, allowing both parameters b and m to be variable. The final result is only accepted if the error ϵ from the second fit is at least 20 % lower than the error ϵ from the first fit. The underlying thinking is that the error in the second fit

will always be lower than the error in the fit, even for random signals, since the second fit allows for more degrees of freedom. In other words, a smaller error in the second fit does not necessarily indicate that the signals are indeed linearly correlated. However, this has to be tested, for example, by calculating the probability of a random signal to achieve the same decrease in the error ϵ. If and how this can be achieved was not analyzed further, though. As a simple alternative, an error decrease of 20 % was set as a threshold, but this value is not based on any statistic criterion. Therefore, further research is recommended.

6.1.3 Validation

The method was validated for a real world example, more specifically, for a fixed-speed motor driving a vacuum pump whose active power demand fluctuates between 600 W and 950 W. It is part of a thermoform machine, which also comprises several Joule heating elements; two variable speed drives; three fixed-speed motors driving different types of conveyor belts; a fan and an external cooling unit consisting of a compressor, a pump and a fan. The active power demand of both the aggregate load and the fixed-speed motor with the continuously variable active power demand is illustrated in Fig. 6.3. The disaggregation method makes use of only the aggregate data. The data of the fixed-speed motor were only used for the evaluation of the algorithm.

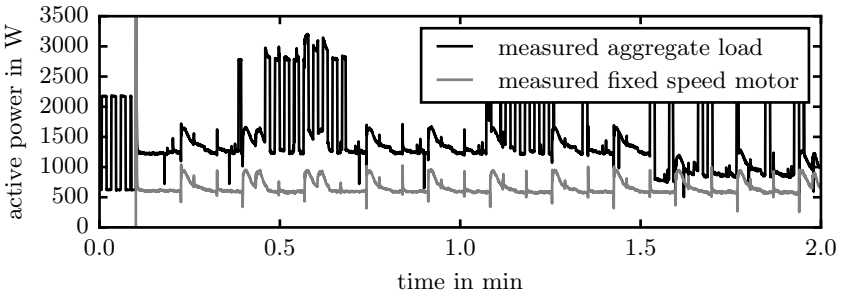

Figure 6.3: Active power demand of the fixed-speed motor with a continuously variable power demand and the aggregate load. Same fixed-speed motor as presented in Fig. 4.2 top and Fig. 5.1.

Step 1 &2: Disaggregate and calculate difference First, the uncontrolled bridge rectifiers were extracted from the aggregate load (see Fig. 6.4). The residual aggregate load was then disaggregated using the method based on

switching events. The result of the latter disaggregation as well as the calculated difference Δp_{agg} is displayed in Fig. 6.4.

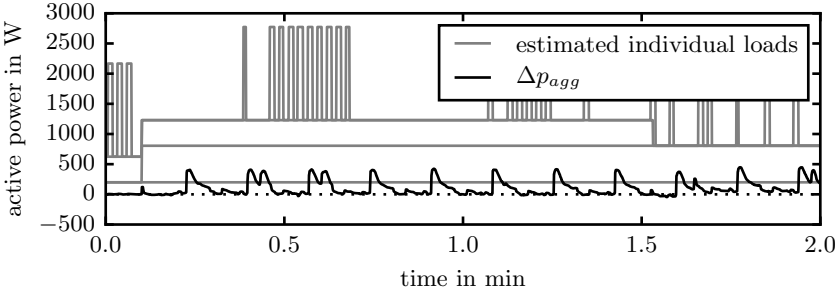

Figure 6.4: Result of the disaggregation method based on switching events

Steps 3 & 4: Identify correlation and perform fit The degree of linear correlation between Δp_{agg} and all aggregate current harmonics was quantified using the Pearson correlation coefficient (see Table 6.1). Δp_{agg} only correlated significantly with the 16th aggregate current harmonic I_{16}^{agg} with a coefficient of 0.80. The second highest correlation coefficient has a significantly lower value of only 0.48. Then, it was tested whether the 16th current harmonic exhibits a significant step change when any of the four estimated two-state loads (see Fig. 6.4) are switched on or off. This was true for only one load, namely the fixed-speed motor driving the vacuum pump. Based on this result, a linear fit was performed between $\Delta p_{agg}(t) + \theta_{FSM}(t) \cdot p_{FSM}$ and I_{16}^{agg} (see Fig. 6.5).

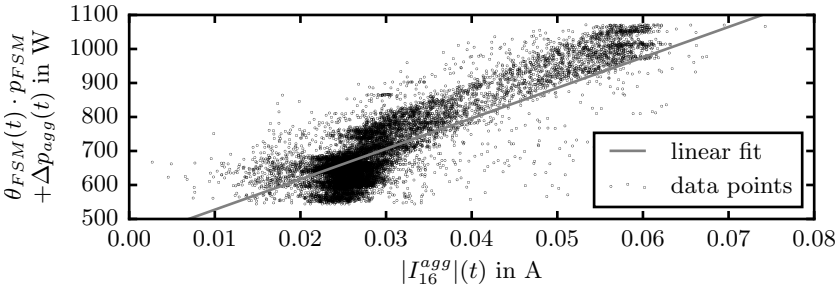

Figure 6.5: Linear correlation between Δp_{agg} and I_{16}^{agg}

While a correlation coefficient value of 0.80 between Δp_{agg} and I_{16}^{agg} does not imply a perfect correlation, the correlation coefficient between the active power demand of the fixed-speed motor driving the vacuum pump p_{FSM}^{meas} and I_{16}^{FSM}

was actually much higher, at 0.94 (see Table 6.1). There are three reasons for the discrepancy, which can be demonstrated with the values in Table 6.1:

- Non-ideal two-state behavior of loads,
- Estimation errors introduced in previous steps,
- Interference of other loads featuring a 16th current harmonic.

Table 6.1: Pearson correlation $\rho(x, y)$ between different current harmonics and the active power demand as well as the harmonic interference ψ_n^{FSM} from other loads according to equation 6.6

n	$\rho\left(\lvert I_n^{agg}\rvert, \Delta p_{agg}\right)$	$\rho\left(\lvert I_n^{agg}\rvert, p_{FSM}^{meas}\right)$	ψ_n^{FSM}	$\rho\left(\lvert I_n^{FSM}\rvert, p_{FSM}^{meas}\right)$
0	0.01	0.12	218 %	0.38
1	0.06	0.18	90 %	0.93
2	0.01	0.11	391 %	0.49
3	0.03	-0.04	418 %	0.57
4	0.02	0.11	460 %	0.51
5	0.04	0.02	614 %	0.66
6	0.04	0.12	519 %	0.46
7	0.02	0.10	785 %	0.64
8	0.14	0.22	404 %	0.51
9	0.07	0.06	788 %	0.54
10	0.19	0.24	276 %	0.58
11	0.12	0.12	2106 %	0.64
12	0.38	0.37	194 %	0.85
13	0.09	0.07	1251 %	0.70
14	0.42	0.48	118 %	0.89
15	0.14	0.16	331 %	0.98
16	0.80	0.91	28 %	0.94
17	0.12	0.16	189 %	0.55
18	0.25	0.58	70 %	0.98
19	0.21	0.14	577 %	0.96
20	0.15	0.61	96 %	0.98
21	0.14	0.28	443 %	0.95
22	0.48	0.58	135 %	0.93
23	0.01	0.12	2733 %	0.86
24	0.02	0.19	240 %	0.87
25	0.17	0.25	2831 %	0.80

If all two-state loads would have operated ideally and the estimation in previous steps would have been perfect, $\rho\left(|I_{16}^{agg}|, \Delta p_{agg}\right)$ would have equaled $\rho\left(|I_{16}^{agg}|, p_{FSM}^{meas}\right) = 0.91$.

The degree to which the current harmonics of other loads interfered with the current harmonics of the fixed-speed motor driving the vacuum pump can be quantified with the following formula:

$$\psi_n^{FSM} = \frac{\sum_{i \neq FSM} |I_n^i|}{|I_n^{FSM}|} \ , \tag{6.6}$$

where the sum iterates through all loads i of the aggregate load excluding the relevant fixed-speed motor with a continuously variable power demand and n refers to the analyzed harmonic. Accordingly, the sum of the 16th current harmonic of all residual loads was 28 % as much as I_{16}^{FSM} (see Table 6.1). If no other load would have generated the 16th current harmonic, the correlation would have equaled $\rho\left(|I_{16}^{FSM}|, p_{FSM}^{meas}\right) = 0.94$.

The values of $\rho\left(|I_n^{FSM}|, p_{FSM}^{meas}\right)$ also demonstrate that the 16th current harmonic was not the only current harmonic that exhibited a significant linear correlation with the active power demand of the fixed-speed motor driving the vacuum pump. Indeed, the 15th, 18th, 19th, 20th and 21st current harmonics demonstrated an even higher correlation than the 16th current harmonic. However, in those cases the interference from other loads was much higher.

Step 5: Estimate using linear fit Using the linear fit obtained in the previous step, the active power demand of the fixed-speed motor driving the vacuum pump was estimated (see Fig. 6.6). The estimation yielded an accuracy of 89 % according to equation 1.1, which satisfies the requirements (see section 1.3).

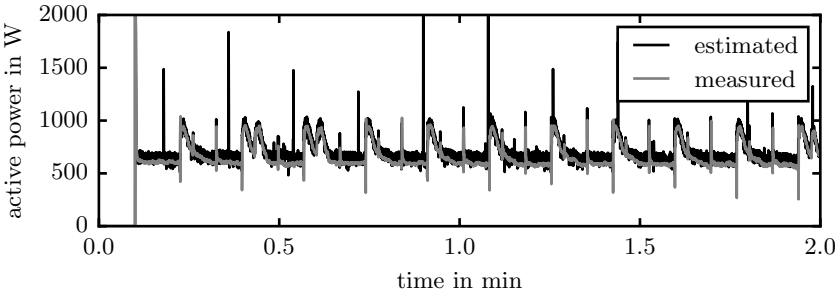

Figure 6.6: Estimated and measured active power demand of the fixed-speed motor with a continuously variable power demand

6.2 Method for extracting uncontrolled bridge rectifiers

6.2.1 Approach

The idea for a new disaggregation method for uncontrolled bridge rectifiers, which were found in all of the variable speed drives analyzed in this thesis, originates from two observations. First, in most cases, the characteristic peaks in the current of an uncontrolled three- or single-phase bridge rectifier are visible in the aggregate current. Second, the current of an ideal uncontrolled bridge rectifier is zero for every region apart from the peaks. Therefore, if the visible peaks in the aggregate current could be filtered or "cut off", the aggregate current could be separated into the current of the uncontrolled bridge rectifier and the current of all residual loads. This approach can be realized by performing the following steps (see Fig. 6.7):

1. Detect the beginning and the ending of peaks by analyzing the curvature of the aggregate current.
2. Identify the type of uncontrolled bridge rectifier - either single-phase or three-phase - by examining the distribution of all estimated peak beginnings and endings.
3. Filter out false positives and false negatives in the estimated current peak beginnings and endings.
4. Estimate the current of the residual loads through interpolation.
5. Estimate the current of the uncontrolled bridge rectifier through a simple subtraction.

A preliminary version of this method has been published in (Gebbe et al. 2017b).

6.2.2 Detailed algorithm

Step 1: Detect beginning and ending of current peaks

The presence of peaks leads to a characteristic shape in the second derivative of the aggregate current corresponding to its curvature, as can be seen in Fig. 6.8. For the two positive peaks in the first half-period, in which the voltage is positive, the following is true: the beginning and end of a positive peak lead to a local maximum in the second derivative of the current, since the curvature of the current increases significantly at those times. In the center of the peaks, the curvature drops and results in a local minimum. Hence, the beginning and

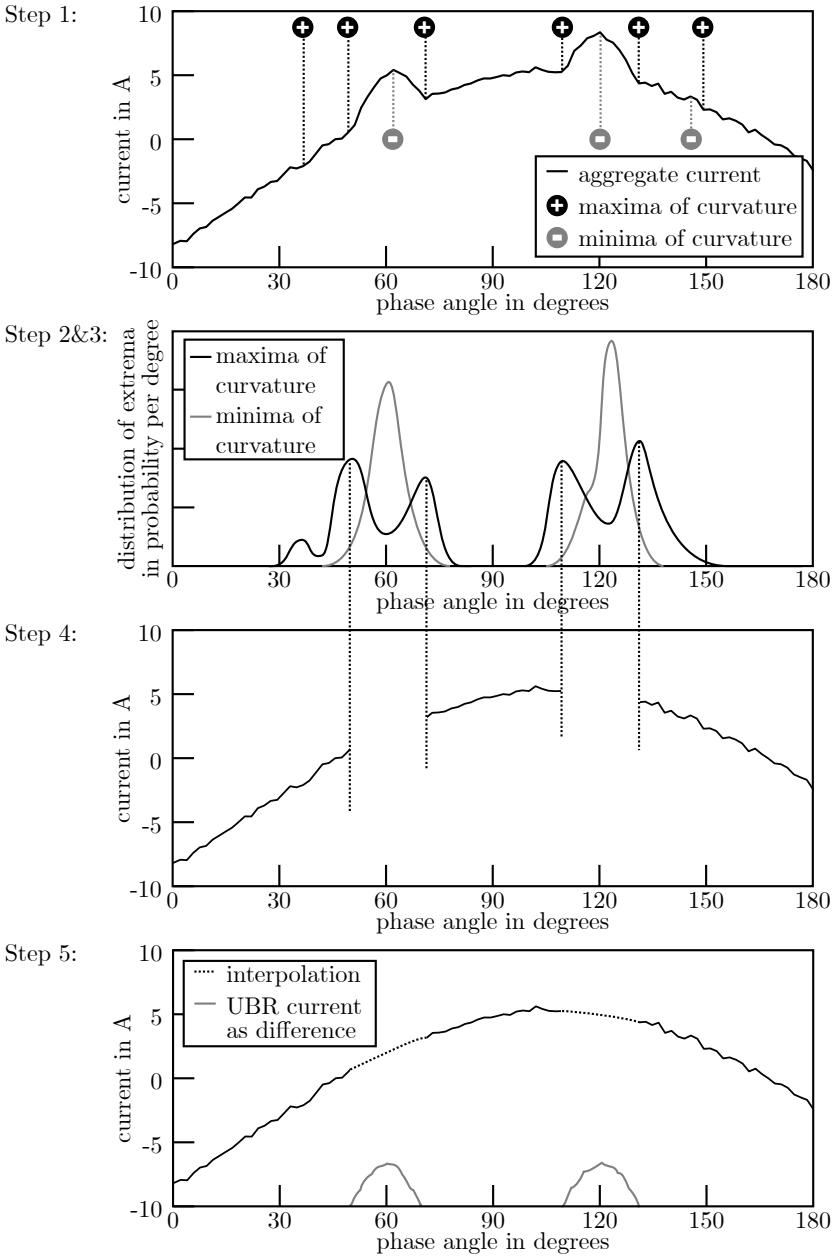

Figure 6.7: Approach for extracting uncontrolled bridge rectifiers

end times of these two peaks can be determined by searching the four largest local maxima in the second derivative of the current, i.e.,

$$\phi_{max} = \underset{\phi}{\operatorname{argmax}} \frac{d^2}{d\phi^2} i_{agg} \ , \tag{6.7}$$

where ϕ_{max} refers to the phase angle with respect to the voltage at which a local maxima of the curvature of the measured aggregate current was found. For half-periods in which the voltage is negative, the same procedure can be performed on the additive inverse of the aggregate current.

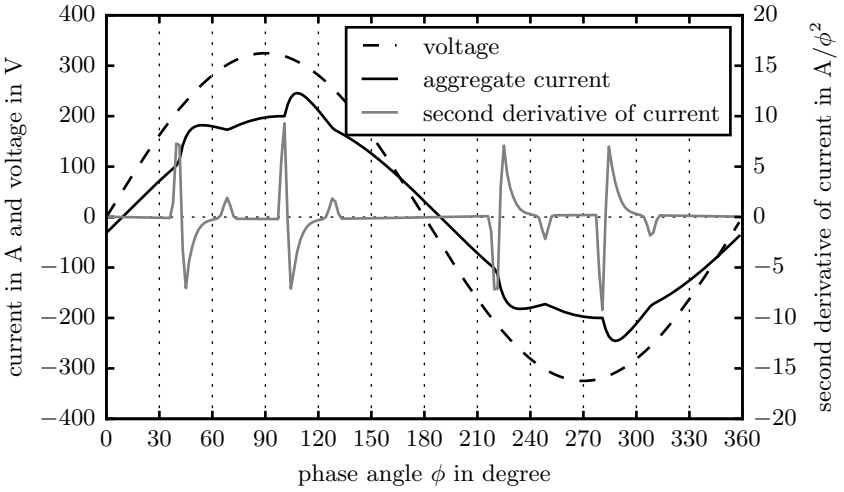

Figure 6.8: Plot of a simulated current, including its second derivative, of an aggregate load comprising an uncontrolled three-phase bridge rectifier

This simple approach works well for ideal signals. However, in real-world signals, the presence of noise and electric loads with current harmonics may lead to either additional peaks in the aggregate current (false positives) or peaks from the uncontrolled bridge rectifier being obscured (false negatives). To handle such signals, the final algorithm is more complex:

First, the current is split into half-periods by detecting the zero crossings of the voltage. While other methods to achieve this result exist, the zero crossing detection is simple and well described in literature (Wall 2003). If the mean voltage in that half-period is negative, the additive inverse of the current is used instead by multiplying the current with (-1). This ensures that all peaks are positive.

Second, the second derivative of the current in each half-period is split into sections with the same sign by performing another zero crossing detection. Then, for each such section the extremum is determined. In other words, a maximum is determined for sections in which the second derivative of the current is positive, and a minimum is determined for sections in which the second derivative of the current is negative.

Third, among those extrema, the six largest maxima and the three lowest minima are chosen for further consideration. While only four maxima and two minima are relevant for a three-phase uncontrolled bridge rectifier, considering more extrema increases the chance of detecting the *relevant* extrema in case of false positives on the one hand. On the other hand, the percentage of false positives among all detected extrema is now at least 33 %.

Step 2: Identify type of uncontrolled bridge rectifier

After detecting the extrema for all half-periods, the distribution of times at which these extrema occur is analyzed (see example in Fig. 6.9). For this purpose, the time is represented as the phase angle with respect to the last zero crossing of the voltage. All extrema occurring at phase angles below 30° or above 150° are discarded since they most likely represent false positives (see simulated data in section A.2).

Ideally, for an uncontrolled *three*-phase bridge rectifier two minima should occur in each half-period around 60° and 120°. Moreover, four maxima should occur in the interval [30°, 150°]. Similarly, for an uncontrolled *one*-phase bridge rectifier, one minimum should occur in each half-period around 90° and two maxima in the interval [30°, 150°] (see section 2.4).

Only if this number of extrema occurs, it is decided that the respective type of rectifier is present in the aggregate load, and the respective disaggregation procedure described in the following steps is performed. Note that it is also possible that the conditions of *both* the three-phase and the single-phase bridge rectifier are fulfilled. In this case, the below-mentioned disaggregation procedure is performed twice: first for a three-phase rectifier using the aggregate current, and afterwards for a single-phase rectifier using the residual current.

Step 3: Filter estimated current peak beginnings and endings

As mentioned above, among the detected extrema, at least 33 % are not relevant. Therefore, the *relevant* extrema need to be detected using the following filtering process. This is achieved in three substeps:

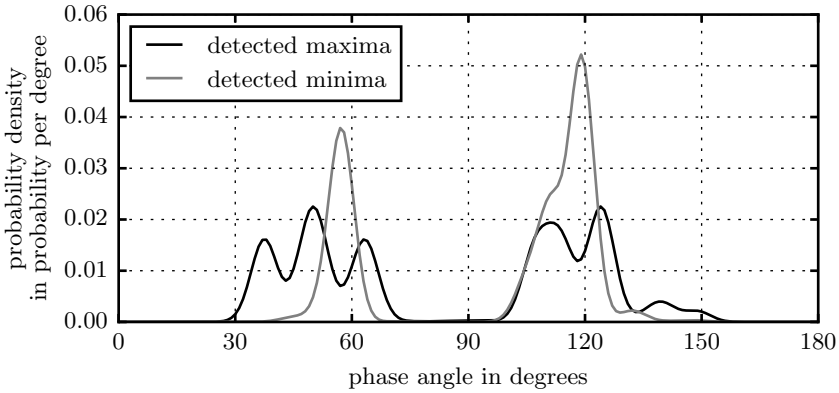

Figure 6.9: Distribution of times (measured in phase angles) at which local maxima and minima were detected for a real world example in which an uncontrolled three-phase bridge rectifier was present

1. Estimate the likely peak center, which is assumed to be constant for all half-periods.
2. Estimate the likely peak width for each half-period.
3. Substitute the estimated values with nearby detected extrema.

Estimate likely peak center First, the actual center of the peaks are found using the detected minima. For an uncontrolled three-phase rectifier two peaks occur at $\phi_{C1} \approx 60°$ and $\phi_{C2} = \phi_{C1} + 60° \approx 120°$, whereas for an uncontrolled single-phase rectifier one peak occurs at $\phi_C \approx 90°$. Moreover, in a first approximation, it can be assumed that the peak centers for a particular uncontrolled bridge rectifier always occur at the same phase angles independent of the load (see section A.2). Therefore, the most likely peak center $\hat{\phi_{C1}}$ for the three-phase rectifier is found by

$$\hat{\phi_{C1}} = \underset{\phi_{C1}}{\operatorname{argmax}} \sum_{\phi_{min}} \mathcal{N}(\phi_{min}, \phi_{C1}, \sigma_C^2) + \mathcal{N}(\phi_{min}, \phi_{C1} + 60°, \sigma_C^2) \qquad (6.8)$$
$$s.\,t. \quad \phi_{C1} \in [60° - 6°, 60° + 6°] \,,$$

where the sum ranges over all phase angles ϕ_{min} for which a minima was found, and $\mathcal{N}(x, \mu, \sigma^2)$ represents the normal distribution.

This can be understood as finding estimate values for ϕ_{C1}, ϕ_{C2}, which overlap the most with any detected local minima ϕ_{min}. It shall be pointed out that using such a likelihood function is robust against outliers, which is not the

case for cost functions that penalize distances. Similarly, the most likely peak center $\hat{\phi_C}$ for the single-phase rectifier is found by

$$\begin{aligned}\hat{\phi_C} = &\underset{\phi_C}{\operatorname{argmax}} \sum_{\phi_{min}} \mathcal{N}(\phi_{min}, \phi_C, \sigma_C^2) \\ &s.\ t. \quad \phi_C \in [90° - 8°, 90° + 8°] \ .\end{aligned} \tag{6.9}$$

Estimate likely peak width Second, the most likely width ϕ_W of the current peaks is determined using the detected maxima. It is assumed that the peak width varies over time given a varying load. In the case of the three-phase rectifier it is further assumed that the peak width is the same for both peaks in the same half-period. Hence, for the three-phase rectifier the beginning and end of the two peaks can be defined as

$$\begin{aligned}\phi_{b1} =& \hat{\phi_{C1}} - 0.5 \cdot \phi_W \\ \phi_{e1} =& \hat{\phi_{C1}} + 0.5 \cdot \phi_W \\ \phi_{b1} =& \hat{\phi_{C1}} + 60° - 0.5 \cdot \phi_W \\ \phi_{e2} =& \hat{\phi_{C1}} + 60° + 0.5 \cdot \phi_W \ ,\end{aligned} \tag{6.10}$$

where the subscript $b1$ refers to the beginning of the first peak, $e1$ denotes the end of the first peak, $b2$ indicates the beginning of the second peak and $e2$ represents the end of the second peak per half-period.

Similarly, the beginning and end of the one peak in case of the single-phase rectifier can be defined as

$$\begin{aligned}\phi_b =& \hat{\phi_C} - 0.5 \cdot \phi_W \\ \phi_e =& \hat{\phi_C} + 0.5 \cdot \phi_W \ .\end{aligned} \tag{6.11}$$

The most likely peak width $\hat{\phi_W}$ for each half-period H is then found for the three-phase rectifier by

$$\begin{aligned}\hat{\phi_W}(H) = &\underset{\phi_W}{\operatorname{argmax}} \sum_{\phi_{max} \in H} + \mathcal{N}(\phi_{max}, \phi_{b1}, \sigma_W^2) + \mathcal{N}(\phi_{max}, \phi_{e1}, \sigma_W^2) \\ &\qquad + \mathcal{N}(\phi_{max}, \phi_{b2}, \sigma_W^2) + \mathcal{N}(\phi_{max}, \phi_{e2}, \sigma_W^2) \\ &s.\ t. \quad \phi_W(H) \in [6°, 60°] \quad \text{and} \quad |\phi_W(H) - \phi_W(H-1)| \leq 6° \ .\end{aligned} \tag{6.12}$$

Similarly, the most likely peak width $\hat{\phi_W}$ for the single-phase rectifier is determined by

$$\hat{\phi_W}(H) = \underset{\phi_W}{\operatorname{argmax}} \sum_{\phi_{max} \in H} + \mathcal{N}(\phi_{max}, \phi_b, \sigma_W^2) + \mathcal{N}(\phi_{max}, \phi_e, \sigma_W^2) \qquad (6.13)$$

$$s.\,t. \quad \phi_W(H) \in [6°, 120°] \quad \text{and} \quad |\phi_W(H) - \phi_W(H-1)| \leq 6° \,.$$

Substitute estimated values with nearby detected extrema Based on the estimated peak center and peak width, all likely peak beginnings and endings $\phi_{b1}, \phi_{e1}, \phi_{b2}$ and ϕ_{e2} or ϕ_b and ϕ_e can be calculated (see equations above). These estimate values can be substituted by a phase angle ϕ_{max} for which a maximum was actually detected if ϕ_{max} is close to one of the estimated values.

An exemplary result for a three-phase uncontrolled bridge rectifier is presented in Fig. 6.10 with regard to the detected phase angles ϕ_{max} corresponding to the input to step 3 and the final values for $\phi_{b1}, \phi_{e1}, \phi_{b2}$ and ϕ_{e2} for each half-period corresponding to the output of step 3.

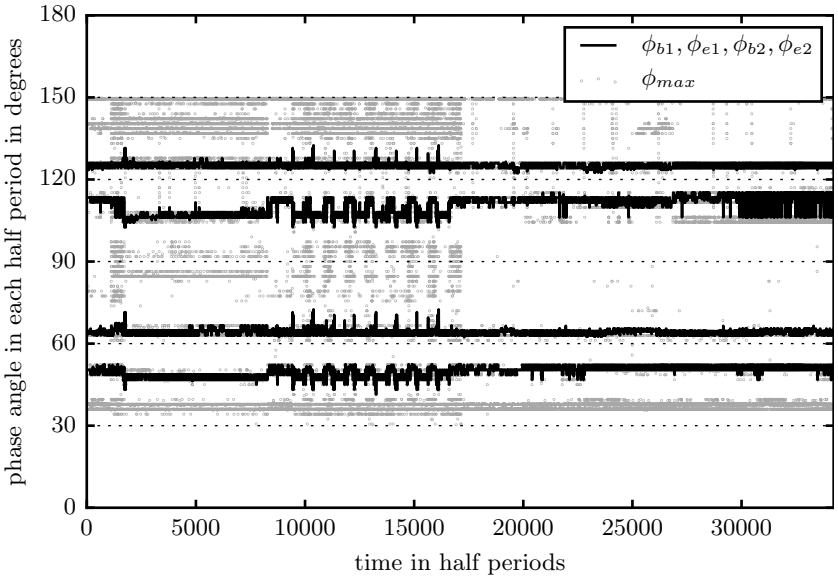

Figure 6.10: Plot of all detected phase angles ϕ_{max} as well as all final phase angles $\phi_{b1}, \phi_{e1}, \phi_{b2}$ and ϕ_{e2}. Same real-world example as in Fig. 6.9.

Step 4: Estimate current of residual loads through interpolation

After the peak beginnings and endings have been detected, the residual current (i.e., the current of all residual loads) is estimated. Since the current of the uncontrolled bridge rectifier is zero outside the peaks, the residual current equals the aggregate current in these regions. For the regions corresponding to the peaks, the residual current is not known, and it is thus estimated via an interpolation.

In the simplest approach, the interpolation is performed linearly. Therefore, the current values at the beginning and at the end of a peak are connected with a line that can be expressed mathematically as:

$$i_{res}(\phi) = \begin{cases} \left(1 - \frac{\phi-\phi_b}{\phi_e-\phi_b}\right) i_{agg}(\phi_b) + \left(\frac{\phi-\phi_b}{\phi_e-\phi_b}\right) i_{agg}(\phi_e) & \dots \text{ if } \phi \in [\phi_b, \phi_e] \\ i_{agg}(\phi) & \dots \text{ else} \end{cases} , \tag{6.14}$$

where i_{res} represents the current of all residual loads, i_{agg} the measured aggregate current, and ϕ_b and ϕ_e refer to the estimated peak beginning and ending. This approach works well if the undefined region (i.e., the peak) is narrow, and it has the advantage of being computationally efficient.

However, if the undefined region is large, the linear approximation of the residual current fails because the current is in fact curved instead of linear. In these cases, more sophisticated interpolations are recommended. If the total harmonic distortion of the residual current is low, its undefined region can be interpolated using a single sine wave with variable amplitude and phase difference but a fixed frequency of $\omega = 2\pi f = 2\pi/(2 \cdot T_H)$, where T_H represents the duration of the half-period. If, on the other hand, the total harmonic distortion is large, multiple sine waves with fixed frequencies can be used for the interpolation. Their parameters can be inferred by, e.g., a least squares fit to the already defined region of the residual current.

Step 5: Estimate current of uncontrolled bridge rectifiers

After the residual current has been estimated, the current of the uncontrolled bridge rectifier can be calculated by simply subtracting the residual current from the aggregate current:

$$i_{UBR} = i_{agg} - i_{res} \ . \tag{6.15}$$

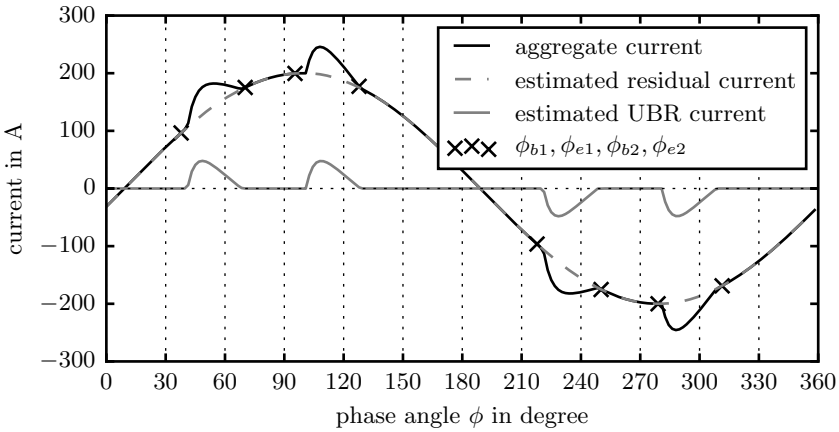

Figure 6.11: Plot of the estimated current from the uncontrolled bridge rectifier (UBR) and the estimated residual current.

6.2.3 Validation

The improved algorithm was evaluated against the four deficits of the existing disaggregation method based on correlation. These deficits were described in detail in section 5.2 and are summarized below:

- A low accuracy,
- A high susceptibility to other loads exhibiting current harmonics,
- An inapplicability if the aggregate load comprises both a three-phase and a single-phase uncontrolled bridge rectifier,
- An inability to disaggregate the current directly.

6.2.3.1 Low accuracy

In order to verify that the new disaggregation algorithm yields a greater accuracy than the ones described in section 5.2, the following experiment was performed:

An aggregate load, consisting of a three-phase uncontrolled bridge rectifier and a linear load, was simulated. The current of the linear load could be described as a pure sinus with a peak magnitude of 200 A, which was approximately twice as high as the peak current magnitude of the uncontrolled bridge rectifier (see Fig. 6.11). For the uncontrolled bridge rectifier, the same simulation data as described in section 5.2 and section A.2 were used.

The improved disaggregation algorithm described above was then applied to the voltage and aggregate current of these two electric loads. The disaggregation result of the uncontrolled bridge rectifier was then evaluated in terms of the measurement accuracy (see eq. 1.1). The accuracy ranged between 95 and 100 % for all scenarios (see Table 6.2) and thus fulfilled the required accuracy of at least 85 %.

Table 6.2: Accuracy of the improved disaggregation method for the different rectifiers defined in section 5.2

		Type of rectifier					
		A	B	C	D	E	F
R_{load}	10 Ω	100 %	100 %	99 %	100 %	99 %	100 %
	15 Ω	100 %	99 %	100 %	98 %	99 %	100 %
	20 Ω	97 %	99 %	100 %	100 %	100 %	100 %
	30 Ω	99 %	100 %	100 %	100 %	99 %	100 %
	40 Ω	99 %	97 %	100 %	100 %	100 %	100 %
	80 Ω	99 %	99 %	100 %	99 %	100 %	100 %
	160 Ω	99 %	99 %	100 %	99 %	100 %	100 %
	320 Ω	99 %	100 %	100 %	100 %	97 %	100 %
	640 Ω	100 %	100 %	100 %	100 %	100 %	100 %
	1000 Ω	100 %	100 %	100 %	100 %	100 %	95 %

6.2.3.2 Susceptibility to current harmonics from other loads

In another experiment, it was demonstrated that the new disaggregation is also more robust against the presence of other electric loads generating similar current harmonics as the uncontrolled bridge rectifier. Therefore, one of the simulated currents described in section 5.2 was used again to represent the current of an uncontrolled bridge rectifier (rectifier A, $R_{load} = 40\ \Omega$). Another electric load was defined, whose first and fifth harmonics equaled the first and fifth harmonics of the uncontrolled bridge rectifier in magnitude and phase. All other harmonics of this load were defined as zero.

Again, the improved disaggregation algorithm described above was applied to the voltage and aggregate current of these two electric loads, and the result was evaluated in terms of the accuracy defined in eq. 1.1. In this case, the residual current was interpolated using a mixture of sinus-waves of different frequencies. The result was that the current of the uncontrolled bridge rectifier was estimated with an accuracy of 97 % (see Fig. 6.12). This is a significant advantage compared to the previous method by Laughman et al. (2003); Lee et al. (2005), which yielded an accuracy of 0 % (see section 5.2).

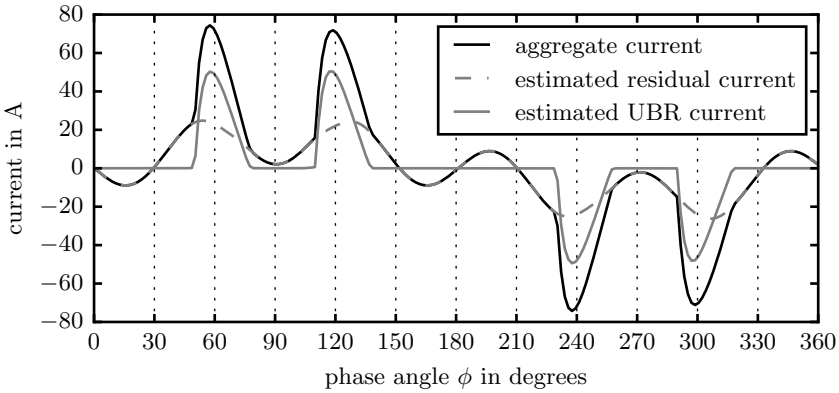

Figure 6.12: Disaggregation result when another load with current harmonics is present

6.2.3.3 Inapplicability if two different types of uncontrolled bridge rectifier are present

The previous disaggregation method could not be applied to an aggregate load comprising both a single-phase *and* a three-phase uncontrolled bridge rectifier (see section 5.2.3). In contrast, the improved disaggregation method can be applied to such an aggregate load. For the case described in section 5.2.3, the disaggregation result is presented in Fig. 6.13. The method achieved disaggregation accuracies of 98-99 % for all three loads.

6.2.3.4 Inability to extract the current

The previous disaggregation methods could only estimate the active power demand or the fundamental harmonic, both of which are defined for one period (see section 2.2). In contrast, the improved disaggregation methods directly estimates the current and thus hundreds of values per period (depending on the sample rate). This is beneficial if further methods require one to analyze either the current of the uncontrolled bridge rectifier or of the residual loads. An example of such a method is the classification described in section 6.4.

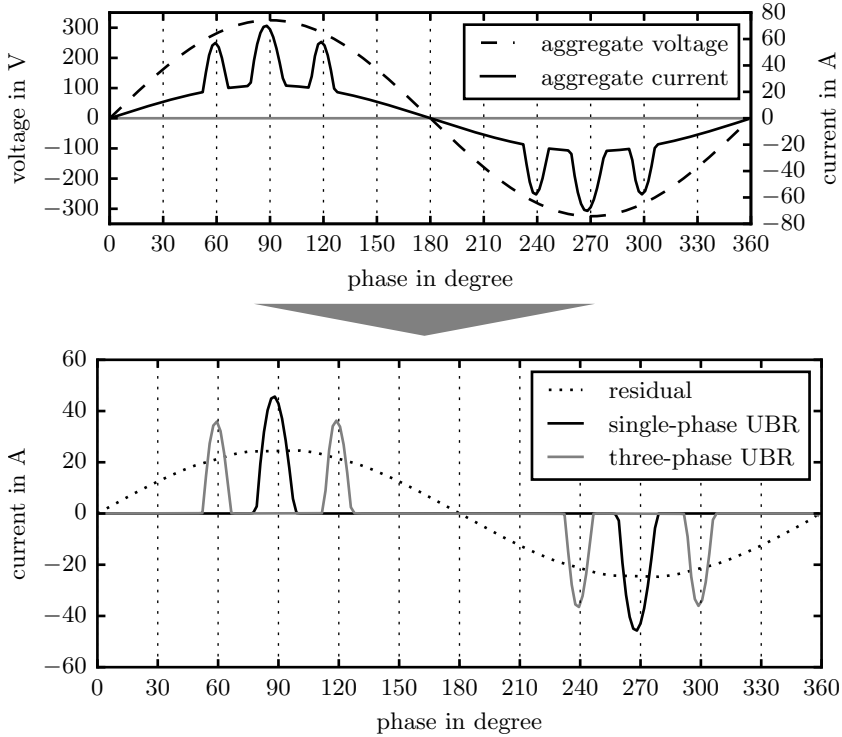

Figure 6.13: An aggregate load comprising both a single-phase and a three-phase uncontrolled bridge rectifier (UBR) (top) can be successfully disaggregated with the improved method (bottom).

6.3 Method for detecting switching events

6.3.1 Approach

The improved approach for detecting events consists of functions which are similar to the ones used in the previous approach described in section 5.3. It comprises three steps (see Fig. 6.14):

1. Determine the probability of a step change using the function ξ already described in section 5.3, albeit with improved robustness.
2. Reconstruct the signal using $\hat{f}^{mod}$.
3. Determine the step-change magnitude based on the reconstructed signal using Δf^{mod} .

The idea for the algorithm can be thought of as a mixture of the event detection approach by Luo et al. (2002) and the original event detection by Hart (1985). While the probability of step changes is calculated using the method proposed in Luo et al. (2002), their magnitude is determined in a way that is more similar to Hart (1985) than Luo et al. (2002). Hart (1985) determines the step-change magnitude by calculating the difference between steady states. The advantage of this is that the reconstructed signal always approximately equals the original signal. While steady states may not be apparent due to noise or continuously variable loads, a similar approach is used here: first, *quasi* steady states are calculated using $\hat{f}^{mod}$, and then the step changes between these quasi steady states are determined using Δf^{mod}.

6.3.2 Detailed algorithm

Step 1: Determine probability using function ξ

To determine the probability of a step change function, the same function ξ as described in detail in section 5.3 is used. However, ξ can lead to undesired results in case of low values of σ_P. This problem and a solution will be described next.

Moreover, an alternative function ξ^{mod} for determining step changes is briefly presented. While this alternative function is not used in the final combined method, it does aid in the understanding of the event detection process, including its challenges, and it may be useful in other scenarios.

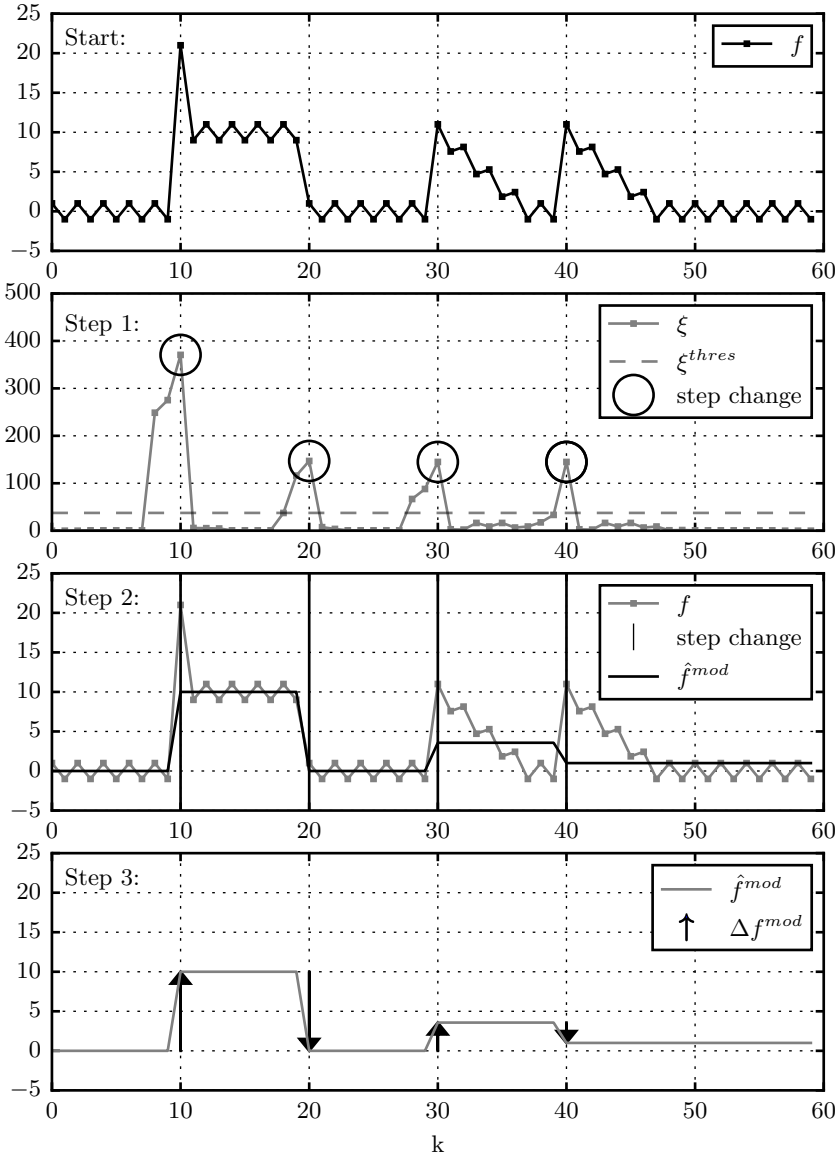

Figure 6.14: Improved approach for detecting events

Improved robustness against low values of σ_P As Luo et al. (2002) already mentioned, low values of σ_P can yield undesired detection results compared to human intuition. Therefore, they proposed setting a lower limit to σ_P as $\sigma_P \overset{!}{\geq} 1\,\% \cdot \mu_P$.

However, this limitation does not suffice in some cases. This can be proven with an exemplary signal f derived from real data, illustrated in Fig. 6.15 at the top. The signal f and its standard deviation are defined as follows:

$$f \approx \begin{cases} 0 & \dots k < 15 \\ 10 & \dots k \geq 15 \end{cases}, \tag{6.16}$$

$$\sigma(f) \approx \begin{cases} 0.25 & \dots k < 10 \\ 1 & \dots k \geq 10 \end{cases}.$$

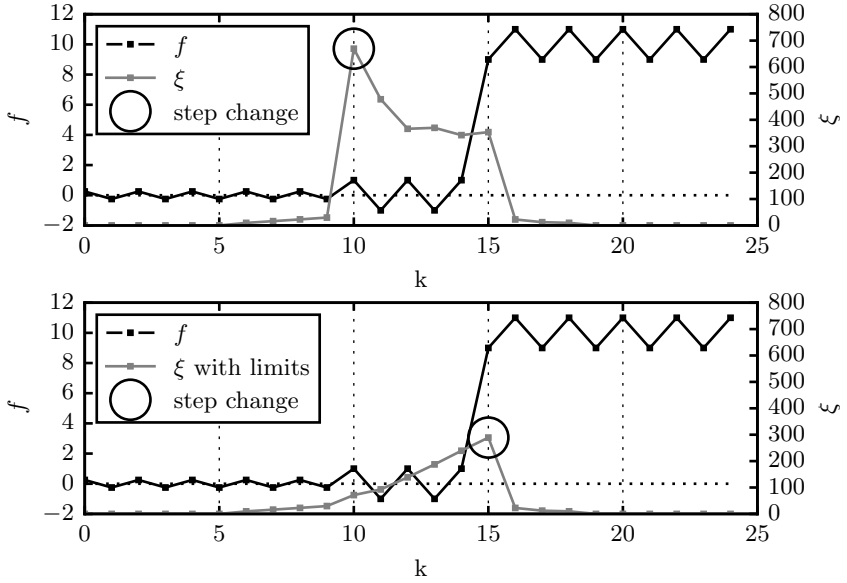

Figure 6.15: Probability of step changes without (top) and with limiting z_i (bottom). $N_D = 6$ was chosen here.

While the desired result is to detect the step change at $k = 15$, ξ actually determines the most likely step change at $k = 10$ due to the low value of $\sigma(f)$

for $k < 10$. A solution is to constrain z_i in equation 5.4 as

$$z_i^{mod} = \begin{cases} 10 & \text{if } z_i > 10 \\ z_i & \text{else} \end{cases} . \tag{6.17}$$

The constant value of 10 is chosen specifically for the example above. For real data, a value of 100 was found to be helpful. With this limitation of z_i, ξ determines the most likely step change at $k = 15$, as desired.

Alternative function for determining probability It is possible to define a modified function for determining the probability of step changes that is robust against narrow peaks. Such a function ξ^{mod} will be presented next and its robustness will be proven. However, since the step change in the active power demand of some motors with a particularly large inrush current rather resembles a narrow peak than a step change (see Fig. 6.16), it is actually necessary to also detect narrow peaks. Therefore, ξ^{mod} was not considered further.

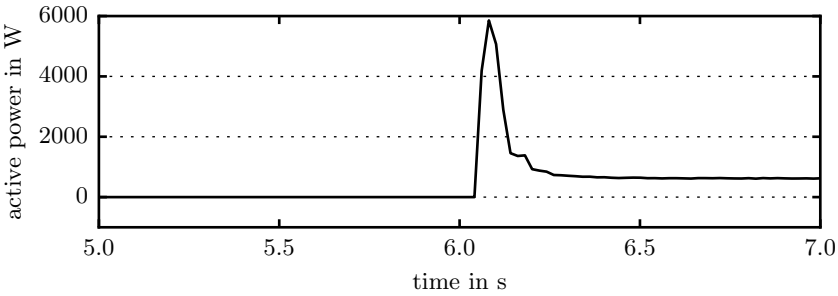

Figure 6.16: Measured active power demand of a motor being switched on

The alternative function for determining the probability $\xi^{mod} : \mathbb{Z} \mapsto \mathbb{R}$ can be defined as

$$\xi_k^{mod} = \frac{N_D}{2} \left(\frac{\mu_D - \mu_P}{max(\sigma_D, \sigma_P)} \right)^2 . \tag{6.18}$$

For the two signals f^s and f^p defined in subsection 5.3.1, the test statistic yields the following values:

$$\text{for } f^s : \quad \xi_{k^*}^{mod} \overset{\text{see eq. 5.5}}{=} \frac{N_D}{2} \left(\frac{m}{\sigma} \right)^2 , \tag{6.19}$$

$$\text{for } f^p : \quad \xi_{k^*}^{mod} \overset{\text{see sec. A.5}}{\approx} \left(\frac{1}{2} \right)^2 .$$

Thus, ξ^{mod} yields the same result as ξ for the signal f^s, or more generally speaking for $\sigma_P \approx \sigma_D$, but a significantly lower result for the signal f^p by a factor of $(m/\sigma)^2$. Assuming that $\xi^{thres} = (N_D/2) \cdot 5^2$ and $(m/\sigma)^2 \gg 5^2$, the following inequalities hold true: $\xi^{mod}_{k^*}(f^p) \ll \xi^{thres} \ll \xi^{mod}_{k^*}(f^s)$. This means, that the signal f^s would be classified as a step change, but not f^p, which is *in principle* the desired result.

Step 2: Reconstruct signal using $\hat{f}^{mod}$

A signal with quasi steady states is reconstructed by calculating the median of the original signal between two detected step changes. To this end, it is assumed that step changes were detected at times $s_1, s_2, \ldots$. The reconstructed signal $\hat{f}^{mod}$ can then be defined as

$$\hat{f}^{mod}_k \equiv median(f_i | \operatorname*{argmax}_{s_j \leq k} s_j \leq i < \operatorname*{argmin}_{k < s_j} s_j) \ . \tag{6.20}$$

At the beginning of a signal, no previous step change exists. In this case, the median is taken from the beginning of the signal until the first detected step change s_1. Similarly, at the end of a signal, the median is taken from the last detected step change until the end of the signal.

Step 3: Determine step changes using Δf^{mod}

Based on the reconstructed signal, the magnitude of a step change is simply calculated as the difference between the current and previous quasi steady states:

$$\Delta f^{mod}_{s_i} \equiv \hat{f}^{mod}_{s_i} - \hat{f}^{mod}_{s_{i-1}} \tag{6.21}$$

6.3.3 Validation

The improved algorithm was evaluated against the following two deficits, which are explained in detail in section 5.3:

- Low robustness against narrow peaks,
- Dissimilarity between reconstructed and original signals.

Low robustness against narrow peaks Since the magnitude of step changes is inferred from the median of signal values, narrow peaks do not affect the step-change magnitude at all under the condition that the residual part of the quasi state is longer than the peak width. This is also evident in Fig. 6.14, in which the magnitude of the step change at $k = 10$ was determined correctly despite the narrow peak due to its inrush current.

Dissimilarity between reconstructed and original signals In contrast to the previous method, the reconstructed signal is directly inferred from the original signal. Thus, they are similar. In particular, it is impossible that estimation errors in $\hat{f}^{mod}$ add up, which was the case in the previous method (compare $k > 20$ in Fig. 5.5 and Fig. 6.14).

6.4 Method for classifying fixed-speed motors

In this section, a simple, generally valid classifier is sought that can differentiate motors according to their mechanical load using the measured aggregate current during the transient state of a turn-on event. To this end, two separate conditions must be met:

- A classification must be possible using features calculated from the measured *motor* current,
- The features describing the *motor* current need to be accurately extracted from the measured *aggregate* current.

The first condition is examined in the following subsection 6.4.1, i.e., a method is searched that can classify motors according to their mechanical load using the measured *motor* current. This method and its classification results are currently being published in (Gebbe et al. 2019). The second condition is analyzed in subsection 6.4.4, in which a suitable disaggregation method for deriving the motor current is proposed and evaluated. A preliminary version of that disaggregation method has been published in (Bashir 2017).

6.4.1 Approach

In order to classify motors according to their mechanical output using the measured *motor* current, features from the turn-on transient current were calculated. The transient behavior of the current was used because it is said to be "intimately related to the physical task [a] load performs" (Sultanem 1991) (see subsection 5.4).

As explained in section 2.5, a classifier can be either manually specified or automatically learned based on existing data. The latter approach was chosen here. This means that a classifier was constructed based on training data, and the accuracy of this constructed classifier was determined for test data. This process can be divided into five steps (see Fig. 6.17):

1. Acquire a data set, i.e., measure the currents of several motors driving different types of mechanical loads.
2. Normalize the measured motor currents so that unwanted influence factors are filtered out.
3. Extract features from the motor transient currents.
4. Identify and select suitable features.
5. Classify the transient currents using the extracted suitable features.

The result of the classification in terms of the classification accuracy is then evaluated in subsection 6.4.3.

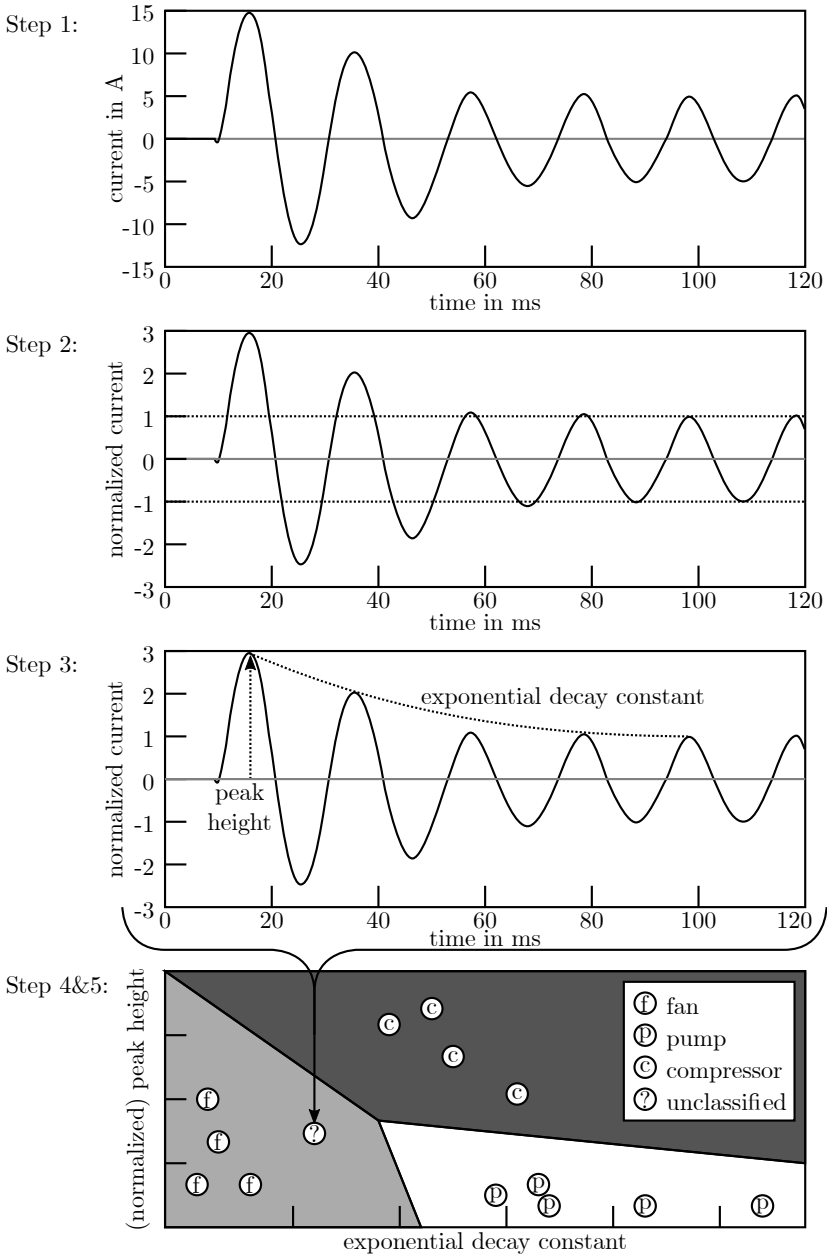

Figure 6.17: Approach for classifying a turn-on transient current

6.4.2 Detailed algorithm

Step 1: Acquire data set

The data set consisted of 21 motors from eight different machines (see Table 6.3). In total, these motors drove eight pumps, four compressors, six fans and three other types of mechanical loads. The vacuum pump is listed as a compressor, since it also transports a gas from one side to the other while increasing its pressure. Only fixed-speed motors were considered because the current of motors with a uncontrolled bridge rectifier featuring an uncontrolled bridge rectifier deviates significantly from a sinus (see subsection 2.4) and would thus require a different treatment.

Table 6.3: List of the analyzed motors categorized according to the containing machine and the type of mechanical load

Machine	Pump	Compressor	Fan	Other mech. load
Thermoform machine - vacuum pump		1		
Thermoform machine - conveyor belt				1
Thermoform machine - motor for winding				1
Thermoform machine - cooling unit	1	1	1	
Heated washing basin	1			
Milling machine - fan for spindle			1	
Milling machine - lubricant pump	1			
Milling machine - cooling lubricant pump	1			
Milling machine - hydraulic pump	1			
Motor driving a generator				1
Pedestal fan			1	
Cooling unit for selective laser sintering machine 1	1	1	1	
Cooling unit for selective laser sintering machine 2	1	1		
Ultrasonic cleaner - fan			1	
Ultrasonic cleaner - fan for drying			1	
Ultrasonic cleaner - circulation pump	1			
Total	**8**	**4**	**6**	**3**

For each motor 2-53 turn-on events were recorded (385 turn-on events in total). For each turn-on event, the current and voltage were recorded for 300 ms, corresponding to approximately 15 periods. Each turn-on event can also be referred to as an item in the context of machine learning.

Step 2: Normalize current

Before the classification, the current was modified in two ways. First, the current of each motor was normalized by dividing it by its peak value during the steady state. Thus, all normalized currents had the same steady-state peak magnitude of 1 A and the only difference between the motors was the transient behavior of the current.

Second, the current was partitioned into half-periods using a zero-crossing approach. The first two half-periods of each turn-on event were omitted for calculating the features. Moreover, the current was potentially multiplied with (-1) such that the current was positive in the third half-period. The reason for this modification was that the transient current is significantly affected by the exact point in time at which the motor turns on with respect to the last zero crossing of the voltage. This effect is the strongest for the first two half-periods (see Fig. 6.18 top). In contrast, after the modification, the current transients of different turn-on events belonging to the same motor often looked nearly identical (see Fig. 6.18 bottom).

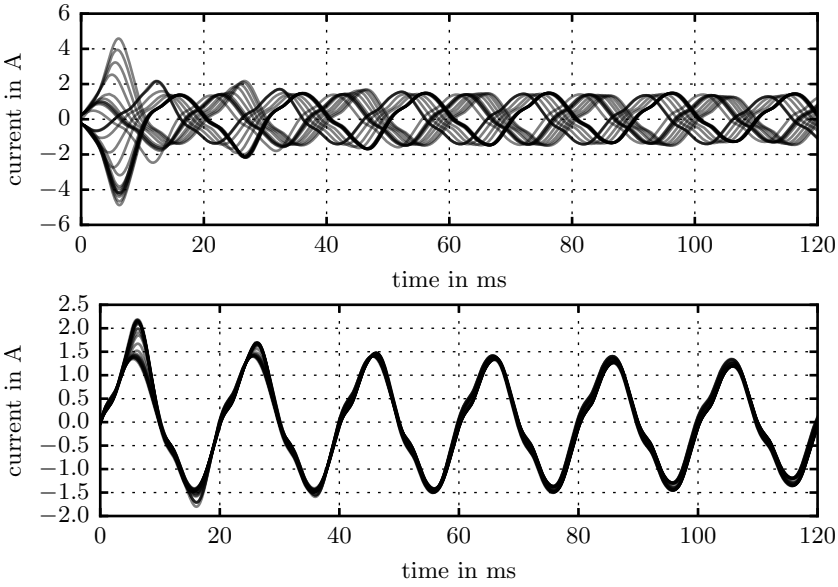

Figure 6.18: Transient current of 27 turn-on events of the heated washing basin before (top) and after (bottom) omitting the first period

Step 3: Define and calculate features

For each turn-on event, several features were calculated. For this purpose, only the time scale of the second to sixth periods of the current after the turn-on event was considered, which corresponds to the first approximately 20-120 ms after a turn-on event. While later times would probably provide useful features too, there is a higher chance that another turn-on event occurs during that time period. For this reason, the duration of the transient was *not* used as a feature, since it can be much longer than 120 ms. The following features were calculated (see summary in Table 6.4).

Table 6.4: List of all features calculated in the case study

Feature category	Number of features in category
Exponential decay constant	4
Line slope constant	4
Peak values, absolute and relative	20
Energy, absolute and relative	10
Energy sum, absolute and relative	10
Magnitude of harmonics	100
Total harmonic distortion of harmonics	5
Presence of local extrema	10
Presence of inflection points	10
Sum	**173**

Exponential decay constant An exponential function of the form $i(t) = i_{max} \cdot e^{-\lambda t} + i_{steady}$ was fitted to the current peaks and the parameter λ was used as a feature. More exactly, this function was fitted to four different signals resulting in four different features: the maxima of the positive half-periods of the current, the minima of the negative half-periods, the maxima of the half-periods of the absolute value of the current and the maxima of the half-periods of the instantaneous power p_{inst}. Thus, five values were considered when fitting the current, and ten values were considered when fitting either the absolute value of the current or the instantaneous power.

Linear slope constant Analogous to calculating the exponential decay constant, a linear slope constant m was calculated by fitting a function of the form $i(t) = i_{max} \cdot m + i_{steady}$. It was also calculated for the four signals specified above.

Current peak values Another set of features comprised the peak values of the current in the second to sixth periods, i.e., the local maxima or minima of each of the corresponding half-periods. In total, five local maxima and five local minima were used as features. These features represent absolute values and make sense in this chapter, since all currents were normalized (see above). However, for a generally valid classifier, relative values are preferable. These can be achieved either by dividing the peak values by the peak current value of the steady state (as was done in this case study) or by dividing them by one of the values themselves. The latter approach was also tested by dividing each peak value by the peak value corresponding to the second half-period of the third period. This particular peak was chosen because it had the lowest coefficient of variation among all 10 peak values. Concluding, both the absolute and the relative peak values were used as features.

Energy Inspired by Chang et al. (2007), the energy of the transient, defined as $e(t_0, \Delta_t) = \int_{t_0}^{t_0+\Delta_t} p_{inst}(t)dt$, was used as a feature. More precisely, the energy of each period from the second to sixth periods was used (five values) along with the *sum* of the energy ranging from the second to either the second, third, fourth, fifth or sixth period (five values). Since these values represent absolute values again, in addition to the absolute values, relative values were calculated by dividing the energy in each period by the energy of the sixth period. The sixth period was chosen because the energy in this period represented the lowest coefficient of variation among the energy of the five periods.

Current harmonics Similar to Leeb et al. (1995), the current harmonics for each period from the second to sixth periods was calculated using a fast Fourier transformation. Only the relative magnitude of the first 20 harmonics was used with respect to the magnitude of the first harmonic, resulting in 100 features in total. Moreover, for each period the total harmonic distortion was calculated, resulting in five more features.

Presence of additional local extrema and inflection points In a perfect sinus signal, there is only one local extrema in the middle of each half-period. However, some currents exhibited multiple local extrema in half-periods. This phenomenon was captured with one feature per half-period, which took the value 1 whenever multiple local extrema appeared. Similarly, an inflection point, at which the curvature of a signal changes, only appears for a perfect sinus when its value approaches zero. In some half-periods, additional inflection points were observed though, and in these cases, a corresponding feature adopted the value 1 and otherwise 0.1 (a value of 0 led to issues when calculating the coefficient of variation).

Step 4: Identify and select suitable features

While a classifier could be constructed using all 173 features, such a classifier would not be considered simple, and it may be difficult to interpret. Instead, a classifier based on only a handful of the most useful features was preferred. A useful feature should exhibit two characteristics. First, the feature values within one class should vary little. This can be quantified using the coefficient of variation defined as $COV = \sigma/\mu$. Second, a high classification accuracy should be achieved using only this feature.

The first characteristic could be checked easily. For each feature, the coefficient of variation within the same motor class (not the same mechanical load type class) was calculated. If the mean coefficient of variation over all 21 motors was above one, the feature was not considered to be a useful feature. In this way, 12 out of the 173 features were omitted, including all four exponential decay constants, amongst others. The residual 161 features were kept for further examination.

The second characteristic is more complex to check, since an actual classification has to be performed. This involves choosing a classifier, training it and determining its accuracy (see details in the next step 5). Such a classification was performed using each of the 161 features *individually*. Based on these results, only the top 50 features resulting in the highest classification accuracy were selected for further processing

Step 5: Classify transient currents

The actual classification can be subdivided into the following five substeps:

1. Prepare the data set to facilitate the classification process.
2. Split the data set into training and test set.
3. Choose a classifier.
4. Train a classifier.
5. Choose a classification accuracy measure.

Prepare data set Before the classification all features were rescaled to $[0, 1]$. Otherwise, features with a high magnitude are likely to dominate the classification process. Furthermore, the number of turn-on events of all motors was equalized to 20. This meant that for some motors, only a fraction of the recorded turn-on events was considered for training and evaluating the classifier, while for other motors, turn-on events were duplicated. Without this modification, the classifier would have prioritized the correct classification of motors with many turn-on events over motors with fewer turn-on events.

Split data set In order to train and evaluate the classifier, the data set was split into a training set for training the classifier and a test set for evaluating the classifier. This was performed using the stratified k-fold cross validation technique with $k = 20$ (Refaeilzadeh et al. 2009). One weakness of the data set was that the number of turn-on events per type of mechanical load was not equal. In machine learning terms, the data set is said to be imbalanced. As a consequence, the classifier would prioritize the correct classification of the class with the highest number of turn-on events, whereas it should consider all classes as equally important. The equal treatment of classes was achieved by modifying the cost function during the training procedure. Therefore, in scikit-learn the parameter class weight was set to "balanced".

Choose classifier Two of the most frequently employed supervised classification techniques are neural networks and support vector machines. While neural networks tend to require a large number of samples (Gebbe et al. 2017c), support vector machines "are well suited to deal with learning tasks where the number of features is large with respect to the number of training instances" (Maglogiannis 2007, p. 13). Since this condition was true for this case study (the number of potential features was approximately half the number of the samples), the support vector machine was chosen. It was implemented using the function "sklearn.svm.SVC" from the python module scikit-learn (Pedregosa et al. 2011). One of the parameters to further specify the support vector machine classifier is the choice of the kernel. Here, three kernels were tested: a linear kernel, a polynomial kernel and a radial basis function kernel.

Train classifier Training the classifier means fitting the parameters of the mathematical model of the support vector machine to the training data such that the classification accuracy is maximized. To this end, the function "fit" provided by scikit-learn was used.

Choose accuracy measure The classification accuracy of the trained classifier was evaluated using the test data. To this end, the predicted labels $\hat{y}$ were compared with the actual labels y. A straightforward classification accuracy measure is the accuracy defined as

$$accuracy(y, \hat{y}) \equiv \frac{1}{N_{items}} \sum_{l \in L} |y_l \cap \hat{y}_l| \ , \tag{6.22}$$

where N_{items} refers to the number of items, and L represents the set of labels. However, this indicator can be misleading. Imagine a case with $N_{items} = 100$, where 10 of the items have the label "A" and the residual 90 the label "B". A classifier which would assign all items to category "B" would have an accuracy of 90 % because 90 items are classified correctly.

Due to this disadvantage, the macro-averaged f1 score was used here. It is defined as

$$
\begin{aligned}
f1_{macro}(y,\hat{y}) \equiv & \frac{2 \cdot p(y,\hat{y}) \cdot r(y,\hat{y})}{p(y,\hat{y}) + r(y,\hat{y})} \text{ , where} \\
r(y,\hat{y}) \equiv & \frac{1}{|L|} \sum_{l \in L} \frac{|y_l \cap \hat{y}_l|}{|y_l|} \text{ and} \\
p(y,\hat{y}) \equiv & \begin{cases} 0 & \text{if } |\hat{y}_l| = 0 \\ \frac{1}{|L|} \sum_{l \in L} \frac{|y_l \cap \hat{y}_l|}{|\hat{y}_l|} & \text{else} \end{cases} ,
\end{aligned}
\tag{6.23}
$$

where $p(y,\hat{y})$ is referred to as precision and $r(y,\hat{y})$ as recall.

For the example described above, the f1 score yields a more helpful classification accuracy measure:

$$
\begin{aligned}
r(y,\hat{y}) = & \frac{1}{2}\left[\frac{0}{10} + \frac{90}{90}\right] = 0.50 \\
p(y,\hat{y}) = & \frac{1}{2}\left[0 + \frac{90}{100}\right] = 0.45 \\
f1_{macro}(y,\hat{y}) \approx & 0.47 \text{ .}
\end{aligned}
\tag{6.24}
$$

6.4.3 Validation

Several classifiers were assessed that differed in terms of the used label of the turn-on events (either the motor or the type of mechanical load), the type of kernel of the support vector machine (linear, polynomial or radial basis function) and the number of considered features (all 161 features with a suitable coefficient of variation, only one of those 161 features or all 1225 possible pairwise combinations of the top 50 useful features). Among the classifiers using only one or two features, only the f1 score of the classifiers yielding the highest f1 score is reported in Table 6.5. Moreover, for classifiers using the mechanical load type as the label, all samples belonging to the category "other type of mechanical loads" were discarded in the training and evaluation phase, since it was not clear whether they were actually similar to each other. Therefore, only the three classes fans, pumps and compressors remained in this case.

When classifying according to the type of mechanical load, f1 scores between 54 and 98 % were achieved with the exception of one f1 score with the value of only 33 % (see Table 6.5). This low score was probably a result of the high number of variable parameters compared to the low number of turn-on events. Similarly, when classifying according to the motor, f1 scores between 50 and 97 % were attained. The features with which the highest accuracies

Table 6.5: Resulting f1 scores for different classifiers (the polynomial kernel is abbreviated to "poly" and the radial basis function kernel to "rbf")

Label	Number of features	Kernel	f1 score	Feature(s), with which f1 score was achieved
Mech. load	161	linear	98 %	
Mech. load	161	poly	33 %	
Mech. load	161	rbf	85 %	
Mech. load	2	linear	79 %	Total harmonic distortion in period 5 + Relative magnitude of 15th harmonic in period 4
Mech. load	2	poly	64 %	Relative peak value in half-period 10 + Presence of inflection points in half-period 6
Mech. load	2	rbf	80 %	Total harmonic distortion in period 5 + Relative magnitude of 15th harmonic in period 4
Mech. load	1	linear	59 %	Total harmonic distortion in period 5
Mech. load	1	poly	54 %	Relative peak value in half-period 11
Mech. load	1	rbf	66 %	Total harmonic distortion in period 5
Motor	161	linear	97 %	
Motor	161	poly	86 %	
Motor	161	rbf	93 %	
Motor	2	linear	76 %	Linear slope constant of the local minima of the current + Sum of absolute energy from period 2 to 3
Motor	2	poly	68 %	Sum of absolute energy from period 2 to 5 + Relative magnitude of seventh harmonic in period 4
Motor	2	rbf	76 %	Linear slope constant of the local minima of the current + Sum of absolute energy from period 2 to 3
Motor	1	linear	52 %	Absolute peak value in half-period 10
Motor	1	poly	50 %	Absolute energy in period 5
Motor	1	rbf	52 %	Absolute peak value in half-period 10

were achieved varied significantly depending on the choice of kernel and label. Among them were the following features:

- The total harmonic distortion in the fifth period,
- The relative magnitude of the 15th current harmonic in the fifth period,
- The linear slope constant of the local minima of the current,
- The absolute current peak values in the tenth half-period as well as the relative peak value in the tenth and eleventh half-period,
- The sum of the absolute energy from period two to three,
- The presence of inflection points in the sixth half-period.

While some features such as the linear slope constant or the sum of the absolute energy from periods two to three clearly describe the transient behavior, other features are extracted from the fifth or sixth period where the transient state of some motors seemed to have already ended.

In conclusion, a classifier was found that can differentiate motors according to their mechanical load with an f1 score of 98 %. However, this classifier is certainly not simple as it uses 161 features. In contrast, if only two of the most useful features are used for classification, an f1 score of at most 80 % is achieved. This example indicates that it is unlikely that a generally valid classifier was found. In other words, the classifier with an f1 score of 98 % would likely misclassify any turn-on events from new motors. This can also be graphically seen in the scatter plots using two features in Fig. 6.19 and Fig. 6.20, in which no strict classification borders separating the different load types are evident. Only some tendencies are apparent such that most motors driving fans had a low total harmonic distortion, a small linear slope and a low energy, compared to motors driving other types of loads.

The high classification accuracy of 98 % according to the mechanical load type can rather be explained by the fact that the motors themselves could be differentiated well with an f1 score of 97 % using all features and with an f1 score of 76 % using only two features (see Table 6.5). This can also be seen in Fig. 6.20, in which the turn-on events belonging to the same motor are grouped closely together, and different clusters for the motors are apparent. This means that two motors can be distinguished with a high certainty using only transient features, even when their steady state value is the same.

The fact that this study did not find a simple, generally valid and sufficiently accurate classifier separating motors according to their mechanical loads does not mean that such a classifier does not exist. In order to conduct the search for such a classifier more thoroughly, the use of electromechanical models with which different types of motors and different types of mechanical loads can be simulated is recommended. However, such simulations are complex (Boghos & Al Jazi 2007; Mohan 2014) and were thus not carried out in this study.

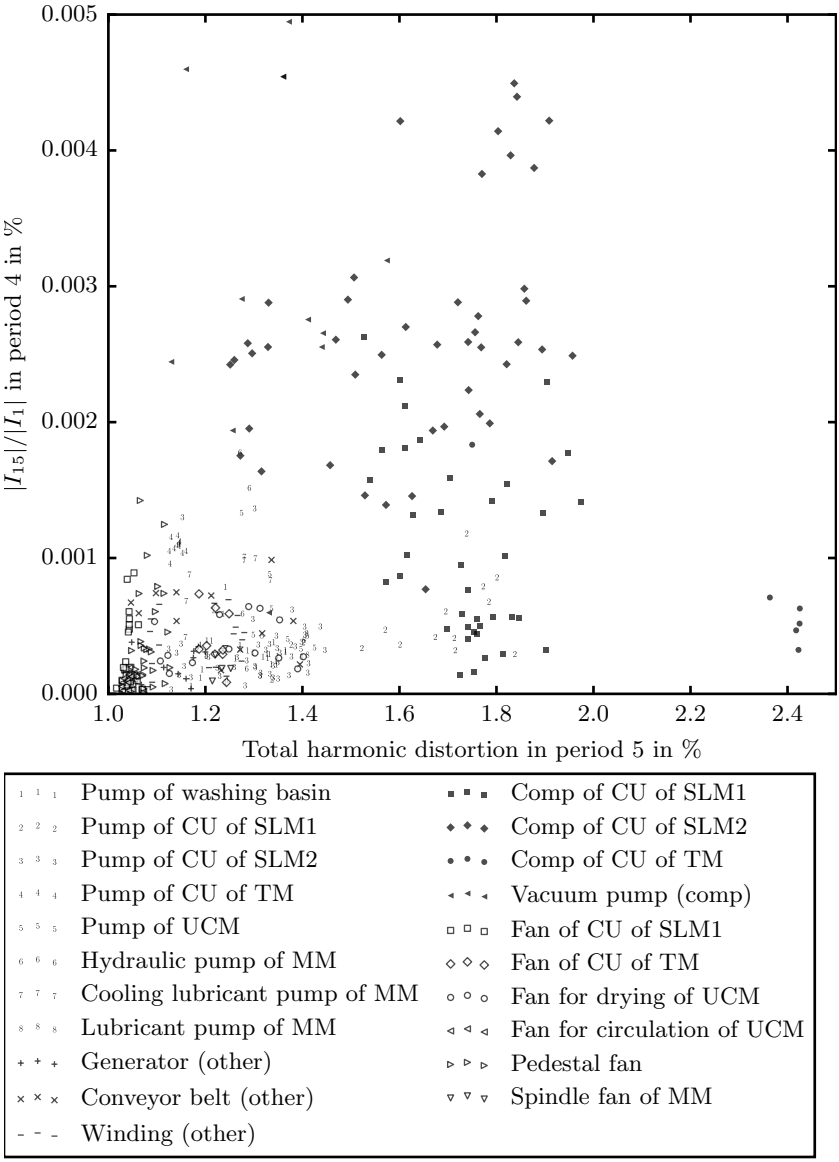

Figure 6.19: Scatter plot of turn-on events. CU=cooling unit, SLM=selective laser sintering machine, TM= thermoform machine, MM=milling machine, UCM=ultrasonic cleaning machine.

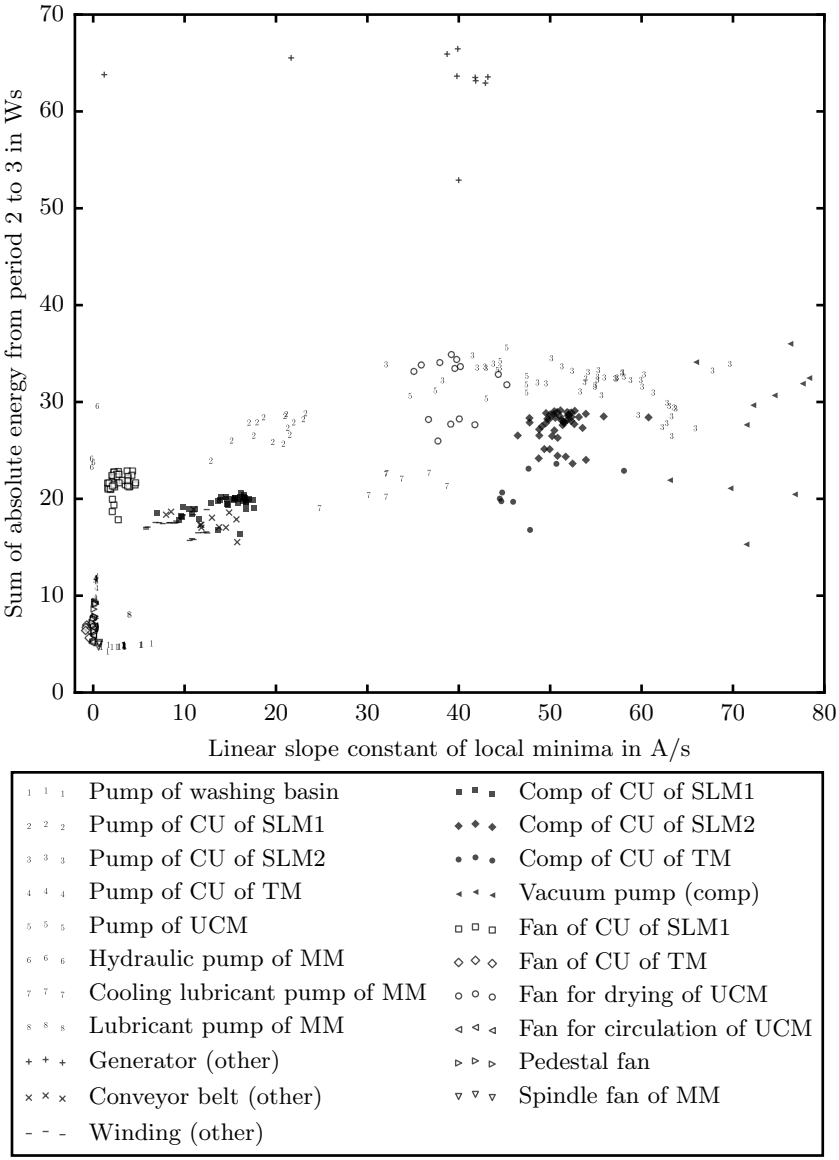

Figure 6.20: Scatter plot of turn-on events. CU=cooling unit, SLM=selective laser sintering machine, TM= thermoform machine, MM=milling machine, UCM=ultrasonic cleaning machine.

6.4.4 Method for extracting transient motor currents

6.4.4.1 Approach

A simple approach for extracting the turn-on transient motor current from an aggregate load is to subtract the measured aggregate current *before* the turn-on event from the aggregate current *after* the turn-on event, assuming that the behavior of all other loads does not change:

$$\begin{aligned} \hat{i}_{motor}^{after}(t) &= i_{agg}^{after}(t) - i_{other}^{after}(t) \\ &\approx i_{agg}^{after}(t) - i_{agg}^{before}(t) \ , \end{aligned} \tag{6.25}$$

where i_{motor} represents the motor current, i_{agg} denotes the aggregate current, i_{other} refers to the current of all other loads and the superscripts before and after indicate the time periods before and after a turn-on event respectively.

However, as indicated in section 5.4, previous works have neither performed this kind of disaggregation nor analyzed its accuracy in comparison with the measured motor current. Instead, it has been implicitly suggested to only extract the feature(s) of the motor current from the feature(s) of the aggregate current. This can be expressed mathematically as follows:

$$\begin{aligned} \vartheta\left(i_{motor}^{after}\right) &= \vartheta\left(i_{agg}^{after} - i_{other}^{after}\right) \\ &\approx \vartheta\left(i_{agg}^{after} - i_{agg}^{before}\right) \\ &= \vartheta\left(i_{agg}^{after}\right) - \vartheta\left(i_{agg}^{before}\right) \ . \end{aligned} \tag{6.26}$$

where ϑ represents a *linear* function, i.e., $\vartheta(a+b) = \vartheta(a) + \vartheta(b)$, with which a feature can be calculated. The majority of the features, including, for example, the active power and the complex current harmonics, are calculated using linear functions. In contrast, the functions used to calculate, e.g., the electric properties $\cos(\phi)$ or the total harmonic distortion are *not* linear.

While this approach is valid, the direct extraction of the motor current instead of the extraction of the feature(s) of the motor current can be helpful. This is because if the motor current can be extracted with an accuracy of 100 % , then it is certain that all features based on the current can also be extracted with an accuracy of 100 %. However, the opposite is not true: if one feature, such as the active power demand, was extracted with an accuracy of 100 %, it does not mean that all other features, e.g., the seventh current harmonic, can also be extracted with an accuracy of 100 %. Therefore, the analysis of the extraction accuracy of the motor current is a helpful indicator for answering the question regarding whether a classification using only the measured aggregate current can be as successful as a classification using the measured motor current.

A new approach is thus proposed, with which the motor current can be extracted from the aggregate current, and its accuracy is evaluated. The approach comprises four steps (see Fig. 6.21):

1. Acquire a data set, i.e., measure the aggregate current as well as the motor current for evaluation purposes.
2. Filter out the current of uncontrolled bridge rectifiers in the aggregate current.
3. Extrapolate the aggregate current before the turn-on event.
4. Estimate the motor current as the difference between the measured aggregate current and the extrapolated aggregate current.

6.4.4.2 Detailed Algorithm

Step 1: Acquire data set The same dataset as described in subsubsection 6.4.2 was used, where not only the current of the motor but also the aggregate current of the whole machine was measured with a time synchronization of approximately 1 μs.

Step 2: Filter uncontrolled bridge rectifier Many aggregate currents exhibited sharp peaks due to the presence of an uncontrolled bridge rectifier in variable speed drives. These peaks were often not perfectly periodic, and they were thus difficult to extrapolate in the subsequent step. To remedy this issue, the current of the uncontrolled bridge rectifier was filtered out using the new disaggregation method described in 6.2. This disaggregation prior to classification is also planned for in the complete preliminary disaggregation concept (see Fig. 4.6). It shall be pointed out that any of the old methods for filtering uncontrolled bridge rectifier could not have been employed for this purpose, as they do not target the current directly. The benefit of this filtering is evaluated in subsubsection 6.4.4.3.

Step 3: Extrapolate aggregate current In order to extract the motor current from the aggregate current, a simple subtraction as described in equation 6.27 is possible. However, this can lead to errors if the measured aggregate current before the turn-on event exhibits non-periodic irregularities. A more robust approach is to infer the *average* periodic behavior of the aggregate current before the turn-on event and then extrapolate it. This was achieved by first performing a discrete Fourier transformation (see subsection 2.1) over $N_{period} = 15$ periods, followed by an inverse discrete Fourier transformation using only those frequencies that are multiples of N_{period}. Moreover, all frequencies below N_{period} were included in the inverse Fourier transform so

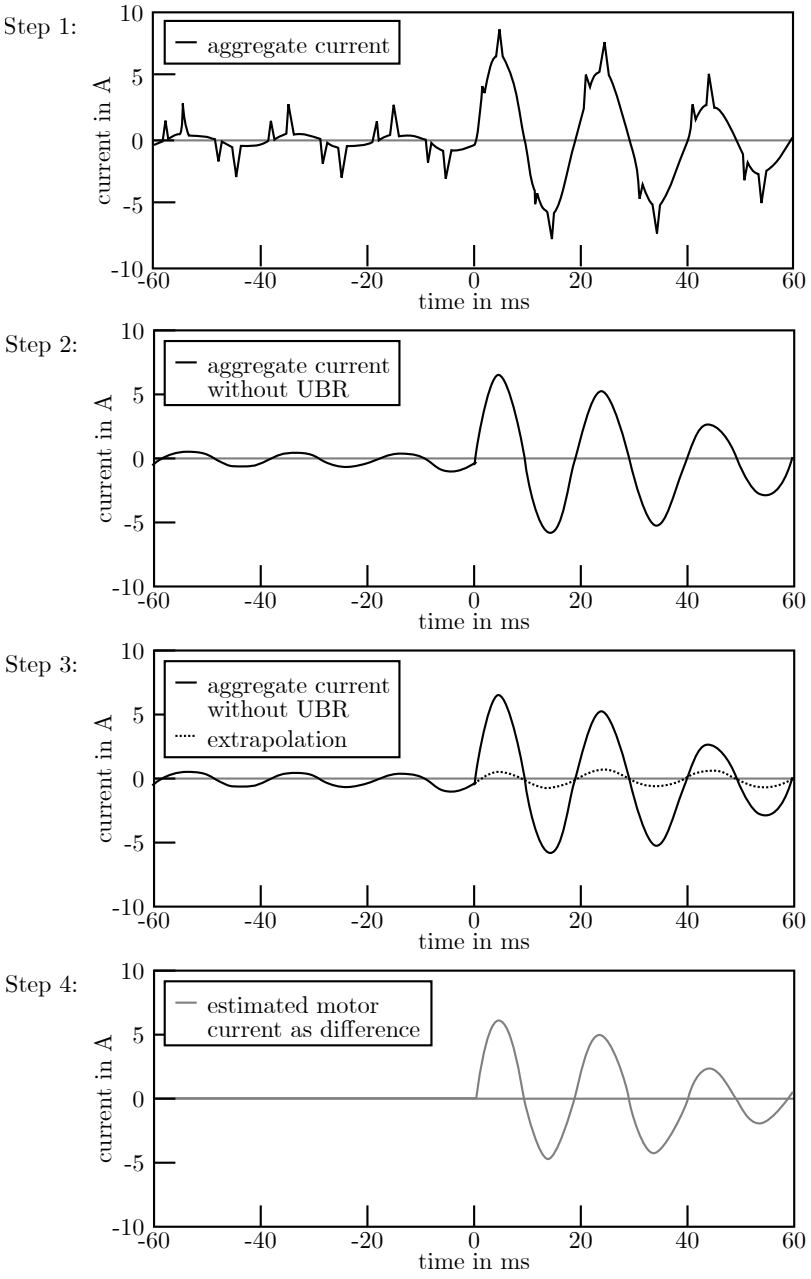

Figure 6.21: Approach for extracting the turn-on transient motor current from an aggregate current

that any underlying slow oscillations of the current due to, e.g., a varying mechanical load could be modeled.

The value of N_{period} can be chosen freely within certain limits. If a low value of N_{period} is chosen (e.g., $N_{period} = 3$), the averaging window is short, and the current inferred through the inverse Fourier transform may be affected by non-periodic irregularities. On the other hand, if a high value of N_{period} is chosen (e.g., $N_{period} = 50$), it is likely that other turn-on events occur during such a long time period and that the assumption of a periodic aggregate current in that time period is not fulfilled.

The accuracy of the estimated aggregate current using the inverse Fourier transform $\hat{i}_{agg}$ was assessed with the following indicator:

$$\epsilon_{agg} = \frac{\int |\hat{i}_{agg}^{before}(t) - i_{agg}^{before}(t)| dt}{\int |i_{agg}^{before}(t)| dt} \ . \tag{6.27}$$

For the calculation of the error ϵ_{agg} the time interval [t_0-300 ms, t_0-10 ms] was used, where t_0 refers to the time of the turn-on event. This time interval corresponds approximately to the last 15 periods before the turn-on event.

Step 4: Estimate motor current The current of the motor was then estimated through a simple subtraction:

$$\hat{i}_{motor}^{after}(t) = i_{agg}^{after}(t) - \hat{i}_{agg}^{after}(t) \ . \tag{6.28}$$

The accuracy of the estimation was evaluated in terms of

$$\epsilon_{motor} = \frac{\int |\hat{i}_{motor}^{after}(t) - i_{motor}^{after}(t)| dt}{\int |i_{motor}^{after}(t)| dt} \ . \tag{6.29}$$

For the calculation of the error ϵ_{motor}, the time interval [t_0+20 ms, t_0+180 ms] was used, which approximately corresponds to the second to eighth full periods. Any subsequent periods were irrelevant since they were not used for the classification of the turn-on events (see feature definitions in subsection 6.4.1).

6.4.4.3 Validation

Two aspects of the new extraction method are evaluated in the this subsubsection:

- The benefit of step 2, i.e,. filtering out the current of uncontrolled bridge rectifiers;
- The accuracy of the extraction of the transient motor current quantified in terms of ϵ_{motor} and ϵ_{agg}.

Benefit of filtering out uncontrolled bridge rectifiers By filtering out uncontrolled bridge rectifiers, the errors ϵ_{agg} and ϵ_{motor} could be reduced for approximately 75 % of the 244 turn-on events (see Fig. 6.22, where the errors were determined both with and without filtering the uncontrolled bridge rectifier current). While both errors could be reduced by a factor of 70-100 % for the majority of the turn-on events, for some turn-on events the errors were even reduced by a factor of up to 10 % (see example in Fig. 6.23). For a minority of the turn-on events, the error increased when the uncontrolled bridge rectifier current was filtered. The reason for an increase was that the filtering of the uncontrolled bridge rectifier current did not work perfectly and thus introduced more non-periodic irregularities than before. It shall be pointed out that in such cases the increase in the errors was almost always below 10 %, though.

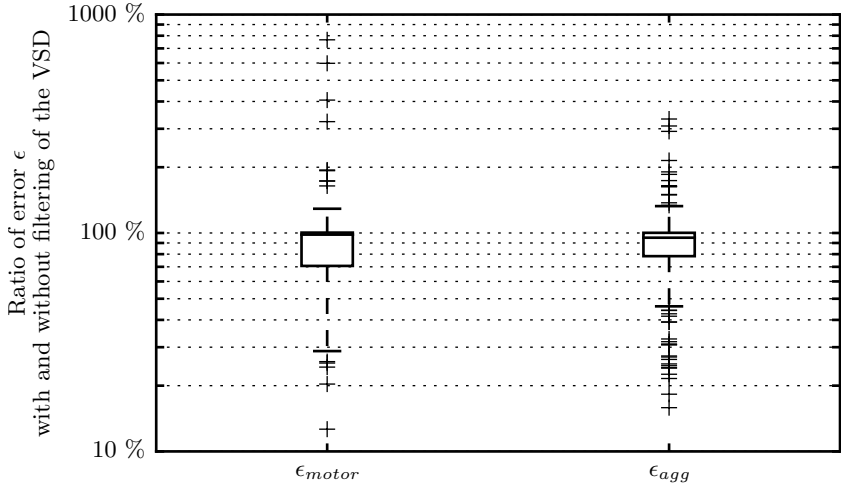

Figure 6.22: The ratio of the errors ϵ_{motor} and ϵ_{agg} with and without filtering of the uncontrolled bridge rectifier (UBR) for 244 turn-on events

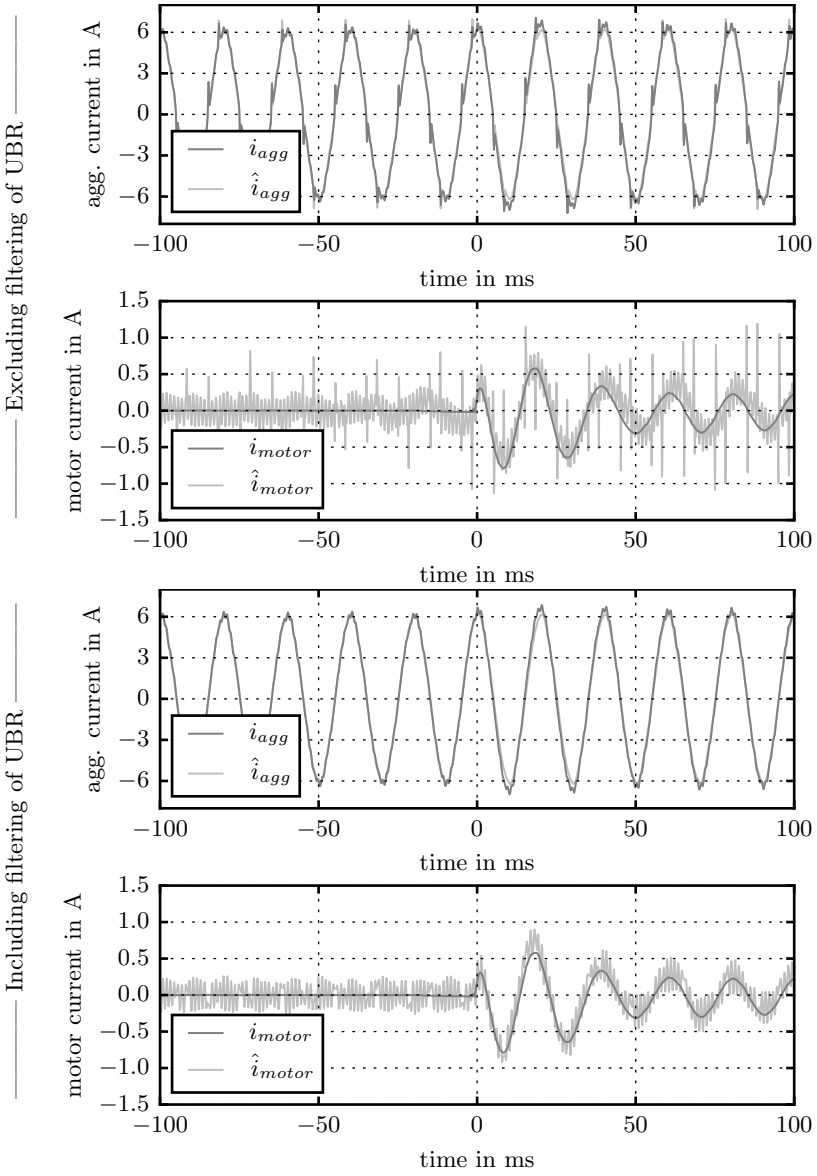

Figure 6.23: Aggregate current and motor current without filtering of the uncontrolled bridge rectifier (top two rows, $\epsilon_{motor} = 116$ %) and with such filtering (bottom two rows, $\epsilon_{motor} = 65$ %)

Accuracy of extraction The error ϵ_{motor} in the extraction of the motor current varied significantly for all 420 turn-on events, ranging from less than 0.3 % to 3,000 % with a median of 5 % (see left subplot in Fig. 6.24). This median error can be interpreted as a success, since an error of $\epsilon_{motor} = 5$ % means that the feature values calculated from the extracted motor current $\hat{i}_{motor}$ would also likely deviate by 5 % or less from the feature values calculated from the measured motor current i_{motor}. Moreover, even motor currents that have been estimated with an error of $\epsilon_{motor} = 65$ % demonstrate a macrosopic behavior that is similar to the one of the measured motor current (see bottom row in Fig. 6.22). Therefore, features such as the linear slope or the energy per half-period might still be calculated accurately. To conclude, *if* a classification of the motors using the measured *motor* current would be possible, then it is likely that the same classification could be achieved using only the measured *aggregate* current.

Next, the reasons for both the large spread of the error ϵ_{motor} and the error being larger than 10 % for some turn-on events is analyzed. To this end, it is helpful to represent the error ϵ_{motor} as a multiplication of two factors:

$$\begin{aligned}
\epsilon_{motor} \equiv & \frac{\int |\hat{i}^{after}_{motor}(t) - i^{after}_{motor}(t)| dt}{\int |i^{after}_{motor}(t)| dt} \\
= & \frac{\int |(i^{after}_{agg}(t) - \hat{i}^{after}_{other}(t)) - i^{after}_{motor}(t)| dt}{\int |i^{after}_{motor}(t)| dt} \\
= & \frac{\int |\hat{i}^{after}_{other}(t) - i^{after}_{other}(t)| dt}{\int |i^{after}_{motor}(t)| dt} \\
\approx & \frac{\int |\hat{i}^{before}_{other}(t) - i^{before}_{other}(t)| dt}{\int |i^{after}_{motor}(t)| dt} \\
= & \frac{\int |\hat{i}^{before}_{agg}(t) - i^{before}_{agg}(t)| dt}{\int |i^{after}_{motor}(t)| dt} \\
= & \underbrace{\frac{\int |\hat{i}^{before}_{agg}(t) - i^{before}_{agg}(t)| dt}{\int |i^{before}_{agg}(t) dt|}}_{=\epsilon_{agg}} \underbrace{\frac{\int |i^{before}_{agg}(t)| dt}{\int |i^{after}_{motor}(t)| dt}}_{\equiv \kappa} .
\end{aligned} \tag{6.30}$$

This means that a low ϵ_{motor} can only be achieved with a low value of ϵ_{agg} and a low value of κ. This makes sense: a high error ϵ_{agg} means that the aggregate current could only be fitted poorly using the inverse Fourier transform. In this case, the motor current will likely be estimated with a high error too. On the other side, a high value of κ means that the current of the motor is much smaller than the sum of the currents of all other loads. In that case, even small deviations in ϵ_{agg} can lead to large errors of ϵ_{motor}.

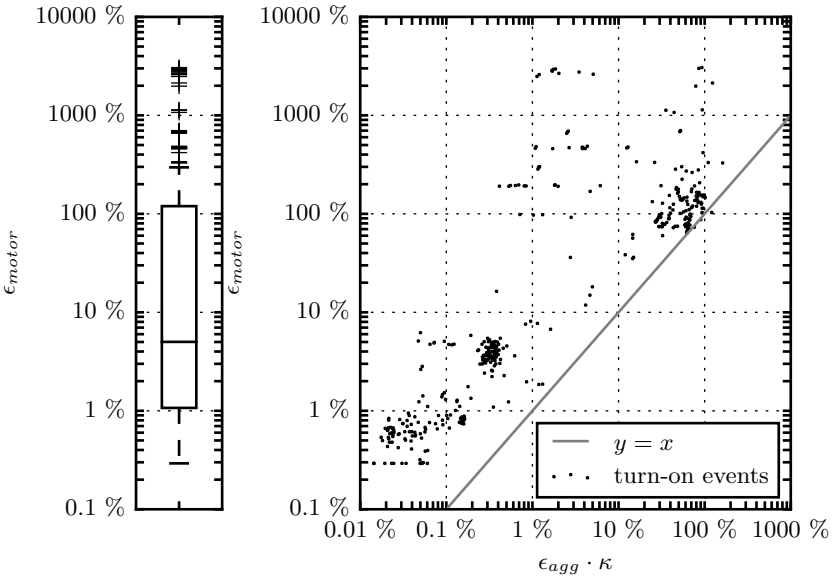

Figure 6.24: Evaluation of the error ϵ_{motor} with respect to $\epsilon_{motor} \cdot \kappa$

That the relation derived in equation 6.30 holds true, is demonstrated in Fig. 6.24. In most cases, ϵ_{motor} is a few percent larger than $\epsilon_{agg} \cdot \kappa$. The fact that it is not equal but slightly larger is due to the following two reasons. First, $|\hat{i}_{other}^{after} - i_{other}^{after}|$ was approximated in equation 6.30 with $|\hat{i}_{other}^{before} - i_{other}^{before}|$. In general though, the difference will be larger in the time interval *after* the turn-on event than in the time interval *before* the turn-on event, since $\hat{i}_{other}$ is estimated based on the time period *before* the turn-on event. Second, the measurement of both the aggregate current and the motor current comprises inherent measurement inaccuracies from, e.g., the current clamps in the order of magnitude of a few percent.

Some turn-on events do not follow equation 6.30. More specifically, the inequalities $\epsilon_{motor} > 10 \cdot \epsilon_{agg} \cdot \kappa$ and $\epsilon_{motor} > 10\ \%$ hold true for 57 turn-on events. In all of these events, another switching event occurred either at the same time as the turn-on event of the motor or during the first periods of the transient. In these cases, an accurate extraction is not possible.

In short, it has been demonstrated that large errors of ϵ_{motors} can be either explained by overlapping switching events or by a high value of $\epsilon_{agg} \cdot \kappa$. In this paragraph, it is analyzed whether ϵ_{agg} or rather κ is responsible for large values of ϵ_{motors}. To this end, both factors are plotted as a scatter plot in Fig. 6.25. It can be observed that for the majority of the cases $\epsilon_{agg} < \kappa$, and also $\epsilon_{agg} \leq 20\ \%$ almost always. All turn-on events with $\epsilon_{agg} > 20\ \%$ can be

attributed to two machines whose current was significantly affected by the presence of an uncontrolled bridge rectifier in a variable speed drive. For these machines the filtering of the uncontrolled bridge rectifier did not always work perfectly, resulting in a high estimation error ϵ_{agg}.

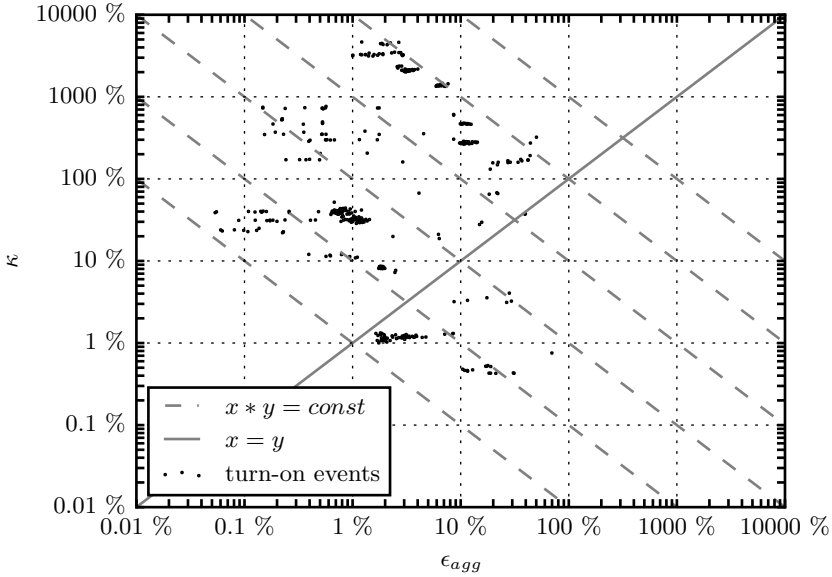

Figure 6.25: Evaluation of the influencing factors ϵ_{agg} and κ. The dashed lines represent a constant value of $\epsilon_{motor} \cdot \kappa = \{0.01\%, 0.1\%, 1\%, 10\%, 100\%, 1000\%\}$ and thus correspond to the vertical grid lines in Fig. 6.24

In summary, an error ϵ_{motor} of above approximately 10 % was a result of one of the following conditions:

- Another electric load switched on or off either at the same time as the turn-on event of the examined motor or during its transient state.
- The current magnitude of the motor was very small compared to the current magnitude of all other loads. In this case, even small approximation errors ϵ_{agg} led to large errors in ϵ_{motors}.
- In two machines variable speed drives featuring uncontrolled bridge rectifiers were present and they could not always be effectively filtered. In these cases, the average aggregate current $\hat{i}_{agg}^{before}$ was estimated with an error ϵ_{agg} of larger than 20 %, which makes the correct estimation of $\hat{i}_{motor}^{after}$ unlikely.

7 Implementation

The combined measurement method based on disaggregation, illustrated in Fig. 6.1, was implemented in python 3.5.3, resulting in several thousand lines of code. Some noteworthy details concerning the implementation of the disaggregation method based on switching events as well as concerning the employed measurement equipment are explained in section 7.1 and section 7.2 respectively.

The combined measurement method, *excluding* the labeling, was then applied to seven machines used in manufacturing. The labeling was omitted, since the labeling using the transient current was already analyzed with real data in section 6.4. Other labeling methods, e.g., based on the power factor, represent the state of the art and were thus not further examined in this thesis. The results of the measurements are presented in section 7.3, and they are critically discussed in section 7.4.

7.1 Details concerning event detection and clustering

While most individual disaggregation methods presented in Fig. 6.1 were described in detail in the respective sections in chapter 6, only part of the disaggregation method based on switching events, namely the detection of the events, was explained in section 6.3. The missing information is presented next:

Switching events were detected by applying the function ξ defined in equation 5.3 to the residual aggregate active power $p_{residual}$. While it is possible to additionally use other electric properties for the event detection, it was found that the events were most pronounced in the active power, the reactive power and the fundamental current harmonic. More exactly, the signal-to-noise ratio, which was measured as the median of a running coefficient of variation, was found to be the highest in those signals.

For each detected switching event, the step-change magnitude in the electric properties active and reactive power as well as the real and imaginary parts of the current harmonics I_1, I_3, I_5, I_7 and I_9 were calculated according to equation 6.21. Only a fraction of all possible current harmonics was used because the other ones exhibited a lower signal-to-noise ratio. A lower signal-to-noise ratio means that the detected step-change magnitude of an ideal two-state

load would not always be the same. Therefore, the inclusion of a harmonic with a low signal-to-noise ratio would likely deteriorate the clustering result. Based on the step changes of the real and imaginary parts of the five current harmonics, their norms were calculated. These norms, plus the active and reactive power, formed the feature vector, which characterizes each event.

In two cases, two different two-state loads were observed to act together as a multi-state load. This means that they turned on at exactly the same time but turned off at different times. In these cases, the turn-on event was manually split into two events. This manual intervention could be automated in the future, as several approaches have already been presented in literature (see subsection 3.7.1).

The events were then clustered based on the *absolute* feature vector so that turn-on and turn-off events were assigned to the same cluster. Before clustering, each feature was rescaled to the interval $[0, 1]$. The features corresponding to the active power, the reactive power and the norm of the first current harmonic were weighed twice as much as the residual features, since their signal-to-noise ratio was higher. For the clustering task, the agglomerative clustering method using the average Euclidean distance between clusters was employed, since its result can be easily retraced using the graphical representation as a dendrogram (Rousseeuw 1987). An important parameter is the threshold distance, above which clusters are considered to be different. This parameter effectively determines the number of clusters. In this thesis, it was chosen manually with the help of the resulting dendrogram. However, several approaches exist for determining the parameter automatically (Halkidi et al. 2001; Milligan & Cooper 1985; Wagner & Wagner 2004), and they could be implemented in the future. Also, the validity of a cluster can be checked by requiring that all events in one cluster should alternate between turning on and turning off.

One or two cluster typically comprised dozens of false positive events with a low step-change magnitude. Such clusters were automatically discarded by examining the coefficient of variation of the absolute active power step changes in each cluster and analyzing the alternation between the turn-on and turn-off events.

7.2 Measurement equipment

The aggregate current and voltage were measured with a sample frequency of 10 kHz using a data acquisition hardware of type DS-NET from the company DEWESoft GmbH. A V4-HV module was used for measuring the voltage, and a V8 module combined with current clamps was employed to measure the current. As current clamps, the model WZ12B from the company GMC-I Messtechnik GmbH were used, for which a measurement error of $\epsilon(t) = \pm 1.5\ \% \cdot i(t) \pm 1mA$

is stated. Even though they are only specified for a frequency range of 45 Hz to 500 Hz, it was experimentally determined by both the author and the manufacturer that they measure a current with a frequency of 10 kHz with an attenuation factor of only a few percent (see Fig. 7.1). According to the Nyquist–Shannon sampling theorem (Shannon 1949), the current clamps are thus appropriate for calculating the highest current harmonic used in this implementation, which is the ninth harmonic correlating to a frequency of 450 Hz.

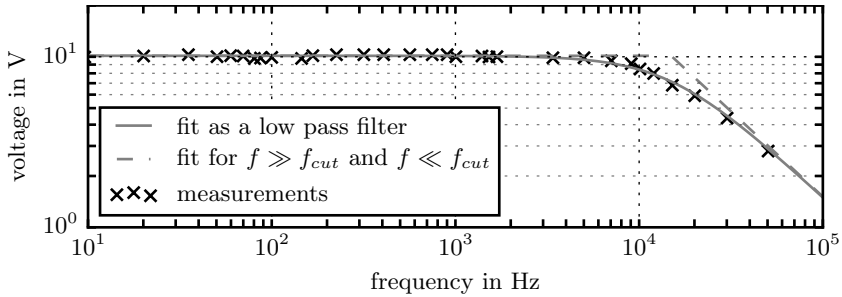

Figure 7.1: Measured frequency response of the utilized current clamps in this thesis, determined using an analog signal generator. To the measured data a first-order low pass filter was fitted as $v(f) = v_0/\sqrt{1 + (f/f_{cut})^2}$. The current clamps return a voltage signal.

In order to assess the result of the disaggregation method, not only the current and the voltage of the aggregate load were measured with the hardware, but also the current of all individual loads with a time synchronicity of approximately 1 μs.

7.3 Results for application examples

The complete disaggregation method was applied to seven aggregate loads:

- Thermoform machine,
- Selective laser machine - phase one,
- Selective laser machine - phase two,
- Vacuum-based handling equipment for carbon composites,
- Milling machine,
- External cooling device,
- Heated washing basin.

These machines were chosen out of the 18 machines analyzed in section 4.2 based on the following criteria: accessibility to the machine, availability of measuring the voltage and current of all individual loads and the informative value of the disaggregation result, i.e. how much insight about the capabilities of the combined aggregation method can be gained from the application example.

The informative value was low if an aggregate power could be easily disaggregated into its constituent parts. This was the case, if only one or two individual loads consumed any noticeable electric power or if few switching events were recorded. In contrast, the informative value was also low if the aggregate power could *not* be easily disaggregated into its constituent parts because of already known limitations of the combined disaggregation method. For example, the machine for folding cardboard boxes comprised 13 variable speed drives and apart from that only a small DC power supply with a negligible power demand compared to those (see section A.1). Since all 13 variable speed drives are of the three-phase type, they cannot be distinguished using the method for extracting uncontrolled bridge rectifiers. Moreover, the power demand of the DC power supply can also not be extracted due to its negligible amount. Thus, the combined disaggregation method detects only one load, which represents the sum of all variable speed drives. Showing this result is of little informative value. Another example is represented by machines in which a one-phase uncontrolled bride rectifier is connected between two phases instead of between a phase and the neutral line. While this electric structure results in the same kind of peaks as described in section 2.4, the peaks appear at different times which are not taken into consideration currently in the current algorithm (see subsection 6.2). As such an electric structure was rare, it was not further analyzed.

The seven selected aggregate loads listed above are representative without loss of generality as they comprise the four most frequent load classes (see section 4.2), i.e., fixed-speed motors, motors fed by a variable speed drive, Joule heating elements and rectifiers, in different combinations and variations

(e.g., a motor driving a pump and a motor driving a fan) plus a semiconductor laser. Therefore, it can be assumed that equivalent disaggregation results can be achieved for any other machine which consists of these four load classes. This conditions holds true for the majority of the machines (see section 4.2).

Most of the machines listed above represent a three-phase load. In these cases, only the most interesting phase in terms of number of loads and number of switching events was chosen for the application. In the case of the selective laser machine, the aggregate load in each phase differed significantly though. Therefore, two phases were analyzed for this machine. Only a fraction of the measured time was used for the application, since most events were repetitive, and thus no additional information was gained by presenting a longer time period. Moreover, it simplified the graphical presentation of the disaggregation results.

The disaggregation results illustrated in Fig. 7.2 to 7.8 are presented using the following elements:

- An area chart in which the *estimated* active power demand $p_{est} : \mathbb{Z} \mapsto \mathbb{R}$ of each load is displayed.
- A table in which the actual loads corresponding to the estimated loads are described. If a load comprises a single-phase or three-phase uncontrolled bridge rectifier, it is marked in the description as (UBR1ph) or (UBR3ph), respectively. Moreover, the table lists three quantitative indicators:
  - The *measured* energy of the load calculated as $e = \sum_k |p_{meas,k}|$.
  - The error of the disaggregation result quantified as $\Delta e = \sum_k |p_{meas,k} - p_{est,k}|$. Therefore, the calculated active power demand was downsampled to 10 periods or approximately 200 ms as stated in the norm (IEC 61000-4-30:2015 2015).
  - The accuracy calculated as $acc = 1 - \Delta e/e$, which coincides with the definition in eq. 1.1. It shall be noted that even in case of a perfect disaggregation, the accuracy is likely to be a few percent less than 100 % due to the inaccuracies of the measurement hardware. A weighted average accuracy was also determined for the aggregate load and it is denoted by the description "Sum".
- A caption text in which the disaggregation result is briefly commented, especially if an accuracy $acc \ll 85$ % was achieved.

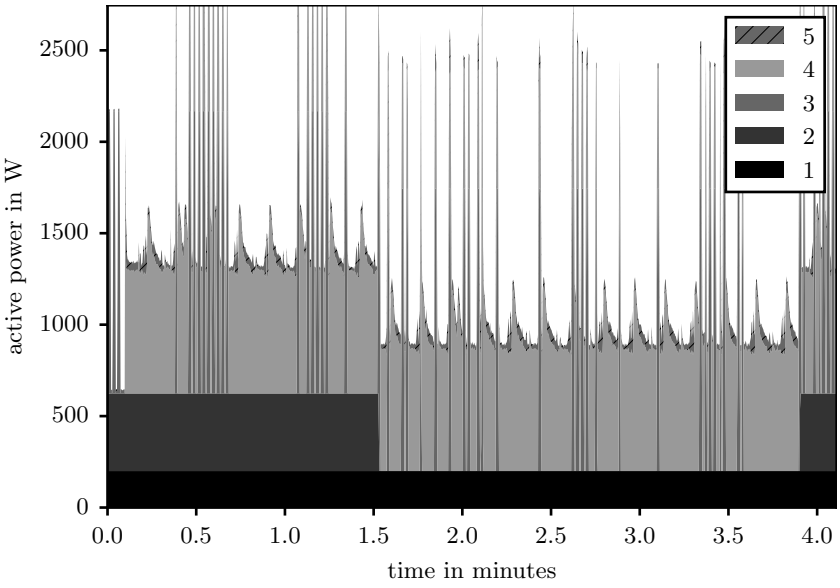

Label	Load	e in Wh	Δe in Wh	acc
1	Rest: Two motors for winding, two fans, DC supply, conveyor belt	14.2	1.7	88 %
2	External cooling device	16.3	4.0	76 %
3	Heating	17.3	1.2	93 %
4	Motor driving a vacuum pump	43.5	4.7	89 %
5	Two variable speed drives (UBR3ph)	4.1	0.1	97 %
	Sum	**95.4**	**11.7**	**88%**

Figure 7.2: Disaggregation result for a thermoform machine. Apart from the external cooling device, all loads were extracted with an accuracy of nearly 90 % or more. Particular attention can be paid to the power demand of the fixed-speed motor driving the vacuum pump. Despite its continuous variation it was estimated with an accuracy of 89 %. Similarly, the two variable speed drives comprising a three phase uncontrolled bridge rectifier were extracted with an accuracy of 97 % despite their low contribution to the aggregate power demand. The low accuracy of the external cooling device can be explained by the fact that four turn-on and four turn-off events with a magnitude of only 80 W between 1.5 and 4 minutes were falsely classified as noise. A more intelligent clustering algorithm is likely to classify these events correctly.

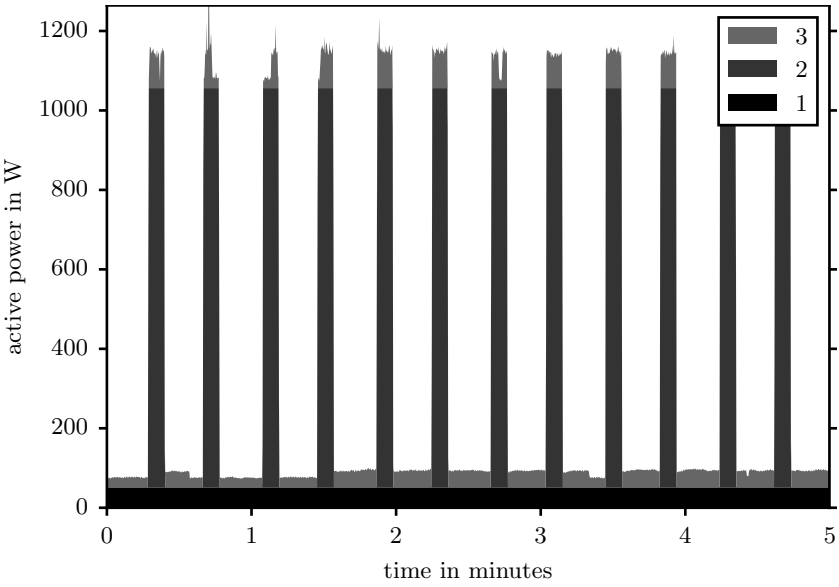

Label	Load	e in Wh	Δe in Wh	acc
1	Baseload of laser		*included below*	
2	Laser	26.8	1.5	95%
3	DC power supply (UBR3ph)	3.6	1.5	59%
	Sum	**30.4**	**2.9**	**90%**

Figure 7.3: Disaggregation result for the first phase of a selective laser machine. This phase only comprises two loads: a laser and a three-phase DC power supply. The laser was identified as two separate loads corresponding to the base load and the additional power demand when activated. Its power demand was estimated with an accuracy of 95 %. The residual DC power supply featuring a three-phase uncontrolled bridge rectifier was extracted with an accuracy of only 59 %. The reason is that the current of the activated laser was not perfectly sinusoidal but was instead characterized by a large share of high-frequency harmonics resulting in a jagged shape. Therefore, the two typical current peaks of the three-phase uncontrolled bridge rectifier were barely observable in the aggregate current.

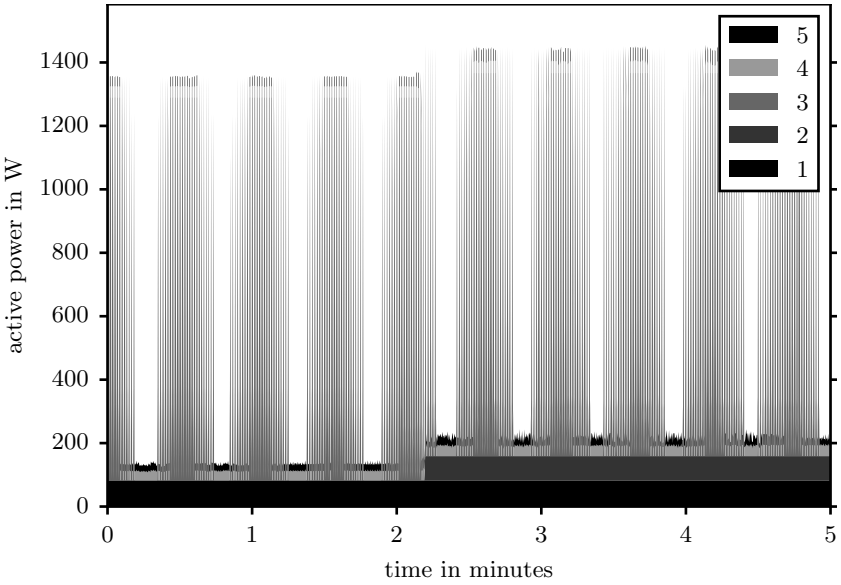

Label	Load	e in Wh	Δe in Wh	acc
1	Computer and fan	7.6	0.8	89%
2	Air circulation fan	5.8	2.2	62%
3	Heating	32.8	5.2	84%
4	DC supply (UBR3ph)	3.2	1.0	69%
5	Motor for lifting platform (UBR1ph)	2.2	0.5	77%
	Sum	**51.6**	**9.7**	**81%**

Figure 7.4: Disaggregation result for the second phase of a selective laser machine. The load with the highest energy demand was a heating element, which was extracted with an accuracy of only 84 %. In fact, some of its active steady states were not detected at all because they lasted shorter than the detection window length $|D_k|$ of 10 periods (see section 5.3). The motor driving the air circulation fan exhibited an atypical turn-on transient behavior lasting several seconds in which the active power demand varied continuously (see Fig. 7.10), which explains its low accuracy of 62 %. A noteworthy fact is that this aggregate load comprised *both* a single-phase and a three-phase uncontrolled bridge rectifier. Both could be extracted using the method described in section 6.2 with an accuracy of approximately 80 % and 70 %. The error is due to the fact that their current peaks overlapped slightly.

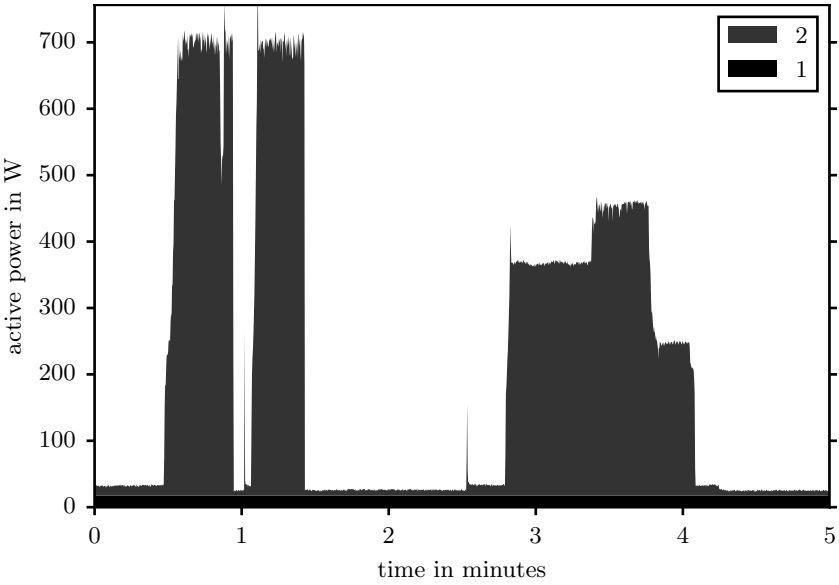

Label	Load	e in Wh	Δe in Wh	acc
1	Two DC power supplies	2.0	0.6	72%
2	Fan (UBR1ph)	16.2	0.7	96%
	Sum	**18.2**	**1.3**	**93%**

Figure 7.5: Disaggregation result for a vacuum-based handling equipment for carbon composites. The active power demand of the aggregate load was dominated by a fan whose motor was controlled by a variable speed drive featuring a single-phase uncontrolled bridge rectifier. Its power demand was extracted with 96 % accuracy. This example reveals that the disaggregation method for uncontrolled bridge rectifiers also works well for scenarios in which the rectifier contributes a dominant share to the aggregate active power demand. The residual power demand can be linked to two DC power supplies, which were estimated with an accuracy of 72 %. The error is due to the fact that the power demand of the fan was estimated a few percent too high in the inactive phases. This small relative error for the fan translated into a high relative error for the power supplies, since the power demand of the fan was significantly higher than that of the power supplies.

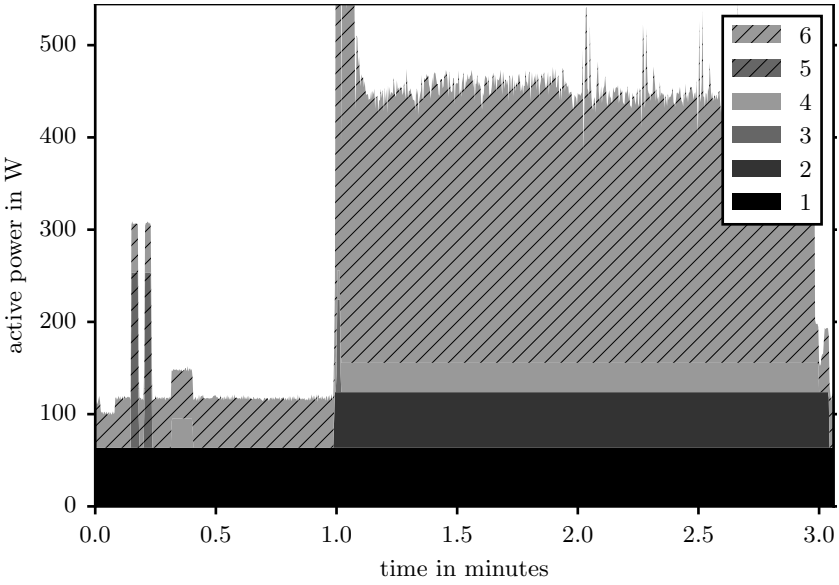

Label	Description of load	e in Wh	Δe in Wh	acc
1	Residual loads: pump for lubricants and electronics	2,62	0,63	76%
2	Fan for spindle	1.85	0.27	85%
3	*False positive*	0.00	0.02	∞
4	Pump for cooling lubricant	0.72	0.40	45%
5	Pump for hydraulic	0.21	0.03	87%
6	Variable speed drive (UBR3ph)	11.53	0.83	93%
	Sum	**16.9**	**2.2**	**87%**

Figure 7.6: Disaggregation result for a milling machine. The variable speed drive, the hydraulic pump and the spindle fan were extracted with accuracies of 85 % and more. Despite this suitable result, the low estimation error of 7 % for the variable speed resulted in an overestimation of the active power demand of the pump for the cooling lubricant which led to an accuracy of only 45 %. The imperfect disaggregation of the variable speed drive also yielded a false positive with a brief active state at around 1:00 min. Shortly before this false positive, the cooling lubricant pump and the spindle fan turned on simultaneously. This event was spitted manually, since the two loads turned off at separate times.

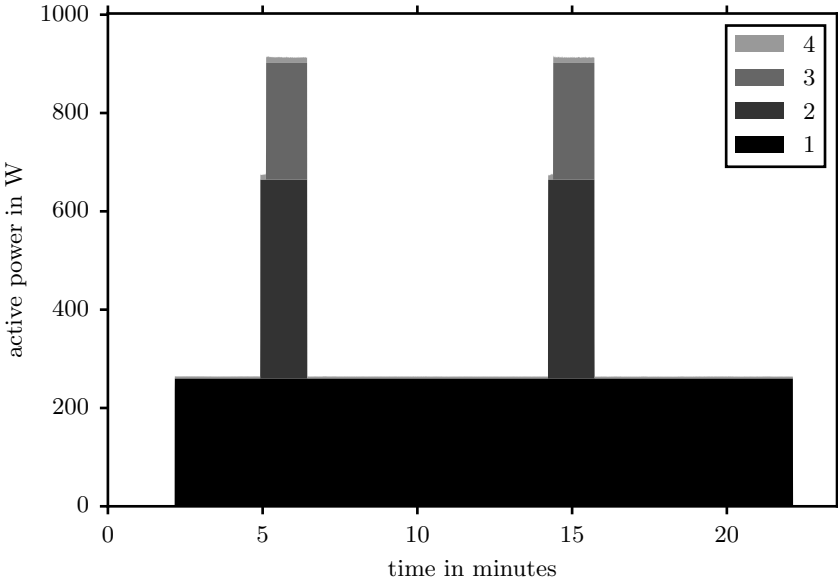

Label	Description of load	e in Wh	Δe in Wh	acc
1	Pump	86.9	0.5	100%
2	Compressor	23.8	3.5	85%
3	Fan	4.0	6.7	-68%
4	DC power supply (UBR3ph)	1.2	0.5	58%
	Sum	**115.9**	**11.1**	**90%**

Figure 7.7: Disaggregation result for an external cooling device. While the power demand of the pump and compressor were extracted with a satisfactory accuracy of 100 % and 85 % respectively, the accuracy for the fan was in fact negative, corresponding to a disaggregation error ϵ of 168 %. The reason is that the turn-on event exhibited an atypical shape due to the oscillating power demand of the compressor (see Fig. 7.9), resulting in an overestimation of the step-change magnitude. Oscillations of the current also masked the current peaks of the DC power supply, whose active power demand was small compared to the other loads. This explains its rather low accuracy of only 58 %.

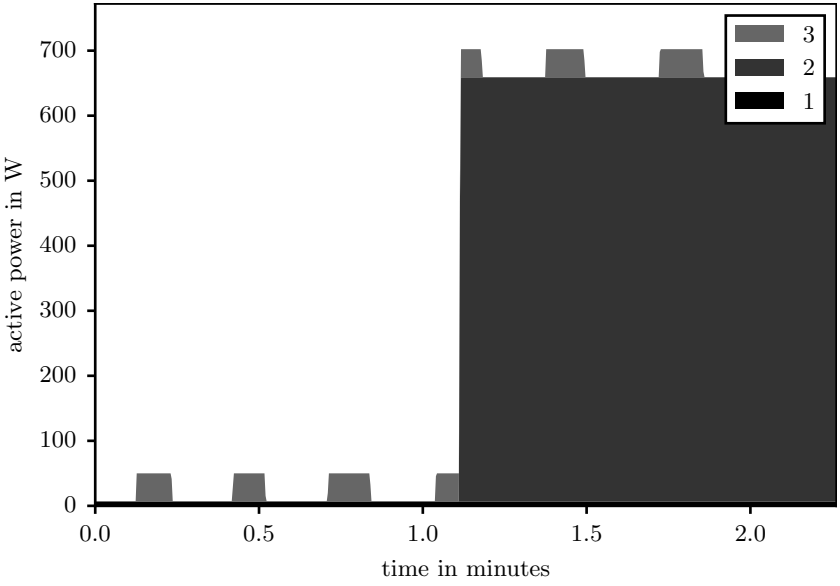

Label	Description of load	e in Wh	Δe in Wh	acc
1	Air pump	0.21	0.01	93%
2	Heating element	12.51	0.04	100%
3	Water pump	0.63	0.03	95%
	Sum	**13.35**	**0.08**	**99%**

Figure 7.8: Disaggregation result for a heated washing basin. The operating behavior of all three loads in this machine resembled that of an ideal two-state load. Therefore, their power demand could be estimated with accuracies above 90 %. The measured active power demand of the air pump varied slightly in correlation with the switching events of the heating element and the water pump. However, it is believed that the power demand of the air pump was *actually* constant and that the observed fluctuations were an effect of unwanted electromagnetic interference in the current clamp due to the air pump's low power demand of only 6 W.

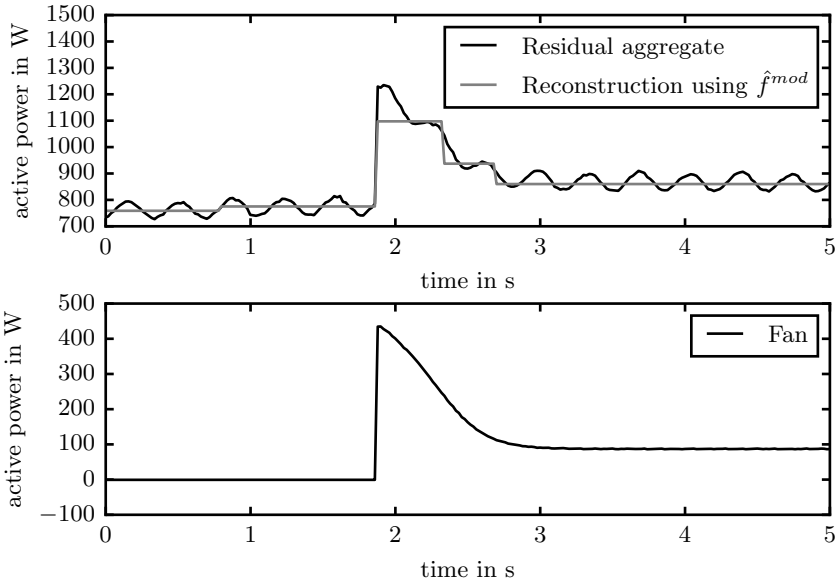

Figure 7.9: Due to the oscillations of the active power demand of the residual aggregate load (induced by the compressor), the turn-on event of the fan was falsely interpreted as a series of one large positive step change and two negative ones instead of just one positive step change. Only the large positive step change was used for estimating the fan's active power demand magnitude, which explains the significant overestimation of its active power demand.

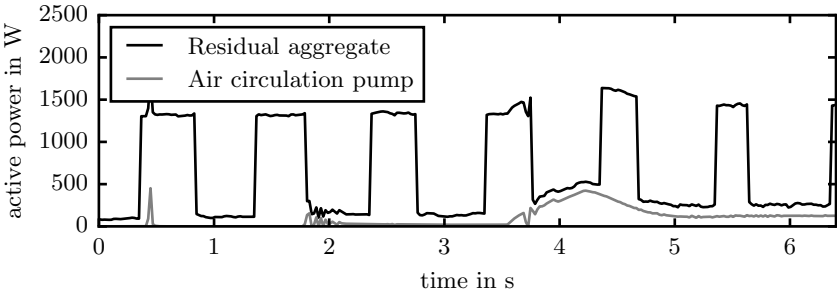

Figure 7.10: Upon being turned on, the motor driving the air circulation pump exhibited a continuously variable active power demand over several seconds until a steady state was reached. This turn-on behavior stands in contrast to that of an ideal two-state load.

7.4 Discussion of results

For all but one aggregate load, an average weighted accuracy of 85 % or more was achieved. Moreover, for a majority of the individual loads, an accuracy of at least 85 % could be achieved with the proposed measurement method. Notably, the active power demand of loads featuring an uncontrolled bridge rectifier was estimated with accuracies of close to 100 % in most cases despite its challenging continuously variable shape. Even if both a three-phase and a single-phase uncontrolled bridge rectifier were present in the aggregate load (see Fig. 7.4), they could be extracted separately, albeit with lower accuracies of only approximately 80 % and 70 %. Similarly, the challenging continuously variable power demand of a fixed-speed motor with a fluctuating mechanical load was estimated with a suitable accuracy of 89 % (see Fig. 7.2).

If an accuracy of approximately 85 % was not achieved for an individual load, it was due to one of the following reasons:

- If the power demand of an uncontrolled bridge rectifier was extracted with an accuracy of less than 85 %, its current peaks were barley observable either due to overlapping current peaks in the presence of both a single-phase and a three-phase uncontrolled bridge rectifier (see Fig. 7.4) or due to the high-frequency noise of other loads with a much higher power demand than the uncontrolled bridge rectifier.
- Any estimation errors resulting from the disaggregation method for uncontrolled bridge rectifier are effectively passed on to the estimated two-state loads (see Fig. 6.1). Thus, even errors that were small in comparison to the active power demand of the uncontrolled bridge rectifier resulted in large errors relative to loads whose active power demand is much smaller than that from the uncontrolled bridge rectifier.
- Some two-state loads exhibited an active power demand shape at turn-on that deviated significantly from the one of ideal two-state loads (see Fig. 7.10, Fig. 7.9 and the brief operating states of the heating in Fig. 7.4).
- In one case, the turn-on events of two-state loads with a comparatively low power demand were masked by the active power demand fluctuations of a fixed-speed motor with a varying mechanical load (see Fig. 7.2). More precisely, some of these fluctuations were erroneously detected as switching events, which led to a large number of false positives. *Actual* switching events, whose step-change magnitude was of the same order of magnitude as the false positive events, were thus indistinguishable.

In order to handle these situations in the future, several improvement options are presented next. Since the three different disaggregation methods illustrated in Fig. 6.1 work independently of each other, they are also reviewed separately.

Disaggregation method for uncontrolled bridge rectifier In order to improve the disaggregation of uncontrolled bridge rectifiers, several sanity checks can be added to make the algorithm more robust. First, it was observed that the estimated current of uncontrolled bridge rectifiers sometimes changes the sign within some half-periods, which stands in contrast to reality. Therefore, the algorithm could be constrained in such a way that the sign of the estimated current of the uncontrolled bridge rectifiers is always constant for one half-period. Second, in the case of the three-phase uncontrolled bridge rectifier, it could be checked that the two peaks in each half-period have a similar shape. Third, the disaggregation method based on the correlation between the active power demand and current harmonics (see subsection 3.7.3) could be performed in parallel and used in cases in which the peaks are masked due to the high-frequency currents of other loads. Fourth, it seems worthwhile to research whether a correlation also exists between the active power demand and high-frequency voltage noise.

Disaggregation method based on switching events First, when detecting the events, the test statistic by Luo yields different results when applied "from left to right" than "from right to left" (see Fig. 7.11). Mathematically speaking, let $f : \mathbb{Z} \mapsto \mathbb{R}$ be a discrete signal and let $\widetilde{f}$ be its horizontally symmetric with respect to the y-axis defined as $\widetilde{f}_k = f_{-k}$. Then, $\xi_{-k}(\widetilde{f}) \neq \xi_k(f)$. Such behavior does not coincide with human intuition and it might hence be beneficial to perform the test statistic twice - once from left to right and once from right to left - and then combine the detection results.

Second, some loads exhibited a large inrush current when being turned on, which results in a transient peak. Sometimes, part of this peak was falsely identified as a steady state (see Fig. 7.9) which resulted in an overestimation of the step-change magnitude. In these cases, it is necessary to test whether the detected step changes might be false positives. This check can be performed either during the event detection or during the clustering step.

Third, many loads in machines draw approximately the same current on all three phases so that their events in the three phases should occur simultaneously, too. This knowledge is currently not used at all. Instead, all phases are dealt with independently.

Fourth, the current clustering method is rather simple in the sense that it groups events based on only the distance between their feature vectors. It is easy to envision a clustering algorithm that also examines whether events in the cluster alternate perfectly between turn-on and turn-off events. Moreover, the sum of the estimated active power demands can be compared against the measured aggregate active power demand while comparing different clustering alternatives.

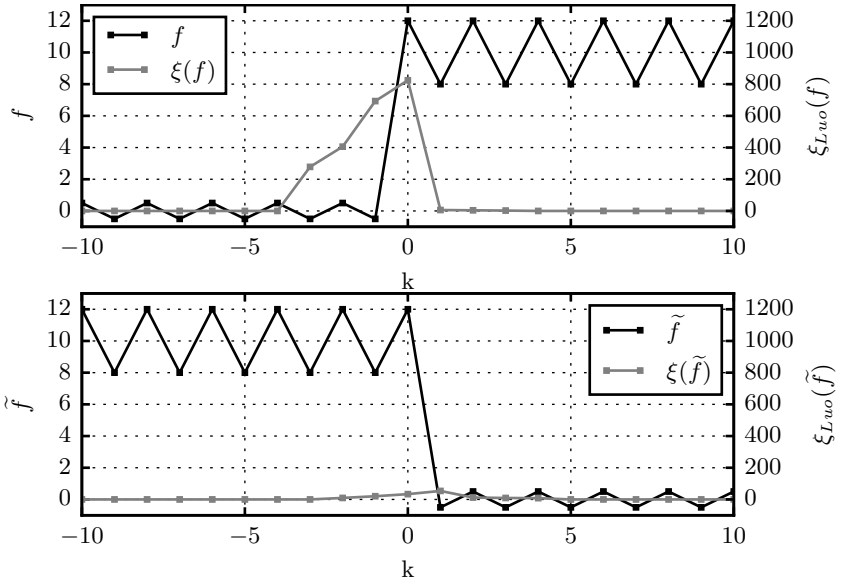

Figure 7.11: The test statistic ξ defined in eq. 5.3 yields different results when performed from left to right than from right to left. This is shown here by applying the test statistic to the original signal f (top) and to the horizontally flipped signal $\widetilde{f}$ (bottom).

Disaggregation method for varying fixed-speed motors If the fluctuations in the power demand mask the switching events of actual two-state loads, it is conceivable that the event detection is performed again *after* the disaggregation of the relevant fixed-speed motor. This should result in less false positives and thus make it easier to detect actual switching events.

Apart from that, one of the most important things is to gain a better understanding of why the correlations between the active power demand and even harmonics occur (see section 6.1). Based on a better understanding it is likely that the disaggregation procedure can be further improved.

8 Evaluation

The proposed measurement method has already been evaluated in Tab. 3.3 according to the requirement criteria described in section 1.3. However, based on the findings in chapter 7, the evaluation of the technical aspects is performed more thoroughly now in section 8.1. Moreover, the economic aspect is analyzed in greater detail in section 8.2.

8.1 Technical evaluation

As stated in section 1.3, it is required that the identified loads contribute at least 80 % to the aggregate active power demand. This requirement was met by all application examples presented in section 7.3. In several cases, some small loads could not be extracted individually but were estimated as one aggregate load instead. This was true for several loads referred to as "rest" in the case of the thermoform machine (see Fig. 7.2), for the computer and fan in the case of the selective laser machine (Fig. 7.4) and for the lubricant pump and electronics in the case of the milling machine (see Fig. 7.6). However, in all three cases, these loads only represented approximately 15 % of the aggregate load. In other words, all loads contributing 85 % to the aggregate active power demand were successfully identified individually.

Another requirement was that the identified loads are measured with an accuracy of approximately 85 % or greater. This was true for the majority of the identified loads presented in section 7.3. For loads with accuracies below 85 %, several improvement options have been proposed in section 7.4. Implementing these will almost certainly increase the accuracy on average and thus probably fulfill the requirement of an accuracy of 85 % for all loads.

The results from the application examples can be generalized to new machines in the sense that the seven examples represent different combinations of the four most frequent load classes, i.e., fixed-speed motors, motors fed by a variable speed drive, Joule heating elements and rectifiers supplying different kinds of electronics (see section 4.2). If a new machine also comprises only these four load classes, it can be assumed that the proposed measurement method yields comparable results.

8.2 Economic evaluation

The algorithms presented in this thesis need to be implemented in a user friendly software. This software could run either online or offline and either directly on the measurement device or on, e.g., a personal computer which may or may not always be connected to the device. Since monitoring the voltages and currents of a three-phase system at 10 kHz and 24 bit would result in a significant data stream of close to 1 GByte/h (8 signals · 10000 Hz · 24 bit · 1/8 byte/bit · 3600 s/h = 864 MByte/h), it is assumed that the data are processed online directly at the measurement device instead of first being transferred to another computing device.

In this scenario, one company would develop and sell a measurement device with the incorporated algorithms to interested manufacturing companies. Therefore, the economic benefit has to be evaluated from two viewpoints:

- From the viewpoint of a manufacturing company using the device,
- From the viewpoint of the vendor who develops and sells the device.

From the viewpoint of the user

As indicated in section 1.3, a manufacturing company does not *directly* benefit from measuring the active power demands of its machines. Instead, performing measurements can lead to the detection of previously unknown energy efficiency deficits. By remedying these deficits, the current and future energy costs can be decreased, which results in cost savings. According to section 1.2, the measurement equipment is required to cost less than 10,000 €, and the setup time for the measurement is required to last less than one hour. That efficiency measures concerning the electricity consumption can be profitable under these circumstances shall be demonstrated next with an example.

An efficiency measure is an investment option for the manufacturer. It requires initial expenses for planning the efficiency measure (c_{plan}) and actually modifying the machine (c_{mod}) and it yields annual cost savings ($\dot{c}_{savings}$). Such investments are typically expected to have a payback period of three years ($t_{payback}$). This can be expressed as:

$$\frac{c_{plan} + c_{mod}}{\dot{c}_{savings}} \overset{!}{\leq} t_{payback} \ . \tag{8.1}$$

The planning costs c_{plan} involve buying a piece of mobile measurement equipment, which can be easily moved from one machine to another ($c_{equipment}$). Moreover, the measurements must be setup (c_{setup}) and analyzed ($c_{analysis}$) for several machines ($N_{examined}$). One measurement of a machine, including

the subsequent analysis, will not always generate one or more relevant ideas for potential efficiency measures. Here, it will be assumed that five measurements result in one relevant idea. This idea has to be further detailed (c_{detail}), before it can be executed. Concluding, the planning costs c_{plan} consist of the following elements:

$$c_{plan} = c_{equipment} + N_{examined} \cdot (c_{setup} + c_{analysis}) + c_{detail} \ . \tag{8.2}$$

The costs of modifying a machine comprise the necessary material ($c_{material}$) as well as internal or external services ($c_{service}$). A type of machine is often owned not only once but several times ($N_{machines}$) by a manufacturing company, potentially in plants at different locations. Then it would be advantageous to carry out the efficiency measure not only for one but for all machines. In this case, the modification cost c_{mod} can be calculated as follows:

$$c_{mod} = N_{machines} \cdot (c_{material} + c_{service}) \ . \tag{8.3}$$

Last, the cost savings are determined by the average reduction in the active power demand of a machine Δp times the annual operating time $\dot{t}_{operating}$ and the electricity price c_{elec}. They scale with the number of machines for which the efficiency measure is carried out ($N_{machines}$). In short,

$$\dot{c}_{savings} = N_{machines} \cdot \Delta p \cdot \dot{t}_{operation} \cdot c_{elec} \ . \tag{8.4}$$

Based on the exemplary numbers listed in Tab. 8.1 whose order of magnitude was drawn from interviews with experts and (BDEW 2018; Dreessen 2017; Gleich 2014; Neugebauer 2013; Reinhart et al. 2016), a payback time of three years is feasible:

$$\frac{c_{plan} + c_{mod}}{\dot{c}_{savings}} = \frac{20,000\ € + 100,000\ €}{40,000\ €/\text{a}} = 3\ \text{a} \ . \tag{8.5}$$

While the numbers listed in Table 8.5 are only exemplary, they show that the cost savings are typically in the order of magnitude of several ten thousand euros and that the personnel costs for planning an efficiency measure quickly amount to 10,000 €. Compared to these numbers, purchasing a measurement equipment for 10,000 € or less is not a significant investment.

Table 8.1: Exemplary values for parameters used in eq. 8.5

Parameter	Subparameters	Value
c_{plan}	$c_{equipment}$ in €	10,000
	$N_{examined}$	5
	c_{setup} in €	200
	$c_{analysis}$ in €	800
	c_{detail} in €	5,000
c_{mod}	$N_{machines}$	10
	$c_{material}$ in €	5,000
	$c_{service}$ in €	5,000
$\dot{c}_{savings}$	Δp in kW	10
	$\dot{t}_{operation}$ in h/a	4,000
	c_{elec} in €/kWh	0.10

From the viewpoint of the vendor

In this subsection it will be demonstrated that a price of 10.000 € is realistic and that under such conditions, the vendor can make a profit. The price p consists of the following elements:

$$p = (c_P + \frac{c_{add} + c_{overhead}}{N_{devices}}) \cdot \frac{1}{1 - m_P} \cdot \frac{1}{1 - m_T} \cdot (1 + t) \cdot \frac{1}{1 - d} \ , \qquad (8.6)$$

where c_P represents the costs of obtaining a device with which the aggregate current and voltage can be measured; c_{add} refers to the additional costs of implementing the disaggregation and labeling algorithms, which are being distributed over $N_{devices}$ sold devices; $c_{overhead}$ denotes the overhead costs of the vendor for, e.g., rent, administrative staff and marketing; m_P is the profit margin of the vendor; m_T is the gross profit margin of a potential intermediary trading company; t represents any taxes and d refers to any discounts, including a cash discount.

Several devices already exist that can simultaneously measure the voltage and the current of a three-phase (aggregate) load. Therefore, it is assumed that such a device is purchased rather than developed from scratch. The price of this type of device for end customers excluding taxes ranges from approximately 350 € (e.g., Janitza UMG 96RM-E) to 1,300 € (e.g., a Beckhoff CX5140 embedded PC with a EL3773 oversampling terminal) depending on the computing power and other features. Three of the current clamps used in this thesis cost an additional 450 €. Based on these numbers, and taking volume discounts into account, it seems realistic that a company can procure a device with sufficient computing power and modifiability for approximately $c_P = 1,500$ €.

Next, the new disaggregation and labeling algorithms need to be implemented on the existing hardware device. These additional development costs shall be estimated to be approximately $c_{add} = 1$ mio. €, which typically suffices to finance a development team of five people over two years. If these costs are distributed over $N_{devices} = 500$ sold devices, the additional costs per device are 2,000 €. The estimated number of 500 sold devices seems to be a conservative estimation given that in Germany alone there are 200,000 manufacturing companies of which approximately 5,000 have more than 250 employees and often more than one plant (Gude 2017).

The overhead costs of the company are also estimated conservatively at $c_{overhead} = 1$ mio. € based on the idea that it may take five years to sell $N_{devices} = 500$ devices and that the annual overhead costs amount to 200,000 €.

Finally, the profit margins of the company selling the devices are assumed to be $m_P = 15$ %, and the gross profit margin of a potential intermediary trading company $m_T = 25$ %. No value-added tax needs to be paid, since the device is not sold to an end consumer, therefore $t = 0$. Furthermore, discounts of $d = 5$ % are postulated.

These numbers result in a price of less than 10.000 €:

$$\begin{aligned} p =& (c_P + \frac{c_{add} + c_{overhead}}{N_{devices}}) \cdot \frac{1}{1 - m_P} \cdot \frac{1}{1 - m_T} \cdot (1 + t) \cdot \frac{1}{1 - d} \\ =& (1,500\ € + \frac{1,000,000\ € + 1,000,000\ €}{500}) \\ & \cdot \frac{1}{1 - 0.15} \cdot \frac{1}{1 - 0.30} \cdot (1 + 0) \cdot \frac{1}{1 - 0.05} \\ =& (1,500\ € + 2,000\ € + 2,000\ €) \cdot \frac{1}{1 - 0.15} \cdot \frac{1}{1 - 0.30} \cdot (1 + 0) \cdot \frac{1}{1 - 0.05} \\ =& 9,082\ € \ . \end{aligned} \tag{8.7}$$

While the numbers provided above are again only exemplary, they demonstrate that the additional development costs per unit and the overhead costs per unit are larger than the costs for obtaining a suitable hardware device. Here, the development and overhead costs were estimated rather high given that a working algorithm was already presented in this thesis. However, even in this case, a price of 10,000 € or less seems realistic.

9 Summary

In this thesis, a measurement method was sought to determine the active power demand of machines components in a more economical manner than by acquiring the current and voltage of each load individually. To this end, several alternative measurement methods were assessed at first. The most suitable method works by only measuring the active power demand of the aggregate load (i.e., the entire machine) and then automatically disaggregating it into its parts based on a detailed analysis of the electric properties. While this measurement method has been proven to be successful for determining the active power demand of residential household devices, it has never been applied to a machine used in manufacturing before.

Since the suitability of this measurement method depends on the types of loads and their operating behavior, 151 electric loads in manufacturing machines were classified next. The four most prevalent load classes were fixed-speed motors (38 % of all loads), motors controlled by a variable speed drive (26 %), Joule heating elements (15 %) and rectifiers supplying electronic loads such as programmable logic controllers (13 %). While most of these loads had only two operating states (i.e., on and off), fixed-speed motors with a varying mechanical load and motors controlled by a variable speed drive exhibited a continuously variable active power demand, which is more challenging to determine through disaggregation.

Based on this analysis, the suitability of the already existing disaggregation methods developed for residential household devices was evaluated for the four most prevalent load classes, thereby revealing several deficits. First, no disaggregation algorithm existed with which the continuously variable active power demand of fixed-speed motors could be extracted. Second, the existing disaggregation method for variable speed drives featuring uncontrolled bridge rectifiers had several disadvantages, most notably a low disaggregation accuracy unless training data are provided. Third, the disaggregation algorithm suited to loads with only two operating states yielded imprecise results if narrow peaks in the active power demand were present due to, e.g., inrush current. Fourth, no algorithm existed with which fixed-speed motors could be classified according to their mechanical load, even though its feasibility has been indicated in literature and such an automatic classification would be desirable from a user's perspective.

For each of these four deficits, a new, improved method was developed and for each new method, the general approach was presented first, followed by the detailed algorithm and a validation. The new methods were then merged into a combined measurement method based on disaggregation, which was implemented in the programming language python.

The combined measurement method was applied to seven real aggregate loads, which represented different types of machines used in manufacturing and comprised three to eleven electric components. In all cases, the majority of the electric components could be identified through the disaggregation. More specifically, the extracted loads contributed at least 85 % to the active power demand of the aggregate load. Moreover, the active power demand of the loads could be estimated with an accuracy of 85 % or more in the majority of the cases. The weighted *average* accuracy ranged between 87 and 93 % for six out of the seven aggregate loads. Some remaining challenges were pointed out for which potential future solutions were proposed. As a result, an estimation accuracy of 85 % or more seems achievable for all loads in the near future.

Apart from this technical evaluation, it could be demonstrated that the implementation of the developed algorithms on a measurement device would be economically profitable for both a manufacturing company using the measurement device and a vendor who develops and distributes the device.

In conclusion, the combined measurement method based on disaggregation has been proven to represent a highly economical and a sufficiently accurate alternative, compared to the current state-of-the-art measurement method. Its application would allow companies to increase their energy efficiency more rapidly and more cost effectively.

Besides tweaking the methods that were already implemented in this thesis, there are several additional promising approaches to be researched in the future:

- Patel et al. (2007) and Gupta et al. (2010) stated that the use of voltage oscillations in the kilohertz to megahertz range allows one to differentiate between the switching events of lights of the same model, since each light is wired slightly differently. Such voltage oscillations were not investigated in this thesis due to the lack of a suitable measurement device. However, they could prove to be similarly useful to distinguish motors of the same type. Moreover, the magnitudes of the voltage oscillations might correlate with a continuously variable active power demand of a load and thus improve their disaggregation accuracies.
- Many loads in machines used in manufacturing draw approximately the same current on all three phases. Therefore, there is a strong link between all three measured phases. This link has currently not been utilized at all. Instead, each phase was dealt with independently.

- Apart from measuring the voltage and current of the aggregate load, it is also possible to monitor the operating states of the individual loads (Gebbe et al. 2014; Panten et al. 2016). Using the operating status of all loads, a disaggregation can be performed as a simple linear regression. While depending *purely* on the operating status signals of all loads is questionable, since they may be difficult to acquire, the *additional* use of any potential operating status signal is likely to improve the disaggregation accuracy.
- The disaggregation method currently estimates an active power demand for each identified load without stating a confidence level. Calculating such a confidence level seems feasible by taking into account the validity of the result and the difficulty of the signal to be disaggregated. This confidence level would help users to asses the disaggregation result.

A Appendix

A.1 Classification of electric loads

The table of all 151 classified electric loads is presented in the following.

machine	component name	variable speed drive + motor	motor + fan	motor + pump	motor + compressor	motor + other mechanical load	Joule heating	electro-magnetic induction + Joule heating	rectifier + electronic load (e. g. programmable logic controller)	phase angle control (light dimmer)	rectifier + resonant inverter + impact ionization (compact fluorescent lamp)	rectifier + high frequency inverter + inverse piezoelectric effect (ultrasound)	rectifier + boost converter + LED-TFT	rectifier + radiative recombination (e.g., semiconductor laser)	hot cathode in magnetron (microwave)	rectifier + high frequency inverter + capacitor (plasma generator)
Vacuum based handling equipment for carbon composites	fan		1													
	VSD controlled fan	1														
	VSD controlled fan	1														
	VSD controlled fan	1														
	VSD controlled fan	1														
	24 V rectifier + analog cards								1							
	24 V rectifier + diverse electronic								1							
Six axis industrial robot	fan		1													
	VSD + several motors	1														
	24 V rectifier								1							
Machine for unfolding cardboard boxes	VSD + motor	1														
	VSD + motor	1														
	VSD + motor	1														
	VSD + motor	1														
	VSD + motor	1														
	VSD + motor	1														
	VSD + motor	1														
	VSD + motor	1														
	VSD + motor	1														
	VSD + motor	1														
	VSD + motor	1														
	24 V rectifier								1							
External cooling device 1	compressor				1											
	pump			1												
	fan		1													
	fan		1													
External cooling device 2	compressor				1											
	pump			1												
	24 V rectifier								1							

machine	component name	variable speed drive + motor	motor + fan	motor + pump	motor + compressor	motor + other mechanical load	Joule heating	electro-magnetic induction + Joule heating	rectifier + electronic load (e. g. programmable logic controller)	phase angle control (light dimmer)	rectifier + resonant inverter + impact ionization (compact fluorescent lamp)	rectifier + high frequency inverter + inverse piezoelectric effect (ultrasound)	rectifier + boost converter + LED-TFT	rectifier + radiative recombination (e.g., semiconductor laser)	hot cathode in magnetron (microwave)	rectifier + high frequency inverter + capacitor (plasma generator)
Optical quality control system for battery separator foils	rectifier for PC								1							
	lighting										1					
	fan		1													
	VSD + motor for winding	1														
	VSD + motor for winding	1														
	rectifier for electronics								1							
	24 V rectifier								1							
	40 V rectifier								1							
	rectifier for electronics								1							
Selective laser sintering machine 1	laser													1		
	VSD + motor	1														
	VSD + motor	1														
	circulation pump			1												
	heating						1									
	15 V rectifier								1							
	24 V rectifier								1							
	fan		1													
Selective laser sintering machine 2	circulation pump			1												
	heating						1									
	fan		1													
	VSD + motor for coating	1														
	VSD + motor for lifting	1														
	laser													1		
	24 V rectifier								1							

machine	component name	variable speed drive + motor	motor + fan	motor + pump	motor + compressor	motor + other mechanical load	Joule heating	electro-magnetic induction + Joule heating	rectifier + electronic load (e. g. programmable logic controller)	phase angle control (light dimmer)	rectifier + resonant inverter + impact ionization (compact fluorescent lamp)	rectifier + high frequency inverter + inverse piezoelectric effect (ultrasound)	rectifier + boost converter + LED-TFT	rectifier + radiative recombination (e.g., semiconductor laser)	hot cathode in magnetron (microwave)	rectifier + high frequency inverter + capacitor (plasma generator)
Thermoform machine	heating						1									
	cooling device - fan		1													
	cooling device - pump			1												
	cooling device - compressor				1											
	vacuum pump				1											
	conveyor belt					1										
	motor for winding					1										
	VSD controlled main drive	1														
	VSD controlled molding station	1														
	fan		2													
Heated washing basin	pump			1												
	heating						1									
	gas pump		1													
Water jet cutting machine	VSD + several motors	1														
	brake					1										
	water pump			1												
	24V rectifier								1							
	15V rectifier								1							
Milling machine	pump for cooling lubricant			1												
	pump for lubricant			1												
	hydraulic pump			1												
	fan for spindle		1													
	VSD + several motors	1														
	vacuum pump				1											
Plasma cleaning system	fan		1													
	plasma generator															1
	rectifier for PC								1							

machine	component name	variable speed drive + motor	motor + fan	motor + pump	motor + compressor	motor + other mechanical load	Joule heating	electro-magnetic induction + Joule heating	rectifier + electronic load (e. g. programmable logic controller)	phase angle control (light dimmer)	rectifier + resonant inverter + impact ionization (compact fluorescent lamp)	rectifier + high frequency inverter + inverse piezoelectric effect (ultrasound)	rectifier + boost converter + LED-TFT	rectifier + radiative recombination (e.g., semiconductor laser)	hot cathode in magnetron (microwave)	rectifier + high frequency inverter + capacitor (plasma generator)
Ultrasonic cleaning system, large	2 ligthming for cabinet box and machine										2					
	13 heating elements						13									
	2 fans for drying		2													
	2 fans for circulation		2													
	3 ultrasound generators											3				
	3 fans for ultrasound generator		3													
	6 circulation pumps			6												
	2 motors for transport	2														
	5 motors for each cleaning station	5														
	fan for 5 motors		1													
	1 fan in the cabinet box		1													
	1 rectifier for electronics								1							
Ultrasonic cleaning system, small	heating						1									
	ultrasound generators											1				
	fan		1													

machine	component name	variable speed drive + motor	motor + fan	motor + pump	motor + compressor	motor + other mechanical load	Joule heating	electro-magnetic induction + Joule heating	rectifier + electronic load (e. g. programmable logic controller)	phase angle control (light dimmer)	rectifier + resonant inverter + impact ionization (compact fluorescent lamp)	rectifier + high frequency inverter + inverse piezoelectric effect (ultrasound)	rectifier + boost converter + LED-TFT	rectifier + radiative recombination (e.g., semiconductor laser)	hot cathode in magnetron (microwave)	rectifier + high frequency inverter + capacitor (plasma generator)
Food shredding machine	heating						1									
	fan for pump		1													
	fan for cabinet box		1													
	24V rectifier								1							
	step motor					1										
	main motor					1										
	VSD controlled feeder screw	1														
	VSD controlled mixing shaft	1														
	VSD controlled feed pump	1														
	vacuum pump				1											
	fan		1													
	24V rectifier								1							
Food mixing machine 1	heating for cabinet box						1									
	lamp										1					
	heating for control panel						1									
	24V rectifier								1							
	VSD controlled motor	1														
	VSD controlled motor	1														
	motor for lifting					1										
	vacuum pump				1											
Food mixing machine 2	heating for cabinet box						1									
	lamp										1					
	24V rectifier								1							
	motor for mixing shaft					1										
	motor for lifting					1										

A.2 Simulation of a three-phase uncontrolled bridge rectifier

For the simulation of a three-phase uncontrolled bridge rectifier with different parameters for C, R_{series} and L_{series} the program LTspice XVII was used. However, the simulation of the ideal circuit diagram shown in Fig. A.1 did not converge. Hence, several modifications were made to the ideal circuit in order to enable convergence:

- Addition of the resistances R3, R4 and R5 with a value of 1 $\mu\Omega$,
- Addition of an internal series resistances of 10 $m\Omega$ for the three voltage sources,
- Selection of the real diode model MUR460 for all six diodes instead of using an idealized diode,
- Usage of the alternate solver in LTspice XVII.

These modifications resulted in a more realistic circuit shown in Fig. A.1. The simulated voltage and current of phase 1 is shown in figures A.2 and A.3 for $R_{load} \in [10, 15, 20, 30, 40, 80, 160, 320, 640, 1000]\ \Omega$. Based on these results, the active power demand p and the harmonics I_5 and I_7 were calculated.

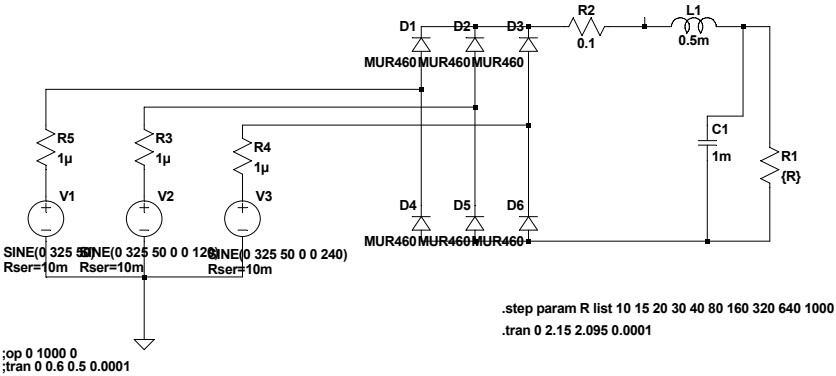

Figure A.1: Screenshot of the circuit diagram in LTspice

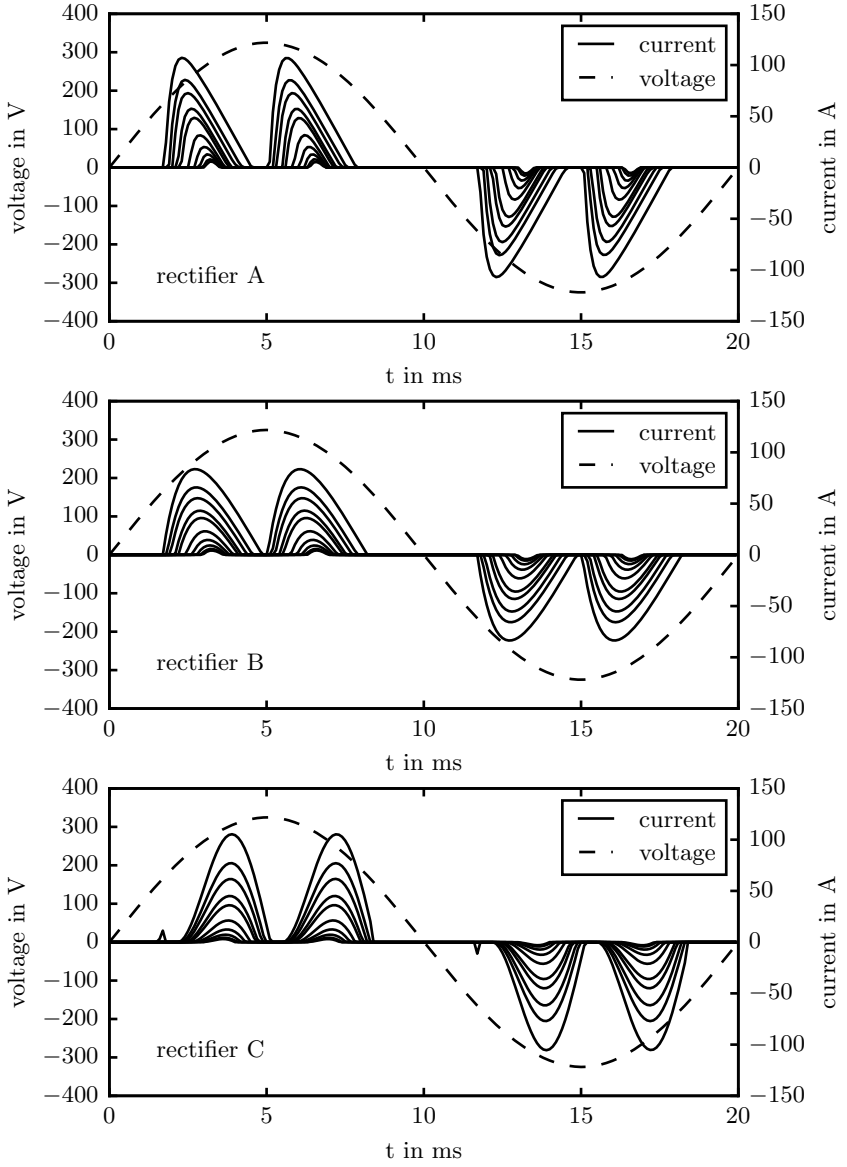

Figure A.2: Simulated current and voltage for rectifiers A, B and C for a varying load

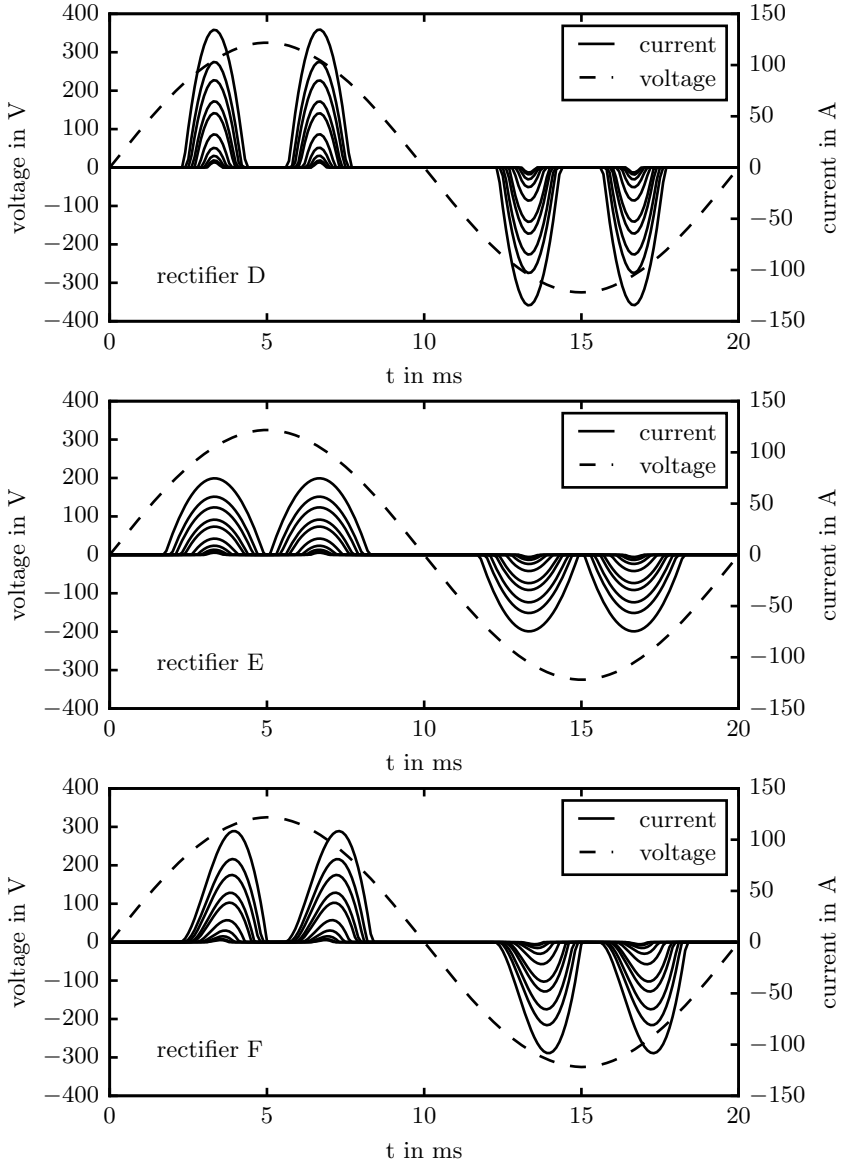

Figure A.3: Simulated current and voltage for rectifiers D, E and F for a varying load

A.3 Deficit of the mapping function by Wichakool et al.

In Wichakool et al. (2009, 2015) the mapping function relates not only one but multiple aggregate current harmonics to the first current harmonic of e. g. an uncontrolled bridge rectifier so that the mapping function takes the form $I_1^{UBR} = F(I_5^{agg}, I_7^{agg}, \dots)$. Based on the first current harmonic, the active power demand of the uncontrolled bridge rectifier can be calculated (see subsection 3.7.3). This mapping function is mathematically derived based on the representation of the signal using the Fourier transform (see section 2.1).

If the mapping function uses *all* aggregate current harmonics as inputs and if the uncontrolled bridge rectifier is the only device which generates current harmonics, the mapping function is in fact 100% accurate. However, this assumption is unlikely to be met in practice and Wichakool et al. (2009, 2015) themselves suggest to only use a few aggregate current harmonics as inputs based on heuristics. Then, the mapping function ceases to be exact and the same deficits as described in section 5.2 hold true.

Method described in Wichakool et al. (2009) The idea presented in (Wichakool et al. 2009) bases on the fact that the current of any of the three phases $i : \mathbb{R} \mapsto \mathbb{R}$ can be described as a product of a switching function $x : \mathbb{R} \mapsto \mathbb{R}$ known a priori and the rectified current through the resistor or inductor $r : \mathbb{R} \mapsto \mathbb{R}$:

$$i(t) = x(t) \cdot t(t) \tag{A.1}$$

Any signal, even a non-periodic one, can be represented as a Fourier series similar to the inverse discrete Fourier transform described in section 2.1, which results in

$$\begin{aligned} i(t) = \sum_{k=-\infty}^{\infty} I_k e^{jk\omega t} &= \sum_{l=-\infty}^{\infty} X_l e^{jl\omega t} \cdot \sum_{m=-\infty}^{\infty} R_m e^{jm\omega t} \\ &= \sum_{l} \sum_{m} X_l R_m e^{j(l+m)\omega t} \\ &= \sum_{n} \underbrace{\sum_{m} X_{n-m} R_m}_{\hat{=} I_n} e^{jn\omega t} \end{aligned} \tag{A.2}$$

, where $I_k, X_l, R_m \in \mathbb{C}\ \forall k, l, m$ and in the last line the index l has been substituted by $n = l + m$. The limits of the sums are omitted for simplicity reasons but always range from $-\infty$ to $+\infty$.

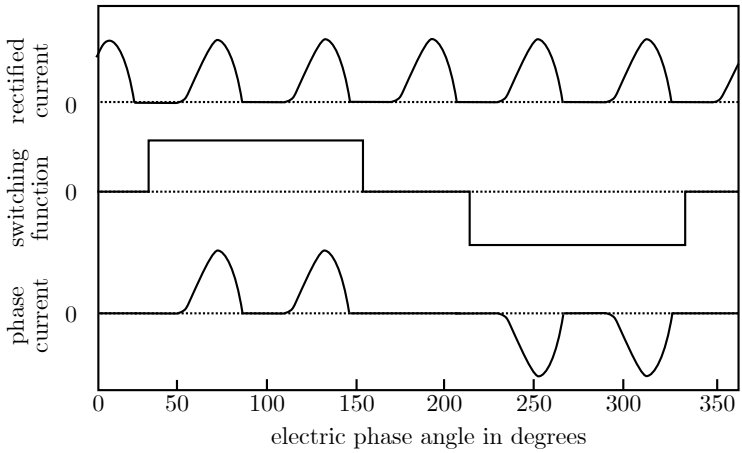

Figure A.4: Exemplary signal of the rectified current (top), the switching function (middle) and the phase current (bottom) (Wichakool et al. 2009)

This means that the coefficient I_k can be calculated as

$$I_k = \sum_m X_{k-m} R_m \tag{A.3}$$
$$\Leftrightarrow \underline{I} = X\underline{R}$$

, where $\underline{I}$ and $\underline{R}$ are vectors and X is a square matrix.

The vector $\underline{I}$ can be split into $\underline{I_1}$ containing the Fourier coefficients I_1 and I_{-1} and $\underline{I_{res}}$ containing all residual Fourier coefficients:

$$\begin{bmatrix} \underline{I_1} \\ \underline{I_{res}} \end{bmatrix} = \begin{bmatrix} X_1 \\ X_{res} \end{bmatrix} \underline{R} \tag{A.4}$$
$$\Rightarrow \underline{I_1} = X_1 \underline{R}$$

This equation represents a way to calculate $\underline{I_1}$ if X_1 and $\underline{R}$ are given. In fact, X_1 (and X_{res}) can be easily calculated, since the function $x(t)$ is known a priori. The vector $\underline{R}$ can be inferred from the equation

$$\underline{I_{res}} = X_{res}\underline{R} \tag{A.5}$$

under the condition that $\underline{I_{res}}$ is given and that X_{res} has at least as many linearly independent rows as columns. The last condition is not met because X_{res} actually has exactly two rows less than columns due to the detachment of $\underline{X_1}$ from the square matrix X. Because of that, Wichakool et al. (2009) propose to reduce the number of columns by only considering a subset M

of Fourier coefficients ($R_m|m \in M$). More specifically, Wichakool et al. (2009) argue that an ideal rectified current r has a periodicity of six. In this case, only Fourier coefficients which are multiples of six are non-zero, i. e. $R_0, R_6, R_{-6}, R_{12}, R_{-12}, \ldots$. Similarly, only a set K of Fourier coefficients of $\underline{I_{res}}$ are chosen such that $|K| = |M|$. Here, Wichakool reasons that even Fourier coefficients are in general zero for AC-systems due to their odd waveform symmetry (Chapman 2005). Moreover, all coefficients which are a multiples of three are zero under a balanced three-phase voltage (Wichakool et al. 2015). Last, they deduce that the magnitude of the Fourier coefficients i_k decreases with increasing k. Concluding, the most relevant coefficients in decreasing order are $I_5, I_{-5}, I_7, I_{-7}, I_{11}, I_{-11}, \ldots$. With these simplifications equation A.4 can be approximated as

$$\begin{aligned} \underline{I_1} &= X_1 \underline{R} \\ &\approx X_1^M \underline{R^M} \\ &= X_1^M \left(X_{res}^{K,M}\right)^{-1} \underline{I_{res}^K} \end{aligned} \tag{A.6}$$

, where vectors and matrices with superscripts M or K represent the described subset of their original versions.

In summary, Wichakool et al. (2009) analytically derived an equation to calculate the first current harmonic based on higher order current harmonics. In a case study, this estimator achieved disaggregation accuracies of close to 100 %. However, the aggregate load in the study was very simple: it consisted only of a 50 W light bulb and a 300 W variable speed drive featuring an uncontrolled bridge rectifier. And despite the advantages of the method, it has some drawbacks:

- Most importantly, the rectified current r is approximated with only $|K|$ Fourier coefficients. This may lead to significant approximation errors. As Wichakool et al. (2009) themselves state, r often does not have a perfect periodicity of six, resulting in a lot more non-zero coefficients such as $r_2, r_4, r_8, \ldots$. This approximation error could be reduced by increasing $|K|$. This would require to increase $|M|$ too, though, meaning that more and higher current harmonics have to be used for the estimation of $\underline{I_1}$. However, such higher harmonics have the disadvantage of being more susceptible to interference (Ciccolella & Canavero 1995; Rich 1982; Xu et al. 1996), which implies a larger measurement error.
- As Wichakool et al. (2009) clearly state, it is assumed that all harmonics $k \in K$ are generated only by the variable speed drive. The larger $|K|$, the less likely this condition is to be met in practice.
- As Wichakool et al. (2009) also indicate, one risk is that the matrix $X_{res}^{K,M}$ is singular and thus cannot be inversed.

Method described in Wichakool et al. (2015) In a following paper, WICHAKOOL ET AL. (2015) described another idea to extract uncontrolled bridge rectifier. It originates from the representation of the current of a variable speed i as the inverse Fourier transform (see eq. 2.3). It can be rewritten as

$$\underbrace{\begin{bmatrix} i_0 \\ i_1 \\ i_2 \\ \vdots \\ i_{N-1} \end{bmatrix}}_{=\underline{i}} = \underbrace{\begin{bmatrix} 1 & 1 & \cdots & 1 \\ 1 & e^{2\pi j \cdot 1 \cdot 1/N} & \cdots & e^{2\pi j (N-1) \cdot 1/N} \\ 1 & e^{2\pi j \cdot 1 \cdot 2/N} & \cdots & e^{2\pi j (N-1) \cdot 2/N} \\ \vdots & \vdots & \vdots & \vdots \\ 1 & e^{2\pi j \cdot 1 \cdot (N-1)/N} & \cdots & e^{2\pi j (N-1)(N-1)/N} \end{bmatrix}}_{\equiv A} \underbrace{\begin{bmatrix} I_0 \\ I_1 \\ I_2 \\ \vdots \\ I_{N-1} \end{bmatrix}}_{\equiv \underline{x}} \tag{A.7}$$

The matrix A can be easily calculated for any given N. Hence, if $\underline{i}$ is given and $\underline{x}$ is unknown, eq. A.7 represents a system of linear equations. Since the columns of A are pairwise orthogonal (see eq. 2.4) and thus linearly independent, the system has one unique solution. Wichakool now uses the fact, that the current of the variable speed drive is zero for $(i_k = 0 \mid k/N \cdot 360° \in [-30°, 30°] \cup [150°, 210°])$. If eq. A.7 is limited to those k's, the number of rows of $\underline{i}$ and matrix A are reduced to $1/3 \cdot N$. Then, the columns of this reduced matrix A and the rows of vector $\underline{x}$ are permutated such that $\underline{x} = [I_1, \underline{I_{others}}, \underline{I_{input}}]^T$, where the vector $\underline{I_{others}}$ has a length of $1/3 \cdot N - 1$ and $\underline{I_{input}}$ a length of $2/3 \cdot N$. eq. A.7 then becomes

$$\begin{bmatrix} 0 \\ 0 \\ 0 \\ \vdots \\ 0 \end{bmatrix} = \tilde{A} \begin{bmatrix} I_1 \\ \underline{I_{others}} \\ \underline{I_{input}} \end{bmatrix} , \tag{A.8}$$

where $\tilde{A}$ represents matrix A with the reduced rows and permutated columns. $\tilde{A}$ has N/3 rows and N columns, hence this system of linear equations has no unique solution, but is underdetermined. Only the relationship between different harmonics can be calculated by bringing $\tilde{A}$ into a reduced row echolon form using the Gaussian elimination method:

$$\begin{bmatrix} 0 \\ 0 \\ 0 \\ \vdots \\ 0 \end{bmatrix} = \begin{bmatrix} 1 & \underline{0} & C_{goal} \\ \underline{0} & \mathbb{1} & C_{others} \end{bmatrix} \begin{bmatrix} I_1 \\ \underline{I_{others}} \\ \underline{I_{input}} \end{bmatrix} , \tag{A.9}$$

where $\mathbb{1}$ represents the identity matrix.

From the equation described above, the estimator for the first harmonic can be deduced:

$$\Rightarrow I_1 = -C_{goal}\underline{I_{input}} \tag{A.10}$$

While the derivation of this estimator is elegant and creative, its applicability is very limited. As mentioned above, $\underline{I_{input}}$ has a length of $2/3 \cdot N$. In this thesis the number of samples per period is $N = 200$, that means that the values of approximately 133 harmonics of the aggregate current are used to estimate the first harmonic I_1 of the variable speed drive. It is implicitly assumed that all of these 133 harmonics of the current of the variable speed drive equal the measured aggregate current. This requirement seems unlikely to be met in practice, especially for high frequency harmonics, which are more sensitive to interferences (Ciccolella & Canavero 1995; Rich 1982; Xu et al. 1996). Because of that, Wichakool only used one to three harmonics for the estimation in his example instead of 133. However, it is not exactly stated, which harmonics shall be chosen, even though the choice affects the estimator C_{goal} significantly. This shall be demonstrated with the following simple example:

Let $k_0/N = 0$ and $k_1/N = 29/360$, $\underline{I_{input}} = I_5$ and $\underline{I_{others}} = I_{11}$, then A.7 becomes:

$$\begin{bmatrix} 0 \\ 0 \end{bmatrix} = \begin{bmatrix} 1 & 1 & 1 \\ e^{2\pi j \cdot 1 \cdot 29/360} & e^{2\pi j \cdot 11 \cdot 29/360} & e^{2\pi j \cdot 5 \cdot 29/360} \end{bmatrix} \begin{bmatrix} I_1 \\ I_{11} \\ I_5 \end{bmatrix} \tag{A.11}$$

$$\Rightarrow 0 = \begin{bmatrix} 1 - e^{2\pi j \cdot (1-11) \cdot 29/360} & 0 & 1 - e^{2\pi j \cdot (5-11) \cdot 29/360} \end{bmatrix} \begin{bmatrix} I_1 \\ I_{11} \\ I_5 \end{bmatrix}$$

$$\Rightarrow I_1 = -\underbrace{\frac{1 - e^{2\pi j \cdot (5-11) \cdot 29/360}}{1 - e^{2\pi j \cdot (1-11) \cdot 29/360}}}_{C_{goal}} I_5 = (-0.92 - 1.48j) \cdot I_5 = 1.74 \cdot e^{1.74i} \cdot I_5$$

However, if $\underline{I_{others}} = I_{17}$ is chosen instead, the estimator changes significantly:

$$\Rightarrow I_1 = (0.07 + 0.11j) \cdot I_5 = 0.13 \cdot e^{0.13i} \cdot I_5 \tag{A.12}$$

In fact, the hypothesis, that the relationship between I_1 and only a few ($\ll 2/3 \cdot N$) other harmonics $\underline{I_{input}}$ is determined by the fact that a third of the signal i is zero, is mistaken. This will be shown in the following with the help of a counterexample. In Fig. A.5 three different signals i are shown, which all fulfill the criterion ($i_k = 0 \mid k/N \cdot 360° \in [-30°, 30°] \cup [150°, 210°]$). However,

the relationship of the harmonics differs significantly among the three signals as shown in Table A.2.

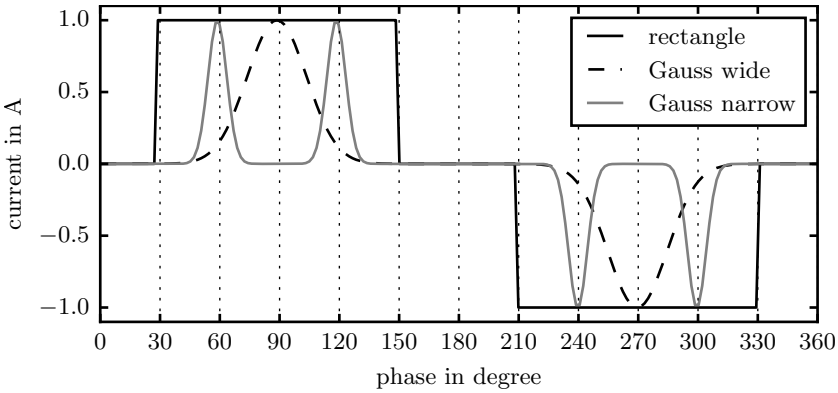

Figure A.5: Three different signals, whose values are all zero between $\phi \in [-30°, 30°] \cup [150°, 210°]$

Table A.2: Calculated harmonics of the three signals presented in A.5. All even harmonics are zero, since the three signals are odd.

	rectangle	Gauss wide	Gauss narrow
$\lvert I_1/I_1 \rvert$	100%	100%	100%
$\lvert I_3/I_1 \rvert$	1%	76%	2%
$\lvert I_5/I_1 \rvert$	20%	45%	90%
$\lvert I_7/I_1 \rvert$	15%	20%	86%
$\lvert I_9/I_1 \rvert$	1%	7%	4%
$\lvert I_{11}/I_1 \rvert$	9%	2%	64%
$\lvert I_{13}/I_1 \rvert$	8%	0%	58%
$\lvert I_{15}/I_1 \rvert$	1%	0%	4%
$\lvert I_{17}/I_1 \rvert$	6%	0%	35%
$\lvert I_{19}/I_1 \rvert$	6%	0%	31%
$\lvert I_{21}/I_1 \rvert$	1%	0%	3%
$\lvert I_{23}/I_1 \rvert$	4%	0%	15%
$\lvert I_{25}/I_1 \rvert$	4%	0%	13%

A.4 Detailed deficits concerning classifying motors

Paper	Proposed feature	Classifier	Loads in case study	Classification accuracy using proposed feature
Sultanem (1991)	duration of transient i determined by analyzing crest current values	not specified	Appliances in one household, to which a complete disaggregation algorithm including clustering and labeling was applied. Appliances not further specified	No focus on classification using only transient features and no quantitative results. Just said that the "length of the transient is not always [a] reliable [feature]".
Leeb (1993); Leeb et al. (1993); Norford & Leeb (1996)	p, q, $\lvert I_3\rvert, \lvert I_3\rvert^2$ during most varying part of transient (dubbed v-section)	patter discrimination via transversal filter	Four loads: instant-start fluorescent lamp, rapid-start fluorescent lamp, two three-phase induction motors with ratings of 0.25 hp and 0.33 hp	No quantification apart from the sentence "[the classifier] performs remarkably well".
Leeb et al. (1995)	time-varying Fourier coefficients of v-section of current i	patter discrimination via transversal filter	Same as in Leeb,AMP1993	No quantification apart from the sentence "all events are correctly identified".
Cole & Albicki (1998)	linear slope of active power p when being turned on	not specified	A compressor of heat pump and a washing machine	No classification is performed and thus no accuracy is reported. It is only stated that the linear approximation of p yields an approximation error of less than 5 %.
Cox et al. (2006)	time-varying Fourier coefficients of voltage	not specified	At least four loads: 1 kW heater, 0.33 single-phase induction motor, three-way incandescent lamp, rapid-start fluorescent lamp	It is stated that "the system has been able to identify nearly all loads". However, neither details of the classification nor quantifiable classification results are shown. Instead, is is only shown graphically that the feature varies significantly for different appliances.
Patel et al. (2007)	coefficients of fast Fourier transform from voltage v in the frequency range between 0-50 kHz	support vector machine (kernel not specified)	Six different residential houses, whose appliances are not further specified. It is only reported that house 1 comprises 41 different appliances.	Accuracy of 84-92 % reported for the six houses using only the proposed feature

Paper	Proposed feature	Classifier	Loads in case study	Classification accuracy using proposed feature
Chang et al. (2007); Yang et al. (2007)	energy $e(t_0, \Delta_t) = \int_{t_0}^{t_0+\Delta_t} p_{inst}(t)$	neural network trained either by backpropagation or by learning vector quantization	Five loads: three induction motors (95 hp, 140 hp, 300 hp), one induction motor controlled by a variable speed drive (95 hp), one load bank ($R = 4\ \Omega$) supplied by an uncontrolled three-phase bridge rectifier	Classification is performed not only with the proposed feature but also with p, q and the total harmonic distortion of voltage as well as current. Hence, the proposed feature was not directly assessed. In the case of overlapping turn-on events, the inclusion of the proposed feature increases the classification accuracy slightly.
Chang et al. (2008)	energy $e(t_0, \Delta_t) = \int_{t_0}^{t_0+\Delta_t} p_{inst}(t)$	neural network trained by backpropagation	Case 1: two three-phase induction motors rated 2.6 hp and 4.7 hp and a R-L-linear load whose real and reactive power resembles the 4.7 hp motor. Case 2: 119 W dehumidifier, 590 W vacuum cleaner, R-L linear load whose real and reactive power resembles the 590 W vacuum cleaner	Classification is performed not only with the proposed feature, but also with p and q. The Inclusion of the proposed feature increases classification accuracy significantly though, from approximately 40 % to 100 %.
Chang et al. (2010, 2012)	energy $e(t_0, \Delta_t) = \int_{t_0}^{t_0+\Delta_t} p_{inst}(t)$	neural network trained by backpropagation	Case 1: two three-phase induction motors rated 160 hp and 123 hp supplied by variable voltage drives and a load bank supplied by a controlled three-phase bridge rectifier (six pulse thyristor rectifier). Case 2: a single-phase induction motor rated 0.2 hp, a three phase induction motor rated 1 hp and a three phase R-L linear load Case 3 and 4 are equivalent to case 1 and 2 in (Chang et al. 2008)	Classification is performed not only with the proposed feature, but also with p and q. In case 1, the classification accuracy is already 100 % without the inclusion of the proposed feature. In case 2, the inclusion of the proposed feature increases the accuracy from 95 % to 100 %. Case 3 and 4 are equivalent to case 1 and 2 in (Chang et al. 2008)

Paper	Proposed feature	Classifier	Loads in case study	Classification accuracy using proposed feature
Chang et al. (2012)	energy $e(t_0, \Delta_t) = \int_{t_0}^{t_0+\Delta_t} p_{inst}(t)$ and duration of transient $p_{inst}(t)$ determined by coefficients from either discrete wavelet transform or short time Fourier transform	neural network trained by back-propagation	Same four cases as in Chang2010, chang2012	Classification is also performed using only both proposed features. Then, the classification accuracy reaches 100 % (case 1), 83-92 % (case2), 94-97 % (case 3) and 79-83 % (case 4) depending on whether the transient duration is determined using either the discrete wavelet transform or the short time Fourier transform.

Table A.3: Detailed summary of the papers presented in the paragraph title "transient features" in subsection 3.7.1

A.5 Calculation of ξ for f^p

The test statistics will be calculated for point k^* and thus $P = \{k^* - 1, k^* - 2, \ldots, k^* - N_P\}$ and $D = \{k^*, k^* + 1, \ldots, k^* + (N_D - 1)\}$. In order to simplify the derivation, the following abbreviated notation is introduced:

$$(f_k^p | k \neq k^*) = \mu_P \pm \sigma \mathrel{\widehat{=}} \begin{cases} \mu_P + \sigma & \text{for even } k \\ \mu_P - \sigma & \text{for odd } k \end{cases} \tag{A.13}$$

Using this notation, first, the mean and standard deviation for both the pre-event and detection window are calculated:

$$\begin{aligned} \mu_P =& \frac{1}{N_P} \sum_{k \in P} f_k \\ =& \frac{1}{N_P} \sum_{k \in P} \mu_P \pm \sigma \\ \approx& \mu_P \end{aligned} \tag{A.14}$$

$$\begin{aligned} \mu_D =& \frac{1}{N_D} \sum_{k \in D} f_k \\ =& \frac{1}{N_D} \left[(N_D - 1)(\mu_P \pm \sigma) + (\mu_P + m \pm \sigma) \right] \\ =& \mu_P + \frac{1}{N_D} \left[\underbrace{(N_D - 1)(\pm\sigma)}_{\ll m} + (m \pm \sigma) \right] \\ \approx& \mu_P + \frac{m}{N_D} \end{aligned} \tag{A.15}$$

$$\begin{aligned} \sigma_P =& \sqrt{\frac{1}{N_P} \sum_{k \in P} (f_k - \mu_P)^2} \\ =& \sqrt{\frac{1}{N_P} \sum_{k \in P} (\mu_P \pm \sigma - \mu_P)^2} \\ =& \sigma \end{aligned} \tag{A.16}$$

$$\sigma_D = \sqrt{\frac{1}{N_P}\sum_{k\in P}(f_k-\mu_D)^2} \tag{A.17}$$

$$= \sqrt{\frac{1}{N_D}\left[(N_D-1)\left(\mu_P \pm \sigma - \left(\mu_P + \frac{m}{N_D}\right)\right)^2 + \left(\mu_P + m \pm \sigma - \left(\mu_P + \frac{m}{N_D}\right)\right)^2\right]}$$

$$= \sqrt{\frac{1}{N_D}\left[(N_D-1)\left(\frac{\pm N_D\sigma - m}{N_D}\right)^2 + \left(m + \frac{\pm N_D\sigma - m}{N_D}\right)^2\right]}$$

$$\approx \sqrt{\frac{1}{N_D}\left[(N_D-1)\left(\frac{-m}{N_D}\right)^2 + \left(m + \frac{-m}{N_D}\right)^2\right]}$$

$$\approx \sqrt{\frac{1}{N_D}\left(\frac{m}{N_D}\right)^2 [(N_D-1) + (N_D-1)^2]}$$

$$= \frac{m}{N_D}\sqrt{\frac{N_D-1}{N_D}\left[1 + (N_D-1)\right]}$$

$$\approx \frac{m}{\sqrt{N_D}}$$

Based on these values, the test statistic ξ can be approximated as:

$$\begin{aligned}
\xi_{k^*}(f^p) =& N_D ln\left(\frac{\sigma_P}{\sigma_D}\right) + \frac{1}{2}\sum_{k\in D}\left[-\left(\frac{f_k-\mu_D}{\sigma_D}\right)^2 + \left(\frac{f_k-\mu_P}{\sigma_P}\right)^2\right] \qquad \text{(A.18)}\\
=& N_D ln\left(\frac{\sigma}{m/\sqrt{N_D}}\right)\\
&+ \frac{1}{2}(N_D-1)\left[-\left(\frac{-\mu_P \pm \sigma - (\mu_P + m/N_D)}{m/\sqrt{N_D}}\right)^2 + \left(\frac{\mu_P \pm \sigma - \mu_P}{\sigma}\right)^2\right]\\
&+ \frac{1}{2}\left[-\left(\frac{-\mu_P + m \pm \sigma - (\mu_P + m/N_D)}{m/\sqrt{N_D}}\right)^2 + \left(\frac{\mu_P + m \pm \sigma - \mu_P}{\sigma}\right)^2\right]\\
=& - N_D ln\left(\frac{1}{\sqrt{N_D}}\frac{m}{\sigma}\right)\\
&+ \frac{1}{2}(N_D-1)\left[-\left(\frac{\pm N_D\sigma - m}{\sqrt{N_D}m}\right)^2 + (1)^2\right]\\
&+ \frac{1}{2}\left[-\left(\frac{N_D m \pm N_D\sigma - m}{\sqrt{N_D}m}\right)^2 + \left(\frac{m}{\sigma}\right)^2\right]\\
\approx& \underbrace{\underbrace{- N_D\, ln\left(\frac{1}{\sqrt{N_D}}\frac{m}{\sigma}\right)}_{<\frac{1}{\sqrt{N_D}}\frac{m}{\sigma}} + \frac{1}{2}\underbrace{(N_D-1)\left[-\frac{1}{N_D}+1\right]}_{\ll(m/\sigma)^2} + \frac{1}{2}\left[\underbrace{N_D + \left(\frac{m}{\sigma}\right)^2}_{\approx(m/\sigma)^2}\right]}_{<\sqrt{N_D}\frac{m}{\sigma}\ll(m/\sigma)^2}\\
\approx& \frac{1}{2}\left(\frac{m}{\sigma}\right)^2
\end{aligned}$$

The modified function ξ^{mod} yields:

$$\begin{aligned}
\xi_{k^*}^{mod}(f^p) =& \frac{N_D}{2}\left(\frac{\mu_D - \mu_P}{max(\sigma_D, \sigma_P)}\right)^2 \\
=& \frac{N_D}{2}\left(\frac{(\mu_P + m/N_D) - \mu_P}{max(m/\sqrt{N_D}, \sigma)}\right)^2 \\
=& \frac{N_D}{2}\left(\frac{m/N_D}{m/\sqrt{N_D}}\right)^2 \\
=& \frac{N_D}{2}\frac{1}{N_D} \\
=& \frac{1}{2}
\end{aligned} \tag{A.19}$$

Bibliography

Abele & Reinhart 2011

Abele, E.; Reinhart, G.: Zukunft der Produktion. Hanser München 2011.

Abele et al. 2011

Abele, E.; Sielaff, T.; Schiffler, A.; Rothenbücher, S.: Analyzing energy consumption of machine tool spindle units and identification of potential for improvements of efficiency. In: Glocalized solutions for sustainability in manufacturing. Springer 2011, pp. 280–285.

Abele et al. 2014

Abele, E.; Sielaff, T.; Beck, M.: Schlussbericht zum Projekt Maxiem. Technical Report, TU Darmstadt PTW, 2014.

Abele et al. 2015

Abele, E.; Panten, N.; Menz, B.: Data collection for energy monitoring purposes and energy control of production machines. procedia CIRP 29 (2015), pp. 299–304.

Adabi et al. 2015

Adabi, A.; Mantey, P.; Holmegaard, E.; Kjaergaard, M. B.: Status and challenges of residential and industrial non-intrusive load monitoring. In: IEEE Conference on Technologies for Sustainability, SusTech 2015, 2015. pp. 181–188.

Ahuja et al. 1990

Ahuja, R. K.; Mehlhorn, K.; Orlin, J.; Tarjan, R. E.: Faster algorithms for the shortest path problem. Journal of the ACM (JACM) 37 (1990) 2, pp. 213–223.

Akbar & Khan 2007

Akbar, M.; Khan, Z. A.: Modified Nonintrusive Appliance Load Monitoring For Nonlinear Devices. In: IEEE International Multitopic Conference, INMIC 2007, 2007, volume 80. pp. 1–5.

Anderson 2014

Anderson, K. D.: Non-Intrusive Load Monitoring: Disaggregation of Energy by Unsupervised Power Consumption Clustering Electrical and Computer Engineering. Ph.D. thesis, Carnegie Mellon University, 2014.

Anderson et al. 2012

Anderson, K. D.; Berges, M.; Ocneanu, A.; Benitez, D.; Moura, J. M.: Event Detection for Non Intrusive Load Monitoring. In: 38th Annual Conference on IEEE Industrial Electronics Society, IECON 2012, 2012. pp. 3312–3317.

Ataby et al. 2014

Ataby, D.; Dornmair, R.; Hamacher, T.; Keller, F.; Reinhart, G.: Flexibilisierung des Stromverbrauchs in Fabriken. In: 13. Symposium Energieinnovation, TU Graz, 2014.

Auinger 2001

Auinger, H.: Efficiency of electric motors under practical conditions. Power Engineering Journal 15 (2001) 3, pp. 163–167.

Balzert et al. 2017

Balzert, H.; Schäfer, C.; Schröder, M.: Wissenschaftliches Arbeiten. 2nd edition. Springer 2017.

Bansal 2017

Bansal, S.: Deep learning for obtaining a detailed energy breakdown from smart meter data, Presentation at European NILM Workshop 2017 in London, 2017, http://www.nilm.eu/.

Baranski & Voss 2004a

Baranski, M.; Voss, J.: Detecting patterns of appliances from total load data using a dynamic programming approach. In: 4th IEEE International Conference on Data Mining, ICDM 2004, 2004a. pp. 327–330.

Baranski & Voss 2004b

Baranski, M.; Voss, J.: Genetic algorithm for pattern detection in NIALM systems. In: IEEE International Conference on Systems, Man and Cybernetics 2004, 2004b. 4, pp. 3462–3468.

Barker et al. 2013

Barker, S.; Kalra, S.; Irwin, D.; Shenoy, P.: Empirical characterization and modeling of electrical loads in smart homes. In: International Green Computing Conference, IGCC 2013, 2013.

Barros et al. 2007

Barros, J.; de Apraiz, M.; Deigo, R. I.; Apráiz, M. D.; Diego, R. I.: Analysis of second order harmonic voltages in power systems. In: International Conference on Renewable Energy and Power Quality 2007, 2007, volume 1. pp. 1–5.

Barsim et al. 2014

Barsim, K. S.; Streubel, R.; Yang, B.: An approach for unsupervised non-intrusive load monitoring of residential appliances. In: Proceedings of the 2nd International Workshop on Non-Intrusive Load Monitoring, 2014. pp. 1–5.

Bashir 2017

Bashir, A.: Disaggregation of Electric Loads Based on Transient Currents. Master's thesis, Fachhochschule Südwestfalen, 2017, supervised by Christian Gebbe.

Batra et al. 2014

Batra, N.; Kelly, J.; Parson, O.; Dutta, H.; Knottenbelt, W.; Rogers, A.; Singh, A.; Srivastava, M.: NILMTK: An Open Source Toolkit for Non-intrusive Load Monitoring. In: Proceedings of the 5th International Conference on Future Energy Systems. ACM 2014. pp. 265–276.

BDEW 2018

BDEW: Bundesverband der Energie-und Wasserwirtschaft e.V. - Strompreisanalyse Haushalte und Industrie Januar 2018, 2018, https://www.bdew.de/media/documents/180109_BDEW_Strompreisanalyse_Januar_2018.pdf, accessed: 2018-03-17.

Behrendt et al. 2012

Behrendt, T.; Zein, A.; Min, S.: Development of an energy consumption monitoring procedure for machine tools. CIRP Annals-Manufacturing Technology 61 (2012) 1, pp. 43–46.

Berges et al. 2009

Berges, M.; Goldman, E.; Matthews, H. S.; Soibelman, L.: Learning Systems for Electric Consumption of Buildings. In: Proceedings of the ASCE International Workshop on Computing in Civil Engineering 2009, 2009. pp. 1–10.

Berges et al. 2010a

Berges, M.; Goldman, E.; Matthews, H. S.; Soibelman, L.: Enhancing electricity audits in residential buildings with nonintrusive load monitoring. Journal of Industrial Ecology 14 (2010a) 5, pp. 844–858.

Berges et al. 2010b

Berges, M.; Soibelman, L.; Matthews, H. S.: Leveraging data from environmental sensors to enhance electrical load disaggregation algorithms. In: Proceedings of the 13th International Conference on Computing in Civil and Building Engineering, 2010b, volume 30.

Berges et al. 2011

Berges, M.; Asce, a. M.; Goldman, E.; Matthews, H. S.; Soibelman, L.; Anderson, K. D.: User-Centered Nonintrusive Electricity Load Monitoring for Residential Buildings. Journal of computing in civil engineering 25 (2011) 6, pp. 471–480.

Bernard & Marx 2016

Bernard, T.; Marx, M.: Unsupervised Learning Algorithm using multiple Electrical Low and High Frequency Features for the task of Load Disaggregation. In: Proceedings of the 3rd international workshop on NILM, 2016.

Bernard et al. 2015

Bernard, T.; Wohland, D.; Klaassen, J.; Vom Bogel, G.: Combining several distinct electrical features to enhance nonintrusive load monitoring. In: International Conference on Smart Grid and Clean Energy Technologies, ICSGCE 2015, 2015. pp. 139–143.

BMW AG 2018

BMW AG: Sustainable Value Report 2016, 2018, https://www.bmwgroup.com/content/dam/bmw-group-websites/bmwgroup_com/ir/downloads/en/2016/BMW-Group-SustainableValueReport-2016--EN.pdf, accessed: 2018-03-17.

Boghos & Al Jazi 2007

Boghos, H.; Al Jazi, A.: Asynchronous Machines. Damascus, Syria: DU (2007).

Böhner et al. 2014

Böhner, J.; Hamacher, M.; Reger, A.; Steinhilper, R.: Derivation of measures for energy efficient machine design by evaluating energy consumption data. Procedia CIRP 15 (2014), pp. 437–442.

Bonfigli et al. 2018

Bonfigli, R.; Felicetti, A.; Principi, E.; Fagiani, M.; Squartini, S.; Piazza, F.: Denoising autoencoders for Non-Intrusive Load Monitoring: Improvements and comparative evaluation. Energy and Buildings 158 (2018), pp. 1461–1474.

Borši et al. 2003

Borši, M.; Ili, D.; Milanovi, N.; Ferkovi, L.; Daponte, P.; Cimitile, A.: Estimation of the Uncertainty in Measurement of the electric energy. In: Proceedings of the XVII IMEKO World Congress. IMEKO 2003. pp. 865–867.

Bracewell 1978

Bracewell, R. N.: The Fourier Transform and Its Applications. McGraw-Hill 1978.

Brecher et al. 2010

Brecher, C.; Herfs, W.; Heyers, C.; Klein, W.; Triebs, J.; Beck, E.; Dorn, T.: Ressourceneffizienz von Werkzeugmaschinen im Fokus der Forschung. wt Werkstattstechnik online 100 (2010) 7/8, pp. 559–564.

Brecher et al. 2012

Brecher, C.; Bäumler, S.; Jasper, D.; Triebs, J.: Energy efficient cooling systems for machine tools. In: Leveraging Technology for a Sustainable World. Springer 2012, pp. 239–244.

Brossog et al. 2014

Brossog, M.; Kohl, J.; Merhof, J.; Spreng, S.; Franke, J.: Energy consumption and dynamic behavior analysis of a six-axis industrial robot in an assembly system. Procedia CIRP 23 (2014), pp. 131–136.

Brossog et al. 2015

Brossog, M.; Bornschlegl, M.; Franke, J. et al.: Reducing the energy consumption of industrial robots in manufacturing systems. The International Journal of Advanced Manufacturing Technology 78 (2015) 5-8, pp. 1315–1328.

Brüggemann & Laumeyer 2013

Brüggemann, H.; Laumeyer, M.: Effiziente Programmierung senkt den Energieverbrauch von Robotern. Maschinenmarkt (2013).

Buddingh 2003

Buddingh, P. C.: Even Harmonic Resonance - An Unusual Problem. IEEE Transactions on Industry Applications 39 (2003) 4, pp. 1181–1186.

Budeanu 1927

Budeanu, C.: Puissances reactives et fictives. 2. Impr. Cultura nationala 1927.

Camps et al. 1994

Camps, O. I.; Robertson, D.; Mayer, J.: Wavelets and power system transients: feature detection and classification. In: The SPIE International Symposium on Optical Engineering in Aerospace Sensing, 1994, volume 2242. pp. 474–487.

Chang et al. 2007

Chang, H.-H.; Yang, H.-T.; Lin, C.-L.: Load Identification in Neural Networks for a Non-intrusive Monitoring of Industrial Electrical Loads. In: International Conference on Computer Supported Cooperative Work in Design, CSCWD 2007. Springer 2007. pp. 664–674.

Chang et al. 2008

Chang, H.-H.; Lin, C. L.; Yang, H.-T.: Load recognition for different loads with the same real power and reactive power in a non-intrusive load-monitoring system. In: International Conference on Computer Supported Cooperative Work in Design, CSCWD 2008, 2008, volume 2. pp. 1122–1127.

Chang et al. 2010

Chang, H.-H.; Lin, C. L.; Lee, J. K.: Load identification in nonintrusive load monitoring using steady-state and turn-on transient energy algorithms. In: Proceedings of the 14th International Conference on Computer Supported Cooperative Work in Design, CSCWD 2010, 2010. pp. 27–32.

Chang et al. 2012

Chang, H.-H.; Chen, K.-l.; Tsai, Y. P.; Lee, W. J.: A New Measurement Method for Power Signatures of Nonintrusive Demand Monitoring and Load Identification. IEEE Transactions on Industry Applications 48 (2012) 2, pp. 764–771.

Chapman 2005

Chapman, S.: Electric machinery fundamentals. Tata McGraw-Hill Education 2005.

Chaudhary 2015

Chaudhary, S.: Integrated Motors & Machine-mounted Drives Report - 2015. Technical Report, IHS Technology - Manufacturing Technology, 2015.

Ciccolella & Canavero 1995

Ciccolella, A.; Canavero, F. G.: Stochastic prediction of wire coupling interference. In: Proceedings of the IEEE International Symposium on Electromagnetic Compatibility 1995, 1995. pp. 51–56.

Cole & Albicki 1998

Cole, A.; Albicki, A.: Data extraction for effective non-intrusive identification of residential power loads. In: IEEE Instrumentation and Measurement Technology Conference, IMTC 1998, 1998, volume 2. pp. 812–815.

Cox et al. 2006

Cox, R.; Leeb, S. B.; Shaw, S. R.; Norford, L. K.: Transient event detection for nonintrusive load monitoring and demand side management using voltage distortion. In: Applied Power Electronics Conference and Exposition, APEC 2006, 2006. pp. 1751–1757.

Czarnecki 1997

Czarnecki, L. S.: Budeanu and Fryze : Two frameworks for interpreting power properties of circuits with nonsinusoidal voltages and currents. Electrical Engineering 80 (1997) Teoria de Potência, pp. 359–367.

Czarnecki 2011

Czarnecki, L. S.: Power theories and meta-theory of powers in electrical circuits. Przeglad Elektrotechniczny (Electrical Review) 87 (2011) 8, pp. 198–201.

Daimler AG 2018

Daimler AG: Sustainability Report 2016, 2018, https://www.daimler.com/documents/sustainability/other/daimler-sustainability-report-2016.pdf, accessed: 2018-03-17.

Denkena et al. 2013

Denkena, B.; Park, H.-S.; Behrens, B.-A.; Henjes, J.; Bertys, S.; Dahal, P.; Lüken, I.; Klassen, A.: Development of a concept to optimize the energy efficiency in forging process chains. International Journal of Precision Engineering and Manufacturing 14 (2013) 7, pp. 1229–1236.

Denkena et al. 2014

Denkena, B.; Helmecke, P.; Hülsemeyer, L.: Energy efficient machining with optimized coolant lubrication flow rates. Procedia CIRP 24 (2014), pp. 25–31.

Denkena et al. 2015

Denkena, B.; Helmecke, P.; Hülsemeyer, L.: Energy efficient machining of Ti–6Al–4V. CIRP Annals 64 (2015) 1, pp. 61–64.

Dickie 1951

Dickie, H. F.: ABC inventory analysis shoots for dollars, not pennies. Factory Management and Maintenance 109 (1951) 7, pp. 92–94.

Dietmair & Verl 2009

Dietmair, A.; Verl, A.: Energy consumption forecasting and optimisation for tool machines. MM science journal March (2009), pp. 62–67.

DIN 8580:2003-09 2003

DIN 8580:2003-09: Manufacturing processes - Terms and definitions, division. Standard, Deutsches Institut für Normung e.V. (DIN), 2003.

Directive 2006/42/EC 2006

Directive 2006/42/EC: Machine Directive of the European Parliament and of the Council of 17 May 2006. Directive, 2006.

Dörr et al. 2013

Dörr, M.; Wahren, S.; Bauernhansl, T.: Methodology for energy efficiency on process level. Procedia CIRP 7 (2013), pp. 652–657.

Dreessen 2017

Dreessen, T.: Resource Management at Voith - Green Controlling to Green Factory. 2017. https://www.igcv.fraunhofer.de/de/veranstaltungen/gfb_kolloquium2017.html, presentation at 4th Green Factory Kolloquium 2017 in Augsburg, Germany.

Ducange et al. 2014

Ducange, P.; Marcelloni, F.; Antonelli, M.: A novel approach based on finite-state machines with fuzzy transitions for nonintrusive home appliance monitoring. IEEE Transactions on Industrial Informatics 10 (2014) 2, pp. 1185–1197.

Eberspächer & Verl 2013

Eberspächer, P.; Verl, A.: Realizing energy reduction of machine tools through a control-integrated consumption graph-based optimization method. Procedia CIRP 7 (2013), pp. 640–645.

Eberspächer et al. 2014

Eberspächer, P.; Schraml, P.; Schlechtendahl, J.; Verl, A.; Abele, E.: A model-and signal-based power consumption monitoring concept for energetic optimization of machine tools. Procedia CIRP 15 (2014), pp. 44–49.

Egarter et al. 2013

Egarter, D.; Sobe, A.; Elmenreich, W.: Evolving Non-Intrusive Load Monitoring. In: European Conference on the Applications of Evolutionary Computation, EvoApplications 2013. Springer 2013. pp. 182–191.

Egarter et al. 2015

Egarter, D.; Bhuvana, V. P.; Elmenreich, W.: PALDi: Online load disaggregation via particle filtering. IEEE Transactions on Instrumentation and Measurement 64 (2015) 2, pp. 467–477.

Eisele 2014

Eisele, C.: Simulationsgestützte Optimierung des elektrischen Energiebedarfs spanender Werkzeugmaschinen. Ph.D. thesis, Technical University of Darmstadt, 2014.

Elsevier 2018

Elsevier: Scopus citation database, 2018, https://www.scopus.com, accessed: 2018-05-12.

Feynman et al. 2011

Feynman, R. P.; Leighton, R. B.; Sands, M.: The Feynman lectures on physics, Vol. I: The new millennium edition: mainly mechanics, radiation, and heat. Basic books 2011.

Fleischer et al. 2016

Fleischer, J.; Förster, F.; Gebhardt, J.: Sustainable manufacturing through energy efficient handling processes. Procedia CIRP 40 (2016), pp. 574–579.

Frost & Sullivan 2014

Frost & Sullivan: Opportunities in the European Electric Drives Market for Discrete Industries. Technical Report, 2014.

Gebbe et al. 2014

Gebbe, C.; Klemm, F.; Zhai, S.; Reinhart, G.: Estimating Machine Power Consumptions through Aggregated Measurements and Machine Data Acquisition. In: Applied Mechanics and Materials, Trans Tech Publications 2014, volume 655. pp. 61–66.

Gebbe et al. 2015

Gebbe, C.; Reddi, J.; Reinhart, G.: Fine Granular Multistep Method for Improving the Resource Efficiency of Process Chains. The Learning Factory (2015), pp. 66–73.

Gebbe et al. 2017a

Gebbe, C.; Glasschröder, J.; Reinhart, G.: Cost-Efficient Energy Monitoring of Manufacturing Machines Based on Nonintrusive Load Monitoring. In: Applied Mechanics and Materials, Trans Tech Publications 2017a, volume 871. pp. 125–134.

Gebbe et al. 2017b

Gebbe, C.; Göttl, F.; Glasschröder, J.; Reinhart, G.: NILM disaggregation algorithm for variable speed drives. In: 24th CIRP Conference on Life Cycle Engineering, 2017b. [Only available on USB-stick distributed at conference, not online.].

Gebbe et al. 2017c

Gebbe, C.; Tran, C.; Lingenfelser, F.; Glasschröder, J.; Reinhart, G.: Feature Extraction and Classification of the Electric Current Signal of an Induction Motor for Condition Monitoring Purposes. In: Applied Mechanics & Materials. Trans Tech Publications 2017c, volume 856. pp. 244–251.

Gebbe et al. 2019

Gebbe, C.; Bashir, A.; Neuhäuser, T.: Classification of fixed speed motors based on their turn-on transient current [Manuscript submitted for publication and currently in review]. IEEE Transactions on Instrumentation and Measurement (2019).

Ghahramani & Jordan 1996

Ghahramani, Z.; Jordan, M. I.: Factorial hidden Markov models. In: Advances in Neural Information Processing Systems, 1996. pp. 472–478.

Gleich 2014

Gleich, R.: Energiecontrolling. Haufe-Lexware 2014.

GMC LLC 2018

GMC LLC: 2016 Sustainability Report, 2018, http://www.gmsustainability.com/_pdf/downloads/GM_2016_SR.pdf?v2, accessed: 2018-03-17.

Gonçalves et al. 2011

Gonçalves, H.; Ocneanu, A.; Berges, M.; Fan, R. H.: Unsupervised disaggregation of appliances using aggregated consumption data. Environmental Engineering (2011).

Grady 2012

Grady, M.: Understanding power system harmonics. Lecture Notes, Department of Electrical & Computer Engineering, University of Texas at Austin, 2012, https://web.ecs.baylor.edu/faculty/grady/Understanding_Power_System_Harmonics_Grady_April_2012.pdf, accessed 2018-05-26.

Grassl 2015

Graßl, M.: Bewertung der Energieflexibilität in der Produktion. Ph.D. thesis, Technical University of Munich, 2015.

Gude 2017

Gude, J.: Produzierendes Gewerbe und Dienstleistungen im Überblick. In: Statistisches Jahrbuch 2017. Statistisches Bundesamt (Destatis) 2017, chapter 20, https://www.destatis.de/DE/Publikationen/StatistischesJahrbuch/StatistischesJahrbuch.html.

Gulati et al. 2014

Gulati, M.; Ram, S. S.; Singh, A.: An In Depth Study into Using EMI Signatures for Appliance Identification. In: Proceedings of the 1st ACM Conference on Embedded Systems for Energy-Efficient Buildings. ACM 2014. pp. 70–79.

Gupta 2014

Gupta, S.: ElectriSense: Single-Point Sensing Using EMI for Electrical Event Detection and Classification in the Home. Ph.D. thesis, University of Washington, 2014.

Gupta et al. 2010

Gupta, S.; Reynolds, M.; Patel, S.: ElectriSense: single-point sensing using EMI for electrical event detection and classification in the home. In: Proceedings of the 12th ACM international conference on Ubiquitous computing, 2010. pp. 139–148.

Guvensan et al. 2013

Guvensan, M. A.; Taysi, Z. C.; Melodia, T.: Energy monitoring in residential spaces with audio sensor nodes: TinyEARS. Ad Hoc Networks 11 (2013) 5, pp. 1539–1555.

Halkidi et al. 2001

Halkidi, M.; Batistakis, Y.; Vazirgiannis, M.: On Clustering Validation Techniques. Journal of Intelligent Information Systems 17 (2001) 2/3, pp. 107–145.

Hanzelka & Milanović 2008

Hanzelka, Z.; Milanović, J. V.: Principles of electrical power control. In: Power Electronics in Smart Electrical Energy Networks. 2008, chapter 2, pp. 13–53.

Harris & Cahill 2005

Harris, C.; Cahill, V.: Exploiting user behaviour for context-aware power management. In: IEEE International Conference on Wireless And Mobile Computing, Networking And Communications, WiMob 2005, 2005, volume 4. pp. 122–130.

Hart 1985

Hart, G. W.: Prototype Nonintrusive Appliance Load Monitor - Progress Report #2. Technical Report, MIT Energy Laboratory, 1985.

Hart 1992

Hart, G. W.: Nonintrusive appliance load monitoring. In: Proceedings of the IEEE, 1992, volume 80. pp. 1870–1891.

Herrmann et al. 2014

Herrmann, C.; Pries, H.; Hartmann, G.: Energie-und ressourceneffiziente Produktion von Aluminiumdruckguss. Springer-Verlag 2014.

Hochreiter & Schmidhuber 1997

Hochreiter, S.; Schmidhuber, J.: Long short-term memory. Neural computation 9 (1997) 8, pp. 1735–1780.

Hofmann 2000

Hofmann, D.: Common Sources of Errors in Measurement Systems. Quality Assurance (2000).

Holmegaard & Baun Kjaergaard 2016

Holmegaard, E.; Baun Kjaergaard, M.: NILM in an Industrial Setting: A Load Characterization and Algorithm Evaluation. In: IEEE International Conference on Smart Computing, SMARTCOMP 2016, 2016. pp. 1–8.

IEC 60034-1:2017 2017

IEC 60034-1:2017: Rotating electrical machines - Part 1: Rating and performance. Standard, International Electrotechnical Commission, 2017.

IEC 60034-16-1:2011 2011

IEC 60034-16-1:2011: Rotating electrical machines - Part 16-1: Excitation systems for synchronous machines - Definitions. Standard, International Electrotechnical Commission, 2011.

IEC 60050-113:2011 2011

IEC 60050-113:2011: International Electrotechnical Vocabulary - Part 113: Physics for electrotechnology. Standard, International Electrotechnical Commission, 2011.

IEC 60050-131:2002 2002

IEC 60050-131:2002: International Electrotechnical Vocabulary - Part 131: Circuit theory. Standard, International Electrotechnical Commission, 2002.

IEC 60050-151:2001 2001

IEC 60050-151:2001: International Electrotechnical Vocabulary - Part 151: Electrical and magnetic devices. Standard, International Electrotechnical Commission, 2001.

IEC 61000-4-30:2015 2015

IEC 61000-4-30:2015: Testing and measurement techniques - Power quality measurement methods. Standard, International Electrotechnical Commission, 2015.

Jacob 2004

Jacob, E. K.: Classification and categorization: a difference that makes a difference. Library Trends 52 (2004) 3, pp. 515–540.

Jain et al. 1999

Jain, A. K.; Murty, M. N.; Flynn, P. J.: Data Clustering: A Review. ACM Computing Surveys 31 (1999) 3, pp. 264–323.

Jazizadeh et al. 2014

Jazizadeh, F.; Becerik-Gerber, B.; Berges, M.; Soibelman, L.: Unsupervised clustering of residential electricity consumption measurements for facilitated user-centric non-intrusive load monitoring. In: Computing in Civil and Building Engineering (2014), 2014. pp. 1869—-1876.

JCGM 2012

JCGM: The international vocabulary of metrology — basic and general concepts and associated terms (VIM), 3rd edition. Standard, Joint Committee for Guides in Metrology (JCGM), 2012.

Jeltsema 2015

Jeltsema, D.: Budeanu's concept of reactive and distortion power revisited. In: 12th International School on Nonsinusoidal Currents and Compensation, ISNCC 2015, 2015. 4, pp. 68–73.

Jin et al. 2011

Jin, Y.; Tebekaemi, E.; Berges, M.; Soibelman, L.: Robust adaptive event detection in non-intrusive load monitoring for energy aware smart facilities. In: IEEE International Conference on Acoustics, Speech and Signal Processing, ICASSP 2011, 2011. pp. 4340–4343.

Johnson & Willsky 2013

Johnson, M. J.; Willsky, A. S.: Bayesian Nonparametric Hidden Semi-Markov Models. Journal of Machine Learning Research 14 (2013), pp. 673–701.

Juran & Gryna 1951

Juran, J.; Gryna, F.: Juran's Quality Control Handbook, New York City, 1951.

Kelly & Knottenbelt 2015

Kelly, J.; Knottenbelt, W.: Neural NILM: Deep Neural Networks Applied to Energy Disaggregation (2015).

Kim et al. 2011

Kim, H.; Marwah, M.; Arlitt, M.; Lyon, G.; Han, J.: Unsupervised Disaggregation of Low Frequency Power Measurements. In: Proceedings of the 11th SIAM International Conference on Data Mining, 2011. pp. 747–758.

Kohl et al. 2014

Kohl, J.; Spreng, S.; Franke, J.: Discrete event simulation of individual energy consumption for product-varieties. Procedia CIRP 17 (2014), pp. 517–522.

Kolter & Jaakkola 2012

Kolter, J. Z.; Jaakkola, T.: Approximate Inference in Additive Factorial HMMs with Application to Energy Disaggregation. In: Proceedings of the International Conference on Artificial Intelligence and Statistics, 2012, volume XX. pp. 1472–1482.

Kolter & Johnson 2011

Kolter, J. Z.; Johnson, M. J.: REDD: A Public Data Set for Energy Disaggregation Research. In: Workshop on Data Mining Applications in Sustainability (SIGKDD), 2011, volume 25. pp. 59–62.

Koschnick & Sattler 2013

Koschnick, G.; Sattler, B.: Vom Frequenzumrichter zum Drive Controller. Technical Report, Zentralverband Elektrotechnik- und Elektronikindustrie e.V. (ZVEI), 2013.

Koza et al. 1996

Koza, J. R.; Bennett, F. H.; Andre, D.; Keane, M. A.: Automated design of both the topology and sizing of analog electrical circuits using genetic programming. In: Artificial Intelligence in Design'96. Springer 1996. pp. 151–170.

Krishnan 2001

Krishnan, R.: Electric motor drives: modeling, analysis, and control. Prentice Hall, Inc. 2001.

Kübler 2017

Kübler, F.: Ressourceneffizienzorientierte Betriebspunktoptimierung von Fertigungsprozessen. Ph.D. thesis, Universität Bayreuth, 2017.

Lam et al. 2007

Lam, H.; Fung, G.; Lee, W.: A Novel Method to Construct Taxonomy of Electrical Appliances Based on Load Signatures. IEEE Transactions on Consumer Electronics 53 (2007) 2, pp. 653–660.

Langer et al. 2014

Langer, T.; Schlegel, A.; Stoldt, J.; Putz, M.: A model-based approach to energy-saving manufacturing control strategies. Procedia CIRP 15 (2014), pp. 123–128.

Larek et al. 2011

Larek, R.; Brinksmeier, E.; Meyer, D.; Pawletta, T.; Hagendorf, O.: A discrete-event simulation approach to predict power consumption in machining processes. Production Engineering 5 (2011) 5, p. 575.

Laughman et al. 2003

Laughman, C.; Kwangduk Lee; Cox, R.; Shaw, S.; Leeb, S. B.; Norford, L.; Armstrong, P.: Power signature analysis. IEEE Power and Energy Magazine 1 (2003) 2, pp. 56–63.

Lee & Varaiya 2011

Lee, E. A.; Varaiya, P.: Structure and Interpretation of Signals and Systems. 2nd edition. LeeVaraiya.org 2011.

Lee 2003

Lee, K. D.: Electric Load Information System based on Non-Intrusive Power Monitoring by. Ph.D. thesis, Massachusetts Institute of Technology, 2003.

Lee et al. 2005

Lee, K. D.; Leeb, S. B.; Norford, L. K.; Armstrong, P. R.; Holloway, J.; Shaw, S. R.: Estimation of variable-speed-drive power consumption from harmonic content. IEEE Transactions on Energy Conversion 20 (2005) 3, pp. 566–574.

Leeb 1993

Leeb, S. B.: A conjoint pattern recognition approach to nonintrusive load monitoring. Ph.D. thesis, Massachusetts Institute of Technology, 1993.

Leeb et al. 1993

Leeb, S. B.; Kirtley, J. L.; Levan, M. S.; Sweeney, J. P.: Development and Validation of a Transient Event Detector. AMP Journal of Technology 3 (1993), pp. 69–74.

Leeb et al. 1995

Leeb, S. B.; Shaw, S. R.; Kirtley, J. L.: Transient event detection in spectral envelope estimates for nonintrusive load monitoring. IEEE Transactions on Power Delivery 10 (1995) 3, pp. 1200–1210.

Li et al. 2011

Li, W.; Zein, A.; Kara, S.; Herrmann, C.: An investigation into fixed energy consumption of machine tools. In: Glocalized solutions for sustainability in manufacturing. Springer 2011, pp. 268–273.

Liang et al. 2010a

Liang, J.; Ng, S. K.; Kendall, G.; Cheng, J. W.: Load Signature Study - Part I: Basic Concept , Structure and Methodology. IEEE Transactions on Power Delivery 25 (2010a) 2, pp. 551–560.

Liang et al. 2010b

Liang, J.; Ng, S. K.; Kendall, G.; Cheng, J. W.: Load Signature Study - Part II: Disaggregation Framework, Simulation and Applications. IEEE Transactions on Power Delivery 25 (2010b) 2, pp. 561–569.

Liebl et al. 2018

Liebl, C.; Popp, R. S.; Zaeh, M. F.: Approach for a Systematic Energy Data Generation and Evaluation. Procedia CIRP 67 (2018), pp. 63–68.

Luo et al. 2002

Luo, D.; Norford, L. K.; Shaw, S. R.; Leeb, S. B.: Monitoring HVAC Equipment Electrical Loads from a Centralized Location Methods and Field Test Results. ASHRAE Transactions 108 (2002), p. 841.

Maglogiannis 2007

Maglogiannis, I. G.: Emerging artificial intelligence applications in computer engineering: real word ai systems with applications in ehealth, hci, information retrieval and pervasive technologies, volume 160. Ios Press 2007.

Marchildon & Mody 2006

Marchildon, K.; Mody, D.: Pumps, Fans, Blowers and Compressors. In: Kutz, M. (Editor): Mechanical Engineers' Handbook: Energy and Power. John Wiley & Sons, Inc. 2006, volume 4, chapter 22, 3rd edition, pp. 717–752.

Mauch & Yang 2015

Mauch, L.; Yang, B.: A new approach for supervised power disaggregation by using a deep recurrent LSTM network. In: IEEE Global Conference on Signal and Information Processing, GlobalSIP 2015, 2015. pp. 63–67.

Mauch & Yang 2016

Mauch, L.; Yang, B.: A novel DNN-HMM-based approach for extracting single loads from aggregate power signals. IEEE International Conference on Acoustics, Speech and Signal Processing, ICASSP 2016 (2016), pp. 2384–2388.

Microchip Technology Inc. 2008

Microchip Technology Inc.: SMPS AC/DC Reference Design User's Guide (DS70320B). Technical Report, 2008.

Milligan & Cooper 1985

Milligan, G. W.; Cooper, M. C.: An examination of procedures for determining the number of clusters in a data set. Psychometrika 50 (1985) 2, pp. 159–179.

Mohan 2014

Mohan, N.: Advanced electric drives: analysis, control, and modeling using MATLAB/Simulink. John Wiley & sons 2014.

Mohri et al. 2012

Mohri, M.; Rostamizadeh, A.; Talwalkar, A.: Foundations of machine learning. MIT press 2012.

Neugebauer 2013

Neugebauer, R.: Handbuch Ressourcenorientierte Produktion. Carl Hanser Verlag GmbH Co KG 2013.

Neugebauer et al. 2010

Neugebauer, R.; Wertheim, R.; Hochmuth, C.; Schmidt, G.; Dix, M.: Modelling of energy and resource-efficient machining. In: Proceedings of the 4th CIRP Conference on High Performance Cutting, Gifu, 2010. pp. 295–300.

Neugebauer et al. 2012a

Neugebauer, R.; Drossel, W.; Wertheim, R.; Hochmuth, C.; Dix, M.: Resource and energy efficiency in machining using high-performance and hybrid processes. Procedia CIRP 1 (2012a), pp. 3–16.

Neugebauer et al. 2012b

Neugebauer, R.; Putz, M.; Schlegel, A.; Langer, T.; Franz, E.; Lorenz, S.: Energy-sensitive production control in mixed model manufacturing processes. In: Leveraging Technology for a Sustainable World. Springer 2012b, pp. 399–404.

Norford & Leeb 1996

Norford, L. K.; Leeb, S. B.: Non-intrusive electrical load monitoring in commercial buildings based on steady-state and transient load-detection algorithms. Energy and Buildings 24 (1996) 1, pp. 51–64.

OECD 2015

OECD: Frascati manual 2015: guidelines for collecting and reporting data on research and experimental development. OECD Publishing 2015.

Panten et al. 2016

Panten, N.; Abele, E.; Schweig, S.: A Power Disaggregation Approach for fine-grained Machine Energy Monitoring by System Identification. Procedia CIRP 48 (2016), pp. 325–330.

Parson 2013

Parson, O.: Why NIALM shouldn't be modelled as the knapsack or subset-sum problem, 2013, http://blog.oliverparson.co.uk/2013/04/why-nialm-shouldnt-be-modelled-as.html, accessed: 2017-01-01.

Parson 2014

Parson, O.: Unsupervised Training Methods for Non-intrusive Appliance Load Monitoring from Smart Meter Data. Ph.D. thesis, University of Southhampton, 2014.

Parson et al. 2014

Parson, O.; Ghosh, S.; Weal, M.; Rogers, A.: An unsupervised training method for non-intrusive appliance load monitoring. Artificial Intelligence 217 (2014), pp. 1–19.

Patel et al. 2007

Patel, S.; Robertson, T.; Kientz, J. A.; Reynolds, M. S.; Abowd, G. D.: At the Flick of a Switch: Detecting and Classifying Unique Electrical Events on the Residential Power Line. In: International Conference on Ubiquitous Computing, UbiComp 2007. Springer 2007. pp. 271–288.

Patterson 1996

Patterson, M. G.: What is energy efficiency?: Concepts, indicators and methodological issues. Energy policy 24 (1996) 5, pp. 377–390.

Pedregosa et al. 2011

Pedregosa, F.; Varoquaux, G.; Gramfort, A.; Michel, V.; Thirion, B.; Grisel, O.; Blondel, M.; Prettenhofer, P.; Weiss, R.; Dubourg, V. et al.: Scikit-learn: Machine learning in Python. Journal of machine learning research 12 (2011) Oct, pp. 2825–2830.

Pillay & Krishnan 1989a

Pillay, P.; Krishnan, R.: Modeling, simulation, and analysis of permanent-magnet motor drives. I. The permanent-magnet synchronous motor drive. Industry Applications, IEEE Transactions on 25 (1989a) 2, pp. 265–273.

Pillay & Krishnan 1989b

Pillay, P.; Krishnan, R.: Modeling, simulation, and analysis of permanent-magnet motor drives. II. The brushless DC motor drive. IEEE Transactions on Industry Applications 25 (1989b) 2, pp. 274–279.

Popp & Zäh 2014a

Popp, R.; Zäh, M.: Determination of the Technical Energy Flexibility of Production Systems. Advanced Materials Research 1018 (2014a), pp. 365–372.

Popp & Zäh 2014b

Popp, R.; Zäh, M.: Steuerung des Energiebedarfs von Werkzeugmaschinen. wt-online 6 (2014b), pp. 413–417.

Powers et al. 1991

Powers, J.; Margossian, B.; Smith, B.: Using a rule-based algorithm to disaggregate end-use load profiles from premise-level data. IEEE Computer Applications in Power 4 (1991) 2, pp. 42–47.

Putz et al. 2017

Putz, M.; Klocke, F.; Neugebauer, R.: Ressourceneffizienz, Springer 2017, chapter Fraunhofer Leitprojekt E 3-Produktion. pp. 145–174.

Rashid 2007

Rashid, M. H.: Power Electronics Handbook. 3rd edition. Elsevier 2007.

Rasmussen et al. 1997

Rasmussen, C. B.; Ritchie, E.; Arkkio, A.: Variable speed induction motor drive for household refrigerator compressor. In: IEEE International Symposium on Industrial Electronics, ISIE 1997, 1997, volume 2. pp. 655–659.

Recker 2012

Recker, J.: Scientific research in information systems: a beginner's guide. Springer Science & Business Media 2012.

Refaeilzadeh et al. 2009

Refaeilzadeh, P.; Tang, L.; Liu, H.: Cross-validation. In: Encyclopedia of database systems. Springer 2009, pp. 532–538.

Reinhart et al. 2010

Reinhart, G.; Karl, F.; Krebs, P.; Reinhardt, S.: Energiewertstrom: Eine Methode zur ganzheitlichen Erhöhung der Energieproduktivität. ZWF Zeitschrift für wirtschaftlichen Fabrikbetrieb 105 (2010) 10, pp. 870–875.

Reinhart et al. 2016

Reinhart, G.; Steinhilper, R.; Böhner, J.; Gebbe, C.; Glasschröder, J.; Lothes, G.; Müller, T.; Simon, P.; Unterberger, E.; Weeber, M.: Ressourceneffiziente Fabriken - Innovative Praxisbeispiele und zukünftige Handlungsfelder. Fraunhofer Verlag 2016.

Reinhart et al. 2017

Reinhart, G.; Steinhilper, R.; Böhner, J.; Brugger, M.; Chen, Q.; Ellenrieder, S.; Gebbe, C.; Glasschröder, J.; Götz, G.; Jahn, J.; Klein, M.; Küfner, T.; Lothes, G.; Lutter-Günther, M.; Müller, T.; Reger, A.; Schmidt, V.; Schock, C.; Schweda, S.; Teufelhart, S.; Thorenz, B.; Uhlemann, T. H.-J.; Unterberger, E.: Strategien und Methoden der ressourceneffizienten Produktion. Fraunhofer Verlag 2017.

Rich 1982

Rich, A.: Understanding Interference-Type Noise. Analog Dialogue 16 (1982) 3, pp. 16–19.

Ridi et al. 2015

Ridi, A.; Gisler, C.; Hennebert, J.: Processing smart plug signals using machine learning. In: IEEE Wireless Communications and Networking Conference Workshops, WCNCW 2015, 2015. pp. 75–80.

Rohde 2017

Rohde, C.: Erstellung von Anwendungsbilanzen für die Jahre 2013 bis 2016. Technical Report, Fraunhofer-Institut für System- und Innovationsforschung (Fraunhofer ISI), Karlsruhe, 2017.

Rousseeuw 1987

Rousseeuw, P. J.: Silhouettes: A graphical aid to the interpretation and validation of cluster analysis. Journal of Computational and Applied Mathematics 20 (1987), pp. 53–65.

Sanders et al. 1991

Sanders, S. R.; Noworolski, J. M.; Liu, X. Z.; Verghese, G. C.: Generalized averaging method for power conversion circuits. IEEE Transactions on Power Electronics 6 (1991) 2, pp. 251–259.

Scheda 1986

Scheda, F. A.: Transient inrush current in high-efficiency and standard motors. IEEE transactions on industry applications (1986) 1, pp. 145–147.

Schmidhuber 2015

Schmidhuber, J.: Deep learning in neural networks: An overview. Neural networks 61 (2015), pp. 85–117.

Schmitt et al. 2011

Schmitt, R.; Bittencourt, J. L.; Bonefeld, R.: Modelling Machine Tools for Self-Optimisation of Energy Consumption. In: Glocalized Solutions for Sustainability in Manufacturing, 2011. pp. 253–257.

Schoofs et al. 2010

Schoofs, A.; Guerrieri, A.; Delaney, D. T.; O'Hare, G. M.; Ruzzelli, A. G.: Annot: Automated electricity data annotation using wireless sensor networks. In: 7th Annual IEEE Communications Society Conference on Sensor Mesh and Ad Hoc Communications and Networks, SECON 2010, IEEE 2010. pp. 1–9.

Sclater & Traister 2003

Sclater, N.; Traister, E. J.: Handbook of Electrical Design Details. 2nd edition. McGraw-Hill 2003.

Senft 2012

Senft, S.: Roboter energieeffizient steuern und programmieren. etz elektrotechnik & automation 5 (2012), pp. 2–3.

Shannon 1949

Shannon, C. E.: Communication in the presence of noise. Proceedings of the IRE 37 (1949) 1, pp. 10–21.

Shao et al. 2012

Shao, H.; Tech, V.; Marwah, M.: A Temporal Motif Mining Approach to Unsupervised Energy Disaggregation. In: 1st International Workshop on Non-Intrusive Load Monitoring, 2012. pp. 1–2.

Shaw & Laughman 2007

Shaw, S. R.; Laughman, C.: A Kalman-filter spectral envelope preprocessor. IEEE Transactions on Instrumentation and Measurement 56 (2007) 5, pp. 2010–2017.

Shenkman 2006

Shenkman, A. L.: Transient analysis of electric power circuits handbook. Springer Science & Business Media 2006.

Siegwart 1974

Siegwart, H.: Produktentwicklung in der industriellen Unternehmung. Haupt 1974.

Simon 2015

Simon, U.: Verfahren der Bewegungsplanung zur Energieminimierung bei Maschinen und Robotern. In: Fachtagung Vernetzt Planen und Produzieren, VPP 2015, 2015. Sonderheft 21, pp. 109–118.

Srinivasan et al. 2006

Srinivasan, D.; Ng, W. S.; Liew, A. C.: Neural-network-based signature recognition for harmonic source identification. IEEE Transactions on Power Delivery 21 (2006) 1, pp. 398–405.

Steinhilper et al. 2015

Steinhilper, R.; Kübler, F.; Hamacher, M.; Böhner, J.; Fiebach, R.; Volk, D.; Müller, S.; Volk, D.; Kubizek, A.; Wiegärtner, V.: Minimierung nicht wertschöpfender Energieaufwände durch energetische Anlagenoptimierung. Fraunhofer Verlag 2015.

Stoldt et al. 2013

Stoldt, J.; Schlegel, A.; Franz, E.; Langer, T.; Putz, M.: Generic energy-enhancement module for consumption analysis of manufacturing processes in discrete event simulation. In: Re-engineering Manufacturing for Sustainability. Springer 2013, pp. 165–170.

Sultanem 1991

Sultanem, F.: Using appliance signatures for monitoring residential loads at meter panel level. IEEE Transactions on Power Delivery 6 (1991) 4, pp. 1380–1385.

Sung et al. 2002

Sung, D.-U.; Kim, C.-G.; Hong, C.-S.: Monitoring of impact damages in composite laminates using wavelet transform. Composites Part B: Engineering 33 (2002) 1, pp. 35–43.

Suzuki et al. 2008

Suzuki, K.; Inagaki, S.; Suzuki, T.; Nakamura, H.; Ito, K.: Nonintrusive appliance load monitoring based on integer programming. In: SICE Annual Conference, 2008, IEEE 2008. pp. 2742–2747.

Teiwes et al. 2018

Teiwes, H.; Blume, S.; Herrmann, C.; Rössinger, M.; Thiede, S.: Energy Load Profile Analysis on Machine Level. Procedia CIRP 69 (2018), pp. 271–276.

The Nielsen Company LLC 2015

The Nielsen Company LLC: The sustainable imperative, 2015, http://www.nielsen.com/content/dam/corporate/us/en/reports-downloads/2015-reports/global-sustainability-report-oct-2015.pdf, accessed: 2018-03-17.

Uddin & Nadeem 2012

Uddin, M.; Nadeem, T.: EnergySniffer: Home energy monitoring system using smart phones. In: 8th International Conference on Wireless Communications and Mobile Computing Conference, IWCMC 2012, IEEE 2012. pp. 159–164.

USDOE 1997

USDOE: Determining Electric Motor Load and Efficiency. Fact sheet as part of the motor challenge program, U. S. Department of Energy - Office of Energy Efficiency and Renewable Energy, 1997.

Verl et al. 2011a

Verl, A.; Abele, E.; Heisel, U.; Dietmair, A.; Eberspächer, P.; Rahäuser, R.; Schrems, S.; Braun, S.: Modular modeling of energy consumption for monitoring and control. In: Glocalized Solutions for Sustainability in Manufacturing. Springer 2011a, pp. 341–346.

Verl et al. 2011b

Verl, A.; Westkämper, E.; Abele, E.; Dietmair, A.; Schlechtendahl, J.; Friedrich, J.; Haag, H.; Schrems, S.: Architecture for multilevel monitoring and control of energy consumption. In: Glocalized Solutions for Sustainability in Manufacturing. Springer 2011b, pp. 347–352.

VW AG 2018

VW AG: Sustainability Report 2016, 2018, http://sustainabilityreport2016.volkswagenag.com/fileadmin/16_NB/PDF_en/vw-sr2016-en.pdf, accessed: 2018-03-17.

Wagner & Wagner 2004

Wagner, S.; Wagner, D.: Comparing clusterings: an overview. Research report. ISSN 1432-7864, 2004.

Wall 2003

Wall, R.: Simple methods for detecting zero crossing. In: 29th Annual Conference of the IEEE Industrial Electronics Society, IECON 2003, IEEE 2003, volume 3. pp. 2477–2481.

Wang & Zheng 2011

Wang, Z.; Zheng, G.: New method for non-intrusive data extraction and classification of residential appliances. In: Chinese Control and Decision Conference, CCDC 2011, 2011. pp. 2196–2201.

Wang & Zheng 2012

Wang, Z.; Zheng, G.: Residential appliances identification and monitoring by a nonintrusive method. IEEE Transactions on Smart Grid 3 (2012) 1, pp. 80–92.

Wichakool et al. 2009

Wichakool, W.; Avestruz, A. T.; Cox, R.; Leeb, S. B.: Modeling and estimating current harmonics of variable electronic loads. IEEE Transactions on Power Electronics 24 (2009) 12, pp. 2803–2811.

Wichakool et al. 2015

Wichakool, W.; Remscrim, Z.; Orji, U. A.; Leeb, S. B.: Smart metering of variable power loads. IEEE Transactions on Smart Grid 6 (2015) 1, pp. 189–198.

Willeke et al. 2016

Willeke, S.; Ullmann, G.; Nyhuis, P.: Method for an Energy-Cost-Oriented Manufacturing Control to Reduce Energy Costs: Energy Cost Reduction by Using a New Sequencing Method. In: Industrial Engineering, Management Science and Application (ICIMSA), 2016 International Conference on, IEEE 2016. pp. 1–5.

Xu et al. 1999

Xu, W.; Dommel, H. W.; Hughes, M. B.; Chang, G. W. K.; Tan, L.; Chang, G. W. K.; Tan, L.: Modelling Of Adjustable Speed Drives For Power System Harmonic Analysis. IEEE Transactions on Power Delivery 14 (1999) 2, pp. 595–601.

Xu et al. 1996

Xu, X.; Nitta, S.; Mutoh, A.; Jayaram, S.: Study on noise characteristics of multiconductor twisted-pair wire circuit-the case of n= 2. IEEE International Symposium on Electromagnetic Compatibility 1996 (1996), pp. 259–264.

Yang et al. 2007

Yang, H.-T.; Chang, H.-H.; Lin, C. L.: Design a neural network for features selection in non-intrusive monitoring of industrial electrical loads. In: 11th International Conference on Computer Supported Cooperative Work in Design, CSCWD 2007, 2007. pp. 1022–1027.

Yoo et al. 2011

Yoo, J.; Park, B.; Hur, K.: Context awareness-based disaggregation of residential load Consumption. Elsevier 2011, volume 44. pp. 13691–13695.

Zeifman & Roth 2011

Zeifman, M.; Roth, K.: Nonintrusive appliance load monitoring: Review and outlook. IEEE Transactions on Consumer Electronics 57 (2011) 1, pp. 76–84.

Zhou et al. 2015

Zhou, N.; Wang, J.; Wang, Q.; Wei, N.: Measurement-Based Harmonic Modeling of an Electric Vehicle Charging Station Using a Three-Phase Uncontrolled Rectifier. IEEE Transactions on Smart Grid 6 (2015) 3, pp. 1332–1340.

Zimmermann et al. 2012

Zimmermann, J.-P.; Evans, M.; Lineham, T.; Griggs, J.; Surveys, G.; Harding, L.; King, N.; Roberts, P.: Household Electricity Survey: A study of domestic electrical product usage. Intertek (2012), p. 600.

Zoha et al. 2012

Zoha, A.; Gluhak, A.; Imran, M. A.; Rajasegarar, S.: Non-intrusive Load Monitoring approaches for disaggregated energy sensing: A survey. Sensors 12 (2012) 12, pp. 16838–16866.